PhD-FSTC-2018-41
The Faculty of Sciences, Technology and Communication

DISSERTATION

Defense held on 17/05/2018 in Luxembourg

to obtain the degree of

DOCTEUR DE L'UNIVERSITÉ DU LUXEMBOURG

EN PHYSIQUE

by

Artur WACHTEL
Born on 26 December 1986 in Kara-Balta (Kyrgyzstan)

NONEQUILIBRIUM THERMODYNAMICS IN BIOLOGY: FROM MOLECULAR MOTORS TO METABOLIC PATHWAYS

Dissertation defense committee

Dr. Massimiliano Esposito, Dissertation Supervisor
Professor, Université du Luxembourg

Dr. Ludger Wirtz, Chairman
Professor, Université du Luxembourg

Dr. Alexander Skupin, Vice Chairman
Research scientist, Université du Luxembourg

Dr. David Wolpert
Professor, Santa Fe Institute

Dr. Peter Sollich
Professor, Georg-August-Universität Göttingen

This thesis is submitted for the degree *Docteur de l'Université du Luxembourg en Physique*.

Nonequilibrium Thermodynamics in Biology

From Molecular Motors to Metabolic Pathways

by Artur Wachtel

Abstract

Biological systems need to exchange energy and matter with their environment in order to stay functional or “alive”. This exchange has to obey the laws of thermodynamics: energy cannot be created and exchange comes at the cost of dissipation, which limits the efficiency of biological function. Additionally, subcellular processes that involve only few molecules are stochastic in their dynamics and a consistent theoretical modeling has to account for that.

This dissertation connects recent development in nonequilibrium thermodynamics with approaches taken in biochemical modeling. I start by a short introduction to thermodynamics and statistical mechanics, with a special emphasis on large deviation theory and stochastic thermodynamics. Building on that, I present a general theory for the thermodynamic analysis of networks of chemical reactions that are open to the exchange of matter.

As a particularly insightful concrete example I discuss the mechanochemical energy conversion in stochastic models of a molecular motor protein, and show how a similar analysis can be performed for more general models. Furthermore, I compare the dissipation in stochastically and deterministically modeled open chemical networks, and present a class of chemical networks that displays exact agreement for arbitrary abundance of chemical species and arbitrary distance from thermodynamic equilibrium. My major achievement is a thermodynamically consistent coarse-graining procedure for biocatalysts, which are ubiquitous in molecular cell biology. Finally, I discuss the thermodynamics of unbranched enzymatic chains.

Erkenntnis wächst aus Konfusion

→←

Preface

This thesis contains the results of my research on the thermodynamics of chemical reaction networks in the group of Massimiliano Esposito at the University of Luxembourg. It is mainly composed of five studies: three published articles and two manuscripts *in preparation*. They form the chapters 5–9. In order to help the reader who is unfamiliar with the field, I additionally provide a motivational prelude and four introductory chapters. In the motivation I take the biological viewpoint and highlight the relevance of chemical reaction networks. The introduction covers the essential prerequisites and sets the stage for my research: chapter 1 deals with thermodynamics in and out of equilibrium. Chapter 2 covers statistical mechanics, stochastic thermodynamics and large deviation theory. In chapter 3 I introduce elementary chemical reactions in closed volumes and I show how their microscopic (stochastic) and macroscopic (deterministic) dynamics and thermodynamics need to be treated. It is followed by the most important introductory chapter 4 where I discuss open systems with many chemical reactions. I conclude this thesis with a final part where I summarize my achievements and provide a perspective on currently ongoing as well as possible future research. The author contributions for the included research articles are detailed in the appendix. References are given at the end of each chapter.

This thesis was funded by an AFR PhD grand awarded by the National Research Fund Luxembourg (grant number 7865466). Also many individual people supported me and my research. First and foremost I have to thank my PhD supervisor Massimiliano Esposito. Although frequently very busy, he still finds the time to discuss interesting research questions — ranging from the very small details in specific models to the big picture stretching across disciplines. I am indebted to my Master supervisor Jürgen Vollmer, with whom I continue to collaborate and who by now is a dear friend. I am very thankful for the productive collaborations with my coauthors Bernhard Altaner, Matteo Polettini, and Riccardo Rao. Our discussions, individually and in groups of various configurations, were both the source of a lot of confusion, but ultimately also the spark of my understanding. Special respect is due to Riccardo Rao. As my office mate he had to endure my praying chants and unexpected bursts of laughter. I have to thank my friends Fabian Telschow, Caroline Bauer, and Alexandre Lazarescu. Your support was what really kept me afloat. Zu guter Letzt möchte ich meinen Eltern und meinen Brüdern danken. Ihre Unterstützung in allen Lebenslagen und aus der Ferne ist kaum mit Worten aufzuwiegen. Спасибо!

Luxembourg, April 2018
Artur Wachtel

Contents

Motivation

Biology is the natural science that studies living organisms. The known living organisms are classically categorized into different kingdoms of life: *animals*, *plants*, *fungi*, as well as *bacteria*, *archaea*, and sometimes *protista*. We humans ourselves are animals and thus part of the life on Earth. We domesticate other animals and plants for our own survival. Livestock breeding and agriculture provide nourishment and clothing. Forestry supplies us with one of our most important construction materials: wood. Moreover, bacteria and fungi are employed for fermentation, which is an important method to preserve food. The understanding of biology is especially important for modern medicine, since it unveils the microscopic causes for diseases and thus underlies their treatments. Consequently, every progress in the understanding of biological processes has a great potential to increase the quality of our lives.

Modern biology in fact already provides a thorough understanding for the principal organization of living organisms: organs, tissues and cells. The latter can be considered the elementary building block of life itself — subcellular structures are typically not considered "alive". Cells again are internally organized into different organelles and compartments. However, there are only four types of organic molecules that constitute all of the above structures [1]:

Lipids form the membranes that separate the cell from its environment, and the cellular organelles from the rest of the cell. *Carbohydrates* give structural stability to the cells of plants and fungi. Both lipids and carbohydrates serve as long-term storage of energy for the cellular machinery. The latter is primarily composed of *aminoacids* which form polypeptides and proteins. These can catalytically convert other chemicals (enzymes), serve as mechanochemical engines [2, 3], or constitute structural molecules, for example in the cytoskeleton [4]. The *ribonucleic acid* (RNA) and the *deoxyribonucleic acid* (DNA) provide the storage of *information* in four basic letters: **A**denine, **T**hymine[1], **G**uanine and **C**ytosine. The nucleic acids store the blueprints for the construction of proteins and thus carry the hereditary information from one generation of cells and organisms to the next. Especially one nucleobase, *adenine*, serves another purpose. When bound to ribose sugar it can be phosphorylated up to three times, known as *adenosine monophosphate* (AMP), *adenosine diphosphate* (ADP) and *adenosine triphosphate* (ATP). Each of these phosphorylation steps is energetically costly but fully reversible and it was understood that these adenosine phosphates serve as the principal short-term fuel for the cellular machinery [5].

In order to grow and divide, the cell needs to construct these materials from energy as well as from precursor molecules it extracts from its food. This process is known as *anabolism*. The reverse process to break down biological matter for energy is *catabolism*. Together they form the entire *metabolism* of the cell. The metabolism is important to keep the cell operational or "alive" and requires a permanent but selective exchange of matter across the cell's boundary.

By now, this general organization of cellular life is common knowledge and not disputed. However, the exact biochemical *processes* inside living cells are still subject to research: To what extent and exactly how are individual metabolic pathways regulated? How does the cell process and respond to external chemical (mechanical/optical) signals? While proteins are encoded by genes on the DNA,

[1] In RNA, thymine is replaced by the similar **U**racil.

how do they feed back onto the transcriptional and translational processes of the genetic material? The respective experiments are difficult and time consuming. After all, each species, organism, and even each cell is different. This variability extends down even to the microscopic level where the stochastic nature of molecular dynamics leads to intrinsic noise within the cellular machinery. These challenges are currently being faced with automated experimental setups that provide analysis with a high throughput of individual cells or molecules. These methods give access to the genes of a cell (genomics), the activation levels of these genes as messenger RNA transcripts (transcriptomics), the actual abundance of proteins (proteomics), as well as the concentrations (metabolomics) and the fluxes (fluxomics) of various metabolite molecules within the living cell. The integration of all these data has the potential to lead to a systemic understanding of entire cells and even organisms. These approaches are summarized under the term *systems biology* [6, 7].

A consistent integration of all these data into models with predictive power requires a solid theoretical basis. This basis cannot be of purely mathematical nature. In the end, cellular and subcellular processes are based on the *chemical* conversion of molecules and the storage and transport of *energy*. The physical theory that is centered around exchange of energy and matter is *thermodynamics*. It was originally born at the time of the industrial revolution and was aimed at understanding the exact functioning, and improving the efficiency of steam engines. However, it turned out that the range of its applicability is much larger. Modern thermodynamics [8–10] incorporates temporal evolution and deals with small stochastic systems. It is applied in strongly correlated quantum systems [11] and it covers the physical effects of information [12, 13].

While modern nonequilibrium thermodynamics is conceptually capable of treating biochemical processes on a molecular level, there is still a gap between the current understanding of the theory and the systemic scale that is required for a fruitful application in the life sciences.

The goal of my thesis is to narrow this gap. I start from the basic concepts of thermodynamics in its modern formulation, which I introduce in the first two chapters. Then, I present chemical reactions and networks thereof in the following two chapters. Afterwards, I apply these concepts to small and fluctuating molecular motors, and subsequently move up the scales to arrive at large macroscopic pathways. Following this route, we find a lot of uncharted territory and sometimes more questions than answers.

Ultimately, the pursuit of nonequilibrium thermodynamics in biology may pave the way for a system-wide treatment of energy, work, heat and information — a theory of *thermodyn**o**mics*.

References

[1] D. L. Nelson and M. M. Cox. *Lehninger Principles of Biochemistry*. 5th ed. New York: W. H. Freeman and Co., 2008.

[2] F. Jülicher, A. Ajdari, and J. Prost. “Modeling molecular motors”. In: *Reviews of Modern Physics* 69.4 (1997), pp. 1269–1282.

[3] A. B. Kolomeisky and M. E. Fisher. “Molecular Motors: A Theorist’s Perspective”. In: *Annual Review of Physical Chemistry* 58.1 (2007), pp. 675–695.

[4] D. A. Fletcher and R. D. Mullins. “Cell mechanics and the cytoskeleton”. In: *Nature* 463 (2010), pp. 485–492.

[5] F. Lipmann. “Metabolic Generation and Utilization of Phosphate Bond Energy”. In: *Advances in Enzymology*. Ed. by F. F. Nord and C. H. Werkman. Vol. 1. New York: Interscience Publishers, 1941, pp. 99–162.

[6] U. Alon. *An Introduction to Systems Biology: Design Principles of Biological Circuits*. Mathematical and Computational Biology Series. Boca Raton: Chapman and Hall/CRC, 2007.

[7] E. Klipp et al. *Systems Biology*. Weinheim: Wiley-VCH, 2009.

[8] M. Esposito. "Stochastic thermodynamics under coarse graining". In: *Physical Review E* 85, 041125 (2012).

[9] U. Seifert. "Stochastic thermodynamics, fluctuation theorems and molecular machines". In: *Reports on Progress in Physics* 75, 126001 (2012).

[10] S. Ciliberto. "Experiments in Stochastic Thermodynamics: Short History and Perspectives". In: *Physical Review X* 7, 021051 (2017).

[11] M. Esposito, M. A. Ochoa, and M. Galperin. "Quantum Thermodynamics: A Nonequilibrium Green's Function Approach". In: *Physical Review Letters* 114, 080602 (2015).

[12] A. Bérut et al. "Experimental verification of Landauer's principle linking information and thermodynamics". In: *Nature* 483 (2012), pp. 187–189.

[13] J. M. R. Parrondo, J. M. Horowitz, and T. Sagawa. "Thermodynamics of information". In: *Nature Physics* 11.2 (2015), pp. 131–139.

Part I.

Introduction to Thermodynamics & Statistical Mechanics

1. Thermodynamics

Thermodynamics is a universal theory of exchanges and consequently deals with fundamental properties of matter. A good approximation for biological matter is that of a solution that mainly consists of water. This solution is surrounded by some boundary (cell membrane) but can exchange heat and volume, as well as matter with its environment.

In this chapter I provide a modern formulation for thermodynamics that covers both thermodynamic equilibrium [1] as well as nonequilibrium situations [2]. It serves as the foundation of my work. For simplicity, in this chapter I will cover only macroscopic and inert systems. The following chapter 2 deals with microscopic systems and I introduce elementary chemical reactions in chapter 3. The last introductory chapter 4 finally covers the thermodynamics of fully open chemical networks.

The main goal of this chapter is to provide a way to quantify the *dissipation* of a system under biochemically relevant conditions.

1.1. The Laws of Thermodynamics

Thermodynamics studies *exchange processes* between several systems. The two most important exchange quantities are *energy* and *matter*.

A system that releases energy as useful *work* is especially interesting and such systems are referred to as *engine* or *motor*. An obvious question is: how much work can an engine perform? It was understood early on that this work cannot be unlimited. The limits are twofold: (1) All engines require some other form of energy as *fuel* in order to operate. Like the original steam engines, modern engines convert *heat* into *work*. (2) *Heat* can never be fully converted into *work* because of irreversible *dissipation*. These principles are two fundamental laws. Like many laws in physics, the laws of thermodynamics are derived from empirical evidence. They cannot be derived from more fundamental principles.

1.1.1. Thermodynamic Equilibrium: The Zeroth Law

Two otherwise isolated systems are said to be in *thermodynamic equilibrium* if, upon contact, they do in fact not exchange any quantity. The *zeroth law of thermodynamics* states that thermodynamic equilibrium is a transitive relation:

> When the two systems A and B are in thermodynamic equilibrium and the two systems B and C as well, then also A and C, upon contact, will not exchange any quantity and therefore are also in thermodynamic equilibrium.

This is a very idealized concept but it is possible to relax these requirements. While full thermodynamic equilibrium requires that *no* quantity is being exchanged, there are partial equilibria:

- When two systems do not exchange heat: *thermal equilibrium*.
- When two systems do not exchange mechanical work: *mechanical equilibrium*.

- When two systems do not exchange matter: *chemical equilibrium*.

Each of these partial equilibria can be quantified: The quantity characterizing the thermal equilibrium is *temperature*. Likewise, the *pressure* (force per surface area) characterizes mechanical equilibrium with respect to volume work. The analogous quantity for particle exchange is the *chemical potential*. Since a system may be composed of several chemical species and each of them could in principle be exchanged, we have a chemical potential for each species. When otherwise equilibrated, heat (work, matter) will go from higher temperature (pressure, chemical potential) to lower.

Temperature, pressure and chemical potential are *intensive* quantities — in contrast to the *extensive* quantities that are being exchanged. A thermodynamic *reservoir* has no meaningful extensive properties but instead is fully described by its intensive quantities.

1.1.2. Energy Balance: The First Law

The exchanges of a thermodynamic system impact its energy balance. The *first law of thermodynamics* states that

> All the changes of internal energy are either due to work or to heat.

In formal language we write $\Delta E = W + Q$. In this chapter I assume that the exchange processes are continuous. I deal with discontinuous exchange in chapter 2. Due to the continuity, we can reformulate the first law via integrals:

$$\int \mathrm{d}E = \int đW + \int đQ\,. \tag{1.1}$$

The energy E is a *state function*. Its change only depends on the initial and final state of the system. The work W and the heat Q are not given by the state of the system. They depend on the transformation γ that we impose. Therefore, we use *inexact differentials* to express these process-dependent integrals.

The exchanged work, again, can be of different types. For systems with a three-dimensional volume, *mechanical work* is performed against the external pressure p:

$$đW_{\mathrm{mech}} = -p\,\mathrm{d}V\,. \tag{1.2}$$

A one-dimensional system, analogously, performs work by changing the length ℓ against an external force, $đW_{\mathrm{mech}} = -f\,\mathrm{d}\ell$.

Adding one mole of particles of type i from a reservoir at chemical potential μ_i changes the internal energy by means of the *chemical work*:

$$đW_{\mathrm{chem}} = \sum_i \mu_i\,\mathrm{d}n_i\,. \tag{1.3}$$

1.1.3. Entropy Balance: The Second Law

Rudolph Clausius [3, 4] was the first to relate the exchanged heat to a state function. Specifically, he found that for reversible transformations γ, which always remain at thermodynamic equilibrium, the exchanged heat $đQ$ — when scaled by the temperature — is a state function, the *entropy* S:

$$\Delta S = \int_\gamma \mathrm{d}S = \int_\gamma \frac{1}{T} đQ\,. \tag{1.4}$$

He also realized that for irreversible (or dissipative) transformations γ we have an inequality:

$$\Delta S = \int_\gamma \mathrm{d}S > \int_\gamma \frac{1}{T} \text{đ}Q \,. \tag{1.5}$$

This is known as Clausius' version of the *second law of thermodynamics*.

In a modern formulation [2] we prefer to have an equality by quantifying the dissipation by means of the *entropy production*:

$$\int_\gamma \text{đ}\Sigma := \int_\gamma \left(\mathrm{d}S - \frac{1}{T} \text{đ}Q \right) = \Delta S - \int_\gamma \frac{1}{T} \text{đ}Q \geq 0 \,. \tag{1.6}$$

The second law of thermodynamics thus is equivalent to saying that the integrated entropy production is a positive quantity for irreversible processes, while it is zero at thermodynamic equilibrium.

This is also true for cyclic processes, where the integral over every state function vanishes. This means that the entropy production is not a state function on its own. It depends on the process just like work and heat, and we have to use an inexact differential.

1.1.4. Absolute Temperature: The Third Law

The *third law of thermodynamics* states that

> The entropy change associated with any condensed system undergoing a reversible isothermal process approaches zero as the temperature at which it is performed approaches 0 K.

This especially implies that it is impossible to cool a system to absolute zero temperature in a finite number of steps or in a finite amount of time.

The third law is stated here only for completeness — and strictly speaking we need to dig into quantum thermodynamics in order to address it appropriately. Since I am mainly interested in biological systems, absolute zero temperature is not an interesting regime for the purpose of this thesis.

1.2. Nonequilibrium Thermodynamics

When combining the energy and entropy balances we arrive at the fundamental equations of nonequilibrium thermodynamics [2, 5, 6]:

$$\mathrm{d}E = T\,\mathrm{d}S - p\,\mathrm{d}V + \sum_i \mu_i\,\mathrm{d}n_i - T\text{đ}\Sigma \,. \tag{1.7}$$

From this relation we see that *isolated systems* (where the energy, the volume and the chemical composition is fixed) evolve towards bigger entropy:

$$\int \mathrm{d}S = \int \text{đ}\Sigma \geq 0 \,. \tag{1.8}$$

The situation where entropy does not increase is thermodynamic equilibrium where $\text{đ}\Sigma = 0$. This is known as the *maximum entropy principle* for thermodynamic equilibrium. If instead of the energy we fix the entropy, the energy will be minimized — which is known as *minimum energy principle*.

These extremum principles are the reason why energy and entropy are considered *thermodynamic potentials*.

In the context of biological systems, the assumptions that energy, entropy or volume is prescribed is not very realistic. It is more appropriate to consider the temperature and the pressure to be imposed by the environment. In this isothermal–isobaric setting, neither the entropy nor the energy approach their extremum. Instead, the *free enthalpy* or *Gibbs free energy* defined as $G = E - TS + pV$ is the right potential for this case:

$$\mathrm{d}G = -S\,\mathrm{d}T + V\,\mathrm{d}p + \sum_i \mu_i\,\mathrm{d}n_i - T\text{đ}\Sigma\,. \tag{1.9}$$

For closed systems that are thermally and mechanically equilibrated, this relation together with the second law ensures the minimization of the free enthalpy.

1.2.1. Isothermal Energy Conversion

Under isothermal conditions, the second law as formulated above implies that a machine cannot transform heat into work in a continuous (cyclic or steady-state) fashion. Instead, work is always being dissipated into heat. Thus, isothermal energy conversion requires the conversion between different types of work, coming at the cost of dissipation.

In chapter 5 I will investigate the isothermal conversion of chemical work into mechanical work by a molecular motor. The *efficiency* of this process is given by

$$\eta_{\mathrm{II}} \coloneqq -\frac{\oint \text{đ}W_{\mathrm{mech}}}{\oint \text{đ}W_{\mathrm{chem}}} = \frac{\oint p\,\mathrm{d}V}{\oint \sum_i \mu_i\,\mathrm{d}n_i} = \frac{\oint f\,\mathrm{d}\ell}{\oint \sum_i \mu_i\,\mathrm{d}n_i} \leq 1\,. \tag{1.10}$$

The last inequality follows from equation (1.7) and shows that the dissipation sets the essential limits for the efficiency of energy conversion. This limitation makes the dissipation an especially important quantity to determine.

1.2.2. Dissipation under Biochemical Conditions

In *open* systems, the chemical composition can change due to exchange with the particle reservoirs. When additionally the system internally allows for chemical reactions, the matter exchange currents cannot be identified with the change of chemical composition, $\mathrm{d}n_i$. Consequently, open reactive systems can reach *nonequilibrium steady states* even when they are thermally and mechanically equilibrated with their environment. These steady states admit steady exchange of matter which therefore needs to be expressed by inexact differential forms, $\text{đ}n_i$. In this thesis I primarily focus on these nonequilibrium steady states.

With equation (1.9) we can quantify the entropy production of a chemically reacting system in a steady state at fixed temperature and fixed pressure as [2, 6]

$$\text{đ}\Sigma = \sum_i \mu_i\,\text{đ}n_i\,. \tag{1.11}$$

Note that here only the species which are continuously exchanged with the reservoirs need to be taken into account. The internal species satisfy $\text{đ}n_j = \mathrm{d}n_j = 0$ at steady states.

This expression for the entropy production was the main goal of this chapter. However, we are not done yet. For chemical systems in dilute solution that are thermally and mechanically equilibrated we can express the chemical potentials by means of the chemical composition.

1.3. Equilibrium Thermodynamics

At thermodynamic equilibrium, the dissipation in exactly zero. We therefore arrive at the *fundamental relation of equilibrium thermodynamics* [1, 7]

$$\mathrm{d}E = T\,\mathrm{d}S - p\,\mathrm{d}V + \sum_i \mu_i\,\mathrm{d}n_i\,. \tag{1.12}$$

It implies that the equilibrium energy is a function only of the entropy, the volume and the chemical composition of the system. Moreover, at equilibrium the temperature, pressure, and chemical potentials are properties of the *system* and can be written as state functions via the equations of state

$$T(S,V,\{n_i\}) = \frac{\partial E}{\partial S}\,, \qquad p(S,V,\{n_i\}) = -\frac{\partial E}{\partial V}\,, \qquad \mu_j(S,V,\{n_i\}) = \frac{\partial E}{\partial n_j}\,. \tag{1.13}$$

Similarly, the equilibrium free enthalpy is a function of the temperature, the pressure, and the chemical composition:

$$\mathrm{d}G = -S\,\mathrm{d}T + V\,\mathrm{d}p + \sum_i \mu_i\,\mathrm{d}n_i\,. \tag{1.14}$$

The derivatives of the equilibrium free enthalpy provide the entropy, the volume and the chemical potentials as functions of temperature, pressure and chemical composition:

$$S(T,p,\{n_i\}) = -\frac{\partial G}{\partial T}\,, \qquad V(T,p,\{n_i\}) = \frac{\partial G}{\partial p}\,, \qquad \mu_j(T,p,\{n_i\}) = \frac{\partial G}{\partial n_j}\,. \tag{1.15}$$

We see that the extensivity of the energy, the volume and the mole numbers ensures that the entropy and the free enthalpy are extensive as well: all extensive quantities scale with the size of the system. This is mathematically expressed as *homogeneity* of the thermodynamic potentials. Therefore, Euler's theorem for homogeneous functions allows us to integrate the fundamental relation of equilibrium thermodynamics to provide an expression for the absolute value of the thermodynamic potentials:

$$E = T\,S - p\,V + \sum_i \mu_i\,n_i\,, \qquad G = \sum_i \mu_i\,n_i\,. \tag{1.16}$$

This equation is known as *Euler relation.*

1.4. Ideal Fluids

The full dependence of the thermodynamic potentials on their natural variables is not known for most systems of interest. However, sometimes the full dependence is not necessary to make useful statements about the thermodynamics of a system. When *equations of state* are available, they can be integrated to provide just as much information. Since I am mainly interested in the dissipation of a system, I need equations of state for the chemical potential. I focus on *ideal* solutions — which are closely related to mixtures of ideal gases.

1.4.1. The Ideal Gas

The ideal gas takes a special role in thermodynamics: it is one of the few systems that can be solved analytically. It describes the thermodynamic behavior of dilute gases with f degrees of freedom while having negligible interactions between the molecules. The degrees of freedom account for three translations in physical space as well as additional rotational degrees of freedom of the molecules. An ideal gas that is composed of a single particle type is fully described by the two equations of state

$$pV = nRT\,, \qquad E = \frac{f}{2}nRT\,. \tag{1.17}$$

Here, $R \approx 8.314\,\mathrm{J\,K^{-1}\,mol^{-1}}$ is the ideal gas constant. From these equations of state and the fundamental relations, it is possible to derive the chemical potential of the ideal gas [7] as

$$\mu(T,p) = \mu^* \frac{T}{T^*} - \frac{f+2}{2}RT\ln\frac{T}{T^*} + RT\ln\frac{p}{p^*}\,. \tag{1.18}$$

This expression is independent of the total amount n of gas, but is given relative to a reference value μ^* at temperature T^* and pressure p^*. In fact, the Euler relation ensures that the free enthalpy is directly proportional to the chemical potential for every pure substance: $G(T,p,n) = n\,\mu(T,p)$. Thus, the chemical potential accounts for all equilibrium properties of the pure substance.

When mixing several ideal gases, the chemical composition has an impact on the chemical potentials of the different components j in the mixture [7]:

$$\mu_j(T,p,\{n_i\}) = \mu(T,p) + RT\ln\frac{n_j}{\sum_i n_i}\,. \tag{1.19}$$

The argument of the logarithm is known as *molar fraction* of the species j. The composition-independent term is the chemical potential of a pure ideal gas, equation (1.18).

1.4.2. Ideal Dilute Solution

In an *ideal* solution, the energetic interactions of the different components are entirely screened by the solvent. Thus the solutes behave essentially like a mixture of ideal gases. Additionally, in a *dilute* solution the molar fraction is entirely dominated by the solvent. Hence, we can approximate the molar fraction by the *molar concentration* $z_i = \frac{n_i}{V}$, where the volume $V \equiv V(T,p,\{n_i\})$ is defined by eq. (1.15). This decouples the chemical potentials of the different solutes and we arrive at the equation of *ideal dilute solutions*:

$$\mu_i(T,p,z_i) = \mu_i^\circ(T,p) + RT\ln\frac{z_i}{1\,\mathrm{M}}\,. \tag{1.20}$$

The first term, μ°, contains all contributions of the solvent and thus is the chemical potential at the *standard state* with concentration $z_i = 1\,\mathrm{M} = 1\,\mathrm{mol\,dm^{-3}}$. In the following, I will suppress the explicit standard concentration inside the logarithm.

With this equation the Gibbs free energy of an ideal dilute solution is given as

$$G(T,p,\{V\,z_i\}) = V\sum_i \mu_i(T,p,z_i)\,z_i = V\sum_i \mu_i^\circ(T,p) + VRT\sum_i z_i\ln z_i\,. \tag{1.21}$$

In the standard state, it takes the value

$$G^\circ(T,p) = G(T,p,\{V\}) = V\sum_i \mu_i^\circ(T,p)\,. \tag{1.22}$$

Moreover, we can finally express the entropy production in a well stirred system via the concentrations as

$$\text{đ}\Sigma = V \sum_i \mu_i(z_i)\,\mathrm{d}z_i = V \sum_i \left[\mu_i^\circ(T,p) + RT \ln z_i\right] \mathrm{d}z_i \,. \tag{1.23}$$

The equations (1.21) and (1.23) are the central results of this section. They are valid for ideal dilute solutions at a macroscopic scale. In the next chapter, we will extend these concepts to systems of mesoscopic size, and which therefore follow stochastic dynamics. The generalized expressions for the free enthalpy and the dissipation will serve as the starting points for the thermodynamic analysis of reactive systems in chapter 3.

References

[1] H. B. Callen. *Thermodynamics and an Introduction to Thermostatistics*. 2nd ed. New York: Wiley, 1985.

[2] D. Kondepudi and I. Prigogine. *Modern Thermodynamics: From Heat Engines to Dissipative Structures*. 2nd ed. Chichester: John Wiley & Sons, 2015.

[3] R. Clausius. "Ueber eine veränderte Form des zweiten Hauptsatzes der mechanischen Wärmetheorie". In: *Annalen der Physik* 169.12 (1854), pp. 481–506.

[4] R. Clausius. "Ueber verschiedene für die Anwendung bequeme Formen der Hauptgleichungen der mechanischen Wärmetheorie". In: *Annalen der Physik* 201.7 (1865), pp. 353–400.

[5] P. Glansdorff and I. Prigogine. *Thermodynamic theory of structure, stability and fluctuations*. London, New York: Wiley-Interscience, 1971.

[6] S. de Groot and P. Mazur. *Non-Equilibrium Thermodynamics*. Dover Books on Physics Series. New York: Dover Publications, 1984.

[7] R. Hołyst and A. Poniewierski. *Thermodynamics for Chemists, Physicists and Engineers*. Dordrecht: Springer, 2012.

2. Statistical Mechanics

Statistical mechanics provides a microscopic perspective for thermodynamics. It is built on top of a detailed microscopic dynamical description of a macroscopic system. For the purpose of this thesis, I assume an underlying *classical* mechanics. Quantum effects are known to only play a significant role at very low temperatures and hence are most likely negligible for biochemical systems[1].

In this chapter I give an overview of statistical mechanics and how to recover from it the thermodynamics in and out of equilibrium. I cover stochastic dynamics giving rise to a discrete exchange of extensive quantities between a system and its environment. A special focus is on the entropy production in stochastic thermodynamics. It provides the microscopic origin for irreversibility and highlights the statistical nature of the second law of thermodynamics.

2.1. Hamiltonian formulation of Classical Mechanics

A mechanical system is fully described by the positions q and the momenta p of its constituent parts. The positions and momenta of such a system, collected as $\gamma = (q, p)$, evolve in time according to Hamilton's equation of motion [1]:

$$\frac{\mathrm{d}}{\mathrm{d}t}\gamma = I\,\nabla H(\gamma) \qquad \text{where} \qquad I = \begin{pmatrix} 0 & \mathbb{1} \\ -\mathbb{1} & 0 \end{pmatrix}, \qquad \nabla H = \begin{pmatrix} \frac{\partial H}{\partial q} \\ \frac{\partial H}{\partial p} \end{pmatrix}. \tag{2.1}$$

In addition to governing the evolution of time, the Hamiltonian function $H(q, p)$ quantifies the total, i.e. potential and kinetic, energy in the system in the state $\gamma = (q, p)$. This energy function is typically nonlinear which causes also the dynamics to be nonlinear. Due to this nonlinearity, the detailed dynamics is complicated and can be solved analytically only for few simple problems.

The special symplectic structure of this equation ensures that the energy $H(q, p)$ is conserved throughout the time evolution:

$$\frac{\mathrm{d}}{\mathrm{d}t}H(\gamma(t)) = \nabla H(\gamma(t)) \cdot \frac{\mathrm{d}}{\mathrm{d}t}\gamma(t) = \nabla H(\gamma(t)) \cdot I\,\nabla H(\gamma(t)) = \frac{\partial H}{\partial q}\frac{\partial H}{\partial p} - \frac{\partial H}{\partial p}\frac{\partial H}{\partial q} = 0\,. \tag{2.2}$$

This *conservation of energy* is an integral property of Hamilton's equation of motion. It implies that any motion is restricted to the *energy shell* of the initial condition: $H(\gamma(t)) \equiv H(\gamma(0))$.

Hamiltonian systems may have other conserved quantities: linear and angular momentum are typical candidates. This means that the accessible phase space Ω is in fact only a submanifold of the energy shell.

2.2. Equilibrium Statistical Mechanics

The dynamics within the accessible phase space can be assumed to be unpredictable or *chaotic*. Hence, we can assume that the state of the system will visit every part of the accessible phase space infinitely

[1] Nonetheless, the internal structure and stability of a molecule can only be understood with methods from quantum mechanics. However, quantum *coherence* is not relevant across different molecules at ambient temperatures.

often. A more rigorous formulation is the *ergodic hypothesis*: there is a unique function ρ on the accessible phase space Ω such that for almost all observable functions A on Ω and almost all initial conditions $\gamma(0) \in \Omega$ with time evolution $\gamma(t)$ we have

$$\lim_{t\to\infty} \frac{1}{t} \int_0^t A(\gamma(\tau))\,\mathrm{d}\tau = \int_\Omega \rho(x)A(x)\,\mathrm{d}x\,. \tag{2.3}$$

We can especially integrate the constant function $A \equiv 1$ in time to get normalization: $1 = \int_\Omega \rho(x)\mathrm{d}x$. When integrating indicator functions χ_ω of subsets $\omega \subset \Omega$ of the energy shell, we can deduce that the function ρ is furthermore *positive*. In total, ρ is a probability density and characterizes the long-time behavior of the ergodic system. It is often referred to as *ergodic measure*. The importance of the ergodic measure can also be understood in a more physical way: assume a lot of identical copies γ_i of the physical system are prepared with initial conditions sampled from an open neighborhood of (almost) any point $\gamma(0) \in \Omega$. After some *relaxation time* $\tilde{t}$, the average of (almost) every observable A over this *ensemble* of systems tends to the same value as does an average over large times:

$$\lim_{N\to\infty} \sum_{i=1}^{N} A(\gamma_i(t')) = \int_\Omega \rho(x)A(x)\,\mathrm{d}x = \lim_{t\to\infty} \frac{1}{t} \int_0^t A(\gamma(\tau))\,\mathrm{d}\tau \quad \text{for all } t' > \tilde{t}\,. \tag{2.4}$$

Here it is important to realize that the right hand side is independent of the time t'. Frequently, the ensemble on the left hand side is considered a time-dependent probability distribution on its own: we can define

$$\rho_N(x,t) := \frac{1}{N} \sum_{i=1}^{N} \delta(x - \gamma_i(t))\,. \tag{2.5}$$

Then, the ergodic limit is typically written as $\rho_N(x,t') \xrightarrow{N\to\infty} \rho(x)$. This limit is true only for sufficiently large t' and is understood to hold only for almost all points x. Thus, any average taken with respect to either measure takes the same value. Overall, this hypothesis ensures that neither the initial conditions nor the exact dynamics are of importance when it comes to computing averages of physically meaningful observables, such kinetic or potential energy. Knowledge (or good astimates) of the ergidic measure are sufficient to do so.

2.2.1. The Microcanonical Ensemble

For a system with N identical particles in a three dimensional volume V, the total phase space of positions and momenta is $V^N \times \mathbb{R}^{3N}$. Due to interactions between the particles and their container, the linear and angular momentum of the particle system is not conserved. Under the assumption of purely elastic collisions, conservation of energy $E = H(q,p)$ still restricts the available phase space to an energy shell $\Omega(E,V,N) \subset V^N \times \mathbb{R}^{3N}$. What is the ergodic distribution on this energy shell?

Following the work of Boltzmann and Gibbs, the only option is to use the uniform distribution [2]

$$\rho_{\mathrm{mc}}(x) = \frac{1}{|\Omega|} \qquad \text{where} \qquad |\Omega| = \int_\Omega \mathrm{d}x\,. \tag{2.6}$$

This is known as the *microcanonical ensemble*. Indeed, using this ansatz and only considering kinetic energy $H(q,p) = \frac{m}{2}p^2$ it is possible to reproduce the phenomenological equilibrium thermodynamics of the ideal gas (in the limit of $N \to \infty$). In this identification, the thermodynamic equilibrium

entropy measures the available phase space volume as $S(E, V, N) = k_\mathrm{B} \ln |\Omega(E, V, N)|$. Boltzmann's constant $k_\mathrm{B} = \frac{R}{N_\mathrm{A}} \approx 1.38 \times 10^{-23}\,\mathrm{J\,K^{-1}}$ is related to the ideal gas constant R via Avogadro's number $N_\mathrm{A} \approx 6.02 \times 10^{23}\,\mathrm{mol^{-1}}$. I use it here because it is more common in the context of statistical mechanics than is the ideal gas constant.

2.2.2. Gibbs–Shannon Entropy

In a more general setting we have to account for the exchange of energy or volume, so the distribution cannot be restricted to the energy shell. A uniform distribution on the entire unbounded state space, however, cannot be normalized. Consequently, the above ansatz needs to be modified. Gibbs reasoned that the most natural ergodic distribution on the available phase space Ω (now typically the entire phase space) is the one that maximizes the functional [2]

$$\mathcal{S}(\rho) = -k_\mathrm{B} \int_\Omega \rho(x) \ln(\rho(x)) \mathrm{d}x \tag{2.7}$$

while ensuring normalization as well as finite average values for the quantities that can be exchanged. Note that here I suppressed a constant factor with dimension of phase space volume in the argument of the logarithm — this factor does not impact the maximization and results merely in an additive shift in the absolute value of the functional. The quantity in eq. (2.7) measures the (average) amount of *information* you gain from sampling the distribution ρ [3] and it is now known as *Gibbs–Shannon entropy*. The maximum of this information measure represents a state that you have the least prior knowledge about [4]. In this sense it measures the "disorder" in a system. Indeed, for constant energy, volume, and particle numbers we reproduce the microcanonical entropy

$$\max_{\rho \,|\, E,V,N} \mathcal{S}(\rho) = \mathcal{S}(\rho_\mathrm{mc}) = S\left(E, V, N\right) \,. \tag{2.8}$$

2.2.3. The Isothermal–Isobaric Ensemble

In the following, we will account for a closed system that can exchange energy and volume with an *ideal* reservoir. An ideal reservoir never changes its properties, irrespective of the amount of energy or volume that is being exchanged. This reservoir is fully characterized by its temperature T and pressure p.

The system's microstate x is accounting for the entire internal configuration, covering states with different values for energy $E(x)$ and volume $V(x)$. The maximization of the Gibbs–Shannon entropy (when accounting for normalization, as well as a finite mean energy and volume) results in the *isothermal–isobaric ensemble*:

$$\varrho(x) = \frac{1}{\mathcal{Z}\left(T, p, N\right)} \exp\left[-\frac{E(x) + pV(x)}{k_\mathrm{B}T}\right] \tag{2.9}$$

with its partition function

$$\begin{aligned} \mathcal{Z}(T, p, N) &= \int_\Omega \mathrm{d}x \exp\left[-\frac{E(x) + pV(x)}{k_\mathrm{B}T}\right] \\ &= \int_0^\infty \mathrm{d}V \int_0^\infty \mathrm{d}E \exp\left[-\frac{E + pV - T\,S(E, V, N)}{k_\mathrm{B}T}\right] \,. \end{aligned} \tag{2.10}$$

The partition function quantifies the effectively occupied phase space volume. For the isothermal–isobaric ensemble it directly provides the equilibrium free enthalpy as

$$G\left(T, p, N\right) = -k_\mathrm{B}T \ln \mathcal{Z}\left(T, p, N\right) = \langle E \rangle_\varrho + p \left\langle V \right\rangle_\varrho - T\,\mathcal{S}(\varrho) \,. \tag{2.11}$$

2.3. Nonequilibrium Statistical Mechanics

The statistical description on phase space in terms of the partition function and the thermodynamic potentials correctly reproduces equilibrium thermodynamics. In this description, the dynamics of a process plays no role — the dynamics disappears upon maximizing the Gibbs–Shannon entropy. Such a formulation of thermodynamics is inherently incapable of dealing with exchange currents and with relaxation to thermodynamic equilibrium. Hence, we need to consider the dynamics.

The exact microscopic (Hamiltonian) dynamics on phase space is too complicated for a detailed discussion of dynamics. Nonetheless, a *mesoscopic* dynamics in terms of stochastic processes is a viable alternative.

2.3.1. Markov Processes

We can think of an intermediate level of description for the dynamics where, instead of providing a deterministic evolution in time, we partition the available phase space into *mesoscopic states*: $\Omega = \bigcup\{\omega\}$. For the purpose of this thesis, it is sufficient to work with a *discrete* set of mesoscopic states, so that we can take sums over all possible mesoscopic states ω instead of integrals over phase space volumes.

A first simple approximation to dynamics on this space is a *Markov process*, i.e. a memoryless stochastic process. The probability to find a trajectory γ in a state ω at time t is determined solely by the probabilities to find the trajectory in the other states ω' at a previous time $t' < t$. In a time-continuous formulation, the time evolution of this probability evolves according to the *master equation*:

$$\frac{\mathrm{d}}{\mathrm{d}t}\, p_\omega = \sum_{\omega' \neq \omega} w_{\omega,\omega'}\, p_{\omega'} - \sum_{\omega' \neq \omega} w_{\omega',\omega}\, p_\omega \,. \tag{2.12}$$

Here, $w_{\omega,\omega'}$ is the transition rate from state ω' to state ω. A more compact notation for this equation can be achieved by incorporating the *escape rates* $r_\omega := \sum_{\omega' \neq \omega} w_{\omega',\omega}$ as negative entries on the diagonal of the transition matrix

$$\mathbb{W}_{\omega,\omega'} = \begin{cases} w_{\omega,\omega'} & \text{if } \omega \neq \omega' \,, \\ -r_\omega & \text{if } \omega = \omega' \,. \end{cases} \tag{2.13}$$

With this shorthand notation, the master equation can be written in matrix–vector form:

$$\frac{\mathrm{d}}{\mathrm{d}t}\, \boldsymbol{p} = \mathbb{W}\boldsymbol{p} \,, \tag{2.14}$$

which is why this matrix is often referred to as the *generator* of the Markov process.

Under fairly mild conditions, this master equation reaches a unique steady state:

$$0 = \mathbb{W}\boldsymbol{p}^* \,. \tag{2.15}$$

Sufficient for the uniqueness and global stability of this steady state is the *irreducibility* of the transition matrix. A transition matrix is irreducible, if for every pair of states, ω and ω', there is a sequence of states $\omega, \omega_1, \ldots, \omega_n, \omega'$ such that the transition rate from one state to the next does not vanish. In this case, the unique steady-state distribution spans the one-dimensional kernel of the transition matrix — and determining the kernel of $\mathbb{W}$ is equivalent to finding the steady-state distribution for equation (2.14).

We will especially require that $w_{\omega,\omega'} \neq 0 \Leftrightarrow w_{\omega',\omega} \neq 0$. This is known as *microscopic reversibility*: when a transition from one state ω to another state ω' is possible, so is the reverse transition. This does not restrict the exact values of these rates. They may be vastly different — making one almost negligible with respect to the other.

Some transition matrices allow for a special property: a vector $\boldsymbol{\pi}$ is in *detailed balance* with a transition matrix $\mathbb{W}$ if for all pairs of states ω and ω' we have $w_{\omega',\omega}\,\pi_\omega = w_{\omega,\omega'}\,\pi_{\omega'}$. This means that there is no probability current between any state. A direct consequence of detailed balance is that every detailed balanced vector $\boldsymbol{\pi}$ is a steady-state solution to the master equation (2.12). Since we assume the transition matrix to be irreducible, this steady-state solution is furthermore unique. If a transition matrix admits a detailed balanced steady-state solution, this solution can be constructed very easily by starting at any state p_1 and progressing to its neighboring states ω via

$$\frac{\pi_\omega}{\pi_1} = \frac{w_{\omega,1}}{w_{1,\omega}} \tag{2.16}$$

and so on. The value of π_1 is determined a posteriori from normalization $\sum_\omega \pi_\omega = 1$. This construction is obviously only possible if and only if for every sequence of neighboring states $\omega_1, \omega_2, \ldots, \omega_n, \omega_1$ that returns to its starting point, we have

$$\frac{w_{\omega_1,\omega_2} \cdots w_{\omega_n,\omega_1}}{w_{\omega_2,\omega_1} \cdots w_{\omega_1,\omega_n}} = 1\,. \tag{2.17}$$

This equivalent criterion for detailed balance is attributed to Колмогоров[2] [5].

2.3.2. Stochastic Thermodynamics

In order to connect the Markovian dynamics to equilibrium statistical mechanics, we need to associate thermodynamic state functions to the mesoscopic states ω:

$$\text{energy } e_\omega\,, \qquad \text{volume } v_\omega\,, \qquad \text{and} \qquad \text{entropy } s_\omega\,. \tag{2.18}$$

The entropy s_ω of the mesoscopic state ω accounts for the phase space volume attributed to that state during the partitioning of the available phase space. Accounting for it explicitly is necessary to make the upcoming equations invariant under further coarse graining (with appropriate time-scale separation) [6].

With these state functions, we can express the equilibrium distribution from statistical mechanics in the isothermal–isobaric ensemble as

$$p_\omega^{\mathrm{eq}} = \frac{1}{\mathcal{Z}} \exp\left[-\frac{e_\omega + p\,v_\omega - T s_\omega}{k_\mathrm{B} T}\right] = \frac{1}{\mathcal{Z}} \exp\left(-\frac{g_\omega}{k_\mathrm{B} T}\right)\,. \tag{2.19}$$

with the mesoscopic free enthalpy $g_\omega = e_\omega + p\,v_\omega - T\,s_\omega$. The equilibrium energy and the equilibrium volume,

$$E^{\mathrm{eq}} = \langle e \rangle^{\mathrm{eq}} = \sum_\omega e_\omega\, p_\omega^{\mathrm{eq}} \qquad \text{and} \qquad V^{\mathrm{eq}} = \langle v \rangle^{\mathrm{eq}} = \sum_\omega v_\omega\, p_\omega^{\mathrm{eq}}\,, \tag{2.20}$$

are simple averages over the mesoscopic states. The thermodynamic entropy of the equilibrium distribution p_ω^{eq}, in addition, needs to account for the Gibbs–Shannon contribution:

$$S^{\mathrm{eq}} = \sum_\omega p_\omega^{\mathrm{eq}} \left(s_\omega - k_\mathrm{B} \ln p_\omega^{\mathrm{eq}}\right)\,. \tag{2.21}$$

[2] Frequently transliterated as “Kolmogorov” or “Kolmogoroff”.

The equilibrium free enthalpy therefore is given by

$$G^{\mathrm{eq}} = E^{\mathrm{eq}} + p\,V^{\mathrm{eq}} - T\,S^{\mathrm{eq}}\,. \tag{2.22}$$

At thermodynamic equilibrium we have no currents of extensive quantities between the system and its reservoir. This can be ensured microscopically only if all probability currents vanish, so by detailed balance. This identification leads to the requirement

$$\frac{w_{\omega,\omega'}}{w_{\omega',\omega}} = \frac{p^{\mathrm{eq}}_{\omega}}{p^{\mathrm{eq}}_{\omega'}} = \exp\left[-\frac{g_\omega - g_{\omega'}}{k_{\mathrm{B}}T}\right], \tag{2.23}$$

which ensures consistency between dynamics and thermodynamics. Obviously, this requirement is nothing but a rephrasing of the Колмогоров criterion, equation (2.17), in physical terms: the sum of $g_\omega - g_{\omega'}$ along every cycle in the network of states necessarily is zero — otherwise g_ω is not actually a well defined function of the mesoscopic state ω. In a way this can be understood as the stochastic version of the zeroth law.

The description as presented so far is able to cover equilibrium steady states as well as relaxation to equilibrium starting from a nonequilibrium initial condition. Nonequilibrium steady states require multiple reservoirs, which can trigger transitions between the states. The different reservoirs may indeed be associated to different sets of admissible transitions. Whenever a transition between two states ω and ω' may involve different reservoirs, these different choices are dynamically indistinguishable from the perspective of the system. For the interactions with the reservoirs and thus the thermodynamics, however, it is important to do their book keeping separately.

When modeling a mesoscopic system in contact with multiple reservoirs, indexed by ℓ, we therefore decompose the stochastic transition rates as

$$w_{\omega,\omega'} = \sum_{\ell} w^{\ell}_{\omega,\omega'}\,. \tag{2.24}$$

The total transition rates $w_{\omega,\omega'}$ will in general not satisfy detailed balance. Nonetheless, each of these reservoirs alone would impose its own equilibrium upon the system, so we need the detailed balance relation as given in eq. (2.23) for each reservoir individually,

$$\frac{w^{\ell}_{\omega,\omega'}}{w^{\ell}_{\omega',\omega}} = \exp\left[-\frac{e_\omega + p^\ell\,v_\omega - T^\ell\,s_\omega - e_{\omega'} - p^\ell\,v_{\omega'} + T^\ell\,s_{\omega'}}{k_{\mathrm{B}}T^\ell}\right] = \exp\left[-\frac{g^{\ell}_{\omega} - g^{\ell}_{\omega'}}{k_{\mathrm{B}}T^\ell}\right], \tag{2.25}$$

and we call it *local detailed balance*. It reduces to the ordinary detailed balance in the case of a single reservoir. For multiple reservoirs, this provides a consistent nonequilibrium thermodynamic description of the Markovian dynamics known as *stochastic thermodynamics* [6, 7]. The expressions in equations (2.20)–(2.22) provide the correct *nonequilibrium* averages when evaluated for general distributions p_ω. This framework is finally capable of addressing both relaxation to equilibrium as well as nonequilibrium steady states.

I now give the entropy balance, cf. section 1.1.3, within the framework of stochastic thermodynamics.

Using the master equation, the time evolution of the nonequilibrium entropy is

$$\begin{aligned}
\tfrac{\mathrm{d}}{\mathrm{d}t}S &= \sum_{\omega}\left(\tfrac{\mathrm{d}}{\mathrm{d}t}p_\omega(t)\right)\left(s_\omega - k_\mathrm{B}\ln p_\omega(t)\right) - \sum_{\omega} p_\omega \frac{\frac{\mathrm{d}}{\mathrm{d}t}p_\omega}{p_\omega} \\
&= \sum_{\omega}\left(\sum_{\omega'} w_{\omega,\omega'}p_{\omega'}\right)\left(s_\omega - k_\mathrm{B}\ln p_\omega\right) - \underbrace{\sum_{\omega}\tfrac{\mathrm{d}}{\mathrm{d}t}p_\omega}_{=0} \\
&= \sum_{\omega}\left(\sum_{\omega'\neq\omega} w_{\omega,\omega'}p_{\omega'} - w_{\omega',\omega}p_\omega\right)\left(s_\omega - k_\mathrm{B}\ln p_\omega\right) \\
&= \sum_{\omega}\sum_{\omega'} w_{\omega',\omega}\,p_\omega\left(s_{\omega'} - s_\omega + k_\mathrm{B}\ln\frac{p_\omega}{p_{\omega'}}\right).
\end{aligned}$$

This expression is the sum of two terms:

$$\tfrac{\mathrm{d}}{\mathrm{d}t}\langle s\rangle = \langle\Phi\rangle + \langle\Sigma\rangle\,. \tag{2.26}$$

The first quantifies the rate of *entropy flow* from the reservoir:

$$\langle\Phi\rangle = \sum_{\ell}\sum_{\omega}\sum_{\omega'} w^{\ell}_{\omega',\omega}\,p_\omega\left(s_{\omega'} - s_\omega - k_\mathrm{B}\ln\frac{w^{\ell}_{\omega',\omega}}{w^{\ell}_{\omega',\omega}}\right) \tag{2.27}$$

$$= \sum_{\ell}\frac{1}{T^\ell}\sum_{\omega}\sum_{\omega'} w^{\ell}_{\omega',\omega}\,p_\omega\left[e_{\omega'} - e_\omega + p^\ell\left(v_{\omega'} - v_\omega\right)\right] \tag{2.28}$$

$$= \sum_{\ell}\frac{\dot{Q}^\ell}{T^\ell}\,. \tag{2.29}$$

The second accounts for the rate of *irreversible entropy-production*:

$$\langle\Sigma\rangle = k_\mathrm{B}\sum_{\ell}\sum_{\omega}\sum_{\omega'} w^{\ell}_{\omega',\omega}\,p_\omega\ln\frac{w^{\ell}_{\omega',\omega}\,p_\omega}{w^{\ell}_{\omega,\omega'}\,p_{\omega'}} \tag{2.30}$$

$$= \frac{k_\mathrm{B}}{2}\sum_{\ell}\sum_{\omega}\sum_{\omega'}\left(w^{\ell}_{\omega',\omega}\,p_\omega - w^{\ell}_{\omega,\omega'}\,p_{\omega'}\right)\ln\frac{w^{\ell}_{\omega',\omega}\,p_\omega}{w^{\ell}_{\omega,\omega'}\,p_{\omega'}} \geq 0\,. \tag{2.31}$$

For a steady state $\boldsymbol{p}^*$, the entropy production equals the entropy flow into the reservoir, $\langle\Sigma\rangle = -\langle\Phi\rangle$. For a detailed balanced steady state $\boldsymbol{\pi}$, both the entropy production and the entropy flow are zero.

Let us now re-consider the case of a single reservoir with temperature T and pressure p. The detailed balance requirement connects thermodynamic quantities with the transition rates, equation (2.23). This implies that the time derivative of the nonequilibrium free enthalpy is expressed as

$$\tfrac{\mathrm{d}}{\mathrm{d}t}G = -T\langle\Sigma\rangle \leq 0\,. \tag{2.32}$$

Consequently, the positivity of the entropy-production rate ensures the minimization of free enthalpy. This shows the consistency with nonequilibrium thermodynamics as presented in section 1.2. The major difference is that now we have a *dynamics* to refer to — and additionally, this dynamics is *stochastic*. In contrast, equilibrium statistical mechanics imposes the extremum principle without any reference to dynamics.

2.3.3. Large Deviations

We have seen that the rate of entropy production and the rate of entropy flow are anti-symmetric transition observables — they cannot be expressed with a state function. The ensemble averages were given in the previous section. The fluctuations of these quantities need to be expressed on the level of stochastic trajectories [8, 9].

Let γ be a *realization* or *stochastic trajectory* of the Markov process that starts at time $t = 0$ and ends at time $t = \tau$. This realization covers n jumps during that time and visits the states $\gamma_0 = \omega_0, \ldots, \gamma_\tau = \omega_n$. A generic time-averaged observable along this trajectory has to account for the possibility of truly path-dependent contributions (denoted with đ in chapter 1) and for state functions, respectively. Such a time average is written as

$$\mathcal{X}[\gamma_\tau] = \frac{1}{\tau}\sum_{j=0}^{n-1} X^{\text{jump}}_{\omega_{j+1},\omega_j} + \frac{1}{\tau}\int_0^\tau X^{\text{state}}(\gamma_t)\mathrm{d}t\,. \tag{2.33}$$

This expression is a stochastic variable because it depends on the realization of the Markov process. For ergodic Markov processes, this time average will in fact converge (almost surely) to the ensemble average $\langle\mathcal{X}\rangle$ in the limit $\tau \to \infty$.

More specifically, the large-τ scaling of the probability is provided by the *large-deviation rate function* [10, 11]

$$f_\mathcal{X}(x) = -\lim_{\tau\to\infty}\frac{1}{\tau}\ln\mathbb{P}\left(\mathcal{X}[\gamma_\tau] = x\right)\,. \tag{2.34}$$

The minimum of this function is the (almost sure) large time average of the observable: $f_\mathcal{X}(x = \langle\mathcal{X}\rangle) = 0$. The Legendre transform of this rate function is the *scaled cumulant-generating function*

$$\lambda_\mathcal{X}(q) = \lim_{\tau\to\infty}\frac{1}{\tau}\ln\left\langle\exp\left(q\,\tau\,\mathcal{X}[\gamma_\tau]\right)\right\rangle = x\cdot q - f(x)\,. \tag{2.35}$$

Here, the angular brackets denote the average over many realizations of the stochastic process. Again, ergodicity makes sure that this expression does not depend on the choice of initial conditions for the different realizations. From its definition it is clear that the scaled cumulant-generating function is always convex and satisfies $\lambda_\mathcal{X}(0) = 0$. Moreover, the derivatives of the scaled cumulant-generating function, when evaluated at zero, are the *scaled cumulants* of the time average $\mathcal{X}$. The first two scaled cumulants are the (unscaled) mean and the scaled variance:

$$\lambda'_\mathcal{X}(0) = \langle\mathcal{X}\rangle\,, \qquad\qquad \lambda''_\mathcal{X}(0) = \lim_{\tau\to\infty}\tau\left(\langle\mathcal{X}^2[\gamma_\tau]\rangle - \langle\mathcal{X}[\gamma_\tau]\rangle^2\right)\,. \tag{2.36}$$

The scaling in τ makes sure that the limits do converge to finite values.

The rate function is very often hard to compute, while the scaled cumulant-generating function (SCGF), and thus the cumulants, are more easily accessible. When the transition matrix (or generator) is biased exponentially by $q\mathcal{X}$, the SCGF $\lambda_\mathcal{X}(q)$ is in fact its dominant eigenvalue. In chapter 5 I exploit this connection to calculate the scaled cumulants of physical observables in an analytically exact way.

The time-averaged entropy production along a single trajectory is given by

$$\Sigma[\gamma_\tau] = \frac{k_\mathrm{B}}{\tau}\sum_{j=0}^{n-1}\ln\frac{w^\ell_{\omega_{j+1},\omega_j}p_{\omega_j}}{w^\ell_{\omega_j,\omega_{j+1}}p_{\omega_{j+1}}}\,. \tag{2.37}$$

It satisfies a *detailed fluctuation relation* [12, 13]

$$\frac{\mathbb{P}\left(\Sigma\left[\gamma_\tau\right] = k_\mathrm{B}\sigma\right)}{\mathbb{P}\left(\Sigma\left[\gamma_\tau\right] = -k_\mathrm{B}\sigma\right)} = \mathrm{e}^{\tau\sigma} \tag{2.38}$$

which in turn implies an *integral fluctuation relation*

$$\left\langle \exp\left(-\frac{\tau}{k_\mathrm{B}}\Sigma\right)\right\rangle = 1\,. \tag{2.39}$$

From Jensen's inequality we recover positive average entropy production: $\langle\Sigma\rangle \geq 0$.

This connection ensures that the fluctuation relations are the extension of the second law of thermodynamics to a fluctuating regime. They moreover explicitly show that we can always find trajectories that have a *negative* entropy production and apparently "violate" the second law. However, among all trajectories, these are exponentially rare to be realized and the second law has to be interpreted as a statistical property of physical systems.

The fluctuation relations in fact generalize another result from nonequilibrium statistical mechanics: the fluctuation–dissipation relations [12]. They relate the dissipative *response* of thermodynamic currents (at equilibrium) to the *fluctuations* of these currents (at equilibrium). More specifically, when the total entropy production of a system, $\text{đ}\Sigma = \sum_\alpha J_\alpha\, F_\alpha\, \mathrm{d}t$, is expressed as a bilinear form of currents J_α and forces F_α, then at thermodynamic equilibrium (where currents and forces both vanish) we have

$$k_\mathrm{B}\frac{\mathrm{d}\langle J_\alpha\rangle}{\mathrm{d}F_\beta} = \frac{1}{2}\lim_{\tau\to\infty}\tau\langle J_\alpha J_\beta\rangle_\tau\,. \tag{2.40}$$

Since the average currents vansih at equilibrium, the limit on the right hand side is the scaled co-variance of the two current quantities as introduced in eq. (2.36).

The most iconic instance of a fluctuation–dissipation relation is the Einstein–Smoluchowski relation for Brownian motion. In this case the dissipation is $\text{đ}\Sigma = v\cdot\frac{\tilde{F}}{T}\,\mathrm{d}t$. Here, the current quantity of interest is the drift velocity v (or displacement per unit time) and the corresponding thermodynamic force is just the mechanical force $\tilde{F}$ on the Brownian particle, scaled by temperature T. The velocity, in turn, is a linear function of the force: $v = \tilde{\mu}\tilde{F}$, where $\tilde{\mu}$ is the *mobility* of the Brownian particle. Therefore, the response of the drift velocity to the thermodynamic force is $T\frac{\mathrm{d}v}{\mathrm{d}\tilde{F}} = T\tilde{\mu}$. The second moment of the displacement per unit time *decreases* in time like $2D/\tau$ with the diffusion constant D. Thus, the scaled variance is just $2D$ and the Einstein–Smoluchowski relation [14, 15] for Brownian motion reads

$$k_\mathrm{B}T\tilde{\mu} = D\,. \tag{2.41}$$

The central message of this chapter is that stochastic thermodynamics, as formulated here, is capable of describing the thermodynamics of mesoscopic physical systems which follow stochastic dynamics. It encompasses thermodynamic equilibrium, but can also treat nonequilibrium situations — transient or at a steady state. In this stochastic setting, the second law as introduced as an *inequality* in chapter 1 needs to be understood statistically. Moreover, it can be re-phrased as *equalities* for the statistical properties of stochastic trajectories known as the the fluctutation relations, eqs. (2.38) and (2.39). These relation in fact also generalize the fluctuation–dissipation relations. I will come back to the fluctuation–dissipation relations in chapters 5 and 6 and investigate to what extent these relations are still true *out of thermodynamic equilibrium.*

References

[1] R. Abraham and J. E. Marsden. *Foundations of Mechanics.* 2nd ed. Providence, Rhode Island: AMS Chelsea Publishing, 2008.

[2] H. B. Callen. *Thermodynamics and an Introduction to Thermostatistics.* 2nd ed. New York: Wiley, 1985.

[3] C. E. Shannon. "A mathematical theory of communication". In: *The Bell System Technical Journal* 27.3 (1948), pp. 379–423.

[4] E. T. Jaynes. "Information Theory and Statistical Mechanics". In: *Physical Review* 106.4 (1957), pp. 620–630.

[5] A. Kolmogoroff. "Zur Theorie der Markoffschen Ketten". In: *Mathematische Annalen* 112.1 (1936), pp. 155–160.

[6] M. Esposito. "Stochastic thermodynamics under coarse graining". In: *Physical Review E* 85, 041125 (2012).

[7] U. Seifert. "Stochastic thermodynamics, fluctuation theorems and molecular machines". In: *Reports on Progress in Physics* 75, 126001 (2012).

[8] U. Seifert. "Entropy Production along a Stochastic Trajectory and an Integral Fluctuation Theorem". In: *Physical Review Letters* 95, 040602 (2005).

[9] C. Van den Broeck and M. Esposito. "Ensemble and trajectory thermodynamics: A brief introduction". In: *Physica A: Statistical Mechanics and its Applications* 418 (2015). Proceedings of the 13th International Summer School on Fundamental Problems in Statistical Physics, pp. 6–16.

[10] H. Touchette. "The large deviation approach to statistical mechanics". In: *Physics Reports* 478.1–3 (2009), pp. 1–69.

[11] R. Chetrite and H. Touchette. "Nonequilibrium Markov Processes Conditioned on Large Deviations". In: *Annales Henri Poincaré* 16.9 (2014), pp. 2005–2057.

[12] J. L. Lebowitz and H. Spohn. "A Gallavotti–Cohen-Type Symmetry in the Large Deviation Functional for Stochastic Dynamics". In: *Journal of Statistical Physics* 95.1–2 (1999), pp. 333–365.

[13] D. J. Searles and D. J. Evans. "Fluctuation theorem for stochastic systems". In: *Physical Review E* 60.1 (1999), pp. 159–164.

[14] A. Einstein. "Über die von der molekularkinetischen Theorie der Wärme geforderte Bewegung von in ruhenden Flüssigkeiten suspendierten Teilchen". In: *Annalen der Physik* 322.8 (1905), pp. 549–560.

[15] M. von Smoluchowski. "Zur kinetischen Theorie der Brownschen Molekularbewegung und der Suspensionen". In: *Annalen der Physik* 326.14 (1906), pp. 756–780.

Part II.

Introduction to Chemical Reaction Networks

3. Elementary Chemical Reactions

A *chemical reaction* is a transformation of some molecules, called *reactant molecules* to some other *product molecules* by rearrangements of atomic nuclei and electronic bonds. A single chemical reaction in itself is already a complicated process, when accounting for the exact quantum mechanical dynamics of molecules: electrons delocalize and tunnel between the attractive potentials of different nuclei or molecules. Furthermore, the exact interaction potentials for all different molecules are not known — although there are several numerical approaches to quantify these processes to some approximation.

For the purpose of this thesis, it is enough to have an understanding of chemical reactions on a mesoscopic level. The net balance for a chemical reaction is written as

$$\sum_{i=1}^{s} \nu_i \, Z_i \rightleftharpoons \sum_{i=1}^{s} \bar{\nu}_j \, Z_j \, . \tag{3.1}$$

Here, ν_i is the *stoichiometric coefficient* of the species Z_i as a reactant for the reaction and $\bar{\nu}_i$ is the respective stoichiometric coefficient as a product. I will use the symbol $N_i = \bar{\nu}_i - \nu_i$ to express the net stoichiometric change of this reaction. Note that I assume all reactions to be reversible. When a chemical reaction (from left to right in equation (3.1)) is possible, so is its reverse reaction (from right to left). The main reason for this assumption is *microscopic reversibility*.

The main assumption behind a thermodynamic treatment of chemical reactions on a mesoscopic level is that the chemically reactive mixture is in a dilute solution. The solvent mediates the transport of heat and the exchange of volume. It furthermore screens the individual reactive molecules from each other, ensuring that the chemical composition with arbitrary particle numbers is a locally stable configuration of the entire system. I will denote the particle numbers of the species Z_i with exactly the same symbol, meaning the state of the system is $\boldsymbol{Z} = (Z_1, \ldots, Z_s) \in \mathbb{N}_0^s$. With the solvent as a mediator it is furthermore reasonable to impose the external temperature T and the external pressure p and to consider the entire reactive solution to be thermally and mechanically equilibrated. Additionally, I will assume a well-stirred system without any spatial inhomogeneities in particle abundances.

The chemical reaction with net stoichiometric difference $\boldsymbol{N} = (N_1, \ldots, N_s)$ therefore is a transition from the locally equilibrated state $\boldsymbol{Z}$ to the locally equilibrated state $\boldsymbol{Z} + \boldsymbol{N}$. I restrict the presentation in this chapter to *elementary* reactions which overcome a single potential barrier in their interaction landscape during this transition. The thermodynamic treatment of more complicated, catalytic reactions will be addressed in chapter 8. Assuming an elementary reaction, its dynamics is a stochastic jump process on a one-dimensional lattice that is spanned by $\boldsymbol{N}$. This is very similar to a birth–death process and can be visualized as in figure 3.1.

In this chapter I deal with the thermodynamics and dynamics of a single elementary chemical reaction in a closed volume, namely from which no particles can be exchanged. In addition to the description as a stochastic process I address the dynamics as a differential equation in the macroscopic limit. The case of several elementary chemical reactions that can exchange matter with their environment will be addressed in the following chapter 4.

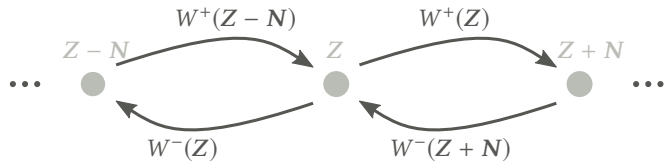

Figure 3.1.: Stochastic process for a single chemical reaction. It resembles a kind of birth–death process with specific changes in particle numbers per reaction event instead of just ±1. Additionally, the transition rates depend on the state. Moreover, the chemical reaction only interconverts different chemical species. Therefore, the total mass in the system is conserved and the reachable state space is finite: on right (left) end of the one-dimensional lattice some particle number Z_i is smaller than the respective stoichiometric coefficient ν_i as a reactant ($\bar{\nu}_i$ as a product) which makes another forward (backward) reaction impossible. Thus the particle numbers for each reachable state are always non-negative. The explicit transition rates given in section 3.2 have this property by construction.

3.1. Energetics of Elementary Reactions

We saw the macroscopic description of ideal dilute solutions already in section 1.4.2. Here, I provide a complementary view based on equilibrium statistical mechanics which allows us to treat *discrete* particle numbers.

The thermodynamic potential for the isothermal–isobaric ensemble is the free enthalpy G and in section 2.2.3 I showed that it can be expressed by the partition function

$$G(T, p, \boldsymbol{Z}, n_{\text{solv}}) = -k_{\text{B}} T \ln \mathcal{Z}(T, p, \boldsymbol{Z}, n_{\text{solv}}) \,. \tag{3.2}$$

Note that in general, the free enthalpy depends on *all* particle numbers for solutes $\boldsymbol{Z}$ and the mole number n_{solv} of the solvent.

The diluteness assumption leads to independence of the different solutes and we can write the partition function of the entire system as a *product* over the different solutes, treating the solvent implicitly:

$$\mathcal{Z}(T, p, \boldsymbol{Z}, n_{\text{solv}}) = \prod_{i=1}^{s} \frac{[\mathcal{Z}_i(T, p, n_{\text{solv}})]^{Z_i}}{Z_i!} \,. \tag{3.3}$$

The factorial term accounts for possible overcounting of indistinguishable states. We now introduce the free enthalpy of each solute species $g_i = -k_{\text{B}} T \ln \mathcal{Z}_i$ to express the free enthalpy of the entire system as

$$G(T, p, \boldsymbol{Z}, n_{\text{solv}}) = -k_{\text{B}} T \sum_{i=1}^{s} Z_i \ln \mathcal{Z}_i(T, p, n_{\text{solv}}) + k_{\text{B}} T \sum_{i=1}^{s} \ln Z_i! \tag{3.4}$$

$$= \sum_{i=1}^{s} (Z_i \, g_i + k_{\text{B}} T \ln Z_i!) \,. \tag{3.5}$$

Here and in the following, I suppress the dependence on the temperature, the pressure, and the solvent.

As a consequence, the free-enthalpy difference of the chemical reaction in equation (3.1) is given by

$$\Delta_\mathrm{r} G = G(\boldsymbol{Z} + \boldsymbol{N}) - G(\boldsymbol{Z}) = \sum_{i=1}^{s} \left[N_i \, g_i + k_\mathrm{B} T \ln(Z_i + N_i)! - k_\mathrm{B} T \ln Z_i! \right] . \tag{3.6}$$

In the following, I switch back to quantifying entropy with the ideal gas constant as is customary in (bio)chemistry.

3.2. Rates of Elementary Reactions

For a complete dynamical description as a stochastic process, we need the rate at which reaction events occur.

In order for a chemical reaction to proceed, the reactant molecules need to meet in the reactive solution and form a *complex*. This complex is a metastable configuration that spontaneously dissociates again. We assume this formation and dissociation of complexes to be fast enough and energetically neutral. The probability for all the reactant molecules to meet in the reactive volume is proportional to the multinomial coefficient that counts the possibilities to choose the necessary ν_i molecules out of the total number Z_i for species i:

$$\text{number of complexes} \propto \prod_i \binom{Z_i}{\nu_i} \propto \prod_i \frac{Z_i!}{(Z_i - \nu_i)!} = \prod_i Z_i \, (Z_i - 1) \dots (Z_i - \nu_i + 1) \, . \tag{3.7}$$

Once the complex of reactants is formed, the rate for a chemical reaction only depends on the type of the reaction and thus is a constant k.

Overall, the transition rates between the configurations $\boldsymbol{Z} - \boldsymbol{N}$, $\boldsymbol{Z}$, and $\boldsymbol{Z} + \boldsymbol{N}$ (as visualized in figure 3.1) are

$$\begin{aligned} W^+(\boldsymbol{Z} - \boldsymbol{N}) &= k^+ \prod_{i=1}^{s} \frac{(Z_i - N_i)!}{(Z_i - \bar{\nu}_i)!} , & W^-(\boldsymbol{Z}) &= k^- \prod_{i=1}^{s} \frac{Z_i!}{(Z_i - \bar{\nu}_i)!} , \\ W^+(\boldsymbol{Z}) &= k^+ \prod_{i=1}^{s} \frac{Z_i!}{(Z_i - \nu_i)!} , & W^-(\boldsymbol{Z} + \boldsymbol{N}) &= k^- \prod_{i=1}^{s} \frac{(Z_i + N_i)!}{(Z_i - \nu_i)!} , \end{aligned} \tag{3.8}$$

with some reaction rate constants k^+ and k^- for the forward and backward reaction. These expressions for the transition rates are known as *mass–action rates* for elementary reactions. Note that the factorial dependence on the state ensures nonnegative particle numbers.

3.3. Transition State Theory: The Eyring–Kramers Equation

The transition rates can be connected to the energetics of the elementary reactions. This is done with transition state theory.

Once the reactants have met, the reactant complex evolves in a potential landscape that is in principle very complicated and has a lot of local minima. The exact details of this potential landscape are usually not known and accessible only to computational methods.

Each of the configurations representing the reactant complex and the product complex are considered local minimum of this potential landscape. An *elementary reaction* is a reaction that proceeds

via a single step — overcoming a single saddle point that separates the basins of attraction of the two local minima.

When the thermal noise is not too strong, the rate of this transition can be quantified by the Eyring–Kramers [1–3] equation:

$$k^+ \propto T \exp\left[-\frac{\Delta G^\ddagger}{RT}\right] . \tag{3.9}$$

The barrier is characterized by the *free enthalpy of activation* $\Delta G^\ddagger$. This equation connects the forward transition rate to the energetic landscape. It is derived from a diffusive approximation of the dynamics within that energy landscape. From the microscopic perspective, there is no reason for the reverse process to be forbidden. Consequently, the reverse reaction has a transition rate that has a similar form, however the free enthalpy of activation is different.

Hence, the ratio of forward and backward rate constants is related to the difference of activation energies — which is the *free enthalpy difference* of the transformation of molecules:

$$RT \ln \frac{k^+}{k^-} = -\sum_i N_i \, g_i = -\Delta G^\circ . \tag{3.10}$$

Note that this ratio does not account for the entire free enthalpy difference of the reaction, as it was derived in eq. (3.6). It only accounts for the free enthalpy change due to the transformation of molecules (the analog of the standard state contribution) — it does not account for the additional entropic contribution arising from the factorials of the initial and final states.

With this connection between the reaction rate constants and the free enthalpy of the involved molecules, we see that the total free enthalpy of reaction is connected to the total transition rates and we therefore recover the condition of *detailed balance*:

$$RT \ln \frac{W^+(\boldsymbol{Z})}{W^-(\boldsymbol{Z}+\boldsymbol{N})} = -\sum_i \left[N_i \, g_i + RT \ln (Z_i + N_i)! - RT \ln Z_i!\right] \tag{3.11}$$

$$= G(\boldsymbol{Z}) - G(\boldsymbol{Z}+\boldsymbol{N}) = -\Delta_\mathrm{r} G . \tag{3.12}$$

This ensures that the steady-state distribution of the stochastic process is given by the equilibrium distribution

$$P(\boldsymbol{Z}) = \frac{1}{\mathcal{N}} \exp\left[-\frac{G(\boldsymbol{Z})}{RT}\right] , \qquad \text{where} \qquad \mathcal{N} = \sum_{\boldsymbol{Z}} \exp\left[-\frac{G(\boldsymbol{Z})}{RT}\right] . \tag{3.13}$$

3.4. The Macroscopic Limit and the Law of Mass–Action

In the macroscopic limit, the factorials involving the particle numbers can be approximated with Stirling's formula

$$\ln Z! \approx Z \ln Z - Z .$$

Additionally, the stochastic dynamics described above behaves almost surely deterministically [4]. As a consequence, the state of the system is given by a single value for the *molar concentrations* $\boldsymbol{z} = \boldsymbol{Z}/V$ measured in $\mathrm{M} = \mathrm{mol\,dm^{-3}}$.

The transition rates $W^{\pm}(\boldsymbol{Z})$ in the macroscopic limit are well approximated by the reaction fluxes [4]

$$\phi^{+}(\boldsymbol{z}) = k^{+} \prod_i (z_i)^{\nu_i} \,, \qquad \phi^{-}(\boldsymbol{z}) = k^{-} \prod_i (z_i)^{\bar{\nu}_i} \,. \tag{3.14}$$

Their difference is the macroscopic reaction current

$$J(\boldsymbol{z}) = \phi^{+}(\boldsymbol{z}) - \phi^{-}(\boldsymbol{z}) = k^{+} \prod_i (z_i)^{\nu_i} - k^{-} \prod_i (z_i)^{\bar{\nu}_i} \,. \tag{3.15}$$

The reaction dynamics in the macroscopic limit is given by deterministic differential equations [4] — the rate equations of chemical kinetics

$$\tfrac{\mathrm{d}}{\mathrm{d}t}\boldsymbol{z} = \boldsymbol{N} J(\boldsymbol{z}) \,. \tag{3.16}$$

Note that I absorbed factors of volume into the reaction rate constants.

Additionally, in this limit we recover the expression for the chemical potential of ideal dilute solutions we already saw in equation (1.20) and the total free enthalpy at given concentration $\boldsymbol{z}$:

$$G(\boldsymbol{z}) = V \sum_i z_i \, \mu_i(\boldsymbol{z}) = V \sum_i z_i (\mu_i^{\circ} + RT \ln z_i) \,. \tag{3.17}$$

The free enthalpy of reaction in the macroscopic limit thus takes the form

$$\Delta_{\mathrm{r}} G = \sum_i N_i \left[\mu_i^{\circ} + RT \ln z_i\right] = \Delta_{\mathrm{r}} G^{\circ} + RT \sum_i N_i \ln z_i \,. \tag{3.18}$$

Therefore, the mass–action kinetics ensures a direct connection between the reaction fluxes $\phi^{\pm}$ and the free enthalpy of reaction:

$$-\Delta_{\mathrm{r}} G = RT \ln \frac{\phi^{+}(\boldsymbol{z})}{\phi^{-}(\boldsymbol{z})} \,. \tag{3.19}$$

This is known as *flux–force relation*. It relies significantly on the fact that we deal with elementary reactions that follow mass–action kinetics. The chapter 8 is dedicated to this equation and investigates to which extent it is valid also for kinetics at a coarser level.

The concentrations corresponding to macroscopic thermodynamic equilibrium make both the reaction currents and the free enthalpy of reaction vanish and thus satisfy

$$RT \sum_i N_i \ln z_i^{\mathrm{eq}} = -\Delta_{\mathrm{r}} G^{\circ} = RT \ln \frac{k^{+}}{k^{-}} \,. \tag{3.20}$$

This is commonly referred to as the *law of mass–action* and the quantity

$$K^{\mathrm{eq}} = \prod_i \left(z_i^{\mathrm{eq}}\right)^{N_i} = \exp\left[-\frac{\Delta_{\mathrm{r}} G^{\circ}}{RT}\right] \tag{3.21}$$

is the *equilibrium constant* of the reaction. The law of mass–action is the macroscopic embodiment of the thermodynamic detailed balance condition, cf. equation (2.23), for a single chemical reaction.

References

[1] H. Eyring. “The Activated Complex in Chemical Reactions”. In: *Journal of Chemical Physics* 3.2 (1935), pp. 107–115.

[2] H. Kramers. “Brownian motion in a field of force and the diffusion model of chemical reactions”. In: *Physica* 7.4 (1940), pp. 284–304.

[3] F. Bouchet and J. Reygner. “Generalisation of the Eyring–Kramers Transition Rate Formula to Irreversible Diffusion Processes”. In: *Annales Henri Poincaré* (2016), pp. 1–34.

[4] T. G. Kurtz. “The Relationship between Stochastic and Deterministic Models for Chemical Reactions”. In: *Journal of Chemical Physics* 57.7 (1972), pp. 2976–2978.

4. Open Chemical Reaction Networks

In the previous chapter I dealt with a single chemical reaction in a closed system. Now I address the interactions between many such reactions, and I discuss how a reactive system can reach a nonequilibrium steady state when it exchanges some of its species with the environment.

The generic description of a chemical reaction network is a list of reactions $\rho = 1, \ldots, r$,

$$\sum_{i=1}^{s} \nu_{i,\rho}\, Z_i \underset{-\rho}{\overset{\rho}{\rightleftharpoons}} \sum_{i=1}^{s} \bar{\nu}_{i,\rho}\, Z_i \,. \tag{4.1}$$

Here, each reaction ρ couples to the species Z_i with stoichiometric coefficient $\nu_{i,\rho}$ as a reactant and with stoichiometric coefficient $\bar{\nu}_{i,\rho}$ as a product.

We now have to divide the set of chemical species $Z = X \cup Y$ into the *internal species* X and the *chemostatted species* Y which are exchanged with the environment. This discrimination separates also the stoichiometric coefficients:

$$\sum_{i} \nu_{i,\rho}\, X_i + \sum_{j} \nu_{j,\rho}\, Y_j \underset{-\rho}{\overset{\rho}{\rightleftharpoons}} \sum_{i} \bar{\nu}_{i,\rho}\, X_i + \sum_{j} \bar{\nu}_{j,\rho}\, Y_j \,. \tag{4.2}$$

4.1. Network Stoichiometry

A list of reactions as given in equation (4.1) or (4.2) is not necessarily the most convenient way to deal with the network as a whole. In the previous chapter I already introduced the stoichiometric vector $\boldsymbol{N} = \bar{\boldsymbol{\nu}} - \boldsymbol{\nu}$ for a single reaction. Now we have many reactions ρ and collect their stoichiometric vectors $\boldsymbol{N}_\rho$ in the *stoichiometric matrix*:

$$\mathbb{S} = \left(\boldsymbol{N}_1, \ldots, \boldsymbol{N}_r\right) \,. \tag{4.3}$$

With the additional distinction of internal and chemostatted species we have to separate the stoichiometric matrix into two parts:

$$\mathbb{S} = \begin{pmatrix} \mathbb{S}^X \\ \mathbb{S}^Y \end{pmatrix} \,. \tag{4.4}$$

The entire stoichiometric matrix and its two constituent parts encode information about the entire network that is independent of dynamical or kinetic properties: conservation laws and stoichiometric cycles.

4.1.1. Conserved Quantities

The easiest way to conceptualize conservation laws is by addressing the atomic compositions of molecules.

We can count the number of oxygen atoms in the chemical species i and collect these numbers into a vector $\boldsymbol{\ell}_\mathrm{O} = (\ell_1, \ell_2, \ldots, \ell_s)$. Since each reaction in the network conserves oxygen, the number

of oxygen atoms before and after each reaction is the same. Consequently, the vector $\boldsymbol{\ell}_O$ satisfies $\boldsymbol{\ell}_O \cdot \mathbb{S} = 0$. In fact, chemical reactions conserve the atomic nuclei of all the chemical elements. However, since each chemical reaction typically induces only few local changes in larger molecules, the different nuclei are conserved not just individually. Phosphorous is an example in biochemistry that is typically occurring together with oxygen in the phosphate group. Thus, the conservation of phosphorous and oxygen will not necessarily be independent. The conserved groups of atoms are called *moieties*. In addition to atomic nuclei, the number of electrons is conserved — leading to conservation of charge. The entire network has to respect these conserved quantities or conservation laws.

When the atomic composition of all chemical species are known, it is possible to determine all conserved moieties [1]. In some cases the exact atomic composition of a chemical reaction network might not be known. Nonetheless, we can identify the conservation laws in a chemical reaction network by determining the *co-kernel* of the stoichiometric matrix, i.e. the set of all vectors $\boldsymbol{\ell}$ that satisfy

$$\boldsymbol{\ell} \cdot \mathbb{S} = 0\,. \tag{4.5}$$

Each such vector identifies a linear combination of chemical species that remains untouched by all reactions. The co-kernel is a proper vector space and as such we can choose a set of basis vectors which represent quantities that are conserved independently. All chemical species are composed of atomic nuclei, so we can always find a basis of vectors with *nonnegative* entries. These vectors represent a set of independently conserved moieties.

The fact that the network is open and can exchange all species Y with its environment breaks some of the conservation laws. All the vectors that satisfy

$$\boldsymbol{\ell} \cdot \mathbb{S} = 0 \qquad \text{while} \qquad \boldsymbol{\ell} \cdot \mathbb{S}^Y \neq 0 \tag{4.6}$$

are *broken conservation laws*. Only the vectors $\boldsymbol{\ell}$ that satisfy

$$\boldsymbol{\ell} \cdot \mathbb{S}^X = 0 \tag{4.7}$$

are truly conserved or *unbroken* also in the open network. From the perspective of exchange of matter it is therefore most convenient to construct a basis of the co-kernel of $\mathbb{S}$ that consists of the linearly independent conservation laws satisfying equation (4.7) as well as independent broken conservation laws satisfying equation (4.6). A downside is that this choice of basis, in the worst case, leaves us with conservation laws with negative entries for some species. These conservation laws cannot be interpreted as *moieties*.

4.1.2. Stoichiometric Cycles

We saw that some linear combinations of species are conserved quantities. Some linear combinations of reactions also have a special role. The vectors $\boldsymbol{c}$ that satisfy

$$\mathbb{S}\,\boldsymbol{c} = 0 \tag{4.8}$$

constitute the kernel of the stoichiometric matrix. These vectors form combinations of reactions that, when performed one after the other (with the respective multiplicities), return the system to the state it started from. Consequently, these combinations of reactions are natural cyclic transformations of the system. We therefore call them *stoichiometric cycles*. For closed networks, however, these

stoichiometric cycles are purely *internal*: they do not exchange any particles with the environment. For an open system, we have to consider the vectors $\boldsymbol{c}$ that satisfy

$$\mathbb{S}^X \boldsymbol{c} = 0 \tag{4.9}$$

as the set of *all* stoichiometric cycles. They leave the internal species untouched but *may* exchange particles with the chemostats. All internal cycles satisfying equation (4.8) obviously also satisfy eq. (4.9). There are, however, additional cycles that emerge upon chemostatting, which we therefore call *emergent cycles*. They are characterized by the condition

$$\mathbb{S}^X \boldsymbol{c} = 0 \qquad \text{while} \qquad \mathbb{S}^Y \boldsymbol{c} \neq 0\,. \tag{4.10}$$

These represent all the cyclic transformations of the system that *do* exchange matter with the environment.

4.1.3. The Number of Chemostats

The number $|Y|$ of chemostatted species is closely connected to the number L^{b} of (linearly independent) broken conservation laws and the number C^{e} of (linearly independent) emergent cycles, as first shown by Polettini and Esposito [2].

The rank–nullity theorem states that the dimension of the kernel (the nullity) and the dimension of the image (the rank) of a matrix always add up to the dimension of the domain. This is true both for the matrix as well as its transpose, while their ranks are the same. For the full stoichiometric matrix $\mathbb{S}$ these relations read

$$\operatorname{rank}\mathbb{S} = s - L = r - C^{\mathrm{i}}\,. \tag{4.11}$$

Here, $L = \dim\operatorname{coker}\mathbb{S} = \#\{\text{conservation laws}\}$, $C^{\mathrm{i}} = \dim\ker\mathbb{S} = \#\{\text{internal cycles}\}$. Consequently, for the reduced stoichiometric matrix $\mathbb{S}^X$ we also have

$$\operatorname{rank}\mathbb{S}^X = |X| - L^{\mathrm{u}} = r - C\,, \tag{4.12}$$

where $L^{\mathrm{u}} = \dim\operatorname{coker}\mathbb{S}^X = \#\{\text{unbroken cons. laws}\}$, $C = \dim\ker\mathbb{S}^X = \#\{\text{all cycles}\}$. The difference of these equations yields

$$s - |X| - L + L^{\mathrm{u}} = C - C^{\mathrm{i}} \qquad \Leftrightarrow \qquad |Y| = C^{\mathrm{e}} + L^{\mathrm{b}}\,. \tag{4.13}$$

Note that obviously $|X| + |Y| = s$, $C^{\mathrm{e}} + C^{\mathrm{i}} = C$ and $L^{\mathrm{u}} + L^{\mathrm{b}} = L$.

In total we see that every chemostat that is being introduced into a chemical network either breaks a conservation law or gives rise to an emergent cycle. It is important to realize that not all conservation laws need to be broken before a new cycle can emerge.

4.2. Stochastic Reaction Dynamics

In chapter 3 I discussed a single chemical reaction in a closed container. Its natural mesoscopic dynamics is a birth–death process on a one-dimensional lattice spanned by its stoichiometric vector.

When several reactions are admissible, each reaction will occur independently —resulting in an interconnected network of states, which I call *chemical lattice*. Since the particle number cannot become negative, this lattice is a subset of $\mathbb{N}_0^s$. Possible conservation laws additionally restrict this lattice to be a true subset, which in the case of a closed system is always a finite network of states.

4.2.1. Closed Network

The probability $P(\boldsymbol{Z}, t)$ to observe a *closed* system in state $\boldsymbol{Z}$ at time t evolves according to the *chemical master equation*:

$$\tfrac{\mathrm{d}}{\mathrm{d}t} P(\boldsymbol{Z}, t) = \mathcal{L} P(\boldsymbol{Z}, t)\,, \tag{4.14}$$

with the generator

$$\mathcal{L}P(\boldsymbol{Z}) = \sum_{\rho=1}^{r} \Big[W_\rho^-\big(\boldsymbol{Z} + \boldsymbol{N}_\rho\big)\, P(\boldsymbol{Z} + \boldsymbol{N}_\rho) + W_\rho^+\big(\boldsymbol{Z} - \boldsymbol{N}_\rho\big)\, P(\boldsymbol{Z} - \boldsymbol{N}_\rho) - (W_\rho^+(\boldsymbol{Z}) + W_\rho^-(\boldsymbol{Z}))P(\boldsymbol{Z}) \Big]\,. \tag{4.15}$$

As detailed in section 3.2, its transition rates are

$$W_\rho^+(\boldsymbol{Z}) = k_\rho^+ \frac{\boldsymbol{Z}!}{(\boldsymbol{Z} - \boldsymbol{\nu}_\rho)!}\,, \qquad\qquad W_\rho^-(\boldsymbol{Z}) = k_\rho^- \frac{\boldsymbol{Z}!}{(\boldsymbol{Z} - \bar{\boldsymbol{\nu}}_\rho)!}\,, \tag{4.16}$$

where I employ the abbreviation $\boldsymbol{Z}! \equiv \prod_{i=1}^{s} Z_i!$ for a less cluttered notation.

Note that a reaction ρ can only occur (in forward direction) when the state $\boldsymbol{Z}$ contains at least the minimal number $\boldsymbol{\nu}_\rho$ of reactant molecules. This minimal requirement is different for each reaction. Hence, not all reactions are allowed at all states. This causes a slightly irregular network structure along the boundaries of the chemical lattice, where the particle numbers are small.

The closed system necessarily has to relax to thermodynamic equilibrium. Therefore it must satisfy the detailed balance condition, equation (2.23), or equivalently the cycle criterion of Колмогоров, equation (2.17). Note that the chemical lattice, in general, contains a lot of cycles. Nonetheless, it is easy to verify that the factorial contributions to the transition rates cancel when checking for the cycle criterion. Furthermore, every cycle in the chemical lattice is a combination of reactions that return the system to its initial state and thus it is associated to a vector in $\ker \mathbb{S}$. Note that in this association all cycles of the type $+\rho_1 + \rho_2 - \rho_1 - \rho_2$ correspond to the zero vector. In total, the condition on the reaction network for reaching equilibrium reduces to

$$\sum_\rho c_\rho \, \ln \frac{k_\rho^+}{k_\rho^-} \equiv \boldsymbol{c} \cdot \ln \frac{\boldsymbol{k}^+}{\boldsymbol{k}^-} = 0 \qquad\qquad \text{for all internal cycles } \boldsymbol{c} \in \ker \mathbb{S}\,, \tag{4.17}$$

which is a *small* set of conditions. It was first stated by Wegscheider [3] in the context of deterministic dynamics.

4.2.2. Open Network

When we have an *open* network, particle numbers can change due to reactions or due to exchange. I only consider situations where all connected particle reservoirs are ideal and provide a constant chemical potential μ_j for all chemostatted species Y_j. With this assumption, I especially exploit the equation of ideal dilute solutions, equation (1.20), which connects chemical potentials and concentrations y_j. Thus it is most appropriate to take the macroscopic limit for all the chemostat's particle numbers in the transition rates and consider their concentrations constant:

$$W_\rho^+(\boldsymbol{Z}) = k_\rho^+ \, \boldsymbol{y}^{\boldsymbol{\nu}_\rho} \, \frac{\boldsymbol{X}!}{(\boldsymbol{X} - \boldsymbol{\nu}_\rho)!}\,, \qquad\qquad W_\rho^-(\boldsymbol{X}) = k_\rho^- \, \boldsymbol{y}^{\bar{\boldsymbol{\nu}}_\rho} \, \frac{\boldsymbol{X}!}{(\boldsymbol{X} - \bar{\boldsymbol{\nu}}_\rho)!}\,. \tag{4.18}$$

Here, I use an implicit product over the chemostat's concentrations,

$$\boldsymbol{y}^{\boldsymbol{\nu}_\rho} = \prod_{y_j \in Y} y_j^{\nu_{j,\rho}} ,$$

and absorb several factors of volume into the reaction rate constants. Moreover, the state $\boldsymbol{X}$ only accounts for the particle numbers of the internal species X and thus is in a smaller space. This reduction of dimension from the closed to the open system causes a "collapse" of the chemical lattice, which creates new cycles. They correspond to the *emergent* cycles I introduced in section 4.1.2. This open network still satisfies Wegscheider's conditions on the kinetic rate constants for the *internal cycles*. However, it no longer satisfies detailed balance. The logarithmic ratio of transition rates

$$\ln \frac{W_\rho^+(\boldsymbol{X})}{W_\rho^-(\boldsymbol{X}+\boldsymbol{N}_\rho)} = \ln \frac{k_\rho^+}{k_\rho^-} + \ln \frac{\boldsymbol{X}!}{(\boldsymbol{X}+\boldsymbol{N}_\rho)!} - \boldsymbol{N}_\rho \cdot \ln \boldsymbol{y} \tag{4.19}$$

contains terms that depend on the chemostats and these do not add up to zero along emergent cycles $\boldsymbol{c}_\varepsilon$. Instead, from equation (3.10) we see that they add up to the actual *chemical potential differences* provided by the reservoirs:

$$\boldsymbol{c}_\varepsilon \cdot \ln \frac{\boldsymbol{k}^+}{\boldsymbol{k}^-} - \left(\mathbb{S}^Y \boldsymbol{c}_\varepsilon\right) \cdot \ln \boldsymbol{y} = -\frac{1}{RT} \boldsymbol{\mu}^Y \cdot \mathbb{S}^Y \boldsymbol{c}_\varepsilon \equiv -\frac{\Delta_\varepsilon G}{RT} . \tag{4.20}$$

These are the thermodynamic cycle forces that prevent the system from reaching equilibrium. Generally, they are nonzero and they impose a nonequilibrium steady-state on the system. The maximal number of independent forces is the number of emergent cycles, which in turn is tied to the number of chemostats and the broken conservation laws.

The instantaneous dissipation of an open chemical network in the state $P(\boldsymbol{X})$ can be quantified with the entropy-production rate

$$\begin{aligned}\langle \Sigma \rangle = \frac{R}{2} \sum_\rho \sum_{\boldsymbol{X}} \Bigg[& \Big(W_\rho^+(\boldsymbol{X}-\boldsymbol{N}_\rho)\, P(\boldsymbol{X}-\boldsymbol{N}_\rho) - W_\rho^-(\boldsymbol{X})\, P(\boldsymbol{X}) \Big) \ln \frac{W_\rho^+(\boldsymbol{X}-\boldsymbol{N}_\rho)\, P(\boldsymbol{X}-\boldsymbol{N}_\rho)}{W_\rho^-(\boldsymbol{X})\, P(\boldsymbol{X})} \\ & + \Big(W_\rho^+(\boldsymbol{X})\, P(\boldsymbol{X}) - W_\rho^-(\boldsymbol{X}+\boldsymbol{N}_\rho)\, P(\boldsymbol{X}+\boldsymbol{N}_\rho) \Big) \ln \frac{W_\rho^+(\boldsymbol{X})\, P(\boldsymbol{X})}{W_\rho^-(\boldsymbol{X}+\boldsymbol{N}_\rho)\, P(\boldsymbol{X}+\boldsymbol{N}_\rho)} \Bigg] . \end{aligned} \tag{4.21}$$

In fact, when evaluating this expression at the steady state it is not even necessary to account for the steady-state probability inside the logarithm. These contributions only account for the Gibbs–Shannon entropy, which is a state function and does not change in the steady state.

4.3. Deterministic Reaction Dynamics

As we have seen already in chapter 3, there is a natural way to express the reaction dynamics in the macroscopic limit [4] as deterministic differential equations. The state of a closed system is given by the molar concentrations of all chemical species $\boldsymbol{z} = \frac{\langle \boldsymbol{Z} \rangle}{V}$ and it evolves according to

$$\tfrac{\mathrm{d}}{\mathrm{d}t} \boldsymbol{z} = \sum_{\rho=1}^{r} \left(\nu_{i,\rho} - \bar{\nu}_{i,\rho}\right) \left(k_\rho^+ \prod_i z_i^{\nu_{i,\rho}} - k_\rho^- \prod_i z_i^{\bar{\nu}_{i,\rho}} \right) = \sum_{\rho=1}^{r} \boldsymbol{N}_\rho\, J_\rho(\boldsymbol{z}) = \mathbb{S}\, \boldsymbol{J}(\boldsymbol{z}) . \tag{4.22}$$

It is remarkable how similar this evolution equation is to Hamilton's equation of motion, equation (2.1). The stoichiometric matrix takes the role of the symplectic matrix, and a function of the state of the system is a conserved quantity — irrespective of a lot of the dynamical details. This conservation is built into the mere structure of the equations. The crucial difference is that chemical reaction networks admit many conserved quantities, which in addition all are *linear* functions of the state, in contrast to the nonlinear Hamiltonian function. The latter happens to also dictate the dynamic flow, while chemical reaction currents are not immediately related to conserved quantities.

For an open system we separate the concentrations $\boldsymbol{z} = (\boldsymbol{x}, \boldsymbol{y})$ into internal species X and chemostatted species Y. The state of the system is only given by $\boldsymbol{x}$ whose evolution is governed by

$$\tfrac{\mathrm{d}}{\mathrm{d}t}\boldsymbol{x} = \mathbb{S}^X \boldsymbol{J}(\boldsymbol{x}, \boldsymbol{y})\,. \tag{4.23}$$

The balance for the chemostatted species now reads

$$0 = \tfrac{\mathrm{d}}{\mathrm{d}t}\boldsymbol{y} = \mathbb{S}^Y \boldsymbol{J}(\boldsymbol{x}, \boldsymbol{y}) + \boldsymbol{I} \tag{4.24}$$

and accounts both for reaction currents $\boldsymbol{J}$ and for exchange currents $\boldsymbol{I}$ with the reservoirs. It is not a dynamical equation, since the concentrations of the chemostatted species are imposed by the reservoirs, which I assume constant in time. Moreover, I focus on nonequilibrium steady states for which $\boldsymbol{J} \in \ker \mathbb{S}^X$. The theory itself is more general and can in principle be applied with time-dependent changes of the chemostat's concentrations [5].

The steady-state dissipation rate of such a macroscopic reaction network follows from equation (1.23) and equation (4.24) as

$$đ\Sigma = -V \sum_{y_j \in Y} \mu_j I_j \,\mathrm{d}t = -V \boldsymbol{\mu}^Y \cdot \mathbb{S}^Y \boldsymbol{J}(\boldsymbol{x}, \boldsymbol{y})\,\mathrm{d}t = -V \sum_{\varepsilon} J_\varepsilon\, \Delta_\varepsilon G\,. \tag{4.25}$$

Note that the steady-state current in fact is a linear combination of cycle currents, out of which the internal cycle currents do not contribute to the dissipation. Hence, the dissipation is a bilinear form of cycle forces and cycle currents J_ε.

The relation between this deterministic expression and the stochastic average in equation (4.21) is not necessarily obvious. The steady-state of the nonlinear deterministic system is in general not unique, but can be any attractive fixed point of equation (4.23). In contrast, the stochastic entropy production at the ergodic distribution is unique. I will address the correspondence between these two in chapter 7. A special focus is the regime of small particle numbers where the approximation leading to the deterministic dynamics is no longer valid.

This point marks the end of the introduction to the nonequilibrium thermodynamics of open chemical reaction networks. The central results are the derivations of the entropy production rate in open chemical reaction networks for both the deterministic rate equations, eq. (4.25), and the stochastic master equation, eq. (4.21). The following chapters 5–8 are essentially my research articles and manuscripts. In the following section, I just provide a small yet biologically important example network. It serves as a practical guide for the reader who wants a more hands-on discussion of network stoichiometry, including conservation laws and cycles.

4.4. Example Network: Adenosine Phosphate Reactions

I now give an example reaction network that is particularly important for cellular energetics: the hydrolysis of adenosine phosphates. Apart from water (H_2O) and protons (H^+), it involves the

organic chemical species *adenosine triphosphate* (ATP), *adenosine diphosphate* (ADP), and *adenosine monophosphate* (AMP), as well as inorganic hydrogen phosphate[1] (P_i) and pyrophosphate[2] (PP_i):

$$\begin{aligned} \mathrm{ATP} + \mathrm{H_2O} &\rightleftharpoons \mathrm{ADP} + \mathrm{P}_i + \mathrm{H}^+ \\ \mathrm{ADP} + \mathrm{H_2O} &\rightleftharpoons \mathrm{AMP} + \mathrm{P}_i + \mathrm{H}^+ \\ \mathrm{ATP} + \mathrm{H_2O} &\rightleftharpoons \mathrm{AMP} + \mathrm{PP}_i + 2\,\mathrm{H}^+ \\ 2\,\mathrm{ADP} &\rightleftharpoons \mathrm{ATP} + \mathrm{AMP} \\ \mathrm{H_2O} + \mathrm{PP}_i &\rightleftharpoons 2\,\mathrm{P}_i \end{aligned} \tag{4.26}$$

The stoichiometric matrix for this reaction network is

$$\mathbb{S} = \begin{array}{c} \\ \mathrm{ATP} \\ \mathrm{ADP} \\ \mathrm{AMP} \\ \mathrm{P}_i \\ \mathrm{PP}_i \\ \mathrm{H_2O} \\ \mathrm{H}^+ \end{array} \begin{pmatrix} & & & & \\ -1 & 0 & -1 & 1 & 0 \\ 1 & -1 & 0 & -2 & 0 \\ 0 & 1 & 1 & 1 & 0 \\ 1 & 1 & 0 & 0 & 2 \\ 0 & 0 & 1 & 0 & -1 \\ -1 & -1 & -1 & 0 & -1 \\ 1 & 1 & 2 & 0 & 0 \end{pmatrix} \tag{4.27}$$

The right-nullspace of the stoichiometric matrix is spanned by two cycles:

$$\boldsymbol{c}_1 = \begin{pmatrix} 1 \\ -1 \\ 0 \\ 1 \\ 0 \end{pmatrix}, \qquad \boldsymbol{c}_2 = \begin{pmatrix} 1 \\ 1 \\ -1 \\ 0 \\ -1 \end{pmatrix}. \tag{4.28}$$

The first cycle represents the recombination of two ADP into ATP and AMP, followed by hydrolysis of ATP as well as phosphorylation of AMP back to two ADP. The second cycle represents two consecutive hydrolysis reactions of ATP to ADP and AMP, followed by condensation of two hydrogen phosphates into pyrophosphate and condensation of pyrophosphate with AMP back into ATP. Moreover, both cycles are balanced with respect to protons and water molecules.

The left-nullspace of the stoichiometric matrix is spanned by four conservation laws:

$$\boldsymbol{\ell}_{\mathrm{AMP}} = \begin{array}{c} \\ \mathrm{ATP} \\ \mathrm{ADP} \\ \mathrm{AMP} \\ \mathrm{P}_i \\ \mathrm{PP}_i \\ \mathrm{H_2O} \\ \mathrm{H}^+ \end{array} \begin{pmatrix} & \\ 1 & \\ 1 & \\ 1 & \\ 0 & \\ 0 & \\ 0 & \\ 0 & \end{pmatrix}, \quad \boldsymbol{\ell}_{\mathrm{P}_i} = \begin{array}{c} \\ \mathrm{ATP} \\ \mathrm{ADP} \\ \mathrm{AMP} \\ \mathrm{P}_i \\ \mathrm{PP}_i \\ \mathrm{H_2O} \\ \mathrm{H}^+ \end{array} \begin{pmatrix} & \\ 2 & \\ 1 & \\ 0 & \\ 1 & \\ 2 & \\ 0 & \\ 0 & \end{pmatrix}, \quad \boldsymbol{\ell}_{\mathrm{O}} = \begin{array}{c} \\ \mathrm{ATP} \\ \mathrm{ADP} \\ \mathrm{AMP} \\ \mathrm{P}_i \\ \mathrm{PP}_i \\ \mathrm{H_2O} \\ \mathrm{H}^+ \end{array} \begin{pmatrix} & \\ 0 & \\ 0 & \\ 0 & \\ 1 & \\ 1 & \\ 1 & \\ 0 & \end{pmatrix}, \quad \boldsymbol{\ell}_{\mathrm{H}} = \begin{array}{c} \\ \mathrm{ATP} \\ \mathrm{ADP} \\ \mathrm{AMP} \\ \mathrm{P}_i \\ \mathrm{PP}_i \\ \mathrm{H_2O} \\ \mathrm{H}^+ \end{array} \begin{pmatrix} & \\ 2 & \\ 1 & \\ 0 & \\ 0 & \\ 0 & \\ 0 & \\ 1 & \end{pmatrix}. \tag{4.29}$$

The first conservation law states that adenosine monophosphate is a conserved moiety. The second represents conservation of the phosphate group. The third is conservation of oxygen during hydrolysis, while the last is conservation of protons.

[1] Molecular formula: HPO_4
[2] Molecular formula: P_2O_7

In biochemistry, water and protons are always considered chemostats [6] — they are given by the solvent and the pH value. These two chemostats break the latter two conservation laws, which implies that the system will have a modified equilibrium steady state. I now additionally consider P_i, AMP, and ATP chemostatted, which breaks also the remaining two conservation laws. The only internal species are ADP and PP_i for which the reduced stoichiometric matrix is

$$\mathbb{S}^X = \begin{matrix} \text{ADP} \\ \text{PP}_i \end{matrix} \begin{pmatrix} 1 & -1 & 0 & -2 & 0 \\ 0 & 0 & 1 & 0 & -1 \end{pmatrix} \tag{4.30}$$

The fifth chemostat has no more conservation law to break, so it gives rise to the emergent cycle

$$\boldsymbol{c}_\text{e} = \begin{pmatrix} 1 \\ 1 \\ 0 \\ 0 \\ 0 \end{pmatrix} \tag{4.31}$$

which carries the cycle force

$$-\Delta_\text{e} G = RT \ln \frac{[\text{ATP}][\text{H}_2\text{O}]^2}{[\text{AMP}][\text{P}_i]^2[\text{H}^+]^2 K^\text{eq}} \,. \tag{4.32}$$

This emergent cycle represents double hydrolysis of ATP to AMP via ADP. Pyrophosphate does not appear in this cycle so it remains in chemical equilibrium with the phosphate chemostat.

This analysis of an example network shows the amount of information that is accessible by mere stoichiometry. At no point did we refer to the exact kinetics of the involved reactions, nor to the solution of the dynamical equations. Such kinetic or dynamical information is obviously necessary to make statements about the concentrations, the reaction (or cycle) currents, or the dissipation at the steady state.

References

[1] H. S. Haraldsdóttir and R. M. T. Fleming. "Identification of Conserved Moieties in Metabolic Networks by Graph Theoretical Analysis of Atom Transition Networks". In: *PLoS Computational Biology* 12.11, e1004999 (2016).

[2] M. Polettini and M. Esposito. "Irreversible thermodynamics of open chemical networks. I. Emergent cycles and broken conservation laws". In: *Journal of Chemical Physics* 141, 024117 (2014).

[3] R. Wegscheider. "Über simultane Gleichgewichte und die Beziehungen zwischen Thermodynamik und Reactionskinetik homogener Systeme". In: *Monatshefte für Chemie und verwandte Teile anderer Wissenschaften* 32.8 (1911), pp. 849–906.

[4] T. G. Kurtz. "The Relationship between Stochastic and Deterministic Models for Chemical Reactions". In: *Journal of Chemical Physics* 57.7 (1972), pp. 2976–2978.

[5] R. Rao and M. Esposito. "Nonequilibrium Thermodynamics of Chemical Reaction Networks: Wisdom from Stochastic Thermodynamics". In: *Physical Review X* 6, 041064 (2016).

[6] R. A. Alberty. *Thermodynamics of Biochemical Reactions*. New York: John Wiley & Sons, 2003.

Part III.

Stochastic Thermodynamics of Chemical Reaction Networks

5. Stochastic Thermodynamics of Molecular Motors

A good first application of stochastic thermodynamics to biology is to perform a detailed exploration of the fluctuations in thermodynamic observables of a small but relevant prototypical system. Particularly interesting model systems are molecular motors. These are proteins found in living cells that are capable of exerting mechanical forces. Some motors transport cargo vesicles through the cell — especially on scales where diffusion is not fast enough, like in the axon of neurons. Other molecular motors can attach to different parts of the cytoskeleton in order to manipulate the cell shape, for example in muscle cells. Special types of molecular motors are located on the outer membrane of the cell and power the motion of cilia or flagella — which in turn are used to propel a unicellular organism through its environment, or to create directed fluid flow in multicellular organisms, such as in the trachea of mammals.

From the first law of thermodynamics, equation (1.1), it is clear that molecular motors cannot exert these forces for free. They need a source of energy. Heat is not an option: they are embedded in the aqueous surrounding of the cytosol and hence are thermally equilibrated at the single surrounding temperature T. Therefore, molecular motors need to use chemical energy as fuel. In many cases they act as catalysts that bind adenosine triphosphate (ATP) and release adenosine diphosphate (ADP) as well as hydrogen phosphate (P_i). This hydrolysis reaction, cf. section 4.4, fuels the motor even in a totally isothermal environment. Hence, the molecular motor converts chemical energy to mechanical energy. I introduced the efficiency of this *isothermal energy conversion* in section 1.2.1 and showed how it is limited by the dissipation of the process.

The heat reservoir induces thermal fluctuations in the motor which, compared to the chemical forcing, cannot be neglected. Therefore, a proper treatment of the dynamics and thermodynamics of a molecular motor necessarily needs to take fluctuations in all degrees of freedom into account. This can be done by applying the theory of stochastic thermodynamics as presented in section 2.3.2 to a single molecular motor. The master equation on its small network of states does not satisfy detailed balance, but *local* detailed balance with the chemical and mechanical forces coupling to different transitions.

Here, I want to highlight the connection of this approach to the theory of open chemical networks, which I presented in chapter 4. Generally, we would have to treat the chemical reactions of *many* molecular motors on the large chemical lattice. However, the chemostatting of the fuel and the waste results in the chemical decoupling of the different motor molecules. Each motor molecule remains a conserved moiety throughout the chemical reactions, restricting the chemical lattice to a finite set of states. The additional assumption of a mechanical decoupling makes the different molecular motors entirely independent. Consequently, the mechanochemical master equation describing such a system is equivalent to many copies of that of a single motor molecule.

In this chapter, I provide the reprint of an article that I coauthored. The article presents a thermodynamic analysis of stochastic models for *kinesin*, which is a well studied model system for molecular motors. The two physical currents in this system are the rate of mechanical displacement of the motor (with velocity as mean and diffusion constant as variance) as well as the rate of chemical

turnover (with hydrolysis rate as mean). The thermodynamic forces coupling to these currents are the mechanical load force as well as the chemical potential difference[1] $\mu_{\mathrm{ATP}} - \mu_{\mathrm{ADP}} - \mu_{\mathrm{P}_i}$. In this article we apply an analytical method to calculate the *cumulants* of these two physical currents as functions of these forces. The method revolves around the characteristic polynomial of a biased transition matrix of the master equation, which provides access to the *scaled cumulant generating function* introduced in section 2.3.3. The method is the result of my Master's thesis [1] and was published [2] back to back with its application to the kinesin models [3] in the same issue of *Physical Review E*.

The advantage of using an analytical method is striking. In this system, the current cumulants vary over many orders of magnitude. Having access to the analytical expressions for these cumulants, we are able to determine quantities that are derived from these cumulants and difficult to determine otherwise: the *efficiency* of the energy conversion, the *response* of the currents to changes in the forces, as well as the *ratios* of different cumulants. In the article we find that the chemical turnover and the mechanical displacement of kinesin are *quasi-tightly* coupled. The efficiency of the energy conversion performed by kinesin indicates that it may be optimized by evolution to perform well in a wide range of physiological concentrations of ATP. The ratio of diffusion constant and motor velocity (known as randomness parameter) reveals that kinesin behaves primarily Poissonian — which means that it is as deterministic in its motion as is possible for a reversible stochastic process. Interestingly, the mechanical response of the motor resembles the fluctuation–dissipation relation wherever the displacement velocity vanishes, not only at the true thermodynamic equilibrium —where it is known to hold. Additionally, the kinesin models we analyzed exhibit a region of negative differential mobility far from equilibrium.

References

[1] A. Wachtel. "Fluctuation Spectra and Coarse Graining in Stochastic Dynamics". MA thesis. Göttingen: Georg-August-Universität, 2013. arXiv: 1312.0115.

[2] A. Wachtel, J. Vollmer, and B. Altaner. "Fluctuating currents in stochastic thermodynamics. I. Gauge invariance of asymptotic statistics". In: *Physical Review E* 92, 042132 (2015).

[3] B. Altaner, A. Wachtel, and J. Vollmer. "Fluctuating currents in stochastic thermodynamics. II. Energy conversion and nonequilibrium response in kinesin models". In: *Physical Review E* 92, 042133 (2015).

[1] As customary in biochemistry, we suppress the water and proton that are involved in the hydrolysis.

[2] https://creativecommons.org/licenses/by/3.0/

Fluctuating currents in stochastic thermodynamics. II. Energy conversion and nonequilibrium response in kinesin models

Bernhard Altaner,[1,2] Artur Wachtel,[1,3] and Jürgen Vollmer[1,2]

[1]*Department of Dynamics of Complex Fluids (DCF), Max Planck Institute for Dynamics and Self-Organization (MPI DS), Am Fassberg 17, 37077 Göttingen, Germany*

[2]*Institute for Nonlinear Dynamics, Faculty of Physics, Georg-August University Göttingen, 37077 Göttingen, Germany*

[3]*Complex Systems and Statistical Mechanics, Physics and Materials Science Research Unit, University of Luxembourg, Luxembourg*

(Received 4 May 2015; published 14 October 2015)

Unlike macroscopic engines, the molecular machinery of living cells is strongly affected by fluctuations. Stochastic thermodynamics uses Markovian jump processes to model the random transitions between the chemical and configurational states of these biological macromolecules. A recently developed theoretical framework [A. Wachtel, J. Vollmer, and B. Altaner, Phys. Rev. E **92**, 042132 (2015)] provides a simple algorithm for the determination of macroscopic currents and correlation integrals of arbitrary fluctuating currents. Here we use it to discuss energy conversion and nonequilibrium response in different models for the molecular motor kinesin. Methodologically, our results demonstrate the effectiveness of the algorithm in dealing with parameter-dependent stochastic models. For the concrete biophysical problem our results reveal two interesting features in experimentally accessible parameter regions: the validity of a nonequilibrium Green-Kubo relation at mechanical stalling as well as a negative differential mobility for superstalling forces.

DOI: 10.1103/PhysRevE.92.042133 PACS number(s): 05.70.Ln, 87.10.Mn, 02.50.Ga, 87.15.A−

I. INTRODUCTION

Understanding the complex biochemical processes which are responsible for cellular metabolism is one of the key questions in modern biophysics. The quantitative analysis of so-called molecular motors, which are the small machines transforming different forms of energy into one another, is at the center of these efforts [1–3]. In recent years scientists have developed techniques that allow the systematic observation and manipulation of these biological macromolecules [4]. Under *in vivo* conditions, (electro-)chemical gradients in the cell maintain these systems out of equilibrium. From a thermodynamic perspective, one is interested in the currents of heat, matter, and energy that flow through a molecular motor, because they allow, for instance, the definition of its efficiency.

In analogy to macroscopic engines, molecular motors are described by thermodynamic cycles in a space of biochemical and configurational states. In contrast, the energy scales involved in biochemical energy conversion are only a couple of times larger than the thermal energy. Consequently, thermal fluctuations cannot be neglected, and their dynamics must be modeled as a stochastic process that reproduces the stochastic time series observed in experiments. Stochastic thermodynamics refers to a general framework for a consistent definition of fluctuating work and heat currents on the level of these fluctuating time series [5,6]. The common model for molecular motors are dynamically reversible Markov jump processes, which can be thought of as (memoryless) random walks on a biochemical network of states [3,7–9]. In an accompanying publication [10] we investigated the asymptotic statistics of such systems from the perspective of the cycle topology of the network of states. In particular, we developed an efficient method to calculate all cumulants of arbitrary fluctuating currents analytically.

Here we are interested in the first- and second-order fluctuation statistics, i.e., the expressions for macroscopic average currents (like the motor's velocity) and Green-Kubo time-correlation integrals (like its diffusion constant). To be concrete, we use the analytic nature of our method to analyze the parameter space of different stochastic models for the motor protein kinesin [11–13], which were designed to reflect typical force-spectroscopy experiments [14–17]. Besides illustrating the insights that thermodynamic cycles provide into the motor dynamics, our results uncover interesting model predictions and thus indicate directions for future experimental research: The validity of a nonequilibrium fluctuation dissipation relation at mechanical stalling as well as negative differential mobility, commonly referred to as "getting more from pushing less" [18].

This work is structured as follows. In Sec. II we briefly review the results of Ref. [10]. In contrast to the formal exposition there, here we focus on the implementation of a universally applicable algorithm for the efficient calculation of averages and correlation integrals of fluctuating currents in stochastic thermodynamics. Section III thoroughly discusses how to apply our universal method in the concrete biophysical context of a kinesin model. In Sec. IV we give a detailed account of kinesin's chemical (ATP hydrolysis) and mechanical (displacement) currents as functions of their conjugate chemical and mechanical drivings. We conclude in Sec. V with a discussion of the main conceptional and biophysical insights.

II. FLUCTUATING CURRENTS AND THEIR STATISTICS

In this section we introduce our mathematical notation and—based on the general results presented in Ref. [10]—provide a concise recipe for calculating the averages and

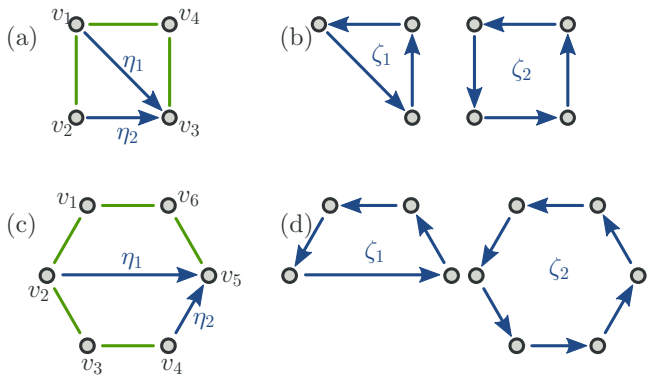

FIG. 1. (Color online) Two different graphs representing Markov models with (a) four states ($N = 4$, $M = 5$) and (c) six ($N = 6$, $M = 7$) states. The unoriented edges marked in green (gray) serve as a spanning tree $\mathcal{T}$. They connect all vertices of the respective graph. The remaining edges, marked as dark blue arrows, are the respective chords $\mathcal{H}$. Here we already indicate an orientation for the chords to provide a reference for the sign of the currents. Each chord η_ℓ gives rise to a fundamental cycle ζ_ℓ. They are shown in panels (b) and (d) for the four- and six-state models, respectively. Regarding the topological cycle structure, both graphs are equivalent. In particular, they have the same number $B = M - N + 1 = 2$ of fundamental cycles.

asymptotic (co-)variances of two fluctuating currents in a dynamically reversible Markov process on a finite state space. Such averages and covariances play a major role in stochastic thermodynamics [8,19,20]: They correspond to physical steady-state currents and time-correlation (Green-Kubo) integrals [21]. To be concrete, we exemplify topological concepts for both a four-state and a six-state Markov process, Fig. 1. In Sec. III we interpret these examples as models for the molecular motor kinesin.

A. Currents for Markovian processes

Memoryless stochastic processes on a finite state space $\mathcal{V} = \{v_1, v_2, \ldots, v_N\}$ are called *Markovian jump processes*. Henceforth, we consider the time-continuous, homogeneous case. A realization, or *trajectory* (γ_k, t_k), of the process starting at time $t_0 = 0$ in a state $\gamma_0 \in \mathcal{V}$ is a collection of jump times $t_k > 0$ and visited states $\gamma_k \in \mathcal{V}$ with $k \in \mathbb{N}$. We interpret it as a time series that contains the outcomes of subsequent measurements performed on a small system like a molecular motor.

Transitions from a state $v_i \in \mathcal{V}$ to a different state $v_j \in \mathcal{V}$ occur at a given constant rate w_j^i. For thermodynamic consistency [6–8,20,21], we require *dynamical reversibility*, i.e., $w_j^i > 0 \Leftrightarrow w_i^j > 0$. With this constraint we draw the state space as a undirected graph $\mathcal{G}$ with the N states as vertices and M admissible transitions as edges, cf. Fig. 1. In addition to dynamic reversibility we assume that the state space is connected, which ensures ergodicity of the process.

An ensemble of trajectories with initial probability distribution $\boldsymbol{p}(0) = (p_1(0), \ldots, p_N(0))$ on $\mathcal{V}$ evolves according to the master equation [22]: $\frac{d}{dt}\boldsymbol{p}(t) = \boldsymbol{p}(t)\mathbb{W}$ or, in components,

$$\frac{d}{dt}p_i(t) = \sum_{j\neq i}\left(p_j w_i^j - p_i w_j^i\right),$$

where we use the convention $w_i^i = -\sum_{j\neq i} w_j^i$. Ergodicity of the process implies that there is a unique steady-state probability distribution $\boldsymbol{\pi}$ satisfying $0 = \boldsymbol{\pi}\mathbb{W}$ to which all initial conditions will converge eventually. The quantities $J_j^i = \pi_i w_j^i - \pi_j w_i^j$ represent the steady-state probability currents between two states v_i and v_j. The special condition where all the steady-state currents vanish, $J_j^i = 0$, is called *detailed balance* or *equilibrium*. Since we are interested in the currents of nonequilibrium systems, we will *not* assume detailed balance in the following.

In order to account for general currents, e.g., changes in energy, entropy, particle numbers, or physical position, we introduce *jump observables*. A jump observable φ assigns a weight φ_j^i to the transition from v_i to v_j, where we require antisymmetry: $\varphi_j^i = -\varphi_i^j$. The *macroscopic average current* $c(\varphi)$ associated to a jump observable φ is

$$c(\varphi) := \frac{1}{2}\sum_{i,j} J_j^i \varphi_j^i. \tag{1}$$

In order to illustrate the concept we provide two examples. For a pair of states (v_i, v_j) we define a simple but important case of jump observable: The *counting observable* $\varphi_{(i,j)}$ counts $+1$ for a transition from state v_i to v_j and -1 for a reverse transition from v_j to v_i. To every other transition it associates a weight of 0. In this case the macroscopic counting rate from v_i to v_j equals the steady-state probability current between these states: $c(\varphi_{(i,j)}) = J_j^i$. This expression obviously vanishes if transitions between v_i and v_j are impossible. In Ref. [10] we emphasized that counting observables form a basis of the space of jump observables: Every jump observable can be expressed as an appropriate linear combination of counting observables.

Another important example is the dissipation in stochastic thermodynamics. It is derived from the jump observable σ that takes the values $\sigma_j^i = \ln \frac{w_j^i}{w_i^j}$. The macroscopic average dissipation

$$c(\sigma) = \frac{1}{2}\sum_{i,j} J_j^i \ln \frac{w_j^i}{w_i^j}$$

is non-negative and vanishes only at equilibrium, i.e., if and only if we have detailed balance.

Kirchhoff's current law states that the currents in an electrical network balance at each vertex v_i. The same is true for the steady-state probability currents J_j^i, and the stationary Master equation formalizes Kirchhoff's *current law* as $\sum_i J_j^i = 0$. In Ref. [8], Schnakenberg discussed an extended analogy between Markov jump processes and Kirchhoff's laws. The fundamental object of Schnakenberg's theory is a set of $B = M - N + 1$ fundamental cycles $\{\zeta_\ell\}$, which describe the topology of a Markov jump process. They are obtained from a spanning tree of the graph representing the network of states, cf. Fig. 1 as well as Sec. II B. For now, think of a fundamental cycle ζ_ℓ as a tuple of consecutive states $(\gamma_0, \gamma_1, \ldots, \gamma_{m(\ell)} = \gamma_0)$ that form a self-avoiding and closed trajectory. Cycles are defined up to cyclic permutations. Adding the contributions of a jump observable φ along the

transitions in a fundamental cycle ζ_ℓ gives its *circulation*,

$$\mathring{\varphi}_\ell := \sum_{k=0}^{m(\ell)} \varphi_{\gamma_{k+1}}^{\gamma_k}. \tag{2}$$

Kirchhoff's *voltage law* states that the voltage drops $V = U_j - U_i$ between vertices of an electric network vanish if integrated along any circuit. Using the notion of circulations, the voltage law reads $\mathring{V}_l = 0$. Another result obtained in this context is the Schnakenberg decomposition of the macroscopic dissipation rate [8]:

$$c(\sigma) = \sum_{\ell=1}^{B} c_\ell \, \mathring{\sigma}_\ell, \tag{3}$$

where c_ℓ is the steady-state probability current associated to the cycle ζ_ℓ [10]. The circulations $\mathring{\sigma}_\ell$ of the dissipation are called the *cycle affinities*. In the context of irreversible thermodynamics [23], the Schnakenberg decomposition (3) identifies the cycle affinities as the generalized forces which are conjugate to the cycle currents c_ℓ.

In an earlier publication [13] the authors pointed out that Schnakenberg's decomposition is equally applicable to other observables φ. As a corollary, one may express the average current $c(\varphi) = \sum_\ell c_\ell \, \mathring{\varphi}_\ell$ using only the cyclic structure of the graph. Figure 1 shows two graphs with four and six states, respectively, but having the same cyclic structure. Collecting all B circulations of an observable φ in a B-tuple gives its *chord representation* $\varphi_{\mathcal{H}} := (\mathring{\varphi}_1, \ldots, \mathring{\varphi}_B) \in \mathbb{R}^B$. The detailed mathematical background of this representation is discussed in Ref. [10].

Here we are interested not only in the macroscopic expectations of currents but also in their higher-order statistics. Consequently, the object of study in this work are *fluctuating currents*. The *instantaneous current* $J_\varphi(t)$ derived from a *jump observable* φ along a trajectory (γ_k, t_k) is defined as

$$J_\varphi(t) = \sum_{k=0}^{\infty} \delta(t - t_k) \, \varphi_{\gamma_k}^{\gamma_{k-1}}.$$

The *time-integrated current*

$$\varphi(T) := \int_{t=0}^{T} J_\varphi(t) dt = \sum_{k=0}^{n(T)} \varphi_{\gamma_k}^{\gamma_{k-1}} \tag{4}$$

thus accounts for the total change of the observable φ along a random trajectory with a random number $n(T)$ of jumps up to time T. Hence, this time integral is a random variable with its own statistics. A typical realization of the time-integrated current, and thus its expectation value, grow linearly in time. Due to ergodicity, the *time-averaged current* $\overline{\varphi}_T := \frac{1}{T}\varphi(T)$ converges to the macroscopic current $c(\varphi)$ in the long-time limit:

$$\overline{\varphi}_T \xrightarrow{T\to\infty} c(\varphi). \tag{5}$$

Equivalently, one can average the fluctuating current over trajectories in the steady-state ensemble: $\langle J_\varphi(t)\rangle = \langle J_\varphi(0)\rangle = c(\varphi)$, where one exploits the fact that the steady state is time independent. This ensures that the macroscopic current $c(\varphi)$ is the expectation value, or mean, of the fluctuating current $J_\varphi(t)$.

Another important statistical measure are the correlations of two currents J_φ and J_ψ. A measure for this correlation is the *Green-Kubo integral*:

$$c(\varphi,\psi) := \int_{t=0}^{\infty} \langle [J_\varphi(0) - c(\varphi)][J_\psi(t) - c(\psi)]\rangle dt \, . \tag{6}$$

Similarly to the case of the average currents, ergodicity allows us to replace the steady-state ensemble average by a time average over the argument of the first current J_φ. As a consequence [21], the correlation integral corresponds to a properly scaled covariance of the time-averaged currents:

$$c(\varphi,\psi) = \lim_{T\to\infty} T \, \mathrm{Cov}[\overline{\varphi}_T, \overline{\psi}_T]. \tag{7}$$

As such, the macroscopic current and the Green-Kubo integral are the first two *scaled cumulants* of the pair $(\overline{\varphi}_T, \overline{\psi}_T)$ of time-averaged currents. Scaled cumulants are defined as derivatives of the *scaled cumulant-generating function*, which can be obtained using methods from large deviation theory [10,21,24,25]. Higher-order derivatives represent higher orders of the statistics, such as skewness and kurtosis.

In our accompanying paper [10] we prove a gauge invariance of the fluctuation statistics and show in detail how Schnakenberg's decomposition is extended to all cumulants of arbitrary observables. In the next section we give a brief review in form of a concise and efficient recipe for the first two orders.

B. Determining averages and (co-)variances of currents

The only ingredients needed for the calculation of the scaled cumulants are the transition matrix $\mathbb{W}$ and the jump observables representing the currents of interest. The elements w_j^i of the transition matrix as well as the jump observables may depend on the (physical) control parameters of the Markov processes in an arbitrary way. In the following, we present a simple yet efficient algorithm for the calculation of the first two scaled cumulants of two jump observables φ and ψ. It consists of three substeps: (1) topological, (2) algebraic, and (3) physical. The first two steps are universal. Only the last step involves the jump observables in question. Note that the algorithm requires neither the steady-state distribution $\boldsymbol{\pi}$ nor the scaled-cumulant generating function. We emphasize this fact because, in general, these quantities are difficult or even impossible to obtain analytically, i.e., in the form of a fully parameter-dependent, symbolic expression. An implementation of this algorithm in *Python* is available as a git repository [26].

1. Topology: Defining fundamental cycles

The first step in the analysis addresses the topology of the graph $\mathcal{G}$ representing a network of states, cf. Fig. 1.

(a) Choose a spanning tree $\mathcal{T}$ for the undirected graph, i.e., an undirected subgraph spanning all vertices but not containing any circuit [green edges in Figs. 1(a) and 1(c)].

(b) Provide an orientation to the $B = N - M + 1$ undirected edges $\eta_\ell \in \mathcal{H}$ left out by the tree $\mathcal{T}$. They are the called *chords* [blue edges in Figs. 1(a) and 1(c)].

(c) Identify the fundamental cycles: For every chord $\eta_\ell \in \mathcal{H}$, its terminus and origin are connected by a unique directed path through the spanning tree. Adding the chord itself as a closure of this path results in the fundamental cycle ζ_ℓ [Figs. 1(b) and 1(d)].

2. *Algebra: Determining the fundamental current cumulants*

The second step of our algorithm involves the determination of the first two (joint) scaled cumulants of the fluctuating currents associated to the chords $\eta_\ell \in \mathcal{H}$.

(a) Write down the characteristic polynomial $\chi_{\mathcal{H}}(\lambda; q_1, q_2, \ldots, q_B) = \det(\mathbb{W}_{\mathcal{H}} - \lambda\mathbb{I})$ of the matrix $\mathbb{W}_{\mathcal{H}}$ with entries

$$(\mathbb{W}_{\mathcal{H}})^i_j = \begin{cases} w^i_j \exp(\pm q_\ell) & \text{if } (i \to j) = \pm\eta_\ell, \\ w^i_j & \text{else.} \end{cases} \tag{8}$$

(b) Identify the coefficients $a_0(\boldsymbol{q})$, $a_1(\boldsymbol{q})$, and $a_2(\boldsymbol{q})$ of $\chi_{\mathcal{H}}(\lambda; \boldsymbol{q}) = \sum_{k=0}^{N} a_k(\boldsymbol{q})\,\lambda^k$, i.e., the coefficients of the constant, the linear, and the quadratic terms.

(c) Calculate the vector $\boldsymbol{c} \in \mathbb{R}^B$ with entries $c_\ell = c(\eta_\ell)$ and the scaled covariance matrix $\boldsymbol{C} \in \mathbb{R}^{B\times B}$ with entries $C_{\ell m} = c(\eta_\ell, \eta_m)$ as follows:

$$c_\ell = -\frac{\partial_\ell a_0}{a_1}, \tag{9a}$$

$$\begin{aligned} C_{\ell m} &= -\frac{\partial^2_{\ell m} a_0}{a_1} - \frac{2(\partial_\ell a_0)(\partial_m a_0)a_2}{a_1^3} \\ &\quad + \frac{(\partial_m a_1)(\partial_\ell a_0) + (\partial_\ell a_1)(\partial_m a_0)}{a_1^2} \\ &= -\frac{\partial^2_{\ell m} a_0 + (\partial_\ell a_1)c_m + (\partial_m a_1)c_\ell + 2a_2 c_m c_\ell}{a_1}, \end{aligned} \tag{9b}$$

where the partial derivatives $\partial_\ell a_k := \frac{\partial a_k(\boldsymbol{q})}{\partial q_\ell}\big|_{\boldsymbol{q}=\boldsymbol{0}}$ and the coefficients a_k are evaluated at $\boldsymbol{q} = \boldsymbol{0}$.

Remark: Higher-order scaled cumulants are similarly accessible. The characteristic equation $0 = \chi_{\mathcal{H}}(\lambda; \boldsymbol{q})$ uniquely defines the entire scaled cumulant-generating function $\lambda_{\mathcal{H}}(\boldsymbol{q})$ with $\lambda_{\mathcal{H}}(\boldsymbol{0}) = 0$. Taking derivatives of the characteristic equation yields linear equations for the cumulants, i.e., the inner derivatives $\partial_{q_i,\ldots,q_j}\lambda_{\mathcal{H}}(\boldsymbol{0})$. Note that higher-order cumulants depend on the coefficients $a_k(q)$ with $k > 2$, and the symbolic expressions become more complex. The first two orders are explicitly given by Eqs. (9). The symbolic manipulations that are necessary to obtain the higher orders are efficiently implemented in modern computer algebra systems. For more details on the procedure and a derivation of Eqs. (9), the reader is referred to our accompanying publication [10].

3. *Physics: Cumulants of jump observables*

The third and final step of the algorithm yields the first two scaled cumulants of the fluctuating currents associated to the jump observables φ and ψ.

(a) Sum the jump observables φ and ψ along the edges of the fundamental cycle ζ_ℓ to obtain the circulations $\mathring{\varphi}_\ell$ and $\mathring{\psi}_\ell$. They are the coordinates of the chord representations $\varphi_{\mathcal{H}}, \psi_{\mathcal{H}} \in \mathbb{R}^B$.

(b) The steady-state average of φ, and of the scaled covariance of φ and ψ, then read

$$c(\varphi) = \boldsymbol{c} \cdot \varphi_{\mathcal{H}} \equiv \sum\nolimits_{\ell=1}^{B} \mathring{\varphi}_\ell\, c_\ell, \tag{10a}$$

$$c(\varphi, \psi) = \varphi_{\mathcal{H}} \cdot \boldsymbol{C}\, \psi_{\mathcal{H}} \equiv \sum\nolimits_{m,\ell=1}^{B} \mathring{\varphi}_\ell\, C_{\ell m}\, \mathring{\psi}_m. \tag{10b}$$

We conclude the section with final remarks on the choice of the spanning tree in step 1, which is *a priori* arbitrary. Different choices yield different chords—and thus different expressions for the fundamental current vector $\boldsymbol{c}$ and the fundamental covariance matrix $\boldsymbol{C}$. Expressions (9) and (10) are universal. In order to calculate the cumulants of any jump observable, no equations need to be solved. Via Eq. (9), any combinatorial complexity is hidden in (the derivatives of) the coefficients a_k of the characteristic polynomial. The latter are calculated in a straightforward way either manually or by using a computer-algebra system. However, the final expressions (10) have fewer terms if some of the circulations $\mathring{\varphi}_\ell$ or $\mathring{\psi}_\ell$ along fundamental cycles vanish. It is thus worthwhile to take a careful look at the particular set of jump observables φ and ψ under consideration and choose a spanning tree that is optimal in that regard.

III. KINESIN

A. Kinesin as a molecular motor

Kinesin is a molecular motor which facilitates transport in eukaryotic cells. It moves along intracellular filaments called microtubules and plays a major role in many biological processes, including mitosis, meiosis, and transport of cellular cargo. The most well-studied variety of kinesin—both experimentally (see, e.g., Refs. [4,15–17] and references therein) and theoretically [11,12,27–30]—is a protein dimer consisting of two identical subunits. Figure 2(a) shows a sketch of kinesin binding its intracellular cargo at its tail end. Kinesin's head end consists of two active sites which bind and unbind to the microtubule in alternating succession, thereby allowing the motor to perform mechanical steps of length $L = 8$ nm [31,32]. Due to the polarity of the microtubule, this motion has a preferred "forward" direction.

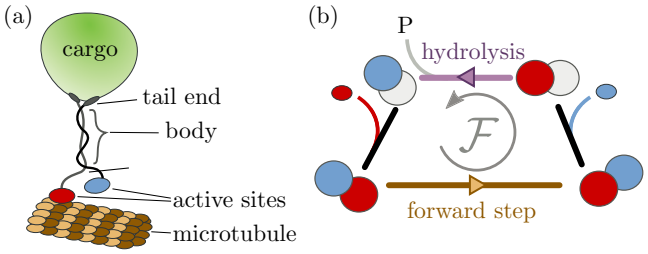

FIG. 2. (Color online) (a) Kinesin is a motor protein consisting of two identical entangled subunits. Cargo is bound at the tail end. The active sites on kinesin's head end bind to the microtubule and act as kinesin's "feet," enabling the molecule to perform directed steps. Kinesin's stepping mechanism is the result of subsequent changes in how strong the active sites bind to the microtubule. The trailing (left) and leading (right) sites are represented by colored ellipses. ATP-laden [red (dark gray)] and empty (light gray) sites bind strongly, whereas an ADP-laden [blue (gray)] site binds only weakly. The succession of chemical compositions shown in panel (b) is called the forward cycle $\mathcal{F}$. Starting from the upper left state, the forward cycle involves (in the counterclockwise direction): (i) Binding of ATP to the (empty) leading site; (ii) a mechanical step (brown edge, bottom), i.e., the exchange of the leading and trailing site; (iii) release of ADP from the (new) leading site; and (iv) hydrolysis (purple edge, top) of ATP into ADP at the trailing site.

The energy necessary for this active directed transport is provided by the hydrolysis of adenosine triphosphate (ATP) into adenosine diphosphate (ADP) and inorganic phosphate (P). Unlike macroscopic motors, small molecular machines operate at low Reynolds numbers and inertia plays no role: Chemical energy is not converted into mechanical energy by a transfer of momentum. Instead, kinesin's mechanical displacement is the result of a complex interplay of the strength of the microtubule binding at the active sites, which depends on their chemical composition. ATP-laden and empty sites bind strongly, while ADP-laden sites bind more weakly [16,17]. Under physiological conditions the mechanochemical interaction can be described by the "forward cycle" depicted in Fig. 2(b) [11]. Models that only treat the forward cycle feature *tight coupling* between the hydrolysis reaction and the stepping: Each hydrolysis of an ATP molecule gives rise to exactly one motor step [14].

B. Experiments and models

An important biophysical question regards the force that kinesin generates for different concentrations of the chemicals ATP, ADP, and P involved in the hydrolysis reaction. Typically, experiments measure this force by linking kinesin to a dielectric colloidal bead which resides in an optical trap [14–16,31]. Involved experimental setups allow the precise control of the pulling force F that the optical trap exerts on the motor against its typical direction of motion. The independent driving parameters are the nondimensionalized force $f := (LF)/(k_BT)$ and the nondimensionalized chemical potential difference $\Delta\mu = \log(K_{\mathrm{eq}}[\mathrm{ATP}]/[\mathrm{ADP}][\mathrm{P}])$, where k_B denotes Boltzmann's constant, T the temperature, K_{eq} the equilibrium constant of the hydrolysis reaction, and $[X]$ the concentration of chemical species X. In the remainder of this work, all physical quantities are expressed in units based on the length scale L, time scale 1s, and energy scale k_BT.

Many experiments probe the stalling force $f_{\mathrm{stall}}(\Delta\mu)$, which is defined as the value of the force needed to bring the motor to a halt for a given chemical potential difference $\Delta\mu$. Under physiological chemical conditions, kinesin hydrolyzes ATP even at stalling forces [15,16]. The exact details of the kinesin stepping mechanism under high mechanical loads remain unknown and several models exist, cf. Refs. [11,12,17] and the references discussed in these publications. While these models differ in their details, they all feature more than only the tightly coupled forward cycle.

A prominent example of a thermodynamically consistent model was introduced in Ref. [11]. There the key idea is to extend the forward cycle shown in Fig. 2(b) by the chemical compositions obtained from exchanging the trailing with the leading active sites, cf. Fig. 3(a). In addition to the forward cycle $\mathcal{F}$, the extended network features six states and has two additional cycles, Figs. 2(b)–2(d): The backward cycle $\mathcal{B}$ represents backward motion under hydrolysis, while the dissipative slip cycle $\mathcal{D}$ represents the futile hydrolysis of two ATP molecules without any stepping [28]. In such a multiple-cycle model, hydrolysis and mechanical displacement are no longer tightly coupled. In Sec. IV A we will address the question of *quasitight coupling*, i.e., situations where the ratio

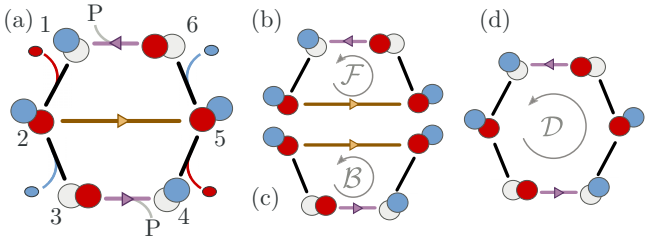

FIG. 3. (Color online) (a) The six-state kinesin model from Ref. [11] extends the forward cycle from Fig. 2(b) by two states. For this model, We use the same spanning tree and chords as in the example shown in Fig. 1(c). Then the fundamental cycles $\zeta_1 \equiv \mathcal{F}$ and $\zeta_2 \equiv \mathcal{D}$ are the forward and dissipative cycles (b) and (d), respectively. The backward cycle (c) is the linear combination $\mathcal{B} = \zeta_2 - \zeta_1$, cf. Ref. [10].

of the average number of chemical and mechanical events predicted by the model is close to unity.

C. Network theory for the kinesin model

In order to study quasitight coupling, energy conversion, and the predicted response to changes in the driving parameters, we apply the algorithm presented in Sec. II B to the six-state model for kinesin, Fig. 3. For the first step of the algorithm, we choose the spanning tree and its chords in the same way as in Figs. 1(c) and 1(d). Consequently, the fundamental cycles $\zeta_1 \equiv \mathcal{F}$ and $\zeta_2 \equiv \mathcal{D}$ correspond to the forward and dissipative cycles, respectively.

The second step of the algorithm requires the determination of the fundamental current vector $\boldsymbol{c}$ and the fundamental covariance matrix $\boldsymbol{C}$. With the enumeration of the vertices as in Fig. 3(a) the matrix $\mathbb{W}_{\mathcal{H}}(q_1,q_2)$ reads:

$$\begin{pmatrix} w_1^1 & w_2^1 & 0 & 0 & 0 & w_6^1 \\ w_1^2 & w_2^2 & w_3^2 & 0 & w_5^2 e^{q_1} & 0 \\ 0 & w_2^3 & w_3^3 & w_4^3 & 0 & 0 \\ 0 & 0 & w_3^4 & w_4^4 & w_5^4 e^{q_2} & 0 \\ 0 & w_2^5 e^{-q_1} & 0 & w_4^5 e^{-q_2} & w_5^5 & w_6^5 \\ w_1^6 & 0 & 0 & 0 & w_5^6 & w_6^6 \end{pmatrix}.$$

It is straightforward to write down its characteristic polynomial $\chi_{\mathcal{H}}(\lambda;q_1,q_2) =: \sum_{k=0}^{6} a_k(q_1,q_2)\lambda^k$ and to extract the coefficients $a_0(q) \equiv \det \mathbb{W}_{\mathcal{H}}(q_1,q_2)$, a_1, and a_2. Differentiating with respect to q_1 and q_2 and evaluating at $q_1 = q_2 = 0$ yields the expressions $\partial_\ell a_k$ appearing in Eqs. (9).

The third step requires the circulations of the jump observables of interest. For the present discussion, we consider the displacement $d = \varphi_{(2,5)}$ and the hydrolysis count $h = \varphi_{(6,1)} + \varphi_{(3,4)}$, which indicate a transition along the brown and purple edges in Fig. 3, respectively. Their matrix representations read

$$d^i_j = \delta_{i,2}\delta_{j,5} - \delta_{i,5}\delta_{j,2}, \tag{11a}$$

$$h^i_j = \delta_{i,6}\delta_{j,1} - \delta_{i,1}\delta_{j,6} + \delta_{i,3}\delta_{j,4} - \delta_{i,4}\delta_{j,3}, \tag{11b}$$

where $\delta_{m,n}$ denotes the Kronecker δ, which yields one if $m = n$ and zero otherwise. The circulations of d and h simply count

the number of the brown and purple edges in the fundamental cycles $\zeta_1 = \mathcal{F}$ and $\zeta_2 = \mathcal{D}$, cf. Figs. 3(b) and 3(d). The chord representations of d and h thus are

$$d_{\mathcal{H}} = (\mathring{d}_1, \mathring{d}_2) = (1,0), \tag{12a}$$
$$h_{\mathcal{H}} = (\mathring{h}_1, \mathring{h}_2) = (1,2). \tag{12b}$$

Note that the choice of the chords is optimal for the calculation of the present variables because one of the entries of $d_{\mathcal{H}}$ vanishes ($\mathring{d}_2 = 0$), while this cannot be achieved for $h_{\mathcal{H}}$. After all, all cycles contain at least one hydrolysis event.

The corresponding macroscopic currents, i.e., the velocity $c(d)$ and the hydrolysis rate $c(h)$ are obtained from Eq. (10) as:

$$c(d) = c_1, \tag{13a}$$
$$c(h) = c_1 + 2c_2. \tag{13b}$$

Their scaled (co-)variances amount to

$$c(d,d) = C_{11},$$
$$c(h,h) = C_{11} + 4C_{12} + 4C_{22},$$
$$c(h,d) = C_{11} + 2C_{12}.$$

In addition to displacement d and hydrolysis count h, we are interested in the jump observable $\sigma^i_j = \ln(w^i_j/w^j_i)$ corresponding to the dissipation. As discussed in Sec. II A its circulations are the cycle affinities. The Hill-Schnakenberg conditions are necessary for the consistency of a Markov jump process with the thermodynamic notion of local equilibrium [3,9]. They state that the affinity of a cycle must express the (nondimensionalized) differences in the potentials of the reservoirs, cf. Refs. [7,8,19]. Upon completing the forward cycle $\mathcal{F} \equiv \zeta_1$, an amount $\Delta\mu$ of chemical energy is used by the system to perform a (dimensionless) amount $-f$ of work against the pulling force. Similarly, a completion of the dissipative cycle $\mathcal{D} \equiv \zeta_2$ uses $2\Delta\mu$ of chemical energy. Consequently, the chord representation of the dissipation reads

$$\sigma_{\mathcal{H}} = (\mathring{\sigma}_1, \mathring{\sigma}_2) = (-f + \Delta\mu, 2\Delta\mu).$$

The Schnakenberg decomposition thus lets us express the average steady-state dissipation by physical parameters and currents through fundamental chords

$$c(\sigma) = (-f + \Delta\mu)c_1 + (2\Delta\mu)c_2. \tag{14}$$

D. The cycle perspective

In the previous section, we expressed observable quantities only by means of their circulations around fundamental cycles and the fundamental first and second chord cumulants. Nowhere in these expressions do the number of states or the choice of a spanning tree appear explicitly. Hence, the same expressions are reproduced by any model with the same cycle topology, as long as the physics along the cycles, i.e., the circulations of antisymmetric jump observables, are the same. As exemplified in Sec II A in Figs. 1(a) and 1(b), one can formulate a model on four states with the same cycle topology as the six-state model described in Fig. 3. Allowing only for single edges between states, such a four-state model is the minimal model featuring two independent cycles. An interesting question is how this model (and other reduced models) compare to more complicated ones.

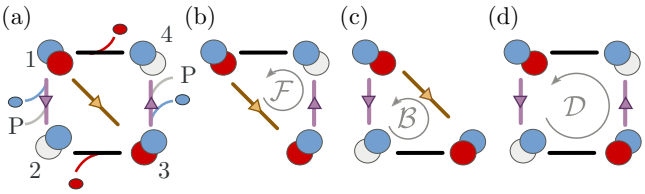

FIG. 4. (Color online) A model with four states, which describes the same physics as the six-state model shown in Fig. 3. In this simpler model we combined the transitions for the ATP hydrolysis on one active site with the ADP release on the other one into a single transition. Details of the model construction are given in the Appendix.

In Ref. [13] we used the idea of preserving the cycle affinities and circulations of jump observables along cycles (together with locality constraints) to develop a coarse-graining algorithm for stochastic models. Its application to the six-state kinesin model produced various topologically equivalent models, which all preserved the fluctuation statistics of the observables of interest almost perfectly. A disadvantage of this coarse-graining algorithm is that the individual transitions in the network of states lose their original interpretation.

In contrast, Fig. 4 shows a four-state model with a clear interpretation of the transitions. This has the advantage that the parametrization of the transition rates is found by the same physical arguments as the ones used in Ref. [11] for the six-state model. Details of the construction of this model are given in the Appendix. We will see in the next section that all the predictions of the six-state model are also found in topologically equivalent four-state models. This observation underlines the virtue of viewing models in ST from the perspective of cycles—an idea that was pioneered by Hill [7,19] and Schnakenberg [8] and has regained considerable attention recently [11,13,28,33,34].

IV. RESULTS

One of the main messages of this work is that the algorithm presented in Sec. II B allows us to probe parametric models used in stochastic thermodynamics in a systematic way. In order to demonstrate the efficiency of our approach, we report on various nontrivial predictions of the six-state kinesin model. At the end of this section we will compare these results with other models.

Throughout this section, we choose the parameter range similar to Ref. [28] and vary $-30 \leqslant f, \Delta\mu \leqslant 30$. Then, in physical units, the pulling force F varies between about -15 and $+15pN$. Following Ref. [11], the chemical potential difference is adjusted by changing the ATP concentration while fixing the other chemical concentrations at physiological values (see Appendix). The physiologically relevant region for the chemical driving parameter is limited to about $20 < \Delta\mu < 30$. Negative values of the chemical potential correspond to extremely low ATP concentrations. In particular,

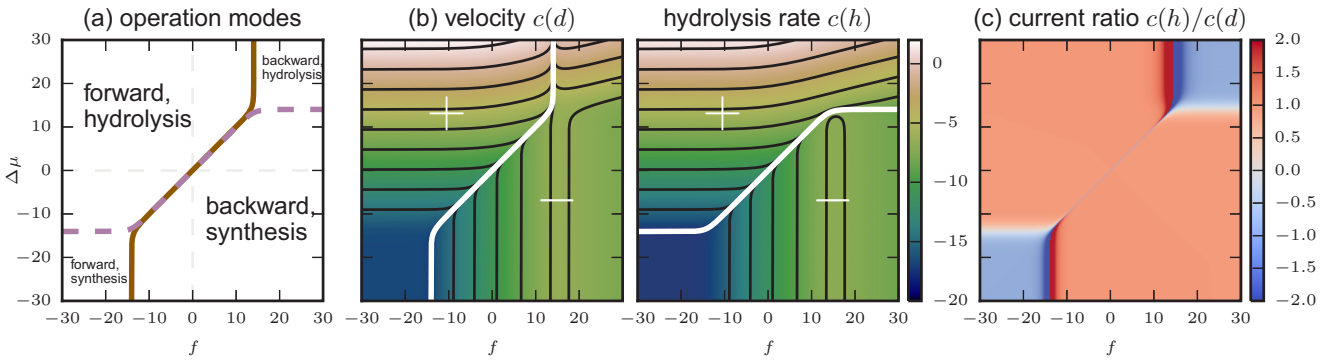

FIG. 5. (Color online) (a) Operation modes as identified in Ref. [28]. (b) Decadic logarithm of the absolute value of the average velocity $c(d)$ (left) and hydrolysis rate $c(h)$ (right). White lines indicate where the currents vanish and correspond to the region boundaries displayed in panel (a). Signs of the currents are indicated as an overlay. Contour lines show that the macroscopic currents are proportional away from these lines. (c) Plotting the ratio $c(h)/c(d)$ makes this proportionality visible directly. The proportionality constant has an absolute value very close to unity, indicating quasitight coupling for most parameter values (see discussion in the main text). Note that the values of the ratio are cropped at absolute values of 2, most prominent in the dark regions surrounding the singularities of the ratio.

the "homeopathic limit" is reached at about $\Delta\mu < -14$: At that point there is less than one ATP molecule in an experiment containing 1 liter of solution.

The reason we still present our results for the entire parameter range $-30 \leqslant f, \Delta\mu \leqslant 30$ is twofold: First, it enables a direct comparison with previous work [11,28]. Second, it demonstrates the effectiveness of our algorithm in predicting results that vary over many orders of magnitude. Still, we emphasize that nontrivial results are encountered exactly in the experimentally accessible region, where we consider the model as valid.

A. Velocity, hydrolysis rate, and their quasitight coupling

Figure 5(a) reproduces a central result of Ref. [28] concerning the operations modes of kinesin. These modes are defined by the signs of the average currents, i.e., of the velocity $c(d)$ and the hydrolysis rate $c(h)$. However, the resulting phase diagram contains no information regarding their magnitude. Based on the expressions (13) we provide a detailed account on their numerical values in Fig. 5(b). Note that these currents vary over about 20 orders of magnitude. This underlines the importance of having analytical expressions to generate the plots. A brute-force numerical approach will either be prohibitively expensive in terms of computer resources or it will suffer from severe inaccuracies when dealing with this vast range of numerical values.

The analytical expressions for the currents also reveal an interesting relation between the average currents. In Fig. 5(c) we plot the ratio $c(h)/c(d)$ of the hydrolysis rate and the velocity. Again, access to the analytical expressions for the currents is crucial to determine the ratio. After all, both its numerator and denominator are of the order 10^{-18} in the lower left corner of the parameter space.

The most prominent feature of Fig. 5(c) is that away from the zero-current lines, the ratio of average hydrolysis rate and velocity takes values very close to ± 1. Consequently, on average, the completion of a cycle yields one mechanical step and one chemical event. We say that chemical and mechanical currents are *quasitightly coupled*. Experimentally, it was found that kinesin hydrolyzes one ATP molecule for each mechanical step [14]. According to the model considered here, quasitight coupling is a generic feature that holds more generally: Even in the region where kinesin moves *backward* while consuming ATP, the absolute values of the currents are locked to a ratio of 1.

Knowing the absolute values of the currents rather than only their signs also allows us to treat kinesin's thermodynamic cycles in more detail. In Ref. [28] this discussion was based on the signs of Hill's (excess) cycle fluxes [7]. With the current ratio we interpret the regions shown in the phase diagram Fig. 5(a) in terms of dominant cycles—at least away from their boundaries: In the upper left and lower right regions the forward cycle $\mathcal{F}$ dominates such that average hydrolysis and velocity are directly proportional, $c(h) \sim c(d)$. The difference between those regions is the angular direction: Counterclockwise completion leads to a forward movement accompanied by ATP hydrolysis, whereas clockwise completion yields backward stepping and ATP synthesis. In contrast, in the upper right and lower left regions hydrolysis and velocity are antiproportional, $c(h) \sim -c(d)$: A counterclockwise (backward, hydrolysis) or a clockwise (forward, synthesis) completion of the backward cycle $\mathcal{B}$ dominates the average dynamics, respectively. This result, which is based on the values of physiological currents, thus complements and extends the discussion presented in Ref. [28].

B. Efficiency of energy conversion

Under physiological conditions, kinesin uses the chemical energy released by the ATP hydrolysis to perform mechanical work. Energy efficiency is one of the most important questions for molecular machines involved in cellular energy conversion [35–37], just as it is for macroscopic machines. A framework for a quantitative analysis is based on the notion of conjugate currents and forces from irreversible thermodynamics [23]. Generally, a complete set of conjugate currents $c(\varphi_i)$ and forces E_i yields the average dissipation as the bilinear form

$$c(\sigma) = \sum_i c(\varphi_i) E_i =: \sum_i c(\sigma_i), \qquad (51)$$

where $\sigma_i = \varphi_i E_i$ denotes the distinct contributions to the entropy production.

Using Eqs. (13) and (14) we find that

$$c(\sigma) = (-f)c(d) + (\Delta\mu)c(h) =: c(\sigma_{\text{mech}}) + c(\sigma_{\text{chem}}). \tag{15}$$

We see that in the kinesin model, velocity $c(d)$ and hydrolysis rate $c(h)$ are conjugate to the negative pulling force $-f$ and the chemical potential $\Delta\mu$, respectively. For a system with two independent contributions to the entropy production, $\sigma = \sigma_1 + \sigma_2$, one may define the efficiency of energy conversion in general terms [36]. To that end note that $c(\sigma)$ is always positive. This, however, does not imply that both contributions $c(\sigma_i)$ are positive. Indeed, systems act as energy converters only if one of the contributions, say, σ_1, is negative. Then, a (positive) average power output $\dot{W}_{\text{out}} := -c(\sigma_1)$ is sustained by a (positive) average power input $\dot{W}_{\text{in}} = c(\sigma_2)$. Note that $c(\sigma_2)$ is positive and larger in magnitude than $c(\sigma_1)$, because $c(\sigma) = c(\sigma_1) + c(\sigma_2) \geqslant 0$ must always hold. Hence, the efficiency of energy conversion is defined as

$$0 \leqslant \hat{\eta} := \frac{\dot{W}_{\text{out}}}{\dot{W}_{\text{in}}} = \frac{|\sigma_1|}{\sigma_2} < 1. \tag{16}$$

It is always positive and smaller than unity.

In the framework of stochastic thermodynamics, this efficiency has been studied under various aspects (cf. e.g., Refs. [35–38]). In Fig. 6, we give the efficiency of energy conversion $\hat{\eta}$ for the kinesin model. The regions A–D correspond to different types of energy conversion where the system acts as either a motor (A and C) or a chemical factory (B and D). Outside these regions both contributions to the entropy production are positive and no energy conversion takes place.

We note the following prediction: For any fixed value of $\Delta\mu$ in the physiological range, i.e., for $20 < \Delta\mu < 30$, the value of the force at maximum efficiency is around $f \approx 10.5$. This suggest that kinesin might be optimized to encounter (elastic) forces of around $5\,pN$, independent of the ATP concentration. It will be interesting to explore the implications of this result for the collaborative behavior of multiple kinesin molecules involved in the viscous transport of organelles.

Finding the parameters of a system that extremize thermodynamic quantities is a generic problem. Recently, many authors have discussed the notion of efficiency at maximum power (see, e.g., Refs. [35,39] and therein). Having fully parameter-dependent symbolic expressions for the various contributions to the entropy production establishes a general (analytic) approach to this optimization problem.

C. Diffusion constant and randomness parameter

So far, we have only investigated average currents, which are also available if the steady-state distribution $\boldsymbol{\pi}$ is known, cf. Eq. (1). Higher-order statistics of fluctuating currents cannot be expressed by means of the stationary distribution only, although a perturbation expansion exists [40]. The method presented here provides direct access to the (co-)variance of fluctuating currents via Eq. (10b), without the knowledge of the stationary distribution.

For motor proteins we are mostly interested in the second scaled cumulant of the time-averaged displacement.

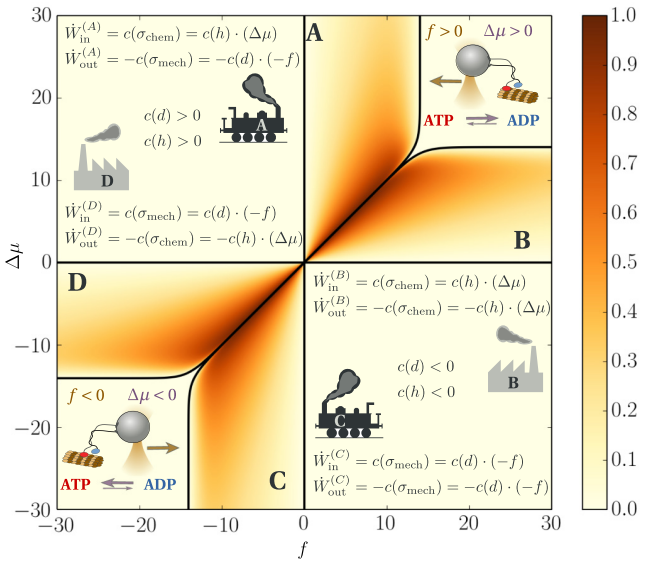

FIG. 6. (Color online) Efficiency of energy conversion in the kinesin model. The four regions A–D correspond to four different ways of energy conversion. In the regions outside the solid curves, no conversion between mechanical and chemical energy takes place. In regions A and C kinesin acts as a motor converting chemical into mechanical energy against the external force. In regions B and D kinesin resembles a chemical factory that uses mechanical energy to produce ATP and ADP, respectively, against the chemical potential provided by the solution. The sketches in the upper right and lower left illustrate the combination of thermodynamic forces acting on the motor in the respective quadrant. In the upper right, kinesin is pulled backward (i.e., against its standard direction of motion) in an ATP-rich environment. In the lower left, kinesin is pushed forward in an ADP-rich environment. Energy conversion occurs only in the regions where both mechanical and chemical currents have the same sign and the forward cycle dominates, cf. Fig. 5.

It quantifies the (linear) scaling of the (fluctuating part of) the mean-square displacement and thus defines (up to a factor of 2) the nonequilibrium diffusion constant $D = D(f, \Delta\mu)$:

$$c(d,d) \equiv \lim_{T\to\infty} \frac{1}{T}(\langle d(T)^2\rangle - \langle d(T)\rangle^2) =: 2D.$$

In Fig. 7(a) we show the diffusion constant in the six-state kinesin model. Like the average velocity, its values span a range of about 20 orders of magnitude. Under physiological conditions ($f = 0, \Delta\mu \approx 25$) the diffusion constant is about 10 orders of magnitude larger than at equilibrium.

A direct measurement of the parameter dependence of D is difficult. An observable that is more easily accessible in experiments is the so-called *randomness parameter* (sometimes called Fano factor) [15,17,41,42],

$$r = \lim_{T\to\infty} \frac{\langle d(T)^2\rangle - \langle d(T)\rangle^2}{\langle d(T)\rangle} = \frac{c(d,d)}{c(d)}. \tag{17}$$

It is a dimensionless measure of the temporal irregularity of the mechanical displacement. While $r = 0$ indicates a deterministic motion without any fluctuations, a value of $|r| = 1$ amounts to a Poisson motor [41]. In Fig. 7(b) we plot its inverse, r^{-1}, which is a smooth function. We see that the

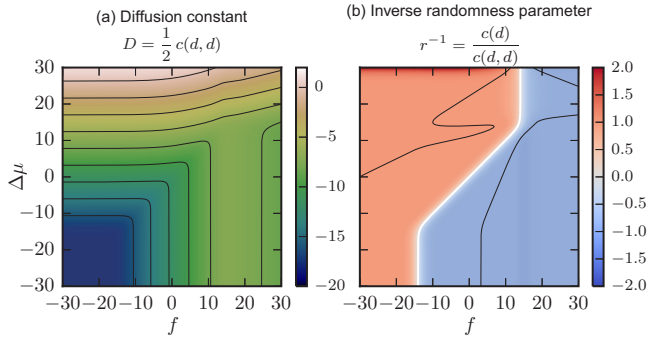

FIG. 7. (Color online) (a) The diffusion constant $D = \frac{1}{2}c(d,d)$ on a decadic logarithmic scale. (b) The inverse randomness parameter $r^{-1} = c(d)/c(d,d) \equiv c(d)/(2D)$ compares the velocity and the diffusion constant. Away from the white stalling line, it obtains an absolute value close to unity. The black solid lines show where $|r| = 1$ holds exactly.

six-state model predicts Poissonian behavior $|r| \approx 1$ in a large area away from the stalling lines. This is in agreement with recent experimental results and theoretical predictions from an alternative model [17].

Our method to calculate the second scaled cumulant and thus the diffusion constant avoids all of the combinatorial complexity of previous approaches [42,43]. Reference [44] treats drift velocity and diffusion in Markovian models formulated for a periodic lattice in arbitrary dimensions. In the present work the topology of physical space is independent from the structure of the graph, which represents the topology of the model: If a system like a molecular motor moves in more than one spatial dimension, one defines a distinct jump observable d_i for each of these dimensions i. Up to a factor of 2, the scaled covariance matrix $c(d_i,d_j)$ then equals the diffusion tensor.

D. Response theory

Equation (15) states that the average velocity $c(d)$ and hydrolysis rate $c(h)$ are conjugate to the mechanical and chemical driving forces $-f$ and $\Delta\mu$. Response theory studies the dependence of averaged currents $\boldsymbol{J} = (c(\varphi_i))_i$ to the conjugate fields $\boldsymbol{E} = (E_i)_i$. For B independent conjugate current-field pairs, $(c(\varphi_i),E_i)_i$, the response matrix $\mathsf{R}(\boldsymbol{E})$ is a $B \times B$ matrix with entries

$$\mathsf{R}_{i,j}(\boldsymbol{E}) := \left.\frac{\partial c(\varphi_i)}{\partial E_j}\right|_{\boldsymbol{E}}. \tag{18}$$

Fluctuation dissipation relations (FDR) relate the response of average currents to their fluctuation statistics. In particular, the Einstein relation relates the mobility of a particle (or its inverse, the friction coefficient) to its diffusion constant. So-called Green-Kubo relations [45] express equilibrium transport coefficients by time-correlation integrals, Eq. (6). Here these time-correlation integrals are obtained as second-order scaled cumulants $c(\varphi_i,\varphi_j)$. The fluctuation relation for the entropy production [6,20] ensures the validity of the following equilibrium FDR [21,24]:

$$\mathsf{R}_{i,j}(\boldsymbol{E} = \boldsymbol{0}) = \frac{1}{2}\,c(\varphi_i,\varphi_j)\big|_{\boldsymbol{E}=\boldsymbol{0}}. \tag{19}$$

With analytical expressions for the average currents $c(\varphi_i)$ one can calculate their derivatives R_{ij}. Because the correlation integrals $c(\varphi_i,\varphi_j)$ are known, our method enables us to probe the nonequilibrium response properties predicted by models of stochastic thermodynamics. As an example, we discuss kinesin's mechanical response using the normalized response coefficient

$$\mathsf{T}_{\text{mech}}(f,\Delta\mu) := \frac{2}{c(d,d)}\frac{\partial c(d)}{\partial(-f)} = -\frac{1}{D}\frac{\partial c(d)}{\partial f}. \tag{20}$$

The equilibrium FDR (19) implies that $\mathsf{T}_{\text{mech}}(0,0) = 1$. As the transition matrix depends smoothly on the driving parameters $(-f,\Delta\mu)$ [11], we expect that there will be a one-dimensional curve in parameter space where $\mathsf{T}_{\text{mech}}(f,\Delta\mu) = 1$.

Figure 8 depicts T_{mech}. As expected, we see that $\mathsf{T}_{\text{mech}}(f,\Delta\mu) = 1$ holds along two lines originating from the origin, such that a nonequilibrium FDR holds for these parameter values. Remarkably, one of these lines coincides with the stalling line $f = f_{\text{stall}}(\Delta\mu)$, i.e., for parameters where the average velocity vanishes.

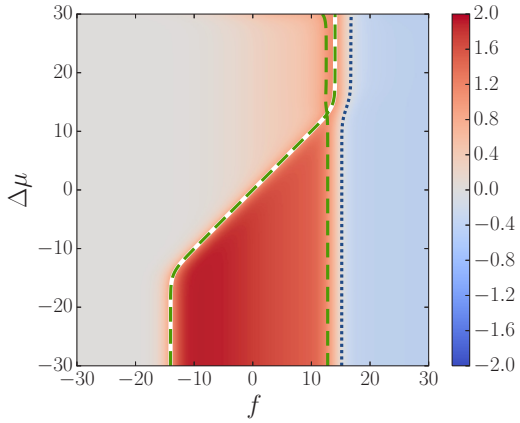

FIG. 8. (Color online) Normalized mechanical response T_{mech}. The dashed green curves indicate $\mathsf{T}_{\text{mech}} = 1$, such that a Green-Kubo FDR (19) holds. One of these curves coincides with the stalling line $f = f_{\text{stall}}(\Delta\mu)$ where the average velocity vanishes (white solid line). The dotted blue line indicates a vanishing transport coefficient. To its right lies a region of negative differential response.

Another nontrivial feature of Fig. 8 is the region where the normalized mechanical response is negative. Since the diffusion constant D is positive, $\mathsf{T}_{\text{mech}} < 0$ implies that the derivative $\partial c(d)/\partial(-f)$ of the mechanical current with respect to its conjugate force is negative. This phenomenon is known as negative differential mobility [46] or, more generally, negative differential response (NDR) [18,47]. The kinesin model predicts negative differential mobility for large-enough pulling forces beyond stalling, i.e., in situations where the motor walks backwards. Then, by pulling more one gets less, i.e., the velocity in pulling direction becomes smaller. This feature might already be visible in the experimental data found in Refs. [16,17]. Although we do not expect to see NDR for arbitrarily high pulling forces in real experiments, explicitly

looking for it in the region for small superstalling forces seems worthwhile.

E. Model comparison

Direct access to the nontrivial features of physical currents allows us to compare different models in detail, both qualitatively and quantitatively. We start by quantitatively comparing the results for the six-state model (Fig. 3) with the simpler four-state model (Fig. 4). Recall that the latter is constructed following the same physical arguments as the former (cf. the Appendix for the details). The results plotted in Figs. 5–8 are all derived from $c(d)$, $c(h)$, and $c(d,d) = 2D$. In Fig. 9 we plot the relative deviations of these quantities between the four-state and the six-state model. Throughout most of the parameter space, they are only a few percentages. This is remarkable, because the observables themselves vary over many orders of magnitude. Note that at the boundaries between different operation modes [Fig. 5(a)], the first cumulants vanish. Hence, we have a divergence in the relative errors unless this happens exactly at the same parameter values in both models.

For the hydrolysis rate $c(h)$ such a divergence is visible in Fig. 9(b) around $(f, \Delta\mu) \simeq (16, 14)$. In principle, this divergence is present wherever $c(h)$ vanishes in the six-state model. In practice, however, the curves of zero average hydrolysis rate $c(h) = 0$ agree almost perfectly, such that the region where the divergence has an effect is extremely small. For most parameters it is hidden due to the finite plotting resolutions and thus not visible in Fig. 9(b). In contrast, the prediction of the stalling forces $f_{\text{stall}}(\Delta\mu)$ agrees exactly between the two models: Figure 9(a) does not exhibit any singularities. In Ref. [13] we introduced a coarse-graining procedure which preserves the cycle topology of a model. By construction, the first cumulants of *all* currents agree between the original and the coarse-grained models. Moreover, the relative error in the diffusion constant is comparable in magnitude to what we see in Fig. 9(c). These *quantitative* results emphasize the value of the cycle perspective introduced in Sec. III D: In order to construct thermodynamically consistent models, one should think of the physics of cycles rather than focusing only on individual transitions.

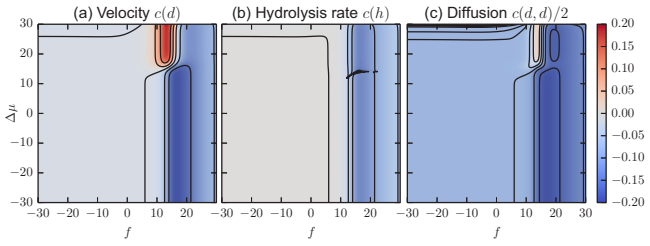

FIG. 9. (Color online) Comparison of our four-state model with the six-state model of Ref. [11]. We show the relative errors $X_4/X_6 - 1$ of the corresponding quantities X_4 and X_6 calculated in the four- and six-state models, respectively. Throughout the parameter range considered, they are almost everywhere well below 15%. Note that for the average hydrolysis rate the relative error diverges close to the line $c(h) = 0$ where the hydrolysis rate in the six-state vanishes. Remarkably, this is not the case for the average velocity, where the stalling lines in both models agree exactly.

Finally, we compare the six-state model to a general model for molecular motors presented in Ref. [48], which was studied in detail in Ref. [12]. Unlike the six-state model studied so far, that model features only two states, which correspond to a strongly and a weakly bound configuration. Multiple transition between these two configurations are possible and represent either an active (i.e., accompanied by a chemical event) or passive displacement along the microtubule. The cycles of the two models differ both in their topology and their interpretation. In particular, the two-state model of Refs. [12,48] has no reference to the "hand-over-hand" stepping mechanism of the forward cycle of Ref. [11], depicted in Fig. 2(b). Moreover, the two-state model was fitted to the experiments of Refs. [14,15], whereas the six-state model used the experimental data from Ref. [16]

Due to the simple structure of the two-state model, an analytical parameter-dependent expression of the scaled cumulant generating function was found in Ref. [12]. Consequently, analytical expression for the scaled cumulants are known and can be compared to the results obtained for the six-state model of Ref. [11], which we used so far. Due to the different nature of the models, we do not expect their predictions to agree quantitatively. In particular, this is the case for parameter values that are far away from values that are realized in the actual experiments, i.e., for small (or even negative) chemical potentials $\Delta\mu$, or negative values of the pulling force. However, for experimentally accessible parameters, it makes sense to look for *qualitative* agreements in the features of the two different kinesin models.

Figure 10 shows the normalized mechanical response Eq. (20) in both models for sensible chemical potential differences ($5 \leqslant \Delta\mu \leqslant 30$) and positive pulling forces. As expected, the models do not agree quantitatively. In particular, the stalling lines are at different positions. However, they show the same qualitative features: the validity of an Einstein FDR at stalling and the emergence of negative differential mobility just above stalling. Together with the experimental hints

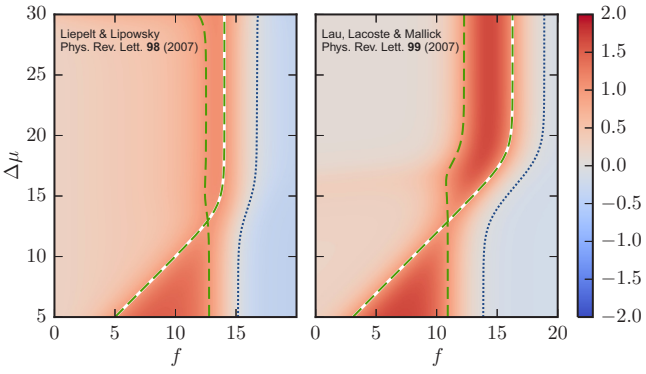

FIG. 10. (Color online) Normalized mechanical response T_{mech} for the six-state model of Ref. [11] studied in the present work (left) and the model from Ref. [12] (right). For experimentally sensible parameters both models predict the same qualitative behavior: The validity of a nonequilibrium Einstein FDR (dashed green curves) at stalling (solid white curve) as well as negative differential response (regions to the right of the dotted blue curve) for superstalling forces. Other features (like the overall structure and magnitude of the response) show the same qualitative behavior of the two models.

from Ref. [16], we consider this agreement as evidence that negative differential mobility is a generic feature of kinesin—a prediction that should be studied by future experiments.

V. CONCLUSION

In the present work, we gave an explicit procedure for the analytical, i.e., fully parameter-dependent, calculation of the statistics of fluctuating currents in stochastic thermodynamics. The algorithm applies to any finite and dynamically reversible Markov model and has been made available as Ref. [26]. We focused on its efficiency in exploring the parameter space of models for the motor protein kinesin, while the mathematical background of the algorithm was the subject of an accompanying paper [10]. In the following we summarize conceptual and physical insights.

From a conceptual point of view, we find the following points particularly noteworthy:

(i) Our algorithm is efficient. After obtaining the fundamental chord cumulants, Eqs. (10) provide fully parameter-dependent expressions for averages and time correlations of arbitrary currents.

(ii) Our algorithm is purely symbolic. Thus it allows simplification and cancellation of zeros. This prevents floating-point inaccuracies even in expressions that vary over many orders of magnitude, cf. Fig. 5(b) or Fig. 7(a).

(iii) Having access to symbolic expressions allows further (algebraic) manipulation and thus the study of derived expressions, cf. Fig. 5(c) or Fig. 7(b). Taking derivatives with respect to external parameters is needed to explore response properties, cf. Eq. (20) and approach (thermodynamic) optimization problems (e.g., efficiency at maximum power, cf. Sec. IV B).

From a physical perspective, our method allows the systematic comparison of the predictions made by various kinesin models, cf. Sec. III. In particular, we gave a detailed account on (quasi-)tight coupling, efficiency of energy conversion, diffusion, and mechanical response for a well-known kinesin model [11] in Secs. IV A–IV D. Moreover, in Sec. IV E we compared these predictions with other models. Regarding the modeling of molecular motors, we emphasize the following:

(i) Current statistics correspond to experimentally observable quantities, like the average motor velocity or its nonequilibrium diffusion constant. Our systematic approach thus extends and unifies previous approaches for calculating these quantities [42–44].

(ii) Thinking of stochastic models in terms of its physical cycles is useful. It allows model reduction, cf. Sec. IV E and Ref. [13].

(iii) Independent models predict two interesting nonequilibrium response properties of kinesin: the validity of a nonequilibrium fluctuation-dissipation relation at mechanical stalling and negative differential mobility for superstalling forces. Both of these predictions lie in realistic parameter regions and can be tested in future experiments.

Modeling the dynamics of molecular motors as random transitions on a biochemical network of states is only one of many appliations of finite Markovian jump processes. The methods established in the present paper apply to any other dynamically reversible model and are easily extended to systems with multiple transitions between states. Thus, they provide a powerful framework to fully explore the physical predictions of any model described by stochastic thermodynamics.

ACKNOWLEDGMENTS

The authors thank Nigel Goldenfeld, Matteo Polettini, and Massimiliano Esposito for insightful discussions. J.V. acknowledges support from a research grant from the "Center for Earth System Research and Sustainability (CliSAP)" at the KlimaCampus Hamburg, while the final version of this manuscript was drafted.

APPENDIX: TRANSITION RATES OF THE FOUR-STATE MODEL FOR KINESIN

The parametrization of the kinesin model on four states (Fig. 4) follows the steps in Ref. [11] for the six-state model (Fig. 3). Transition rates

$$w_j^i := \kappa_j^i \, C_j^i \, \Phi_j^i(f)$$

are obtained as first-order rate constants κ_j^i, which are multiplied by concentration and force-dependent factors. In accordance with first-order rate kinetics, the chemical factor reads

$$C_j^i := \begin{cases} \prod_X [X] & \text{if compound } X \text{ is attached,} \\ 1 & \text{else.} \end{cases}$$

For chemical concentrations which are not too high, the nondimensional chemical potential difference is given by $\Delta\mu = \ln(K_{\mathrm{eq}} \frac{[\mathrm{ATP}]}{[\mathrm{ADP}][\mathrm{P}]})$, where $K_{\mathrm{eq}} = 4.9 \times 10^{11} \mu\mathrm{M}$ is the chemical equilibrium constant for the ATP hydrolysis reaction happening at kinesin's active sites. Like in Ref. [11] we fix $[\mathrm{ADP}] = [\mathrm{P}] = 1\mu\mathrm{M}$ at physiological values and, consequently, vary the concentration of ATP as

$$[\mathrm{ATP}] = \frac{e^{\Delta\mu}}{49} 10^{-10} \mu\mathrm{M}\,.$$

The force-dependent factors Φ_j^i depend on the nondimensionalized pulling force $f = LF/(k_B T)$. They have a different form for mechanical and chemical transitions:

$$\Phi_j^i(f) := \begin{cases} \exp(-\theta f)\,, & \text{if } (i \to j) = (1 \to 3) \\ \exp[(1-\theta) f]\,, & \text{if } (i \to j) = (3 \to 1), \\ \frac{2}{1+\exp[\chi_j^i f]}\,, & \text{else,} \end{cases}$$

where θ and $\chi_j^i = \chi_i^j$ are additional experimental parameters.

For the six-state model the transitions of the forward cycle $\mathcal{F} = \zeta_1$ reflect experimental data. We briefly outline how we use the arguments of Ref. [11] for the parametrization of the four-state model shown in Fig. 4. First note that transitions associated to the edges $(1 \leftrightarrow 3)$ and $(1 \leftrightarrow 4)$ are also present in the six-state model. We thus use similar parametrizations. Transition $(3 \to 4)$ combines ADP release at the leading site with hydrolysis (and immediate P release) at the trailing one. In the six-state model, the same numerical value of the mechanical parameter $\chi_j^i = 0.15$ is used for both of these transitions. We take this as a motivation for using $\chi_4^3 = \chi_3^4 = 0.15$ in the four-state model. Now the only undetermined parameters in the forward cycle are the first-order rate constants κ_4^3 and κ_3^4. The Hill-Schnakenberg

TABLE I. Numerical values of the parameters of the four-state model for kinesin. All first-order reaction rates κ are given in units of s^{-1} or, if attachment of n chemicals is involved, $s^{-1}\,\mu\mathrm{M}^{-n}$. Values correspond to the experimental data in Ref. [16] as stated in Ref. [11]. The equilibrium constant of the ATP hydrolysis reaction is $K_{\mathrm{eq}} = 4.9 \times 10^{11}\,\mu\mathrm{M}$. The parameter $\theta = 0.65$ enters the mechanical factor of the transition rates.

Mechanical transition	$\kappa_3^1 = 3 \times 10^5$	$\kappa_1^3 = 0.24$
Chemical transitions	$\kappa_4^1 = 100$	$\kappa_1^4 = 2.0$
(forward cycle)	$\kappa_3^4 = 2.52 \times 10^6$	$\kappa_4^3 = \frac{K_{\mathrm{eq}}\kappa_3^4\kappa_4^1\kappa_1^3}{\kappa_1^4\kappa_3^1} = 49.3$
Chemical transitions	$\kappa_2^3 = (\frac{\kappa_1^3}{\kappa_3^1})^2\,\kappa_4^1 = 6.4 \times 10^{-11}$	$\kappa_3^2 = \kappa_1^4 = 2.0$
(backward cycle)	$\kappa_1^2 = \kappa_3^4 = 2.52 \times 10^6$	$\kappa_2^1 = \kappa_4^3 = 49.3$
Mechanical load	$\chi_4^3 = \chi_3^4 = \chi_2^1 = \chi_1^2 = 0.15$	$\chi_1^4 = \chi_4^1 = \chi_3^2 = \chi_2^3 = 0.25$

condition $\mathring{\sigma}_1 = -f + \Delta\mu$ for vanishing mechanical driving $f = 0$ yields one additional constraint which can be cast into the expression

$$\frac{\kappa_4^3\kappa_1^4\kappa_3^1}{\kappa_3^4\kappa_4^1\kappa_1^3} \stackrel{!}{=} K_{\mathrm{eq}}.$$

Finally, we take κ_3^4 as a fit parameter that we use to adjust our model to experimental results at the physiological parameter values: We choose it such that the six-state and four-state models yield the same average velocity $c(d)$ for $f = 0$ and $[\mathrm{ATP}] = [\mathrm{ADP}] = [\mathrm{P}] = 1\mu\mathrm{M}$.

The parameters of the remaining transitions are obtained by symmetry. The exception is the first-order constant κ_2^3, associated with ATP release from the leading head. Similarly to Ref. [11] we adjust it in order to account for the Hill-Schnakenberg conditions. On the dissipative cycle $\mathcal{D} = \zeta_2$ this constraint amounts to $\mathring{\sigma}_2 = 2\Delta\mu$ and yields $\kappa_2^3 = (\frac{\kappa_1^3}{\kappa_3^1})^2\,\kappa_4^1$.

At this point, we have determined all the parameters of the four-state model while ensuring the physical and thermodynamic consistency with the original six-state model. Fitting yields $\kappa_3^4 = 2.52 \times 10^6$, which proves to be a good choice globally, cf. Fig. 9. All model parameters are summarized in Table I.

[1] F. Ritort, in *Poincaré Seminar 2003* (Birkhäuser, Basel, 2004), pp. 193–226.
[2] C. Bustamante, J. Liphardt, and F. Ritort, Phys. Today **58**, 43 (2005).
[3] U. Seifert, Eur. Phys. J. B **64**, 423 (2008).
[4] F. Ritort, J. Phys.: Cond. Mat. **18**, R531 (2006).
[5] K. Sekimoto, Suppl. Prog. Theor. Phys. **130**, 17 (1998).
[6] U. Seifert, Rep. Progr. Phys. **75**, 126001 (2012).
[7] T. Hill, J. Theor. Biol. **10**, 442 (1966).
[8] J. Schnakenberg, Rev. Mod. Phys. **48**, 571 (1976).
[9] M. Esposito and C. Van den Broeck, Phys. Rev. E **82**, 011143 (2010).
[10] A. Wachtel, J. Vollmer, and B. Altaner, Phys. Rev. E **92**, 042132 (2015).
[11] S. Liepelt and R. Lipowsky, Phys. Rev. Lett. **98**, 258102 (2007).
[12] A. W. C. Lau, D. Lacoste, and K. Mallick, Phys. Rev. Lett. **99**, 158102 (2007).
[13] B. Altaner and J. Vollmer, Phys. Rev. Lett. **108**, 228101 (2012).
[14] M. J. Schnitzer and S. M. Block, Nature **388**, 386 (1997).
[15] K. Visscher, M. J. Schnitzer, and S. M. Block, Nature **400**, 184 (1999).
[16] N. J. Carter and R. A. Cross, Nature **435**, 308 (2005).
[17] B. E. Clancy, W. M. Behnke-Parks, J. O. L. Andreasson, S. S. Rosenfeld, and S. M. Block, Nat. Struct. Mol. Biol. **18**, 1020 (2011).
[18] R. K. P. Zia and B. Schmittmann, J. Stat. Mech: Theory Exp. (2007) P07012.
[19] T. L. Hill, *Free Energy Transduction in Biology: The Steady-State Kinetic and Thermodynamic Formalism* (Academic Press, New York, 1977).
[20] C. Maes, in *Poincaré Seminar 2003: Bose-Einstein Condensation-Entropy*, edited by J. Dalibard, B. Duplantier, and V. Rivasseau (Birkhäuser, Basel, 2004), p. 145.
[21] J. Lebowitz and H. Spohn, J. Stat. Phys. **95**, 333 (1999).
[22] N. G. van Kampen, *Stochastic Processes in Physics and Chemistry* (Elsevier, Amsterdam, 1992).
[23] S. de Groot and P. Mazur, *Non-Equilibrium Thermodynamics*, Dover Books on Physics Series (Dover, New York, 1984).
[24] D. Andrieux and P. Gaspard, J. Stat. Phys. **127**, 107 (2007).
[25] H. Touchette, Phys. Rep. **478**, 1 (2009).
[26] B. Altaner and A. Wachtel, Git software repository, https://github.com/beralt85/current_cumulants.
[27] D. Lacoste, A. W. C. Lau, and K. Mallick, Phys. Rev. E **78**, 011915 (2008).
[28] S. Liepelt and R. Lipowsky, Phys. Rev. E. **79**, 011917 (2009).
[29] C. Hyeon, S. Klumpp, and J. N. Onuchic, Phys. Chem. Chem. Phys. **11**, 4899 (2009).
[30] W. Zheng, D. Fan, M. Feng, and Z. Wang, Phys. Biol. **6**, 036002 (2009).
[31] K. Svoboda, C. F. Schmidt, B. J. Schnapp, S. M. Block *et al.*, Nature **365**, 721 (1993).
[32] A. Yildiz, M. Tomishige, R. D. Vale, and P. R. Selvin, Science **303**, 676 (2004).
[33] H. Qian, J. Phys.: Condens. Matter **17**, S3783 (2005).

[34] B. Altaner, S. Grosskinsky, S. Herminghaus, L. Katthän, M. Timme, and J. Vollmer, Phys. Rev. E **85**, 041133 (2012).
[35] M. Esposito, K. Lindenberg, and C. Van den Broeck, Phys. Rev. Lett. **102**, 130602 (2009).
[36] G. Verley, M. Esposito, T. Willaert, and C. van den Broeck, Nat. Commun. **5**, 4721 (2014).
[37] M. Polettini, G. Verley, and M. Esposito, Phys. Rev. Lett. **114**, 050601 (2015).
[38] U. Seifert and T. Speck, Eurphys. Lett. **89**, 10007 (2010).
[39] U. Seifert, Phys. Rev. Lett. **106**, 020601 (2011).
[40] M. Baiesi, C. Maes, and K. Netočný, J. Stat. Phys. **135**, 57 (2009).
[41] K. Svoboda, P. P. Mitra, and S. M. Block, Proc. Natl. Acad. Sci USA **91**, 11782 (1994).
[42] Y. R. Chemla, J. R. Moffitt, and C. Bustamante, J. Phys. Chem. B **112**, 6025 (2008).
[43] N. J. Boon and R. B. Hoyle, J. Chem. Phys. **137**, 084102 (2012).
[44] Z. Koza, J. Phys. A: Math. Gen. **32**, 7637 (1999).
[45] E. Helfand, Phys. Rev. **119**, 1 (1960).
[46] O. Bénichou, P. Illien, G. Oshanin, A. Sarracino, and R. Voituriez, Phys. Rev. Lett. **113**, 268002 (2014).
[47] P. Baerts, U. Basu, C. Maes, and S. Safaverdi, Phys. Rev. E **88**, 052109 (2013).
[48] Y. Kafri, D. K. Lubensky, and D. R. Nelson, Biophys. J. **86**, 3373 (2004).

6. Stochastic Thermodynamics for General Finite Systems

In the previous chapter I presented a detailed thermodynamic analysis of a specific model system for molecular motors. We saw that the different currents in the system are quasi-tightly coupled for large parts of the parameter space. Moreover, the system exhibits negative differential mobility far from equilibrium. Nonetheless, at mechanical stalling the response of the displacement velocity agrees with the diffusion constant — reproducing a fluctuation–dissipation relation, but irrespective of the chemical current. A natural question is: how do these features come about, and how generic are they? A subsequent study [1] of my co-author proved that the *localization* of the mechanical force within the network of states is sufficient for such a fluctuation–dissipation relation far from thermodynamic equilibrium.

Is it possible that these features are also present in open chemical reaction networks, even though the emergent cycle forces do not act locally on individual transitions? This latter question is still ongoing research for which I currently do not have a definitive answer. Nonetheless, in the perspectives (chapter 11) I will address some ideas on how to approach this problem, which are inspired by the results that I will present in chapter 7 .

As regards the generality, it is worthwhile to do a small excursion and revisit the theory developed in reference [2]. There, the method to calculate the cumulants relies on analytical expressions for the characteristic polynomial of the biased generator, so that analytical derivatives with respect to the biasing field can be performed with a computer algebra system. However, we realized that it is possible to perform these derivatives explicitly and for general finite systems, at the cost of a slightly increased combinatorial complexity of the expressions.

In this chapter, I provide the preprint for an article *in preparation* explaining our findings. The main result is an iterative equation for a generic cumulant that involves combinations of (i) cumulants of lower order, (ii) hyperbolic functions of cycle forces, as well as (iii) kinetic contributions. Therefore, the major force dependence of the cumulants are hyperbolic functions, and this generic structure explains some of the features we observed in kinesin. Having access to analytical expressions for generic cumulants facilitates a general discussion of the differential response of these cumulants. We especially recover that locality of the force is a sufficient condition for a fluctuation–dissipation relation, and give explicit corrections when this condition is not satisfied. These corrections depend on the system-specific kinetic contributions and still need to be evaluated case-by-case, largely because these kinetic contributions generally also depend on the forces.

References

[1] B. Altaner, M. Polettini, and M. Esposito. “Fluctuation-Dissipation Relations Far from Equilibrium”. In: *Physical Review Letters* 117, 180601 (2016).

[2] A. Wachtel, J. Vollmer, and B. Altaner. “Fluctuating currents in stochastic thermodynamics. I. Gauge invariance of asymptotic statistics”. In: *Physical Review E* 92, 042132 (2015).

The following manuscript is a preprint for
[J. Vollmer, B. Altaner, A. Wachtel. *In preparation.* 2018].
I added pagemarks in the outer margins to provide a continuous pagination throughout the thesis.

Fluctuating currents in stochastic thermodynamics III. Cycle expansion of cumulants

Jürgen Vollmer,[1,2,3] Bernhard Altaner,[4] and Artur Wachtel[5]

[1] *Inst. Nonlinear Dynamics, Faculty of Physics, Georg August University, D-37077 Göttingen, Germany*
[2] *Department of Mathematical Sciences, Politecnico di Torino, Italy*
[3] *Institite for Theoretical Physics, D-04009 University of Leipzig, Germany*
[4] *Physics of Complex Biosystems, Physics Department, Technical University of Munich, James-Franck-Strasse 1, D-85748 Garching, Germany*
[5] *Complex Systems and Statistical Mechanics, Phys. Mat. Sci. Res. Unit, Univ. Luxembourg, Luxembourg*

(Dated: 2018-11-16)

Based on an informed application of Jacobi's formula we derive closed expressions for all cumulants of all antisymmetric obervables of finite Markov processes. This approach provides a fully algebraic representation of the cumulants that does not involve derivatives. The net forces and activities along the cycles play a major role in these expressions—but we also identify additional contributions. The effectiveness of the approach is demonstrated by providing closed expressions for the covariance matrix and the associated response coefficients for currents at arbitrarily strong driving forces.

Keywords: Stochastic Thermodynamics, Scaled Cumulants, Drift, Diffusion, Skewness, Exact Results

I. INTRODUCTION

Modern experimental techniques permit the observation and manipulation of systems at mesoscopic scales. Examples for such mesoscopic systems are bacteria, firing neurons, chemical pathways, and colloidal suspensions in external flows. In general, these systems share two universal features: They behave essentially randomly and follow (statistically) irreversible dynamics. The stochasticity of their dynamics is usually due to fluctuations in energy and particle numbers that arise from the coupling to thermal and chemical reservoirs, respectively. The irreversibility is associated to particle and heat fluxes running through the system.

Mathematically, the dynamics of such systems are often described by Markov processes. Modern statistical physics provides universal sets of tools for their analysis. In particular, the field of stochastic thermodynamics [1] provides a consistent framework for studying thermodynamic properties of fluctuating systems under non-equilibrium conditions.

From the perspective of stochastic thermodynamics, the most important features of non-equilibrium systems are the fluxes of energy and matter that the system exchanges with its environment through various physical mechanisms. When a system connects environments with different values of the intensive quantities, the system experiences a thermodynamic driving force (eg. a temperature gradient, a difference in chemical potential, an external field). The product of the thermodynamic force with its conjugate current (eg. heat, matter, or displacement in the field) gives a distinct contribution to the system's dissipation. [2–4] Importantly, the magnitude of this dissipation is not only determined by the *thermodynamic* parameters describing the environment and thus the magnitude of the thermodynamic forces, but also by the *kinetic* parameters characterizing the system. While thermodynamic parameters prescribe the macroscopic fate of a system in the course of time, kinetic parameters indicate how "active" the system is on the microscopic level. Together they define the average response of the system to a change of external control parameters, as well its flucutations, their skewness and higher-order cumulants.

In this work, we present a framework to study the effect of arbitrary parameter changes on fluctuation statistics of arbitrary thermodynamic current observables to arbitrary order. In particular, our results show that response exhibits universal thermodynamic features which are caused by time-antisymmetric parameters and an additional, non-universal behaviour caused by kinetic parameters. Moreover, the kinetic response properties can still be calculated in a straightforward manner by using combinatorial procedures (graph permutations). As such, the necessary calculations can be done either manually or using the combinatorical libraries that are implemented in common tools for scientific computing, be it symbolic or numeric.

This work is the third part in a series of papers concerned with the statistical properties of the fluctuating thermodynamic currents of extensive quantities. Here we provide further insight into the structure of the response and a framework for efficient calculations. In general the papers target the response to changes in the physical parameters that describe a thermodynamically consistent model. In more mathematical terms, we study the fluctuation spectrum of a current, i.e., the cumulants associated to the corresponding asymptotic probability distribution.

For equilibrium systems, various universal results connecting fluctuations and the response to a change in thermodynamic parameters are known:

- Einstein relations connect the diffusion constant and mobilities [5, 6].
- Green–Kubo integrals allow for the assessment of

non-equilibrium response properties from equilibrium correlation functions [7, 8].

- Onsager identies connect the reciprocal responses of observables to non-conjugate driving parameters. [9–11].

In general, such relations do not hold for systems out of equilibrium, although exceptions have been found under special conditions for stationary non-equilibria [12, 13]. The reason for this is that non-equilibrium steady states are not universal and depend on kinetic parameters. As a consequence, fluctuations in non-equilibrium situations are affected by the excess of *activity* a system experiences by a parameter perturbation [14–16].

Our work is structured as follows:

- Section II: We set the stage by revisiting some concepts from Parts I and II of this series. After that, we give a preview of the main result, where the properties that have been discussed above become evident, without the need for technical details.
- Section III: We show how large deviation theory gives access to the cumulants. In particular, we focus on the algebraic structure of the coefficients obtained from the characteristic polynomial of the skewed transition matrix. The main result is a general closed-form recursion relation for cumulants of arbitrary order based on Laplace' expansion for determinants.
- Section IV: We use Leibniz' permutation formula to explore the important role played by cycles in the network of states. Together with the antisymmetry of physical observables, we identify the general structure of the non-trivial terms in the recursion relation from Sec III. We then discuss novel analytic expressions for currents and response out of equilibrium.
- Section V: We discuss our results and highligh some connections to previous work on linear response out of equilibrium.
- Appendices: In Appendix A, we perform explicit calculations on the simple example system we have used throughout the series.

  In Appendix B, we illustrate the permutation combinatorics for a more complex yet illuminating example.

II. BASIC CONCEPTS AND MAIN RESULT

A. Markov processes and fluctuating currents

We consider a stochastic process that can take N states $v \in \{1, \dots, N\}$. The process is characterized by the probability $p_i(t)$ to find the system in state i at time t. The stochastic process is a Markov process if the evolution of $p_i(t)$ solely depends on the present state. There is no memory of the past evolution. The time evolution of $p_i(t)$ can then be formulated in terms of the transition rates w_j^i. The rates describe how frequently a realization of the stochastic process jumps from state i to state j,

$$\dot{p}_i(t) = \sum_{\substack{j=1 \\ j\neq i}}^{N} (p_j(t)\, w_i^j - p_i(t)\, w_j^i) = \sum_{j=1}^{N} p_j(t)\, w_i^j \tag{1a}$$

with the negative escape rates

$$w_i^i = -\sum_{\substack{j=1 \\ j\neq i}}^{N} w_j^i \,. \tag{1b}$$

Introducing the vector $\boldsymbol{p}(t)$ with components $p_i(t)$ and the $N \times N$ matrix W with entries w_j^i this equation takes the vector form

$$\dot{\boldsymbol{p}}(t) = \mathsf{W}\, \boldsymbol{p}(t) \,. \tag{1c}$$

In the following we consider only Markov processes where the rates w_j^i, and hence also the matrix W, do not depend on time. Moreover, whenever the transition from state i to state j is admissible, so must be the transition from j to i. Formally, this "dynamic reversibility" [17] amounts to the requirement $w_j^i \neq 0 \Leftrightarrow w_i^j \neq 0$ for all $i, j \in \{1, \dots, N\}$.

The set of states $v \in \{1, 2, \dots N\}$ can be viewed as the vertices of a graph , where vertices are connected by edges whenever we find a non-vanishing transition rate between the states. The number of such bidirectional edges is denoted by M. We further assume that the graph is connected.

Time-independence together with the fact that the network is connected and dynamically reversible, implies ergodicity and the existence of a unique steady state [18].

An observable ψ associates the amount ψ_j^i of change of an extensive quantity to each transition from state i to j. The total change of the extensive quantity ψ is a fluctuating time-integrated current, which amounts to the sum of the increments along the trajectory. For a trajectory that starts in a state v_0 and evolves for a time T with τ transitions $v_{j-1} \to v_j, j = 1, \dots, \tau$, we have

$$\Psi(T) = \sum_{j=1}^{\tau} \psi_j^{j-1}.$$

B. Spanning trees and fundamental cycles

A spanning tree for a connected graph with N vertices is a subgraph that connects all vertices by $N-1$ edges. Once a spanning tree is chosen, this leaves $B = M-N+1$ edges of the graph which are called chords. They will be labeled by Greek letters α, β,.... For each chord η_α

we choose and fix an orientation. Adding the chord to the spanning tree creates a circuit. Orienting this circuit along the direction of η_α creates the associated directed fundamental cycle ζ_α.

The fundamental cycles ζ_α form a vector basis for all cycles of the graph. The details of the algebraic and topological properties have been dicussed extensively in [19]. Due to this vector space structure, in what follows we often encounter tuples with B elements that are indexed by α. For briefness of notation we will write B-tuples as vectors and define the scalar product

$$\boldsymbol{a} \cdot \boldsymbol{b} = \sum_{\alpha=1}^{B} a_\alpha b_\alpha.$$

C. Fundamental currents and their cumulants

The fundamental currents Φ_α integrate the number of steps along the chords η_α. Their asymptotic fluctuations are uniquely determined by the scaled cumulant generating function

$$\lambda_*(\boldsymbol{q}) = \lim_{T\to\infty} \frac{1}{T} \ln \langle \exp(\boldsymbol{q}\cdot\boldsymbol{\Phi})\rangle \ .$$

Its derivatives at $\boldsymbol{q} = 0$ are the *scaled cumulants*. A cumulant of order n involves n such derivatives.

For a general n^{th} cumulant we write

$$\mathcal{C}(\alpha_1,\dots,\alpha_n) = \frac{\partial}{\partial q_{\alpha_n}} \cdots \frac{\partial}{\partial q_{\alpha_1}} \lambda_*(\boldsymbol{q})\Big|_{\boldsymbol{q}=\boldsymbol{0}} \tag{2a}$$

where each α_i, $i = 1,\dots,n$ corresponds to one of the fundamental observables defined on the chords. For a finite Markov process the SCGF is differentiable such that the order of applying the derivatives does not matter. Therefore, a cumulant can uniquely be characterized by the multi-index $\boldsymbol{n} = (n_1,\dots,n_B)$ with $n = |\boldsymbol{n}| := \sum_{\alpha=1}^{B} n_\alpha$ that specifies how many derivatives n_α are taken with respect to the entry q_α of $\boldsymbol{q}$. In multi-index notation Eq. (2a) takes the more compact form

$$\mathcal{C}^{\boldsymbol{n}} = \partial_{\boldsymbol{q}}^{\boldsymbol{n}} \lambda_*(\boldsymbol{q})\big|_{\boldsymbol{q}=\boldsymbol{0}} = \lambda_*^{(\boldsymbol{n})}(\boldsymbol{0})\,. \tag{2b}$$

In Wachtel *et al.* [19] we showed that the long-time statistics of a current observable Ψ is equivalent to that of a linear combination of the fundamental currents,

$$\Psi \asymp \sum_{\alpha=1}^{B} \mathring{\psi}_\alpha \Phi_\alpha = \mathring{\boldsymbol{\psi}} \cdot \boldsymbol{\Phi}\,,$$

where $\mathring{\boldsymbol{\psi}} = (\mathring{\psi}_\alpha)_\alpha$ is a B-tuple with entries that give the circulation of the observable ψ around the fundamental cycle ζ_α. More precicely, because of the multi-linearity of the cumulants [20], a general nth cumulant of Ψ reads

$$\sum_{\alpha_1=1}^{B} \mathring{\psi}_{\alpha_1} \sum_{\alpha_2=1}^{B} \mathring{\psi}_{\alpha_2} \cdots \sum_{\alpha_n=1}^{B} \mathring{\psi}_{\alpha_n} c(\alpha_1,\dots,\alpha_n),$$

and is thus fully determined by the nth fundamental cumulants. More generally, this result holds for joint cumulants of several current observables.

D. Nonequilibrium driving forces

A system reaches equilibrium if the stationary state obeys detailed balance. Then, no currents flow in the stationary state. This condition can be made explicit by defining the fundamental forces

$$F_\alpha = \ln \frac{\prod_{(i\to j)\in\zeta_\alpha} w_j^i}{\prod_{(i\to j)\in\zeta_\alpha} w_i^j} = \sum_{(i\to j)\in\zeta_\alpha} \ln \frac{w_j^i}{w_i^j}, \tag{3}$$

as the logarithm of the ratio of the transfer probabilities of traversing the fundamental cycles α in forward and backward direction, respectively. Then, the Kolmogorov cycle criterion guarantees that $\boldsymbol{F} = 0$ is a necessary and sufficient condition for detailed balance and thus equilibrium. In thermodynamically consistent models, the fundamental forces F_α are linear combinations of physical thermodynamic parameters [4, 21].

E. Preview: Main result of this work

Now we have all the pre-requisites in place to present a first glance at the main result of this work: we express the nth cumulant as combinations of cumulants of lower order as well as terms that all have the form

$$\sum_{\boldsymbol{\chi}\in Z_k^{\boldsymbol{m}}} G_k^{\boldsymbol{\chi}} \boldsymbol{\chi}^{\boldsymbol{m}} \mathrm{hyp}_n\Big(\frac{\boldsymbol{\chi}\cdot\boldsymbol{F}}{2}\Big).$$

The different notations will be introduced in detail below. At this point, we give only an overview.

The first sum is over B-tupels $\boldsymbol{\chi}$. They are indicator functions of sets of disjoint cycles $\{\zeta^i\}_i$, where none of the ζ^i have a vertex (and thus also no edge) in common. The corresponding $\boldsymbol{\chi} = (\chi_\alpha)_\alpha$ is defined as the vector with the elements

$$\chi_\alpha\left[\{\zeta^i\}_i\right] = \begin{cases} 1 & \exists i : \eta_\alpha \in \zeta^i, \\ -1 & \exists i : -\eta_\alpha \in \zeta^i, \\ 0 & \text{else.} \end{cases} \tag{4}$$

These $\boldsymbol{\chi}$ are the elements of a set $Z_k^{\boldsymbol{m}}$, where the multi-index $\boldsymbol{m}$ and the integer k prescribe additional topological constraints that must be satisfied by the $\boldsymbol{\chi}$. For simple graphs, most of the sets $Z_k^{\boldsymbol{m}}$ are empty.

The symbol $\boldsymbol{\chi}^{\boldsymbol{m}} \in \{-1,0,1\}$ denotes the product of the entries of $\boldsymbol{\chi}$ according to the multi-index $\boldsymbol{m}$:

$$\boldsymbol{\chi}^{\boldsymbol{m}} := \prod_{\alpha=1}^{B} (\chi_\alpha)^{m_\alpha}, \tag{5}$$

where it is understood that $0^0 = 1$.

The function hyp_n denotes the hyperbolic sine (for n odd) or cosine (for n even). Its argument is one half of the fundamental forces $\boldsymbol{F}$ associated to the entries of $\boldsymbol{\chi}$. This term contains the major dependence of the cumulants on thermodynamic parameters.

Finally, there are the coefficients $G_k^{\boldsymbol{\chi}}$. They are kinetic parameters formed by combinations of the transition rates. In particular, the terms appearing in $G_k^{\boldsymbol{\chi}}$ are formed by the rate products of bi-directional edges $w_j^i w_i^j$ and escape rates w_i^i. As such, they encode aspects of the system's time-symmetric activity [22].

III. CUMULANTS AND LARGE DEVIATION THEORY

The scaled cumulant-generating fucniton and thus the scaled cumulants are accessible using large deviation theory [23, 24]. More precisely, the SCGF is the leading eigenvalue $\lambda_*(\boldsymbol{q})$ of the skewed transition matrix for the chords

$$\hat{\mathsf{W}}(\boldsymbol{q}) = (\hat{w}_j^i : i, j = 1, \dots, N) \tag{6a}$$

$$\text{with} \quad \hat{w}_j^i = \begin{cases} w_j^i \, \exp(+q_\alpha) & \text{if } i \to j = \eta_\alpha \,, \\ w_j^i \, \exp(-q_\alpha) & \text{if } j \to i = \eta_\alpha \,, \\ w_j^i & \text{if } i \to j \in \text{spanning tree.} \end{cases} \tag{6b}$$

Its characteristic polynomial takes the form

$$P(\lambda, \boldsymbol{q}) = \det(\lambda \, \mathsf{1}_N - \hat{\mathsf{W}}(\boldsymbol{q})) = \sum_{k=0}^{N} a_k(\boldsymbol{q}) \, \lambda^k \tag{7}$$

where $\mathsf{1}_N$ is the $N \times N$ identity matrix.

A. Properties of the $a_k(\boldsymbol{q})$

A standard result in (multi)linear algebra is that the coefficients $a_k(\boldsymbol{q})$ of the characteristic polynomial, Eq. (7), are sums of determinants of appropriately chosen submatrices of $\hat{\mathsf{W}}$, or *principal minors*,

$$a_k(\boldsymbol{q}) = (-1)^{N-k} \sum_{\substack{L \subseteq \{1,\dots,N\} \\ |L| = k}} \det \hat{\mathsf{W}}[L] \,. \tag{8}$$

In this work we express these principal minors as determinants of matrices with the same dimension[1] but with modified entries. For a subset $L \subseteq \{1, \dots, N\}$ of states the matrix $\hat{\mathsf{W}}[L]$ has the same elements as $\hat{\mathsf{W}}$ up to the following changes: the elements w_l^l for $l \in L$ are set to one, all other elements in the columns and the rows associated to states in L are set to zero,

$$\hat{\mathsf{W}}[L] = \big(\hat{w}_j^i[L] \colon i, j = 1, \dots, N\big) \quad \text{with} \tag{9a}$$

$$\hat{w}_j^i[L] = \begin{cases} \hat{w}_j^i & \text{if } i \notin L \text{ and } j \notin L \,, \\ 1 & \text{if } i = j \in L \,, \\ 0 & \text{else} \,. \end{cases} \tag{9b}$$

We say that in $\hat{\mathsf{W}}[L]$ the columns and rows of the matrix $\hat{\mathsf{W}}$ associated to the states in L have been *reduced*.

Equation (8) gives rise to the following general properties of the coefficients $a_k(\boldsymbol{q})$ of the characteristic polynomial.

- Up to alternating signs the expressions a_k amount to the sum of all subdeterminants that arise when reducing k rows and the corresponding columns, Eq. (8). Hence, the leading-order coefficient, a_N, always takes the value of 1, the subleading-order coefficient, a_{N-1}, amounts to the negative trace of W, and $a_0 = (-1)^N \det \hat{\mathsf{W}}$.
- The leading-order coefficients do not depend on $\boldsymbol{q}$. In general one can show that the coefficients a_j with $j \in \{N+1-\ell_\alpha, \dots, N\}$ do not depend on q_α when the fundamental cycle associated to α is of length ℓ_α. By construction $\ell_\alpha > 2$ for all cycles. Hence, the three coefficients, a_N, a_{N-1}, and a_{N-2} can not depend on $\boldsymbol{q}$.
- The coefficients of the characteristic polynomial are invariant under the transformation $q_\alpha \to -q_\alpha - F_\alpha$ for all chords α. The symmetry follows by observing that changing the sign of q swaps the role of the forward and the backward direction of the associated fundamental cycle, and that the rates associated to the cycle are swapped by the factors $\exp(\pm F)$ [25].
- Owing to conservation of probability, Eq. (1b), the coefficient a_0 vanishes for $\boldsymbol{q} = \boldsymbol{0}$. As a consequence the characteristic polynomial is solved by $\lambda_*(\boldsymbol{q} = \boldsymbol{0}) = 0$. This root has multiplicity one and all other roots have a negative real part because the Markov process has a unique steady state.

The continuation of this root to values $\boldsymbol{q} \neq 0$ is the scaled cumulant-generating fuction $\lambda_*(\boldsymbol{q})$. Consequently, the derivatives of the SCGF at $\boldsymbol{q} = \boldsymbol{0}$ can be determined via the implicit function theorem Wachtel *et al.* [19], Bruderer *et al.* [26]. In the next two sections we revisit this earlier derivation in order to show how the derivatives in Eq. (2) can be worked out explicitly. To this end, we write derivatives and cumulants in terms of the multi-index $\boldsymbol{n} = (n_1, \dots, n_B)$ that was introduced in Eq. (2b), $a_k^{(\boldsymbol{n})}(\boldsymbol{q}) = \partial_{\boldsymbol{q}}^{\boldsymbol{n}} a_k(\boldsymbol{q})$. We furthermore denote

[1] The more common approach is to remove the columns and rows associated to the vertices in L, leading to a matrix of dimension $(N-k) \times (N-k)$. However, since we only reduce columns and rows symmetrically, the determinant in the end takes the same value. In our setting, the proposed notation facilitates the bookkeeping of multiple reductions since we use the same index set {1, . . . , N} for all stages of reduction.

$\mathcal{C}^{\boldsymbol{n}}$ as $\mathcal{J}^{\boldsymbol{n}}$, $\mathcal{V}^{\boldsymbol{n}}$, and $\mathcal{S}^{\boldsymbol{n}}$ when we wish to indicate that the order of the cumulant is $|\boldsymbol{n}| = 1$, $|\boldsymbol{n}| = 2$, $|\boldsymbol{n}| = 3$, respectively.

B. A Recursion Relation for the Cumulants

In this section we provide a recursion relation for all cumulants, as well as special cases with explicit expressions for the first three cumulants:

The cycle current: amounts to the first cumulant, $\mathcal{C}(\alpha) = \mathcal{J}_\alpha = -\,\partial_{q_\alpha} a_0(\boldsymbol{q})\big|_{\boldsymbol{q}=\boldsymbol{0}} / a_1(\boldsymbol{0})$. This will be shown in Eq. (10a).

The covariance: of the fundamental currents on the cycles α and β is provided by the second cumulant $\mathcal{C}(\alpha,\beta) = \mathcal{V}_{\alpha\beta}$. Its diagonal elements provide the respective diffusivities $2\mathcal{D}_\alpha = \mathcal{V}_{\alpha\alpha}$. In Eq. (10b) we will show that it is a function of $\mathcal{J}_\alpha$, $\mathcal{J}_\beta$ and $\partial_{q_\alpha\, q_\beta} a_0(\boldsymbol{q})$, $\partial_{q_\alpha} a_1(\boldsymbol{q})$, $\partial_{q_\beta} a_1(\boldsymbol{q})$, and a_2 that all must be evaluated at $\boldsymbol{q} = \boldsymbol{0}$.

The skewness: is provided by the third cumulant, $\mathcal{C}(\alpha,\beta,\gamma) = \mathcal{S}_{\alpha\beta\gamma}$. For conciseness we write again $\mathcal{S}_\alpha = \mathcal{S}_{\alpha\alpha\alpha}$. In statistics one commonly normalizes this function with the variance, $\mathcal{S}_\alpha/\mathcal{V}_\alpha^{3/2}$, to characterize how strongly a distribution is skewed. In Eq. (10c) we show how $\mathcal{S}_{\alpha\beta\gamma}$ is related to currents and covariances that have been derived earlier, as well as the third derivative of a_0, second derivatives of a_1, first derivatives of a_2 and on a_3—all evaluated at $\boldsymbol{q} = \boldsymbol{0}$.

The general recursion relation for the cumulants is provided in Eq. (10d). When all derivatives are taken with respect to the same q_α a further simplification can be achieved based on Faà di Bruno's formula. The resulting expression for the n^{th} cumulant is provided in Eq. (11).

1. *First cumulant $\mathcal{J}^{\boldsymbol{n}}$*

For the first cumulant we have $|\boldsymbol{n}| = 1$, *i. e.* $n_l = 1$ for only one particular value of l. In that case the first derivative of $P(\lambda_*(\boldsymbol{q}),\boldsymbol{q})$ only has two terms that do not vanish when evaluating the derivative of P for $\boldsymbol{q} = \boldsymbol{0}$ and $\lambda = 0$,

$$\begin{aligned} 0 &= \partial_{\boldsymbol{q}}^{\boldsymbol{n}} P(\lambda_*(\boldsymbol{q}),\boldsymbol{q})\big|_{\boldsymbol{q}=\boldsymbol{0}} = \partial_{q_{\alpha_l}} P(\lambda_*(\boldsymbol{q}),\boldsymbol{q})\Big|_{\boldsymbol{q}=\boldsymbol{0}} \\ &= \Big[\partial_{q_{\alpha_l}} a_0(\boldsymbol{q}) + a_1(\boldsymbol{0})\, \partial_{q_{\alpha_l}} \lambda_*(\boldsymbol{q})\Big]_{\boldsymbol{q}=\boldsymbol{0}} \\ &= \partial_{q_{\alpha_l}} a_0(\boldsymbol{q})\Big|_{\boldsymbol{q}=\boldsymbol{0}} + a_1(\boldsymbol{0})\, \mathcal{J}_{\alpha_l}\,. \end{aligned}$$

Rearranging terms we find

$$\mathcal{J}^{\boldsymbol{n}} = \mathcal{C}(\alpha_l) = \frac{\partial_{q_{\alpha_l}} a_0(\boldsymbol{q})\Big|_{\boldsymbol{q}=\boldsymbol{0}}}{-a_1(\boldsymbol{0})} = -\frac{a_0^{(\boldsymbol{n})}(\boldsymbol{0})}{a_1(\boldsymbol{0})}\,. \tag{10a}$$

2. *Second cumulant $\mathcal{V}^{\boldsymbol{n}}$*

In order to take the second derivative, $|\boldsymbol{n}| = 2$, of the characteristic polynomial we note that the derivatives of the terms $a_k\lambda_*^k$ for $k > 2$ vanish because $\lambda_*(\boldsymbol{q} = \boldsymbol{0}) = 0$. Employing the multi-index form of the product rule of calculus and exploiting the fact that we can decompose the second derivative with respect to the multi-index $\boldsymbol{n}$ into a sum of multi-indices $(\boldsymbol{m}, \boldsymbol{n}-\boldsymbol{m})$, we find

$$\begin{aligned} 0 &= \partial_{\boldsymbol{q}}^{\boldsymbol{n}} P(\lambda_*(\boldsymbol{q}),\boldsymbol{q})\big|_{\boldsymbol{q}=\boldsymbol{0}} \\ &= a_0^{(\boldsymbol{n})}(\boldsymbol{0}) + \sum_{\boldsymbol{0}\le\boldsymbol{m}\le\boldsymbol{n}} \binom{\boldsymbol{n}}{\boldsymbol{m}} a_1^{(\boldsymbol{n}-\boldsymbol{m})}(\boldsymbol{0})\, \mathcal{C}^{\boldsymbol{m}} + a_2(\boldsymbol{0}) \sum_{\boldsymbol{0}\le\boldsymbol{m}\le\boldsymbol{n}} \binom{\boldsymbol{n}}{\boldsymbol{m}} \mathcal{C}^{\boldsymbol{m}}\, \mathcal{C}^{\boldsymbol{n}-\boldsymbol{m}} \\ &= a_0^{(\boldsymbol{n})}(\boldsymbol{0}) + a_1(\boldsymbol{0})\, \mathcal{V}^{\boldsymbol{n}} + \sum_{\substack{\boldsymbol{0}\le\boldsymbol{m}\le\boldsymbol{n}\\ |\boldsymbol{m}|=1}} \binom{\boldsymbol{n}}{\boldsymbol{m}} a_1^{(\boldsymbol{n}-\boldsymbol{m})}(\boldsymbol{0})\, \mathcal{J}^{\boldsymbol{m}} + a_2(\boldsymbol{0}) \sum_{\substack{\boldsymbol{0}\le\boldsymbol{m}\le\boldsymbol{n}\\ |\boldsymbol{m}|=1}} \binom{\boldsymbol{n}}{\boldsymbol{m}} \mathcal{J}^{\boldsymbol{m}}\, \mathcal{J}^{\boldsymbol{n}-\boldsymbol{m}}\,. \end{aligned}$$

These expressions involve component-wise comparison and binomial factors for multi-indices: For two vectors $\boldsymbol{n} = (n_1,\ldots,n_B)$ and $\boldsymbol{m} = (m_1,\ldots,m_B)$ the expressions $\boldsymbol{m} \le \boldsymbol{n}$ means that each component of $\boldsymbol{m}$ is smaller than or equal to the corresponding component of $\boldsymbol{n}$, $m_\alpha \le n_\alpha$ for each $\alpha \in \{1,\ldots,B\}$. The binomial factors take the common form $\binom{\boldsymbol{n}}{\boldsymbol{m}} = \boldsymbol{n}!/[\boldsymbol{m}!\,(\boldsymbol{n}-\boldsymbol{m})!]$; except that they involve now the multi-index generalization of the factorial, $\boldsymbol{n}! = \prod_{\alpha=1}^{B} n_\alpha!$. Moreover, in this calculation it is understood that $\mathcal{C}^{\boldsymbol{0}} = \lambda_*(\boldsymbol{q} = \boldsymbol{0}) = 0$, and in the third equality the ranges of the sums have been adjusted accordingly.

An expression for $\mathcal{V}^{\boldsymbol{n}}$ is found by rearranging this expression and explicitly working out the non-zero contributions to the sums: In any case we have $\boldsymbol{m}! = 1$ and $(\boldsymbol{n}-\boldsymbol{m})! = 1$. Let us introduce now $\boldsymbol{m}_1$ and $\boldsymbol{m}_2$ with

$|\boldsymbol{m}_1| = |\boldsymbol{m}_2| = 1$ and $\boldsymbol{m}_1 + \boldsymbol{m}_2 = \boldsymbol{n}$. If $\boldsymbol{m}_1 \neq \boldsymbol{m}_2$ then $\boldsymbol{n}! = 1!\,1! = 1$ and the summation index $\boldsymbol{m}$ can take the values $\boldsymbol{m}_1$ and $\boldsymbol{m}_2$. In contrast, when $\boldsymbol{m}_1 = \boldsymbol{m}_2$ then $\boldsymbol{n}! = 2! = 2$ and the summation index $\boldsymbol{m}$ can only take the value $\boldsymbol{m}_1$. Hence, we find

$$\mathcal{V}^{\boldsymbol{n}} = \frac{-1}{a_1(\mathbf{0})}\left[a_0^{(\boldsymbol{n})}(\mathbf{0}) + a_1^{(\boldsymbol{m}_1)}(\mathbf{0})\,\mathcal{J}^{\boldsymbol{m}_2} + a_1^{(\boldsymbol{m}_2)}(\mathbf{0})\,\mathcal{J}^{\boldsymbol{m}_1} + 2\,a_2(\mathbf{0})\,\mathcal{J}^{\boldsymbol{m}_1}\,\mathcal{J}^{\boldsymbol{m}_2}\right]_{\substack{\boldsymbol{m}_1+\boldsymbol{m}_2=\boldsymbol{n}\\ |\boldsymbol{m}_1|=|\boldsymbol{m}_2|=1}} . \tag{10b}$$

3. *Third cumulant $\mathcal{S}^{\boldsymbol{n}}$*

The third derivative of P amounts to the derivative with respect to a multi-index $\boldsymbol{n}$ with $|\boldsymbol{n}| = 3$. It involves the multinomial generalization of the Leibniz formula for products of three and more factors.

$$\begin{aligned}
0 &= \partial_{\boldsymbol{q}}^{\boldsymbol{n}} P(\lambda_*(\boldsymbol{q}),\boldsymbol{q})\big|_{\boldsymbol{q}=\mathbf{0}} \\
&= a_0^{(\boldsymbol{n})}(\mathbf{0}) + a_1(\mathbf{0})\,\mathcal{S}^{\boldsymbol{n}} + \sum_{\substack{\mathbf{0}\le\boldsymbol{m}\le\boldsymbol{n}\\ 0<|\boldsymbol{m}|<|\boldsymbol{n}|}} \binom{\boldsymbol{n}}{\boldsymbol{m}}\, a_1^{(\boldsymbol{n}-\boldsymbol{m})}(\mathbf{0})\,\mathcal{C}^{\boldsymbol{m}} + \sum_{\substack{\mathbf{0}\le\boldsymbol{m}_0,\boldsymbol{m}_1,\boldsymbol{m}_2\le\boldsymbol{n}\\ \boldsymbol{m}_0+\boldsymbol{m}_1+\boldsymbol{m}_2=\boldsymbol{n}\\ |\boldsymbol{m}_1|,|\boldsymbol{m}_2|>0}} \frac{\boldsymbol{n}!}{\boldsymbol{m}_0!\,\boldsymbol{m}_1!\,\boldsymbol{m}_2!}\, a_2^{(\boldsymbol{m}_0)}(\mathbf{0})\,\mathcal{C}^{\boldsymbol{m}_1}\,\mathcal{C}^{\boldsymbol{m}_2} \\
&\quad + a_3(\mathbf{0}) \sum_{\substack{\mathbf{0}\le\boldsymbol{m}_1,\boldsymbol{m}_2,\boldsymbol{m}_3\le\boldsymbol{n}\\ \boldsymbol{m}_1+\boldsymbol{m}_2+\boldsymbol{m}_3=\boldsymbol{n}\\ |\boldsymbol{m}_1|,|\boldsymbol{m}_2|,|\boldsymbol{m}_3|=1}} \frac{\boldsymbol{n}!}{\boldsymbol{m}_1!\,\boldsymbol{m}_2!\,\boldsymbol{m}_3!}\,\mathcal{J}^{\boldsymbol{m}_1}\,\mathcal{J}^{\boldsymbol{m}_2}\,\mathcal{J}^{\boldsymbol{m}_3}
\end{aligned}$$

This provides the $\boldsymbol{n}$-skewness as a sum of terms that involve all possibilities to combine an $\boldsymbol{m}_0$ derivative of the coefficient a_k with k cumulants such that $\boldsymbol{m}_0$ and the derivatives involved in the definitions of the cumulants add up to $\boldsymbol{n}$,

$$\begin{aligned}
\mathcal{S}^{\boldsymbol{n}} = \frac{-1}{a_1(\mathbf{0})}\Bigg[& a_0^{(\boldsymbol{n})}(\mathbf{0}) + \sum_{\substack{\mathbf{0}\le\boldsymbol{m}\le\boldsymbol{n}\\ |\boldsymbol{m}|=1}} \frac{\boldsymbol{n}!}{(\boldsymbol{n}-\boldsymbol{m})!}\left(a_1^{(\boldsymbol{n}-\boldsymbol{m})}(\mathbf{0})\,\mathcal{J}^{\boldsymbol{m}} + a_1^{(\boldsymbol{m})}(\mathbf{0})\,\mathcal{V}^{\boldsymbol{n}-\boldsymbol{m}}\right) \\
& + \boldsymbol{n}! \sum_{\substack{\mathbf{0}\le\boldsymbol{m}_0,\boldsymbol{m}_1,\boldsymbol{m}_2\le\boldsymbol{n}\\ \boldsymbol{m}_0+\boldsymbol{m}_1+\boldsymbol{m}_2=\boldsymbol{n}\\ |\boldsymbol{m}_0|,|\boldsymbol{m}_1|,|\boldsymbol{m}_2|=1}} a_2^{(\boldsymbol{m}_0)}(\mathbf{0})\,\mathcal{J}^{\boldsymbol{m}_1}\,\mathcal{J}^{\boldsymbol{m}_2} + \sum_{\substack{\mathbf{0}\le\boldsymbol{m}\le\boldsymbol{n}\\ |\boldsymbol{m}|=2}} \frac{\boldsymbol{n}!}{\boldsymbol{m}!}\,a_2(\mathbf{0})\,\mathcal{J}^{\boldsymbol{n}-\boldsymbol{m}}\,\mathcal{V}^{\boldsymbol{m}} \\
& + 6\,a_3(\mathbf{0})\,\left(\mathcal{J}^{\boldsymbol{m}_1}\,\mathcal{J}^{\boldsymbol{m}_2}\,\mathcal{J}^{\boldsymbol{m}_3}\right)_{\substack{\boldsymbol{m}_1+\boldsymbol{m}_2+\boldsymbol{m}_3=\boldsymbol{n}\\ |\boldsymbol{m}_1|,|\boldsymbol{m}_2|,|\boldsymbol{m}_3|=1}}\Bigg] .
\end{aligned} \tag{10c}$$

The reason that the a_3-contribution in this expression always involves a factor $3! = 6$ can be found by explicitly working out the situation for different choices of the vector $\boldsymbol{n}$ with $|\boldsymbol{n}| = 3$, in immediate generalization of the argument provided to derive the factor 2 in the a_2-contribution of Eq. (10b). Alternatively, one observes that this contribution to $\mathcal{S}^{\boldsymbol{n}}$ results from the term $a_3\,\lambda^3$ of the characteristic polynomial and that a factor 3! emerges when the three derivatives successively act on the factors λ^3, λ^2 and λ.

C. The general Recursion relation for $\mathcal{C}^{\boldsymbol{n}}$

The derivation of the skewness generalizes in a straightforward manner to a general expression for the cumulant, $\mathcal{C}^{\boldsymbol{n}}$, of order $|\boldsymbol{n}| = n$,

$$\mathcal{C}^{\boldsymbol{n}} = \frac{-1}{a_1(\mathbf{0})}\left[a_0^{(\boldsymbol{n})}(\mathbf{0}) + \sum_{\substack{\mathbf{0}\le\boldsymbol{m}\le\boldsymbol{n}\\ 0<|\boldsymbol{m}|<|\boldsymbol{n}|}} \binom{\boldsymbol{n}}{\boldsymbol{m}}\, a_1^{(\boldsymbol{n}-\boldsymbol{m})}(\mathbf{0})\,\mathcal{C}^{\boldsymbol{m}} + \boldsymbol{n}! \sum_{k=2}^{\min(n,N)} \sum_{\substack{\mathbf{0}\le\boldsymbol{m}_0,\ldots,\boldsymbol{m}_k\le\boldsymbol{n}\\ \boldsymbol{m}_0+\cdots+\boldsymbol{m}_k=\boldsymbol{n}\\ |\boldsymbol{m}_1|,\ldots,|\boldsymbol{m}_k|>0}} \frac{a_k^{(\boldsymbol{m}_0)}(\mathbf{0})}{\boldsymbol{m}_0!} \prod_{l=1}^{k} \frac{\mathcal{C}^{\boldsymbol{m}_l}}{\boldsymbol{m}_l!}\right] . \tag{10d}$$

In general, the terms in this expression cannot further be simplified — except for the following observations:

1. When the shortest cycle that is selected by one of the chords is of length $\ell \geq 3$, then the coefficients, $a_k(\boldsymbol{q})$, do not depend on $\boldsymbol{q}$ for $k \geq N - \ell$. Consequently, one may then demand that $\boldsymbol{m}_0 = \boldsymbol{0}$ in the second sum.

2. Moreover, the same product of cumulants appears $k!$ times in the sum when $m_l, l = 1, \ldots, k$ are all different. At expense of slightly more involved combinatorics the number of terms involved in the recursion can then further be reduced.

3. The result for the special case of the n^{th} cumulant $\mathcal{C}^n(\alpha_s) = \partial^n \lambda_*(\boldsymbol{q})/\partial^n q_{\alpha_s}|_{\boldsymbol{q}=\boldsymbol{0}}$, where all derivatives are taken with respect to the same chord, α_s, is analogous to the collection of terms in the derivation of Faà di Bruno's formula for the n^{th} derivative of a composition of functions [27, 28]. After all, $\lambda_*^k(\boldsymbol{q})$ is the composition of $\lambda_*(\boldsymbol{q})$ with $f(x) = x^k$. One thus finds

$$\mathcal{C}^n = -\frac{1}{a_1}\left[a_0^{(n)}(\boldsymbol{0}) + \sum_{m=1}^{n-1}\binom{n}{m} a_1^{(n-m)}(\boldsymbol{0})\,\mathcal{C}^m + n! \sum_{k=2}^{\min(n,N)} k! \sum_{m=1}^{n} \frac{a_k^{(n-m)}(\boldsymbol{0})}{(n-m)!} \sum_{\substack{l_1,\ldots,l_n \\ n=l_1+2l_2+\cdots+nl_n \\ k=l_1+\cdots+l_n}} \prod_{i=1}^{n} \frac{1}{l_i!}\left(\frac{\mathcal{C}^i}{i!}\right)^{l_i}\right] \tag{11}$$

In Eq. (11) it is understood that all derivatives are taken with respect to the same chord. The constraint on n in the last sum guarantees that there are n derivatives. The condition on k states that the term involves k factors with derivatives of λ, *i. e.* it is a term that originates as a derivative of the $a_k\lambda^k$ term of the characteristic polynomial. Eqs. (10) and (11) provide a recursion relation for the cumulants. They involve only cumulants of smaller order and the derivatives $a_k^{(\boldsymbol{m})}(\boldsymbol{q})$ for $k + |\boldsymbol{m}| = |\boldsymbol{n}|$, evaluated at $\boldsymbol{q} = \boldsymbol{0}$.

D. Summary

Equations (10) provide compact expressions for the cumulants that involve only the coefficients $a_k(\boldsymbol{q})$ and their derivatives. In the next section we provide a cycle expansion for the coefficients $a_k(\boldsymbol{q})$. It provides a very effective approach to calculate the derivatives $a_k^{(\boldsymbol{m})}(\boldsymbol{q})$.

IV. CYCLE EXPANSION OF THE CUMULANTS

In the present section, we demonstrate how the coefficients $a_k(\boldsymbol{q})$ are expressed in terms of (sets of) cycles ζ characterized by some B-tuples $\boldsymbol{\chi}$. We will observe that cycles and associated thermodynamic forces $\boldsymbol{F}$ appear as the argument of a hyperbolic cosine, whereas non-universal dependencies are summarized in kinetic factors G. Specifically, we show that the coefficients $a_k(\boldsymbol{q})$ can be written as

$$a_k(\boldsymbol{q}) = (-1)^{N-k}\left[\frac{G_k^{\emptyset}}{2} + \sum_{\boldsymbol{\chi}\in\mathsf{Z}_k} G_k^{\boldsymbol{\chi}}\,\cosh\left(\boldsymbol{\chi}\cdot\left(\boldsymbol{q}+\frac{\boldsymbol{F}}{2}\right)\right)\right]. \tag{12}$$

Here Z_k is (up to a symmetry) a representation of the set of distinct sets of non-intersecting directed cycles, ζ, that do not involve at least k states. Because all cycles on a graph form a vector space [19, 25, 29], the entries of the vector $\boldsymbol{\chi}$ provide a unique characterization of the directed cycles ζ.

Further, $G_k^{\boldsymbol{\chi}}$ are factors that depend on symmetric products $w_j^i\, w_i^j$ of rates and on the diagonal entries of the (skewed) transition matrix $\hat{\mathsf{W}}$, *cf.* Eq. (6). Hence, they do not depend on $\boldsymbol{q}$. Their explicit form will be provided below in Eq. (15b). Taking derivatives with respect to $\boldsymbol{q}$ is straightforward starting from Eq. (12). No knowledge on the skewed transition matrix is needed to evaluate the expressions, and derivatives where one of the components of $\boldsymbol{n}$ takes a value larger than one —*i. e.* $|\boldsymbol{n}|$ does not agree with the number of non-zero components of $\boldsymbol{n}$— are obtained by trivial changes from the case where the non-zero components all take the value of one. In this section we first derive Eq. (12). Subsequently, we use it to provide a cycle expansion for the cumulants.

A. Cycle expansion of $a_k(\boldsymbol{q})$

We derive Eq. (12) based on the expansion, Eq. (8), of $a_k(\boldsymbol{q})$ in terms of $\det \hat{\mathsf{W}}[L]$, and on the Leibniz formula. The Leibniz formula expresses the determinant $\det \mathsf{A}$ of

an $N \times N$ matrix A in terms of sums of products of its components a^i_j,

$$\det \mathsf{A} = \sum_\pi \operatorname{sign}(\pi) \prod_{i=1}^{N} a^i_{\pi(i)} \,. \tag{13}$$

The sum runs over all permutations π of the tuple $(1,\dots,N)$, *i. e.* bijective maps on the set $\{1,\dots,N\}$. The signature $\operatorname{sign}(\pi)$ of the permutation π takes the value $+1$ (-1) if the permutation results from an even (odd) number of neighboring transpositions of the tuple $(1,\dots,N)$.

When evaluating $\det \hat{\mathsf{W}}[L]$, the product in Eq. (13) involves $\prod_{i=1}^N \hat{w}^i_{\pi(i)}[L]$. This product vanishes unless all states specified in L reside on fixed points (*cf.* Eq. (9)), and unless all transition $(i \to \pi(i))$ are admissible in the dynamics. In the following we therefore restrict the sum to the set P_L of permutations that involve only admissible transitions and keep all states in L fixed. In this case

$$\det \hat{\mathsf{W}}[L] = \sum_{\pi\in\mathsf{P}_L} \operatorname{sign}(\pi) \prod_{i\notin L} \hat{w}^i_{\pi(i)} \,. \tag{14a}$$

Every permutation π can be decomposed into cycles, transpositions and fixed points such that each state is either assigned to a cycle in the graph, a transposition along a bi-directional edge of the graph or a fixed point. The state i is assigned to a fixed point if $\pi(i) = i$, and the state i is assigned to a transposition (i,j), $i \neq j$ if $\pi(i) = j$ and $\pi(j) = i$. Otherwise, it is part of a cycle.

Let ν^L_π be the set of fixed points of π, except for those already specified in L. Moreover, let ε_π be the set of (directed) edges selected by π, and ζ_π be the set of cycles selected by π. Because all cycles are uniquely defined by a set of fundamental cycles, we can encode any set of directed cycles ζ_π uniquely with reference to the chords that serve as our basis. To that end we define the B-tuple $\boldsymbol{\chi}_\pi$ as a directed cycle indicator function that encodes how the cycles in ζ_π traverse the chords $\alpha = (i,j)$:

$$\chi_\pi(\alpha) = \begin{cases} +1 & \text{if } (i,j) \text{ is part of a cycle in } \pi, \\ -1 & \text{if } (j,i) \text{ is part of a cycle in } \pi, \\ 0 & \text{else.} \end{cases} \tag{14b}$$

Conversely, every (set of) cycles ζ is uniquely determined by a mapping $\zeta = \zeta(\boldsymbol{\chi})$ where $\boldsymbol{\chi}$ is a B-tuple interpreted as a directed cycle-indicator function. Henceforth, we make use of this mapping between sets of cycles and B-tuples to obtain a more concise notation.

With these notations we can explicitly write out the $\boldsymbol{q}$ dependence of $\det \hat{\mathsf{W}}[L]$,

$$\begin{aligned} \prod_{i\notin L} \hat{w}^i_{\pi(i)} &= \prod_{m\in\nu^L_\pi} \hat{w}^m_m \times \prod_{(i\to j)\in\varepsilon_\pi} \hat{w}^i_j \hat{w}^j_i \times \prod_{(i\to j)\in\zeta_\pi} \hat{w}^i_j \\ &= \prod_{m\in\nu^L_\pi} w^m_m \times \prod_{(i\to j)\in\varepsilon_\pi} w^i_j w^j_i \times \mathrm{e}^{\boldsymbol{\chi}_\pi\cdot\boldsymbol{q}} \prod_{(i\to j)\in\zeta_\pi} w^i_j \end{aligned}$$

By construction of the skewed transition matrix the diagonal elements $\hat{w}^i_i$ of the skewed transition matrix $\hat{\mathsf{W}}$ do not depend on $\boldsymbol{q}$, the factors involving $\boldsymbol{q}$ cancel for transpositions, and they have been written out explicitly in the exponential factors for the longer cycles.

We can further simplify the third factor by using the definition of the driving forces Eq. (3):

$$\mathrm{e}^{\boldsymbol{\chi}\cdot\boldsymbol{q}} \prod_{(i\to j)\in\zeta} w^i_j = \mathrm{e}^{\boldsymbol{\chi}\cdot(\boldsymbol{q}+\boldsymbol{F}/2)} \sqrt{\prod_{(i\to j)\in\zeta} w^i_j \, w^j_i} \tag{14c}$$

This expression holds for any set of directed cycles $\zeta = \zeta(\boldsymbol{\chi}_\pi)$. Notice that it is symmetric with respect to reversing the arbitrary definition of the chord orientation. After all, if the direction of one chord is reversed, the corresponding component in each of the three vectors $\boldsymbol{\chi}$, $\boldsymbol{q}$, and $\boldsymbol{F}$ changes its sign, while the term in the square root is invariant.

Now, we insert Eq. (14a) into Eq. (8) and evaluate the resulting double sum. It involves all partitions of the N states such that k states, denoted by L, are left aside and the others are divided into fixed points, ν, transpositions, ε, and cycles, ζ. In order to effectively evaluate the sum we factor out common terms and perform the summation in different order. To this end we introduce the following sets (*cf.* Fig. 3 in Appendix B for a non-trivial worked example)

Z_k. The set of indicator functions $\boldsymbol{\chi}$ that specify the sets $\zeta = \zeta(\boldsymbol{\chi})$ of non-intersecting cycles that never visit at least k states and are oriented in such a way that the first non-vanishing entry of $\boldsymbol{\chi}$ takes the value 1. This set does not contain the empty set, $\zeta = \emptyset$, which is treated separately. See Appendix B for a worked example.

$\mathsf{E}^{\boldsymbol{\chi}}_k$. The set of sets ε of non-overlapping transpositions along directed edges that neither involve any state visited by the cycles in $\zeta(\boldsymbol{\chi})$ nor at least k other states. To the very least this set contains the empty set, $\varepsilon = \emptyset$.

$\mathsf{F}^{\varepsilon\boldsymbol{\chi}}_k$. The set of sets ν of points that neither involve any state visited by the cycles in $\zeta(\boldsymbol{\chi})$, nor are part of any transpositions in ε, nor involve k other states. This set may contain the empty set, but it need not.

The definition of the set Z_k specifies a constraint on the direction of the cycles. Notice that without this constraint, $\boldsymbol{\chi} \in \mathsf{Z}_k$ would imply that also $-\boldsymbol{\chi} \in \mathsf{Z}_k$, where $-\boldsymbol{\chi}$ contains the directed cycles $\zeta(\boldsymbol{\chi})$ with their orientations reversed. With the constraint present, only one representant of the conjugate pair appears in $\boldsymbol{\chi} \in \mathsf{Z}_k$.

Now observe that the sum Eq. (14a) includes all permutations: In particular, for a permutation with cycles ζ_π with cycle-indicator $\boldsymbol{\chi}_\pi$, there is exactly one other permutation π^* that contains the same fixed points and transpositions, but all the cycles in reversed orientation, *i. e.* $\nu^L_\pi = \nu^L_{\pi^*}$, $\varepsilon_\pi = \varepsilon_{\pi^*}$ but has $\boldsymbol{\chi}_\pi = -\boldsymbol{\chi}_{\pi^*}$.

Permutations that differ only by the orientation of its cycles will constitute a summand that only differs by the sign of the argument of the exponential function in Eq. (14c). They have the same sign, because the sign of a permutation π is determined only by the number of transpositions and is thus independent of the orientation of its cyclic parts. Thus, the two exponential functions appearing for π and π^* can be summarized as a hyperbolic cosine. Altogether, we thus obtain the cycle expansion anticipated in Eq. (12), where each summand appearing in the sum $\sum_{\boldsymbol{\chi}\in Z_k}$ originates from a pair of conjugate exponential factors given by Eq. (14c):

$$\begin{aligned} a_k(\boldsymbol{q}) &= (-1)^{N-k} \sum_{\substack{L\subseteq\{1,\dots,N\}\\ |L|=k}} \sum_{\pi\in\mathsf{P}_L} \operatorname{sign}(\pi)\, \mathrm{e}^{\boldsymbol{\chi}_\pi\cdot(\boldsymbol{q}+\boldsymbol{F}/2)} \sqrt{\prod_{(i\to j)\in\zeta_\pi} w_j^i\, w_i^j} \left(\prod_{(i\to j)\in\varepsilon_\pi} w_j^i w_i^j\right) \left(\prod_{m\in\nu_\pi^L} w_m^m\right) \\ &= (-1)^{N-k} \left[\frac{G_k^\emptyset}{2} + \sum_{\boldsymbol{\chi}\in\mathsf{Z}_k} G_k^{\boldsymbol{\chi}} \cosh\left(\boldsymbol{\chi}\cdot\left(\boldsymbol{q}+\frac{\boldsymbol{F}}{2}\right)\right)\right], \end{aligned} \tag{15a}$$

$$\text{with}\qquad G_k^{\boldsymbol{\chi}} = 2\operatorname{sign}(\zeta(\boldsymbol{\chi}))\sqrt{\prod_{(i\to j)\in\zeta(\boldsymbol{\chi})} w_j^i\, w_i^j} \sum_{\varepsilon\in\mathsf{E}_k^{\boldsymbol{\chi}}} \left[\operatorname{sign}(\varepsilon)\left(\prod_{(i\to j)\in\varepsilon} w_j^i\, w_i^j\right) \sum_{\nu\in\mathsf{F}_k^{\varepsilon\boldsymbol{\chi}}} \prod_{m\in\nu} w_m^m\right]. \tag{15b}$$

Note that the factor of 2 in the definition of the hyperbolic cosine is absorbed into the definition of $G_k^{\boldsymbol{\chi}}$. Evaluation then proceeds by first selecting cycles, then transpositions and finally fixed points such that k states are left aside. Then the products of the rates are evaluated and combined.

B. The derivatives $a_k^{(\boldsymbol{n})}(\boldsymbol{q})$

The first derivative of Eq. (15) with respect to a component q_α of $\boldsymbol{q}$ is

$$\frac{\partial a_k(\boldsymbol{q})}{\partial q_\alpha} = \sum_{\boldsymbol{\chi}\in\mathsf{Z}_k(\alpha)} G_k^{\boldsymbol{\chi}}\, \chi(\alpha)\, \sinh\left(\boldsymbol{\chi}\cdot\left(\boldsymbol{q}+\frac{\boldsymbol{F}}{2}\right)\right). \tag{16}$$

The derivative introduces a factor $\chi(\alpha)$ in the sum, and it turns the hyperbolic cosine into a sine. We may then restrict the sum to summands where $\chi(\alpha)\neq 0$, *i. e.* require that ζ *must* traverse through α. The accordingly restricted set will be denoted as $\mathsf{Z}_k(\alpha)$.

Further derivatives swap sinh to cosh and vice versa. This is accounted for by introducing

$$\operatorname{hyp}_n(x) = \begin{cases} \sinh(x) & \text{for } n \text{ odd},\\ \cosh(x) & \text{for } n \text{ even}. \end{cases} \tag{17a}$$

Moreover, the inner derivative of $\operatorname{hyp}_n(\boldsymbol{\chi}\cdot(\boldsymbol{q}+\boldsymbol{F}/2))$ generates a product of components of $\boldsymbol{\chi}$. For the $\boldsymbol{n}^{\text{th}}$ derivative the overall factor is the product of the element-wise power

$$\boldsymbol{\chi}^{\boldsymbol{n}} = \prod_{\alpha=1}^{B} (\chi(\alpha))^{n_\alpha}. \tag{17b}$$

Here n_α are the components of $\boldsymbol{n}$ and it is understood that $0^0 = 1$.

The resulting cycle expansion should only involve cycles ζ where $\chi(\alpha)\neq 0$ for all α with $n_\alpha > 0$. Only those sets of cycles ζ contribute where ζ traverses through all chords where $\boldsymbol{n}$ has non-vanishing entries. The set of these cycles is denoted as $\mathsf{Z}_k^{\boldsymbol{n}} \subseteq \mathsf{Z}_k$. Hence, we obtain the cycle expansion of the $\boldsymbol{n}^{\text{th}}$ derivative of $a_k(\boldsymbol{q})$,

$$a_k^{(\boldsymbol{n})}(\boldsymbol{0}) = (-1)^{N-k} \sum_{\boldsymbol{\chi}\in\mathsf{Z}_k^{\boldsymbol{n}}} G_k^{\boldsymbol{\chi}}\, \boldsymbol{\chi}^{\boldsymbol{n}}\, \operatorname{hyp}_{|\boldsymbol{n}|}\!\left(\tfrac{\boldsymbol{\chi}\cdot\boldsymbol{F}}{2}\right) \tag{18}$$

with $G_k^{\boldsymbol{\chi}}$ as defined in Eq. (15b). In the remainder of this section we provide the resulting cycle expansions for the cumulants.

C. Cycle expansion of currents

We provide the cycle expansions for the cumulants, Eqs. (10), with the understanding that $a_k^{(\boldsymbol{n})}(\boldsymbol{q})$ is evaluated for $\boldsymbol{q}=\boldsymbol{0}$. In the following we hence suppress the argument of this function.

Inserting Eq. (16) into Eq. (10a) expresses the currents in terms of the forces $\boldsymbol{F}$

$$\mathcal{J}_\alpha = \frac{(-1)^{N+1}}{a_1} \sum_{\boldsymbol{\chi}\in\mathsf{Z}_0(\alpha)} G_0^{\boldsymbol{\chi}}\, \chi(\alpha)\, \sinh\frac{\boldsymbol{\chi}\cdot\boldsymbol{F}}{2}. \tag{19}$$

Here, $\boldsymbol{\chi}\cdot\boldsymbol{F}$ is the net force acting along the cycle(s in) $\zeta(\boldsymbol{\chi})$. By construction, $\boldsymbol{\chi}\cdot\boldsymbol{F}$ always involves the summand F_α (and thus $\chi(\alpha)\in\{-1,+1\}$. Note, however, that the scalar product $\boldsymbol{\chi}\cdot\boldsymbol{F}$ involves additional fundamental forces F_β when ζ also passes through other chords

η_β. Typically $\mathsf{Z}_0(\alpha)$ does not involve many terms and the cycles substantially reduce the amount of terms contributing to G_0^ζ. The terms $G_0^\emptyset$, which contribute the major part of the permutations (*cf.* the example in the appendix) need not be calculated. The main computational effort is therefore spent on evaluating a_1.

D. Cycle expansion of covariances

The expression (10b) for the covariance provides the cycle expansion

$$\mathcal{V}^{\boldsymbol{n}} = \frac{(-1)^{N+1}}{a_1} \Bigg[\sum_{\boldsymbol{\chi}\in\mathsf{Z}_0^{\boldsymbol{n}}} G_0^{\boldsymbol{\chi}}\, \boldsymbol{\chi}^{\boldsymbol{n}}\, \cosh\frac{\boldsymbol{\chi}\cdot\boldsymbol{F}}{2} - \mathcal{J}^{\boldsymbol{m}_1} \sum_{\boldsymbol{\chi}\in\mathsf{Z}_1^{\boldsymbol{m}_2}} G_1^{\boldsymbol{\chi}}\, \boldsymbol{\chi}^{\boldsymbol{m}_2}\, \sinh\frac{\boldsymbol{\chi}\cdot\boldsymbol{F}}{2} - \mathcal{J}^{\boldsymbol{m}_2} \sum_{\boldsymbol{\chi}\in\mathsf{Z}_1^{\boldsymbol{m}_1}} G_1^{\boldsymbol{\chi}}\, \boldsymbol{\chi}^{\boldsymbol{m}_1}\, \sinh\frac{\boldsymbol{\chi}\cdot\boldsymbol{F}}{2} + 2a_2\, \mathcal{J}^{\boldsymbol{m}_1}\, \mathcal{J}^{\boldsymbol{m}_2} \Bigg]_{\substack{\boldsymbol{m}_1+\boldsymbol{m}_2=\boldsymbol{n} \\ |\boldsymbol{m}_1|=|\boldsymbol{m}_2|=1}} . \tag{20a}$$

It involves the hitherto unknown factors $G_1^{\boldsymbol{\chi}}$ and a_2. The former only differ from $G_0^{\boldsymbol{\chi}}$ by the further restriction of the set of admissible cycles ζ and chords ε, and a different choice of the sets $\mathsf{F}_1^{\varepsilon\boldsymbol{\chi}}$ in the inner sum of Eq. (15b). Without substantial additional effort they can be evaluated together with $G_0^{\boldsymbol{\chi}}$.

E. Cycle expansion of higher-order cumulants

The main findings for the second cumulants, Eq. (20a), carry over to higher order. When evaluating the skewness, Eq. (10c), there are the factors $G_2^{\boldsymbol{\chi}}$ and a_3 appearing that have not been determined before,

$$\begin{aligned}\mathcal{S}^{\boldsymbol{n}} = \frac{(-1)^{N+1}}{a_1} \Bigg[& \sum_{\boldsymbol{\chi}\in\mathsf{Z}_0^{\boldsymbol{n}}} G_0^{\boldsymbol{\chi}}\, \boldsymbol{\chi}^{\boldsymbol{n}}\, \sinh\frac{\boldsymbol{\chi}\cdot\boldsymbol{F}}{2} \\ & - \sum_{\substack{\boldsymbol{0}\le\boldsymbol{m}\le\boldsymbol{n} \\ |\boldsymbol{m}|=1}} \frac{\boldsymbol{n}!}{(\boldsymbol{n}-\boldsymbol{m})!} \left(\mathcal{J}^{\boldsymbol{m}} \sum_{\boldsymbol{\chi}\in\mathsf{Z}_1^{\boldsymbol{n}-\boldsymbol{m}}} G_1^{\boldsymbol{\chi}}\, \boldsymbol{\chi}^{\boldsymbol{n}-\boldsymbol{m}}\, \cosh\frac{\boldsymbol{\chi}\cdot\boldsymbol{F}}{2} + \mathcal{V}^{\boldsymbol{n}-\boldsymbol{m}} \sum_{\boldsymbol{\chi}\in\mathsf{Z}_1^{\boldsymbol{m}}} G_1^{\boldsymbol{\chi}}\, \boldsymbol{\chi}^{\boldsymbol{m}} \sinh\frac{\boldsymbol{\chi}\cdot\boldsymbol{F}}{2} \right) \\ & + \boldsymbol{n}! \sum_{\substack{\boldsymbol{0}\le\boldsymbol{m}_0,\boldsymbol{m}_1,\boldsymbol{m}_2\le\boldsymbol{n} \\ \boldsymbol{m}_0+\boldsymbol{m}_1+\boldsymbol{m}_2=\boldsymbol{n} \\ |\boldsymbol{m}_0|=|\boldsymbol{m}_1|=|\boldsymbol{m}_2|=1}} \mathcal{J}^{\boldsymbol{m}_1}\, \mathcal{J}^{\boldsymbol{m}_2} \sum_{\boldsymbol{\chi}\in\mathsf{Z}_2^{\boldsymbol{m}_0}} G_2^{\zeta}\, \boldsymbol{\chi}^{\boldsymbol{m}_0}\, \sinh\frac{\boldsymbol{\chi}\cdot\boldsymbol{F}}{2} + \sum_{\substack{\boldsymbol{0}\le\boldsymbol{m}\le\boldsymbol{n} \\ |\boldsymbol{m}|=2}} \frac{\boldsymbol{n}!}{\boldsymbol{m}!}\, a_2\, \mathcal{J}^{\boldsymbol{n}-\boldsymbol{m}}\, \mathcal{V}^{\boldsymbol{m}} \\ & + 6\, a_3\, \left(\mathcal{J}^{\boldsymbol{m}_1}\, \mathcal{J}^{\boldsymbol{m}_2}\, \mathcal{J}^{\boldsymbol{m}_3}\right)_{\substack{\boldsymbol{m}_1+\boldsymbol{m}_2+\boldsymbol{m}_3=\boldsymbol{n} \\ |\boldsymbol{m}_1|=|\boldsymbol{m}_2|=|\boldsymbol{m}_3|=1}} \Bigg] . \end{aligned} \tag{20b}$$

In general, on the $n = |\boldsymbol{n}|^{\text{th}}$ level of the recursion one must determine a_n and the factors $G^{\boldsymbol{\chi}}_{n-1}$,

$$\mathcal{C}^{\boldsymbol{n}} = \frac{(-1)^{N+1}}{a_1} \left[\sum_{\boldsymbol{\chi}\in\mathsf{Z}_0^{\boldsymbol{n}}} G_0^{\boldsymbol{\chi}}\ \boldsymbol{\chi}^{\boldsymbol{n}}\ \mathrm{hyp}_{|\boldsymbol{n}|}\frac{\boldsymbol{\chi}\cdot\boldsymbol{F}}{2} - \sum_{\substack{\boldsymbol{0}\le\boldsymbol{m}\le\boldsymbol{n}\\ 0<|\boldsymbol{m}|<|\boldsymbol{n}|}} \binom{\boldsymbol{n}}{\boldsymbol{m}} \mathcal{C}^{\boldsymbol{n}-\boldsymbol{m}} \sum_{\boldsymbol{\chi}\in\mathsf{Z}_1^{\boldsymbol{m}}} G_1^{\boldsymbol{\chi}}\ \boldsymbol{\chi}^{\boldsymbol{m}}\ \mathrm{hyp}_{|\boldsymbol{n}|}\frac{\boldsymbol{\chi}\cdot\boldsymbol{F}}{2} \right.$$
$$\left. + \boldsymbol{n}! \sum_{k=2}^{\min(n,N)} (-1)^k \sum_{\substack{\boldsymbol{m}_0,\boldsymbol{m}_1,\dots,\boldsymbol{m}_k\\ \boldsymbol{m}_0+\cdots+\boldsymbol{m}_k=\boldsymbol{n}\\ |\boldsymbol{m}_1|,\dots,|\boldsymbol{m}_k|>0}} \left(\prod_{i=1}^{k}\frac{\mathcal{C}^{\boldsymbol{m}_i}}{\boldsymbol{m}_i!}\right) \sum_{\boldsymbol{\chi}\in\mathsf{Z}_k^{\boldsymbol{m}_0}} \frac{G_k^{\boldsymbol{\chi}}\ \boldsymbol{\chi}^{\boldsymbol{m}_0}}{\boldsymbol{m}_0!}\ \mathrm{hyp}_{|\boldsymbol{n}|}\frac{\boldsymbol{\chi}\cdot\boldsymbol{F}}{2} \right] . \tag{20c}$$

The equations (20) are the central result of this work. We will discuss their implications in the following section. Let us here comment on the combinatorial complexity of the general recursion relation, Eq. (20c). The right hand side appears to involve a lot of terms and suffer from combinatorial explosion in complexity. However, there are additional restricitons hidden in the definition in the objects appearing here which in fact ensure that a lot of terms vanish. Note especially that n is always smaller than N and furthermore $\mathsf{Z}_k^{\boldsymbol{m}}$ must be the empty set when $|\boldsymbol{m}| \ge N-k-3$.

V. DISCUSSION

The cycle expansions (20) reduce the calculation of cumulants to the combinatorical problem of efficiently running through cycle decompositions of the graph defining the Markov process—rather than involving the algebraic computation of determinants and taking their derivatives, as presented in Wachtel *et al.* [19]. Moreover, it is remarkable that they explicitly provide a substantial part of the dependence of the cumulants on the thermodynamic driving forces $\boldsymbol{F}$.

Thermodynamic consistency specifies how the thermodynamic forces are connected to the physical intensive variables that characterize the environment. In constrst, the factors $G_k^{\boldsymbol{\chi}}$ depend on both the intensive variables and other system-dependent parameters. In order to discuss the general aspects of response, we thus need to invoke concrete parametrizations of the rates. However, we can already discuss general insights that can be achieved that do not depend on the choice of parametrization.

A. Stalling forces, ratios of currents and the randomness parameter

Equation (19) provides an extremely efficient way to predict experimentally observable quantities without the need to evaluate all the coefficients. After all, the factor a_1 cancels out when calculating these quantities.

First, note that the ratio of the currents $\mathcal{J}_\alpha$ and $\mathcal{J}_\beta$ amounts to

$$\frac{\mathcal{J}_\alpha}{\mathcal{J}_\beta} = \frac{a_0^{(\alpha)}}{a_0^{(\beta)}} = \frac{\displaystyle\sum_{\boldsymbol{\chi}\in\mathsf{Z}_0(\alpha)} G_0^{\boldsymbol{\chi}}\ \chi(\alpha)\ \sinh\frac{\boldsymbol{\chi}\cdot\boldsymbol{F}}{2}}{\displaystyle\sum_{\boldsymbol{\chi}\in\mathsf{Z}_0(\beta)} G_0^{\boldsymbol{\chi}}\ \chi(\beta)\ \sinh\frac{\boldsymbol{\chi}\cdot\boldsymbol{F}}{2}} . \tag{21}$$

Second, the stalling condition for a single chord current, $\mathcal{J}_\alpha = 0$, can be achieved by solving the implicit equation

$$0 = \sum_{\boldsymbol{\chi}\in\mathsf{Z}_0(\alpha)} G_0^{\boldsymbol{\chi}}\ \chi(\alpha)\ \sinh\frac{\boldsymbol{\chi}\cdot\boldsymbol{F}}{2} . \tag{22}$$

Its solution is a set of force values known as *stalling forces*.

To leading order in the strength of the current $\mathcal{J}_\alpha$, the factors $G_0^{\boldsymbol{\chi}}$ also provide the force dependence of the randomness parameter (also called Fano factor), *i. e.* the ratio of the diffusivity and the associated current. After all, according to Eqs. (10b) and (20a)

$$\frac{\mathcal{V}_\alpha}{\mathcal{J}_\alpha} = \frac{a_0^{(\alpha\alpha)}}{a_0^{(\alpha)}} - 2\,\frac{a_1^{(\alpha)}}{a_1} - \frac{2\,a_2}{a_1}\,\mathcal{J}_\alpha \tag{23a}$$
$$= \frac{\displaystyle\sum_{\boldsymbol{\chi}\in\mathsf{Z}_0(\alpha)} G_0^{\boldsymbol{\chi}}\ \cosh\frac{\boldsymbol{\chi}\cdot\boldsymbol{F}}{2}}{\displaystyle\sum_{\boldsymbol{\chi}\in\mathsf{Z}_0(\alpha)} G_0^{\boldsymbol{\chi}}\ \chi(\alpha)\ \sinh\frac{\boldsymbol{\chi}\cdot\boldsymbol{F}}{2}}$$
$$+ \frac{4}{a_1}\sum_{\boldsymbol{\chi}\in\mathsf{Z}_1(\alpha)} G_1^{\boldsymbol{\chi}}\ \chi(\alpha)\ \sinh\frac{\boldsymbol{\chi}\cdot\boldsymbol{F}}{2} - \frac{2a_2}{a_1}\,\mathcal{J}_\alpha . \tag{23b}$$

The second and third term on the right-hand side are always finite. In contrast, the first term diverges when $\mathcal{J}_\alpha$ approaches zero, *i. e.* in particular in the limit of small driving forces. Hence, $a_0^{(\alpha\alpha)}/a_0^{(\alpha)}$ dominates the randomness parameter in this limit. The numerator and the denominator of this ratio are the same up to the signs $\chi(\alpha) = \pm 1$ and swapping the hyperbolic sine into a cosine. When one of the summands dominates, the dependence reduces to a hyperbolic (co)tangent.

For larger currents the additional terms involve a_1, a_2 and the current $\mathcal{J}_\alpha$. Hence, the terms a_1, a_2 and $G_1^{\boldsymbol{\chi}}$ must be evaluated to evaluate the randomness parameter at large forces.

B. Response theory

Response theory considers the behaviour of a physical observable (*i. e.*, a cumulant) when some physical parameter h that characterizes the transition rates of the system $\mathsf{W}(h)$ is changed. In linear response theory, we usually consider infinitesimal changes $h \to h + \mathrm{d}h$ while keeping all other parameters constant. Thermodynamic response theory is concerned with the response of a physical current to its conjugate driving forces.

In the present context, the fundamental currents J_α and the fundamental driving forces F_α amount to a set of conjugate thermodynamic currents and forces. This means, that the steady-state entropy production Σ can be written as [4, 10, 25, 29]

$$\Sigma = \sum_\alpha J_\alpha F_\alpha. \tag{24}$$

The response coefficients

$$R_{\alpha,\beta} = \frac{\partial \mathcal{J}_\alpha}{\partial F_\beta} \tag{25}$$

characterize the change of the current $\mathcal{J}_\alpha$ in response to varying the thermodynamic force F_β. For the above partial derivative to be well-defined, one assumes that we have a parametrization of the $2E$ transition rates such that the components of the force vector $\boldsymbol{F}$ can be varied independently and that all remaining parameters are set constant, *i. e.* that

$$\mathsf{W} = \mathsf{W}(\boldsymbol{F}, \{2E - B\} \text{ other parameters}). \tag{26}$$

Consequently, we have

$$\mathcal{J}_\alpha = \mathcal{J}_\alpha(\boldsymbol{F}, \{2E - B\} \text{ other parameters})$$

and the partial derivatives $\frac{\partial}{\partial F_\beta}$ are to be taken with all other parameters constant.

Inspection of Eq. (19) reveals that the response coefficient $R_{\alpha,\beta}$ comprises three terms. They account for the derivatives of a_1, $G^{\boldsymbol{\chi}}$ and the $\sinh(\boldsymbol{\chi}\cdot\boldsymbol{F}/2)$, respectively. Moreover, inspection of Eq. (15a) reveals that the derivative of a_1 comprises terms that involve derivatives of $G_k^{\boldsymbol{\chi}}$ and of $\cosh(\boldsymbol{\chi}\cdot\boldsymbol{F}/2)$, respectively. We hence obtain

$$\begin{aligned} R_{\alpha,\beta}(\boldsymbol{F}) = \frac{\partial \mathcal{J}_\alpha}{\partial F_\beta} = -\mathcal{J}_\alpha \, \frac{a_1^{(\beta)}}{2\,a_1} - \mathcal{J}_\alpha \, \frac{(-1)^{N+1}}{a_1} \left[\frac{1}{2} \, \frac{\partial G_1^{\emptyset}}{\partial F_\beta} + \sum_{\boldsymbol{\chi}\in\mathsf{Z}_1} \frac{\partial G_1^{\boldsymbol{\chi}}}{\partial F_\beta} \, \cosh \frac{\boldsymbol{\chi}\cdot\boldsymbol{F}}{2} \right] \\ - \frac{a_0^{(\alpha\beta)}}{2\,a_1} + \frac{(-1)^{N+1}}{a_1} \sum_{\boldsymbol{\chi}\in\mathsf{Z}_0(\alpha)} \frac{\partial G_0^{\boldsymbol{\chi}}}{\partial F_\beta} \, \chi(\alpha) \, \sinh \frac{\boldsymbol{\chi}\cdot\boldsymbol{F}}{2} \,. \end{aligned} \tag{27}$$

In the limit of vanishing thermodynamic forces $\boldsymbol{F} = 0$, the Kolmogorov cycle criterion implies that the stochastic process obeys detailed balance and we have an equilibrium system. Then, all currents $\mathcal{J}_\alpha = 0$ vanish, and only the third term in Eq. (27) remains:

$$\lim_{\boldsymbol{F}\to\boldsymbol{0}} R_{\alpha,\beta}(\boldsymbol{F}) = -\frac{a_0^{(\alpha\beta)}}{2\,a_1}\Big|_{\boldsymbol{F}=\boldsymbol{0}} ,$$

Consequently, at equilibrium the response matrix $R_{\alpha,\beta}$ is symmetric with respect to swapping α and β and therefore Onsager reciprocity holds. Moreover, in this limit also the covariance reduces to

$$\lim_{\boldsymbol{F}\to\boldsymbol{0}} \mathcal{V}_{\alpha,\beta}(\boldsymbol{F}) = -\frac{a_0^{(\alpha\beta)}}{a_1}\Big|_{\boldsymbol{F}=\boldsymbol{0}} = 2R_{\alpha,\beta}(\boldsymbol{0}) \,,$$

as assured by the Green–Kubo relations.

However, this symmetry does no longer hold for non-vanishing $\boldsymbol{F}$, where the derivatives of the $G_k^{\boldsymbol{\chi}}$ play a role. Nonetheless, the first three terms in the covariance, Eq. (20a), are matched by corresponding contributions in the symmetric sum $R_{\alpha,\beta} + R_{\beta,\alpha}$ of the response coefficients, Eq. (27). Thus, out of equilibrium we have to compare the covariance matrix to the symmetric sum of response coefficients:

$$\mathcal{V}_{\alpha\beta} - (R_{\alpha,\beta} + R_{\beta,\alpha}) = 2\,a_2\,\mathcal{J}_\alpha\,\mathcal{J}_\beta + \frac{(-1)^{N+1}}{a_1}\sum_{\boldsymbol{\chi}\in\mathsf{Z}_1}\left(\mathcal{J}_\alpha\,\frac{\partial G_1^{\boldsymbol{\chi}}}{\partial F_\beta} + \mathcal{J}_\beta\,\frac{\partial G_1^{\boldsymbol{\chi}}}{\partial F_\alpha}\right)\cosh\frac{\boldsymbol{\chi}\cdot\boldsymbol{F}}{2} + \frac{(-1)^{N+1}}{2\,a_1}\left(\mathcal{J}_\alpha\,\frac{\partial G_1^{\emptyset}}{\partial F_\beta} + \mathcal{J}_\beta\,\frac{\partial G_1^{\emptyset}}{\partial F_\alpha}\right) - \frac{(-1)^{N+1}}{a_1}\sum_{\boldsymbol{\chi}\in\mathsf{Z}_0}\left(\boldsymbol{\chi}(\alpha)\,\frac{\partial G_0^{\boldsymbol{\chi}}}{\partial F_\beta} + \boldsymbol{\chi}(\beta)\,\frac{\partial G_0^{\boldsymbol{\chi}}}{\partial F_\alpha}\right)\sinh\frac{\boldsymbol{\chi}\cdot\boldsymbol{F}}{2}\,. \tag{28}$$

The first term comes from the covariance and to leading order is quadratic in the forces, while the rest comes from the symmetric sum of response coefficients and its scaling in the forces is determined by the particular force dependence of the functions $G_1^{\boldsymbol{\chi}}$, $G_1^{\emptyset}$, and $G_0^{\boldsymbol{\chi}}$.

The anti-symmetric part of the response coefficients accounts for corrections to the Onsager reciprocity and takes the form

$$R_{\alpha,\beta} - R_{\beta,\alpha} = \frac{\mathcal{J}_\beta\,a_1^{(\alpha)} - \mathcal{J}_\alpha\,a_1^{(\beta)}}{2a_1} - \frac{(-1)^{N+1}}{a_1}\sum_{\boldsymbol{\chi}\in\mathsf{Z}_1}\left(\mathcal{J}_\alpha\,\frac{\partial G_1^{\boldsymbol{\chi}}}{\partial F_\beta} - \mathcal{J}_\beta\,\frac{\partial G_1^{\boldsymbol{\chi}}}{\partial F_\alpha}\right)\cosh\frac{\boldsymbol{\chi}\cdot\boldsymbol{F}}{2} - \frac{(-1)^{N+1}}{2\,a_1}\left(\mathcal{J}_\alpha\,\frac{\partial G_1^{\emptyset}}{\partial F_\beta} - \mathcal{J}_\beta\,\frac{\partial G_1^{\emptyset}}{\partial F_\alpha}\right) + \frac{(-1)^{N+1}}{a_1}\sum_{\boldsymbol{\chi}\in\mathsf{Z}_0}\left(\chi(\alpha)\,\frac{\partial G_0^{\boldsymbol{\chi}}}{\partial F_\beta} - \chi(\beta)\,\frac{\partial G_0^{\boldsymbol{\chi}}}{\partial F_\alpha}\right)\sinh\frac{\boldsymbol{\chi}\cdot\boldsymbol{F}}{2}\,. \tag{29}$$

Also in this case the first term scales quadratic in the forces to leading order in $\boldsymbol{F}$, and the scaling can not easily be worked out for the other three terms.

These results suggest that there can be manifolds in the space of the forces where (symmetric) Green–Kubo and/or Onsager reciprocity relations hold for a system that is not at thermodynamic equilibrium.

A related observation has been reported by Altaner *et al.* [13]. They showed that the response of a current $\mathcal{J}_\alpha$ to its naturally conjugated force F_α is given by the variance of the current whenever "current $\mathcal{J}_\alpha$ stalls internally: all contributing stochastic transitions need to be internally equilibrated; *i. e.* they are microscopically reversible." The additional key assumption in their derivation is in the way that the transition rates depend on the forces: Each force F_β only impacts the transition rates along the chord η_β in an anti-symmtaric way. With this locality and asymmetry assumption, the kinetic terms $G_0^{\boldsymbol{\chi}}$ for $\boldsymbol{\chi}\in\mathsf{Z}_0(\alpha)$ do not depend on F_α and the last term in Eq. (28) vanishes for $\alpha=\beta$. Stalling of the current $\mathcal{J}_\alpha$ then assures that $\mathcal{V}_{\alpha\alpha} = 2\,R_{\alpha,\alpha}$ even out of equilibrium. Note that these conditions are not sufficient to show the Green–Kubo relation for mixed response nor Onsager reciprocity at stalling.

A more detailed discussion of linear response far from equilibrium lies beyond the scope of the present paper. It will be provided in forthcoming work.

C. Activity a la Maes

Recently, it has been shown that the corrections to linear response in out of equilibrium systems originate from an excess in the "activity" or "frenesy" of a system, *i. e.*from an excess in the speed of the time-symmetric microscopic dynamics [14, 30]. In general, "activity"-like observables are observables whose dynamic behaviour is symmetric with respect to a change in the direction of time [22, 31].

More precisely, we consider the response of the fundamental current $\Phi_\alpha(\underline{\omega})$ as a function of the trajectory $\underline{\omega} = (n_k,\tau_k)_{k\in\mathbb{N}}$ with respect to the force F_β. We call $\langle O\rangle^{F_\beta}$ the trajectory ensemble average for some given parameter F_h.

It can then formally be shown [30] that

$$\frac{\mathrm{d}}{\mathrm{d}F_\beta}\langle\Phi_\alpha\rangle^{F_\beta} = \frac{1}{2}\langle\Phi_\alpha,\Phi_\beta\rangle^{F_\beta} - \left\langle\Phi_\alpha;\frac{\partial}{\partial F_\beta}A\right\rangle^{F_\beta} \tag{30}$$

where $\langle A;B\rangle$ indicates the co-variance of two observables.

Upon division by τ and taking the limit $\tau\to\infty$, the left-hand side reduces to the response coefficient and the second term becomes the second scaled cumulant and we obtain

$$R_{\alpha,\beta} - \frac{1}{2}\mathcal{V}_{\alpha,\beta} = \lim_{\tau\to\infty}\frac{1}{\tau}\left\langle\Phi_\alpha;\frac{\partial}{\partial F_\beta}A\right\rangle^{F_\beta}. \tag{31}$$

Importantly, the observable $\frac{\partial A}{\partial F_\beta}$ in the second covari-

ance is called the excess activity. It is given by

$$\frac{\partial}{\partial F_\beta} A = \int_0^\tau \left[\frac{\partial}{\partial F_\beta} \xi(t) - \frac{1}{2} \sum_{k=1}^{\infty} \delta(t - t_k) \frac{\mathrm{d}}{\mathrm{d}F_\beta} \ln(w_{i\to i} w_{j\to j}) \right] \mathrm{d}t,$$

where $\xi(t) = \sum_i \delta(v(t) - v_i) w_i$ is the escape rate associated to the current state of the process.

As such, the excess activity, like the derivatives of the coefficients $\frac{\partial G_k^\chi}{\partial F_\beta}$ only depends on the F_β-derivatives of rates associated to transpositions, $w_{i\to i} w_{j\to j}$ and escape rates w_i. Understanding the connection between the excess activities and $\frac{\partial G_k^\chi}{\partial F_\beta}$ and their physical interpretation in more detail seems like a promising area of research, but is beyond the scope of this manuscript.

D. other topics

- simplify bookkeeping/evaluation of terms by observing that
  - the substitutions $\mathcal{C}^{\boldsymbol{n}} \to \mathcal{C}^{\boldsymbol{n}}/\boldsymbol{n}!$ and $\partial_{\boldsymbol{q}}^{\boldsymbol{n}} \to \partial_{\boldsymbol{q}}^{\boldsymbol{n}}/\boldsymbol{n}!$ absorb all combinatorial terms summarized in the multinomial factors
  - products of cumulants appear multiple times in the sum Eq. (10d). The matching terms can be collected by asking for partitions where matching indices are collected into groups, and an ordering of the terms in the groups is enforced — as shown in the expression Eq. (11) for the n^{th} derivative with respect to a fixed chord.
- multiple transitions between two sites can be coped with by relatively straightforward extensions. Nothing changes if there is at most one chord between two states. When there is more than one chord, *only* the expression for the derivatives, Eq. (18), must be reworked.
- benchmark the improved performance with respect to the previous algorithm Part I, II when calculating $\mathcal{J}$ and $\mathcal{V}$.

E. Outlook

- enhance Altaner/Polettini [13]: revisit response theory based on fluctuation theorem and general expressions for $\mathcal{J}$ and $\mathcal{V}$
- enhance Cohen, Belousov, Rondoni [32]: on relation of (signs of) $\mathcal{J}$, $\mathcal{V}$, $\mathcal{S}$

The general expressions for the cumulants that we have derived here are useful for statistical kinetics [33], where the goal is to use the fluctuations (in form of variance, skewness and kurtosis) of an enzymatic reaction to deduce the interior structure of the catalytic mechanism. The structure is prescribed by the number of states of the enzyme, by their local connections in forms of neighbors, as well as their global connections in forms of cycles. These structural properties have an immediate impact on the cumulants: they provide the overall number of terms as well as their individual combinatorial and kinetic prefactors, as the general recursion relation, Eq. (20c), highlights. In Ref. [34], the authors found (numerical) evidence that ratios of cumulants are bound by the number of the states in unicyclic networks. Our results indicate that this bound is actually given by the size of the smallest cycle in a multi-cyclic network. However, a thorough analysis of the recursion relation will be necessary to confirm this hypothesis.

VI. CONCLUSION

main findings

- in Eq. (10d) we establish a recursion to effectively calculate $\mathcal{C}^{\boldsymbol{n}}$ to all orders of $n = |\boldsymbol{n}|$
- it works for all finite Markov processes and antisymmetric observables
- in order n it requires the computation of the derivatives $a_k^{(\boldsymbol{m})}(\boldsymbol{q} = \boldsymbol{0})$ with $k + |\boldsymbol{m}| = n$
- in Eq. (15) we provide explicit expressions for the derivatives $a_k^{(\boldsymbol{m})}(\boldsymbol{q} = \boldsymbol{0})$. They only involve (sums of) forces for the fundamental cycles of the generating tree and determinants of (typically sparse) submatrices of the transition matrix of the Markov process
- it is sufficient to calculate derivatives where the components of $\boldsymbol{m}$ take values in $\{0, 1\}$. Higher-order derivatives are obtained by trivial changes of sign and the appropriate choice of cosh or sinh in the derivatives
- only terms need to be calculated that are in general independent and non-zero

This provides a huge speed-up with respect to earlier approaches, and it is amenable to numerical evaluation in computer algebra systems.

Results have been illustrated by providing the general solution of the four-state Markov process with a four-cycle and two three-cycles.
We also discussed

- response
- corrections to Green-Kubo

The reduction of numerical effort is particularly severe when calculating ratios of cumulants. After all, a_1 need not be calculated in that case.

ACKNOWLEDGMENTS

J.V. acknowledges discussion with L. Rondoni, Marco Zamparo
A.W. was financially supported by the National Research Fund of Luxembourg in the frame of AFR PhD Grant No. 7865466.

Appendix A: Example: Four States and Two Fundamental Cycles

In this appendix we demonstrate the application of Eqs. (10), (15), and (18) by providing explicit results for the four-state model with two fundamental cycles. With appropriate rates this model describes the motion of kinesin on a microtubule [4, 35, 36]. Moreover, when taking into account translational symmetry (rotation by multiples of $\pi/3$ for the states sketched in Fig. 1 (a)) it also amounts to an asymmetric exclusion process of three particles on six sites. Except for specific examples in Apps. A 2 and A 3 we do not assume a specific functional dependence or symmetries for the transition rates between the four states.

This model has three cycles, 123, 432, and 1243. We choose a parameterization where $1 \to 2$ and $4 \to 3$ are adopted as chords, as shown in Fig. 1(a). Hence, there are two fundamental cycles, $\alpha = 123$ and $\beta = 432$. Moreover, the model as another cycle 1243. It will be interpreted as superposition of the fundamental cycles, $1243 = \alpha + \beta$. The present choice of chords is convenient because it minimizes the amount of calculations to be preformed. The form of all expressions is invariant under swapping

$$\begin{array}{rl} \text{cycles} & \alpha \leftrightarrow \beta \\ \text{states} & 1 \leftrightarrow 4 \\ & 2 \leftrightarrow 3 \end{array} \tag{A1}$$

This informed choice of the parameterization reduces the computational effort by a factor of two.[2]

1. Characteristic polynomial

To define the skewed transition matrix $\hat{\mathsf{W}}$ we introduce factors involving q_α, $-q_\alpha$, q_β, and $-q_\beta$ for the transitions $1 \to 2$, $2 \to 1$, $4 \to 3$, and $3 \to 4$, respectively. Consequently, the skewed transition matrix takes the form

$$\hat{\mathsf{W}}(\boldsymbol{q}) = \begin{pmatrix} w_1^1 & w_1^2\,\mathrm{e}^{-q_\alpha} & w_1^3 & 0 \\ w_2^1\,\mathrm{e}^{q_\alpha} & w_2^2 & w_2^3 & w_2^4 \\ w_3^1 & w_3^2 & w_3^3 & w_3^4\,\mathrm{e}^{q_\beta} \\ 0 & w_4^2 & w_4^3\,\mathrm{e}^{-q_\beta} & w_4^4 \end{pmatrix}. \tag{A2}$$

where we also introduced $\boldsymbol{q} = (q_\beta, q_\alpha)$.

The matrix $\hat{\mathsf{W}}(\boldsymbol{q})$ has a characteristic polynomial of degree four. The following notation allows us to emphasize the importance of the cycles in these expressions and it results in a less cluttered notation,

$$\begin{aligned} w_i &= w_i^i \\ w_{ij} &= w_j^i w_i^j \\ w_{ijk} &= w_j^i w_k^j w_i^k \\ w_{ijkl} &= w_j^i w_k^j w_l^k w_i^l \end{aligned}$$

With this notation the coefficients a_k of the characteristic polynomial read

[2] Note that the symmetry does not refer to the particular numerical values; for instance, $w_1^1 \neq w_4^4$. Rather is is a relation between the functional form of the resulting expressions.

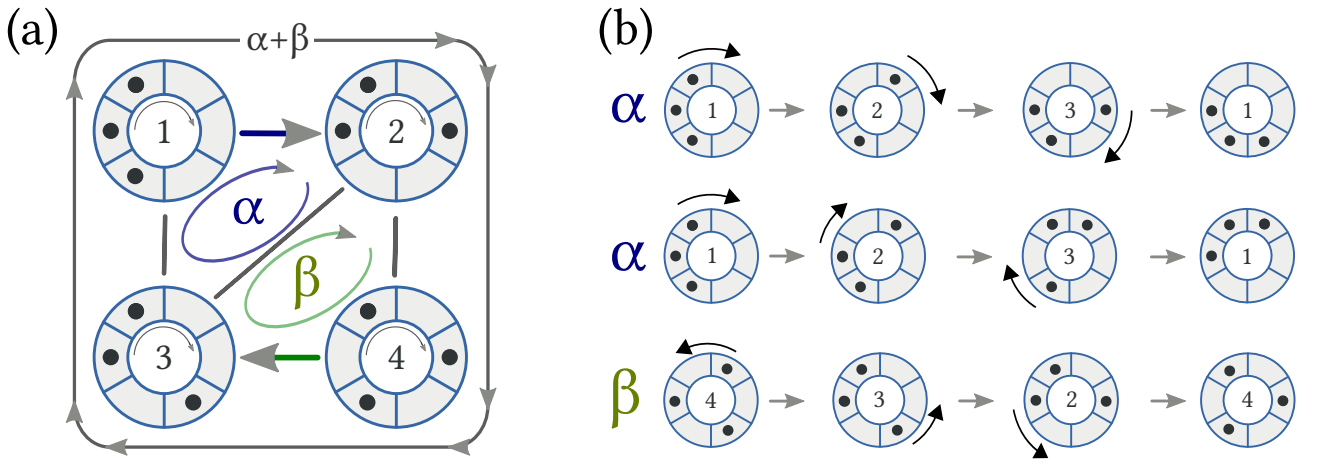

Figure 1. (a) The Markov chain associated to the asymmetric exclusion process of three particles on six sites when one accounts for translational (*i. e.* rotation by multiples of $\pi/3$) symmetry. Each circle shows the position of the three particles. The direction of the arrows in the circle indicates forward (*i. e.* clockwise) motion of particles. The arrows between the states $1 \to 2$ and $4 \to 3$ mark the transitions that will be considered as chords. The remaining transitions form a tree that is connecting the states. Adding a chord to the tree leads to a graph with a single cycle: Cycle $\alpha = 123$ is associated to the chord $1 \to 2$. Cycle $\beta = 432$ is associated to the chord $4 \to 3$. The cycle 1243 will be interpreted as the sum $\alpha + \beta$ of the fundamental cycles α and β. (b) Different realizations of the cycles α and β when one does not reduce the rotational symmetry.

$$a_4 = 1\,, \tag{A3a}$$

$$a_3 = -\mathrm{Tr}(\hat{\mathsf{W}}(\boldsymbol{q})) = -(w_1 + w_2 + w_3 + w_4)\,, \tag{A3b}$$

$$a_2 = +(w_1\,w_2 - w_{12}) + (w_1\,w_3 - w_{13}) + (w_1\,w_4) + (w_2\,w_3 - w_{23}) + (w_2\,w_4 - w_{24}) + (w_3\,w_4 - w_{34})\,, \tag{A3c}$$

$$\begin{aligned} a_1 = &-\big(w_1\,w_2\,w_3 + w_{123}\ \mathrm{e}^{q_\alpha}\ + w_{321}\ \mathrm{e}^{-q_\alpha}\ - w_1\,w_{23} - w_2\,w_{13} - w_3\,w_{12}\big) \\ &-(w_1\,w_2\,w_4 - w_1\,w_{24} - w_4\,w_{12}) - (w_1\,w_3\,w_4 - w_1\,w_{34} - w_4\,w_{13}) \\ &-\big(w_2\,w_3\,w_4 + w_{234}\ \mathrm{e}^{q_\beta}\ + w_{432}\ \mathrm{e}^{-q_\beta}\ - w_2\,w_{34} - w_3\,w_{24} - w_4\,w_{23}\big)\,, \end{aligned} \tag{A3d}$$

$$\begin{aligned} a_0 = \det(\hat{\mathsf{W}}(\boldsymbol{q})) = {}& w_1\,w_2\,w_3\,w_4 - w_1\,w_2\,w_{34} - w_1\,w_3\,w_{24} - w_1\,w_4\,w_{23} - w_4\,w_2\,w_{13} - w_4\,w_3\,w_{12} \\ &+ w_1\ \big(w_{234}\ \mathrm{e}^{-q_\beta}\ + w_{432}\ \mathrm{e}^{q_\beta}\big) + w_4\ \big(w_{123}\ \mathrm{e}^{q_\alpha} + w_{321}\ \mathrm{e}^{-q_\alpha}\big) \\ &+ (w_{12}\,w_{34} + w_{13}\,w_{24}) - \big(w_{1243}\ \mathrm{e}^{q_\alpha+q_\beta} + w_{3421}\ \mathrm{e}^{-q_\alpha-q_\beta}\big)\,. \end{aligned} \tag{A3e}$$

These expressions can either be obtained by direct evaluation of the determinant, Eq. (7) or based on Eq. (15). The process has three cycles $\mathsf{Z}_0 = \{\{\alpha\}, \{\beta\}, \{\alpha+\beta\}\}$.

a_2 The cycles do not contribute to the sum because they involve at least three of the four states. Hence, $a_2 = (-1)^2\, G_2^{\emptyset}$. The terms in brackets refer to the six possibilities to select two states of the four states in the Markov process. In all cases the set E can be empty, and except for the choice $(1, 4)$ they may also form an edge. The factor of -1 accounts then for the signature of ϵ.

a_1 The minus sign in front of all brackets accounts for the factor $(-1)^{N-k}$ because $N - k = 3$. Moreover, in this case the cycles $\mathsf{Z}_1 = \{\{\alpha\}, \{\beta\}\}$ contribute to the sum. When they are selected the other two sets are empty, $\mathsf{E}_1^\alpha = \emptyset$ and $\mathsf{F}_1^\alpha = \emptyset$. Consequently,

the cycles contribute the summands

$$2\sqrt{w_{123}w_{321}}\cosh\left(q_\alpha+\frac{F_\alpha}{2}\right)$$
$$=\sqrt{w_{123}w_{321}}\left(\sqrt{\frac{w_{123}}{w_{321}}}\,\mathrm{e}^{q_\alpha}+\sqrt{\frac{w_{321}}{w_{123}}}\,\mathrm{e}^{-q_\alpha}\right)$$
$$=w_{123}\,\mathrm{e}^{q_\alpha}+w_{321}\,\mathrm{e}^{-q_\alpha} \tag{A4a}$$

$$2\sqrt{w_{432}w_{234}}\cosh\left(q_\beta+\frac{F_\beta}{2}\right)$$
$$=w_{432}\,\mathrm{e}^{q_\beta}+w_{234}\,\mathrm{e}^{-q_\beta} \tag{A4b}$$

The other terms account for contributions with $\zeta=\emptyset$ that involve either a single edge and a fixed point, or three fixed points.

a_0 The terms in the first row account for $\zeta=\emptyset$, and no (first term) or one (five other terms) edge. The second row accounts for the contributions of the cycles α and β that must be complemented by a single fixed point $\mathsf{F}_0^\alpha=\{\{w_4\}\}$ and $\mathsf{F}_0^\beta=\{\{w_1\}\}$, respectively. The last line comprises the contributions where $\zeta=\emptyset$ and ε comprises two edges, and the contribution that accounts for the cycle $\alpha+\beta$,

$$2\sqrt{w_{1243}w_{1342}}\cosh\left(q_\alpha+q_\beta+\frac{F_\alpha+F_\beta}{2}\right)$$
$$=\sqrt{w_{1243}w_{1342}}\left(\sqrt{\frac{w_{1243}}{w_{1342}}}\,\mathrm{e}^{q_\alpha+q_\beta}+\sqrt{\frac{w_{1342}}{w_{1243}}}\,\mathrm{e}^{-q_\alpha-q_\beta}\right)$$
$$=w_{1243}\,\mathrm{e}^{q_\alpha+q_\beta}+w_{1342}\,\mathrm{e}^{-q_\alpha-q_\beta} \tag{A4c}$$

Starting from the expressions Eq. (A3) the derivatives with respect to q_α and q_β can directly be calculated. In the following we rather demonstrate the general approach that should be taken also for more complicated problems: we only determine those terms that are needed to evaluate a given quantity. Moreover, we only provide those terms that are not trivially related by the symmetry, Eq. (A1).

To determine response coefficients we must specify the dependence of the rates on the forces F_α and F_β. To that end we assume that the driving forces act symmetrically along the forward and backward direction of every edge. As a consequence, for $i\neq j$ and $i,j\in\{1,2,3,4\}$ the products $w_j^i w_i^j$ do not depend on the thermodynamic driving forces. The contributions by the cycles are explicitly stated in Eq. (A4), and in addition there are contributions arising from the force dependence of $w_1,\ldots,w_4$.

2. Currents and Response Coefficients

In order to calculate the currents, Eq. (19), we note that $\mathsf{Z}_0(\alpha)=\{\{\alpha\},\{\alpha+\beta\}\}$ Consequently,

$$\mathcal{J}_\alpha=\frac{-1}{a_1}\left[G_0^\alpha\,\sinh\frac{F_\alpha}{2}+G_0^{\alpha+\beta}\,\sinh\frac{F_\alpha+F_\beta}{2}\right],$$

with $F_\alpha=\log(w_{123}/w_{321})$ and $F_\beta=\log(w_{432}/w_{423})$, *cf.* Eq. (3). Moreover,

$$\mathsf{E}_0^\alpha=\emptyset\,,\qquad \mathsf{F}_0^\alpha=\{\{4\}\}\,,\qquad \mathrm{sign}(\alpha)=1\,,$$
$$\mathsf{E}_0^{\alpha+\beta}=\emptyset\,,\qquad \mathsf{F}_0^{\alpha+\beta}=\emptyset\,,\qquad \mathrm{sign}(\alpha+\beta)=-1\,,$$

such that according to Eq. (15b)

$$G_0^\alpha=2\,w_4\sqrt{w_{123}w_{321}}\,, \tag{A6a}$$
$$G_0^{\alpha+\beta}=-2\sqrt{w_{1243}w_{1342}}\,. \tag{A6b}$$

Altogether, we thus obtain

$$\mathcal{J}_\alpha=\frac{-2}{a_1}\left[w_4\sqrt{w_{123}w_{132}}\,\sinh\frac{F_\alpha}{2}+\sqrt{w_{1243}w_{1342}}\,\sinh\frac{F_\alpha+F_\beta}{2}\right]. \tag{A7}$$

The same expression for the current is obtained by evaluating Eq. (10a) based on Eq. (A3).

The current $\mathcal{J}_\beta$ is obtained via the substitution, Eq. (A1). For the ratio of the currents this implies

$$\frac{\mathcal{J}_\alpha}{\mathcal{J}_\beta}=\frac{w_4\sqrt{w_{123}w_{132}}\,\sinh\frac{F_\alpha}{2}-\sqrt{w_{1243}w_{1342}}\,\sinh\frac{F_\alpha+F_\beta}{2}}{w_1\sqrt{w_{432}w_{423}}\,\sinh\frac{F_\beta}{2}-\sqrt{w_{1243}w_{1342}}\,\sinh\frac{F_\alpha+F_\beta}{2}}$$
$$=\frac{\frac{-w_4\sqrt{w_{23}}}{\sqrt{w_{43}w_{42}}}\,\sinh\frac{F_\alpha}{2}+\sinh\frac{F_\alpha+F_\beta}{2}}{\frac{-w_1\sqrt{w_{23}}}{\sqrt{w_{12}w_{13}}}\,\sinh\frac{F_\beta}{2}+\sinh\frac{F_\alpha+F_\beta}{2}} \tag{A8}$$

When plotting the ratio as function of the forces one must watch out that $-w_4=w_2^4+w_3^4$ and $-w_1=w_2^1+w_3^1$ will be functions of the forces, and so will be the factors w_{ij} unless the forces are implemented symmetrically on all transitions $i\to j$.

The stalling forces for the current $\mathcal{J}_\alpha$ are the forces where $\mathcal{J}_\alpha=0$. Due to Eqs. (A7), (A6) and $\sinh(x+y)=\sinh x\,\cosh y+\cosh x\,\sinh y$ they amount to

$$\tanh\frac{F_\alpha}{2}=\sinh\frac{F_\beta}{2}\Big/\left[\frac{w_4\sqrt{w_{23}}}{\sqrt{w_{42}w_{43}}}-\cosh\frac{F_\beta}{2}\right] \tag{A9a}$$
$$=\frac{w_{423}-w_{432}}{2\,(w_2^4+w_3^4)\sqrt{w_{23}}+w_{432}+w_{423}} \tag{A9b}$$

Equation (A9a) is explicit in the forces if w_4 does not depend on the force F_α and if the thermodynamic forces are implemented symmetrically on the transitions, *i. e.* when only the ratios w_j^i/w_i^j depend on the forces while the products w_{ij} do not. Otherwise, Eq. (A9b) provides F_α in terms of the rates, and subsequently Eq. (A9a) can be solved for F_β in order to obtain an implicit description of the dependence.

For the calculation of the response coefficients Eq. (27) we assume from the beginning that the forces are implemented symmetrically. Hence, the terms under the

square root in G_0^α do not depend on the forces. Moreover, for this model the factors $G_1^{\boldsymbol{\chi}}$ take the values, $G_1^\alpha = 2\sqrt{w_{123}w_{321}}$ and $G_1^\beta = 2\sqrt{w_{432}w_{423}}$, and they both do not depend on the forces. To evaluate the derivative of a_1 we have to calculate the derivatives of $G_1^\emptyset$. To that end we observe that

$$\frac{\partial G_1^\emptyset}{\partial F_\alpha} = \sum_{j\in\{1,2,3,4\}} G_2^{\{j\}} \, \frac{\partial w_j}{\partial F_\alpha}$$

where $G_2^{\{j\}}$ denotes those contributions to $G_2^\emptyset$ that do not involve the state j. Thus, we obtain

$$\begin{aligned} R_{\alpha,\alpha}(\boldsymbol{F}) &= \frac{\mathcal{J}_\alpha}{a_1}\,\sqrt{w_{123}w_{321}}\,\sinh\frac{F_\alpha}{2} + \frac{\mathcal{J}_\alpha}{a_1}\sum_{j\in\{1,2,3,4\}} G_2^{\{j\}}\,\frac{\partial w_j}{\partial F_\alpha} \\ &\quad - \frac{1}{a_1}\left[w_4\,\sqrt{w_{123}w_{321}}\,\cosh\frac{F_\alpha}{2} - \sqrt{w_{1243}w_{1342}}\,\cosh\frac{F_\alpha+F_\beta}{2}\right] - \frac{2}{a_1}\,\frac{\partial w_4}{\partial F_\alpha}\,\sqrt{w_{123}w_{321}}\,\sinh\frac{F_\alpha}{2}\,, \qquad \text{(A10a)} \\ R_{\alpha,\beta}(\boldsymbol{F}) &= \frac{\mathcal{J}_\alpha}{a_1}\sqrt{w_{432}w_{423}}\,\sinh\frac{F_\beta}{2} + \frac{\mathcal{J}_\alpha}{a_1}\sum_{j\in\{1,2,3,4\}} G_2^{\{j\}}\,\frac{\partial w_j}{\partial F_\beta} \\ &\quad - \frac{1}{a_1}\left[-\sqrt{w_{1243}w_{1342}}\,\cosh\frac{F_\alpha+F_\beta}{2}\right] - \frac{2}{a_1}\,\frac{\partial w_4}{\partial F_\beta}\,\sqrt{w_{123}w_{321}}\,\sinh\frac{F_\alpha}{2}\,. \qquad \text{(A10b)} \end{aligned}$$

In the equilibrium limit, $\boldsymbol{F}=\boldsymbol{0}$, only the first term in the respective second rows of Eq. (A10) yield non-vanishing values,

$$R_{\alpha,\alpha}(\boldsymbol{0}) = \frac{-w_4\,\sqrt{w_{123}w_{321}} + \sqrt{w_{1243}w_{1342}}}{a_1}\,, \qquad \text{(A11a)}$$

$$R_{\alpha,\beta}(\boldsymbol{0}) = \frac{\sqrt{w_{1243}w_{1342}}}{a_1}\,. \qquad \text{(A11b)}$$

In general $R_{\alpha,\alpha}(\boldsymbol{0}) \neq R_{\beta,\beta}(\boldsymbol{0})$ because $w_4\,\sqrt{w_{123}w_{321}} \neq w_1\sqrt{w_{432}w_{423}}$. In contrast, $R_{\alpha,\beta}(\boldsymbol{0}) = R_{\beta,\alpha}(\boldsymbol{0})$, such that the response matrix is symmetric in the limit of vanishing forces $\boldsymbol{F}$, as required by the Onsager reciprocity.

For non-vanishing driving forces the difference of the two diagonal elements of the response matrix takes the form

$$\begin{aligned} R_{\alpha,\beta} - R_{\beta,\alpha} = \frac{1}{a_1^2}\Bigg[&(w_1-w_4)\,\sqrt{w_{123}w_{321}}\,\sinh\frac{F_\alpha}{2}\,\sqrt{w_{432}w_{234}}\,\sinh\frac{F_\beta}{2} \\ &+ \sqrt{w_{1243}w_{1342}}\,\sinh\frac{F_\alpha+F_\beta}{2}\left(\sqrt{w_{432}w_{234}}\,\sinh\frac{F_\beta}{2} - \sqrt{w_{123}w_{321}}\,\sinh\frac{F_\alpha}{2}\right)\Bigg] \\ &- \frac{1}{a_1^2}\sum_{j\in\{1,2,3,4\}} G_2^{\{j\}}\Bigg[\frac{\partial w_j}{\partial F_\beta}\,w_4\,\sqrt{w_{123}w_{321}}\,\sinh\frac{F_\alpha}{2} - \frac{\partial w_j}{\partial F_\alpha}\,w_1\,\sqrt{w_{432}w_{234}}\,\sinh\frac{F_\beta}{2} \\ &\qquad - \left(\frac{\partial w_j}{\partial F_\beta} - \frac{\partial w_j}{\partial F_\alpha}\right)\,\sqrt{w_{1243}w_{1342}}\,\sinh\frac{F_\alpha+F_\beta}{2}\Bigg] \\ &- \frac{2}{a_1}\left[\frac{\partial w_4}{\partial F_\beta}\,\sqrt{w_{123}w_{321}}\,\sinh\frac{F_\alpha}{2} - \frac{\partial w_1}{\partial F_\alpha}\,\sqrt{w_{432}w_{234}}\,\sinh\frac{F_\beta}{2}\right]. \end{aligned}$$

To leading order the hyperbolic sine functions are linear in their arguments. Consequently, the terms in the first bracket scale quadratically in the forces.

3. Covariances and Green-Kubo relations

According to Eq. (20a) the elements of the covariance matrix $\mathcal{V}^{\boldsymbol{n}}$ take the form

$$\mathcal{V}_{\alpha\alpha} = \frac{-1}{a_1}\left[w_4\,\sqrt{w_{123}w_{132}}\,\cosh\frac{F_\alpha}{2} + \sqrt{w_{1243}w_{1342}}\,\cosh\frac{F_\alpha+F_\beta}{2} - 2\,\mathcal{J}_\alpha\,\sqrt{w_{123}w_{132}}\,\sinh\frac{F_\alpha}{2} + 2\,a_2\,\mathcal{J}_\alpha^2\right] \tag{A12a}$$

$$\mathcal{V}_{\alpha\beta} = \frac{-1}{a_1}\left[\sqrt{w_{1243}w_{1342}}\,\cosh\frac{F_\alpha+F_\beta}{2} - \mathcal{J}_\alpha\,\sqrt{w_{432}w_{423}}\,\sinh\frac{F_\beta}{2} - \mathcal{J}_\beta\,\sqrt{w_{123}w_{132}}\,\sinh\frac{F_\alpha}{2} + 2\,a_2\,\mathcal{J}_\alpha\,\mathcal{J}_\beta\right], \tag{A12b}$$

where it is understood that $\alpha \neq \beta$ in Eq. (A12b). The coefficient a_2 is the only term in these expressions that has not been evaluated before.

The covariance matrix is related to the response matrix by

$$\mathcal{V}_{\alpha\beta} = 2\,R_{\alpha,\beta} - \frac{2\,\mathcal{J}_\alpha}{a_1}\left[a_2\,\mathcal{J}_\beta + \sum_{j\in\{1,2,3,4\}} G_2^{\{j\}}\,\frac{\partial w_j}{\partial F_\beta}\right] + \sqrt{w_{123}w_{132}}\,\sinh\frac{F_\alpha}{2}\left[\mathcal{J}_\beta + 4\,\frac{\partial w_4}{\partial F_\beta}\right]. \tag{A13}$$

This relation also applies for $\alpha = \beta$. It generalizes the Green–Kubo relations of linear response theory, which asserts that $\mathcal{V}_{\alpha\beta} = 2R_{\alpha\beta}$ to leading order in $\boldsymbol{F}$. Away from equilibrium the ratio of the covariance and the response matrix can be noticeably different from two, and again the correction is not necessarily quadratic in the forces $\boldsymbol{F}$. This is easily seen by considering the dependence for $\mathcal{J}_\alpha = 0$. The term $\mathcal{J}_\beta\,\sinh(F_\alpha/2)$ will then be quadratic in $\boldsymbol{F}$, while $\sinh(F_\alpha/2)\,\partial w_4/\partial F_\beta$ will in general be linear.

4. Skewness and Flatness

According to Eq. (20b) the elements of the skewness tensor $\mathcal{S}^{\boldsymbol{n}}$ take the form

$$\mathcal{S}_{\alpha\alpha\alpha} = \mathcal{J}_\alpha\,\left[1 + \frac{3}{a_1}\,\frac{G_0^\alpha}{w_4}\,\cosh\frac{F_\alpha}{2} - \frac{3a_2}{a_1}\mathcal{V}_{\alpha\alpha} - \frac{6a_3}{a_1}\mathcal{J}_\alpha^2\right] + \frac{3}{a_1}\mathcal{V}_{\alpha\alpha}\,\frac{G_0^\alpha}{w_4}\,\sinh\frac{F_\alpha}{2} \tag{A14a}$$

$$\begin{aligned}\mathcal{S}_{\alpha\alpha\beta} = \frac{-1}{a_1}\Bigg[&G_0^{\alpha+\beta}\,\sinh\frac{F_\alpha+F_\beta}{2} - \mathcal{J}_\beta\frac{G_0^\alpha}{w_4}\,\cosh\frac{F_\alpha}{2}\\ &-\mathcal{V}_{\alpha\alpha}\frac{G_0^\beta}{w_1}\,\sinh\frac{F_\beta}{2} - 2\,\mathcal{V}_{\alpha\beta}\frac{G_0^\alpha}{w_4}\,\sinh\frac{F_\alpha}{2} + 2a_2\mathcal{J}_\alpha\mathcal{V}_{\alpha\beta} + a_2\mathcal{J}_\beta\mathcal{V}_{\alpha\alpha} + 6a_3\mathcal{J}_\alpha^2\mathcal{J}_\beta\Bigg].\end{aligned} \tag{A14b}$$

To reduce clutter in this equation we did not insert the explicit form of G_0^α, G_0^β, and $G_0^{\alpha+\beta}$ in this expression, which have been defined in Eq. (A6). The coefficient a_3 is the only term in this expression that has not been evaluated before.

Similarly, a brief calculation that observes Eq. (20c) shows that the kurtosis $\mathcal{K}_{\alpha\alpha\alpha\alpha} = \mathcal{C}(\alpha,\alpha,\alpha,\alpha)$ takes the form

$$\begin{aligned}\mathcal{K}_{\alpha\alpha\alpha\alpha} &= \mathcal{V}_{\alpha\alpha} - \frac{\mathcal{J}_\alpha}{a_1}\left[-2\,\frac{G_0^\alpha}{w_4}\,\sinh\frac{F_\alpha}{2} + 2\,a_2\,(2\,\mathcal{S}_{\alpha\alpha\alpha} - \mathcal{J}_\alpha) + 12\,a_3\mathcal{J}_\alpha\mathcal{V}_{\alpha\alpha} + 24\,a_4\mathcal{J}_\alpha^3\right]\\ &\quad + \frac{\mathcal{V}_{\alpha\alpha}}{a_1}\left[12\,\frac{G_0^\alpha}{w_4}\,\cosh\frac{F_\alpha}{2} - 6\,a_2\mathcal{V}_{\alpha\alpha}\right] - \frac{\mathcal{S}_{\alpha\alpha\alpha}}{a_1}\frac{G_0^\alpha}{w_4}\,\sinh\frac{F_\alpha}{2}\\ &= \mathcal{V}_{\alpha\alpha}\,\left[1 - \frac{3}{a_1^2}\left(\frac{G_0^\alpha}{w_4}\right)^2\,\sinh^2\frac{F_\alpha}{2} + \frac{12}{a_1}\,\frac{G_0^\alpha}{w_4}\,\cosh\frac{F_\alpha}{2} - \frac{6\,a_2}{a_1}\mathcal{V}_{\alpha\alpha}\right]\\ &\quad - \frac{\mathcal{J}_\alpha}{a_1}\Bigg[\frac{3}{2\,a_1}\left(\frac{G_0^\alpha}{w_4}\right)^2\sinh F_\alpha + \frac{G_0^\alpha}{w_4}\,\sinh\frac{F_\alpha}{2}\,\left(-1 + \frac{3}{a_1}\,\frac{G_0^\alpha}{w_4}\,\cosh\frac{F_\alpha}{2} + \frac{6a_2}{a_1}\mathcal{V}_{\alpha\alpha} - \frac{6a_3}{a_1}\mathcal{J}_\alpha^2\right)\\ &\qquad + 2\,a_2\,\mathcal{J}_\alpha\,\left(1 + \frac{6}{a_1}\,\frac{G_0^\alpha}{w_4}\,\cosh\frac{F_\alpha}{2} - \frac{12\,a_2}{a_1}\mathcal{V}_{\alpha\alpha} - \frac{12\,a_3}{a_1}\mathcal{J}_\alpha^2\right) + 12\,a_3\mathcal{J}_\alpha\mathcal{V}_{\alpha\alpha} + 24\,a_4\mathcal{J}_\alpha^3\Bigg].\end{aligned} \tag{A15}$$

In the first step we collected the terms that also appear in the result Eq. (A12a) for $\mathcal{V}_{\alpha\alpha}$. In the second step we

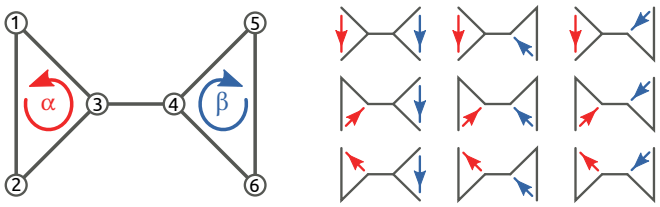

Figure 2. (Left) A graph with six vertices and seven edges. This is the simplest graph with two non-intersecting cycles (red, blue). The two cycles α and β can be recovered from choosing a spanning tree. (Right) The nine different spanning trees (grey) for the graph on the left. The edges not contained in the spanning tree (red, blue) are the *chords* that in turn give rise to the fundamental cycles.

eliminated $\mathcal{S}_{\alpha\alpha\alpha}$ by using Eq. (A14a) In this case a_4 is the only term that has not been evaluated before.

Appendix B: Permutation sets

We now give an explicit example for the decomposition of permulations into cycles, transpositions and fixed points that we employ in the main text. We use the graph with six vertices and seven edges depicted on the left of Fig. 2. A spanning tree for this graph is composed of six vertices and five edges. Thus we have $7-5=2$ chords or fundamental cycles, respectively.

In general, there are $6!=720$ permutations of six objects. However, in this work we only need those permutations of vertices that respect the structure of the graph. Therefore only those cyclic permuations and transpositions are allowed which go along the seven edges of this graph. This already reduces the number of permutations to 40. We represent all the relevant permuations in Fig. 3.

Note that there are two types of permutations: 20 permutations that do not contain any cycle and 20 permutations that involve cycle sets. The permuations without cycles are indispensible to determine the value of the coefficients $a_k(\boldsymbol{q})$, especially $a_1(\mathbf{0})$ appears in all cumulants. Additionally, these permuations encode some of the dependence on the forces $\boldsymbol{F}$. We represent these acyclic permutations in Fig. 3 under $\zeta=\emptyset$ with their transpositions and fixed points emphasized. Note that we only represent those that cannot be obtained from the others by flipping up↔down or left↔right. Their respective multiplicities are denoted explicity.

For the derivatives of the $a_k(\boldsymbol{q})$ with respect to $\boldsymbol{q}$, on the other hand, we only need those permutations that contain (sets of) cycles. Due to symmetry, we in fact need only those cycles sets that are *distinct*, *i. e.* where the indicator function $\boldsymbol{\chi}$ has $+1$ as the first non-zero entry. This leaves only 10 permutations that we group into four cycle sets: $\zeta(\boldsymbol{\chi}=(1,0))=\{\alpha\}$, $\zeta(\boldsymbol{\chi}=(0,1))=\{\beta\}$, $\zeta(\boldsymbol{\chi}=(1,1))=\{\alpha,\beta\}$, and $\zeta(\boldsymbol{\chi}=(1,-1))=\{\alpha,-\beta\}$.

Having identified the cycle sets, we can identify the sets Z_k that contain cycle sets that leave out at least k vertices: $\mathsf{Z}_0=\{\{\alpha\},\{\beta\},\{\alpha,\beta\},\{\alpha,-\beta\}\}$, $\mathsf{Z}_1=\mathsf{Z}_2=\mathsf{Z}_3=\{\{\alpha\},\{\beta\}\}$, $\mathsf{Z}_4=\mathsf{Z}_5=\mathsf{Z}_6=\emptyset$. The set Z_k is the set we need to sum over for the derivatives of the coefficient a_k. For its absolute value, we additionally need to consider $\zeta=\emptyset$.

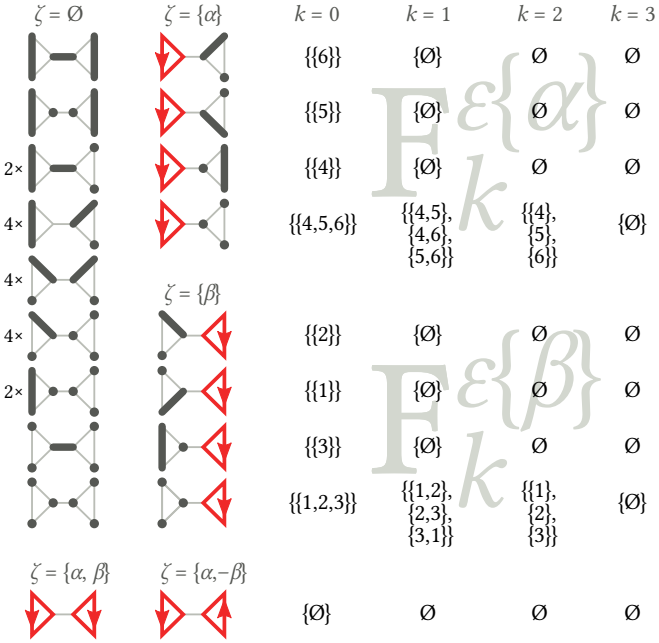

Figure 3. Illustration of the choices for the sets Z_k, $\mathsf{E}_k^{\boldsymbol{\chi}}$, and $\mathsf{F}_k^{\varepsilon\boldsymbol{\chi}}$ for the graph in Fig. 2 with six vertices and seven edges. This is the simplest graph where ζ can comprise two non-intersecting cycles, as sketched in the bottom left. We write $\mathsf{F}_k^{\varepsilon\boldsymbol{\chi}}=\emptyset$ when the cycle set $\zeta(\boldsymbol{\chi})$ and the transposition set ε do not leave out at least k vertices.

Once the cycle sets are chosen, we can continue selecting transpositions and fixed points. The two cycle sets $\zeta=\{\alpha,\beta\}$ and $\zeta=\{\alpha,-\beta\}$ span all six vertices and thus the entire graph. They leave no vertices for transpositions or fixed points thus for them $\mathsf{E}_0^{\boldsymbol{\chi}}=\{\emptyset\}$ and $\mathsf{F}_k^{\emptyset\boldsymbol{\chi}}=\{\emptyset\}$.

In contrast, the cycle sets $\zeta=\{\alpha\}$ and $\zeta=\{\beta\}$ each allow for three possible transpositions, in addition to the fixed points. As indicated in the figure, for $\zeta=\{\alpha\}$, we have $\mathsf{E}_0^{\{\alpha\}}=\mathsf{E}_1^{\{\alpha\}}=\{\emptyset,\{(4,5)\},\{(4,6)\},\{(5,6)\}\}$, while $\mathsf{E}_2^{\{\alpha\}}=\mathsf{E}_3^{\{\alpha\}}=\{\emptyset\}$.

When selecting the cycle set $\zeta=\{\alpha\}$ and the transposition set $\varepsilon=\{(4,5)\}$, we have one vertex free so $\mathsf{F}_0^{\varepsilon\boldsymbol{\chi}}=\{\{6\}\}$ while $\mathsf{F}_1^{\varepsilon\boldsymbol{\chi}}=\{\emptyset\}$, as indicated in the first row in Fig. 3. When not selecting any transposition for the cycle set $\zeta=\{\alpha\}$, the fixed point sets are more complicated: $\mathsf{F}_0^{\varepsilon\boldsymbol{\chi}}=\{\{4,5,6\}\}$, $\mathsf{F}_1^{\varepsilon\boldsymbol{\chi}}=\{\{4,5\},\{4,6\},\{5,6\}\}$, $\mathsf{F}_2^{\varepsilon\boldsymbol{\chi}}=\{\{4\},\{5\},\{6\}\}$, and $\mathsf{F}_3^{\varepsilon\boldsymbol{\chi}}=\{\emptyset\}$. This is depictured in the fourth row in Fig. 3.

We omit writing down the fixed point sets for $\zeta=\emptyset$. They can be constructed from the acyclic permutations depicted in the figure.

[1] Udo Seifert, "Stochastic thermodynamics, fluctuation theorems and molecular machines," Reports on Progress in Physics **75**, 126001 (2012).

[2] S.R. de Groot and P. Mazur, *Non-equilibrium Thermodynamics*, Dover Books on Physics Series (Dover Publications, 1984).

[3] Massimiliano Esposito and Christian Van den Broeck, "Three faces of the second law. i. master equation formulation," Phys. Rev. E **82**, 011143 (2010).

[4] Bernhard Altaner, Artur Wachtel, and Jürgen Vollmer, "Fluctuating currents in stochastic thermodynamics. II. Energy conversion and nonequilibrium response in kinesin models," Phys. Rev. E **92**, 042133 (2015).

[5] A. Einstein, "Über die von der molekularkinetischen Theorie der Wärme geforderte Bewegung von in ruhenden Flüssigkeiten suspendierten Teilchen," Annalen der Physik **322**, 549–560 (1905).

[6] Marian von Smoluchowski, "Zur kinetischen Theorie der Brownschen Molekularbewegung und der Suspensionen," Annalen der Physik **326**, 756–780 (1906).

[7] Melville S. Green, "Markoff random processes and the statistical mechanics of time-dependent phenomena," The Journal of Chemical Physics **20**, 1281–1295 (1952), https://doi.org/10.1063/1.1700722.

[8] R. Kubo, "The fluctuation-dissipation theorem," Reports on Progress in Physics **29**, 255 (1966).

[9] Lars Onsager, "Reciprocal relations in irreversible processes. i." Physical Review **37**, 405–426 (1931).

[10] J.L. Lebowitz and H. Spohn, "A Gallavotti–Cohen type symmetry in the large deviation functional for stochastic dynamics," J. Stat. Phys. **95**, 333 (1999).

[11] D. Andrieux and P. Gaspard, "Fluctuation theorem and onsager reciprocity relations," The Journal of Chemical Physics **121**, 6167–6174 (2004), https://doi.org/10.1063/1.1782391.

[12] U. Seifert and T. Speck, "Fluctuation-dissipation theorem in nonequilibrium steady states," EPL (Europhysics Letters) **89**, 10007 (2010).

[13] Bernhard Altaner, Matteo Polettini, and Massimiliano Esposito, "Fluctuation-dissipation relations far from equilibrium," Phys. Rev. Lett. **117**, 180601 (2016).

[14] Marco Baiesi, Christian Maes, and Bram Wynants, "Fluctuations and response of nonequilibrium states," Phys. Rev. Lett. **103**, 010602 (2009).

[15] Marco Baiesi, Christian Maes, and Bram Wynants, "Nonequilibrium linear response for markov dynamics, i: Jump processes and overdamped diffusions," J Stat Phys **137**, 1094–1116 (2009).

[16] Marco Baiesi, Christian Maes, and Bram Wynants, "The modified sutherland–einstein relation for diffusive nonequilibria," Proceedings of the Royal Society A: Mathematical, Physical and Engineering Sciences **467**, 2792–2809 (2011), arXiv: 1101.3227.

[17] C. Maes, "On the origin and the use of fluctuation relations for the entropy," in *Poincaré Seminar 2003: Bose-Einstein condensation-entropy* (Birkhäuser, Basel, 2004) p. 145.

[18] W. Feller, *An Introduction to Probability Theory and Its Applications*, 3rd ed., Vol. 1 (Wiley, 1968).

[19] Artur Wachtel, Jürgen Vollmer, and Bernhard Altaner, "Fluctuating currents in stochastic thermodynamics. I. Gauge invariance of asymptotic statistics," Phys. Rev. E **92**, 042132 (2015).

[20] P. McCullagh, *Tensor methods in statistics*, Monographs on statistics and applied probability (Chapman and Hall, 1987).

[21] Matteo Polettini, Gregory Bulnes-Cuetara, and Massimiliano Esposito, "Conservation laws and symmetries in stochastic thermodynamics," Physical Review E **94**, 052117 (2016).

[22] Christian Maes and Maarten H. van Wieren, "Time-symmetric fluctuations in nonequilibrium systems," Physical Review Letters **96**, 240601 (2006).

[23] H. Touchette, "The large deviation approach to statistical mechanics," Phys. Rep. **478**, 1–69 (2009).

[24] Raphaël Chetrite and Hugo Touchette, "Nonequilibrium Markov processes conditioned on large deviations," Annales Henri Poincaré **16**, 2005–2057 (2014).

[25] D. Andrieux and P. Gaspard, "Fluctuation theorem for currents and schnakenberg network theory," J. Stat. Phys. **127**, 107–131 (2007).

[26] M Bruderer, L D Contreras-Pulido, M Thaller, L Sironi, D Obreschkow, and M B Plenio, "Inverse counting statistics for stochastic and open quantum systems: the characteristic polynomial approach," New Journal of Physics **16**, 033030 (2014).

[27] Henryk Gzyl, "Multidimensional extension of faa di bruno's formula," Journal of Mathematical Analysis and Applications **116**, 450–455 (1986).

[28] Warren P. Johnson, "The curious history of faà di bruno's formula," The American Mathematical Monthly **109**, 217–234 (2002).

[29] J. Schnakenberg, "Network theory of microscopic and macroscopic behavior of master equation systems," Rev. Mod. Phys. **48**, 571–585 (1976).

[30] Pieter Baerts, Urna Basu, Christian Maes, and Soghra Safaverdi, "Frenetic origin of negative differential response," Physical Review E **88**, 052109 (2013).

[31] C. Maes and K. Netočný, "Canonical structure of dynamical fluctuations in mesoscopic nonequilibrium steady states," EPL (Europhysics Letters) **82**, 30003 (2008).

[32] Roman Belousov, E. G. D. Cohen, and Lamberto Rondoni, "Nonequilibrium langevin dynamics: A demonstration study of shear flow fluctuations in a simple fluid," Phys. Rev. E **96**, 022125 (2017).

[33] Jeffrey R. Moffitt and Carlos Bustamante, "Extracting signal from noise: kinetic mechanisms from a michaelis–menten-like expression for enzymatic fluctuations," FEBS Journal **281**, 498–517 (2014).

[34] Andre C. Barato and Udo Seifert, "Skewness and kurtosis in statistical kinetics," Physical Review Letters **115**, 188103 (2015).

[35] S. Liepelt and R. Lipowsky, "Kinesin's network of chemomechanical motor cycles," Phys. Rev. Lett. **98**, 258102 (2007).

[36] R. Lipowsky, S. Liepelt, and A. Valleriani, "Energy Conversion by Molecular Motors Coupled to Nucleotide Hydrolysis," J. Stat. Phys. **135**, 951–975 (2009).

7. Stochastic Thermodynamics for Open Chemical Networks

The two previous chapters were dedicated to the large-time fluctuations of currents in molecular motors and generic finite Markov processes, respectively. We saw the extraordinarily important role of forces and currents along all the different cycles in the network of states.

This importance in fact poses a problem in generalizing these findings to truly *open* chemical networks, which are not restricted to a finite set of states by some conservation law. After all, the chemical lattice as introduced in chapter 4 is driven out of equilibrium by infinitely many copies of the emergent cycle forces. Additionally, the chemical reaction currents need to count all transitions of the same type in the network. The main problem is that we do not have a general method to compute the steady-state distribution for such an infinite network. Consequently, we first have to address the steady-state distribution and the averages of thermodynamic current quantities in these open chemical networks before we can really address their fluctuations. Especially because fluctuations are not always easy to determine, many studies resort to the deterministic rate equations, which are an *approximation* that is increasingly good in the macroscopic limit, as detailed in section 3.4. Some other approximative approaches include the chemical Langevin equation [1], moment closure approximations [2] and stochastic simulations [3]. All these approximations primarily address the *dynamical* properties of chemical reaction systems. For understanding the *thermodynamic* properties of open chemical networks, however, we have to ask the question about the thermodynamic accuracy of these approximations.

Here, I provide the reprint of an article that I coauthored, where we investigate the behavior of the (average) dissipation in stochastic and deterministic open chemical networks with analytical and computational methods. In this analysis it turns out that a purely topological network quantity — the *deficiency* [4, 5] — plays a crucial role in connecting the chemical master equation with the deterministic rate equations, both from a dynamical and from a thermodynamic perspective. This deficiency provides a classification for cycles that is complementary to the distinction of emergent *vs.* internal that I introduced in section 4.1.2.

The main result of this article is as follows: a nonlinear open chemical network with zero deficiency exhibits many properties that one may expect from an equilibrium system. Its steady state can be computed and is entirely uncorrelated. Additionally, there is an ideal correspondence between the stochastic and the deterministic description. Even the dissipation as quantified by the entropy-production rate, defined for the two cases in equations (4.21) and (4.25), is exactly identical for both dynamics. This is true arbitrarily far from equilibrium and for arbitrary (average) particle numbers — even below one, where the deterministic dynamics is not at all a good approximation. Moreover, we prove by example that the fluctuating dynamics can have a *smaller* entropy-production rate than its deterministic counter part. This contrasts a naïve intuition that fluctuations should increase the dissipation.

References

[1] D. T. Gillespie. “The chemical Langevin equation”. In: *Journal of Chemical Physics* 113.1 (2000), pp. 297–306.

[2] D. Schnoerr, G. Sanguinetti, and R. Grima. “Validity conditions for moment closure approximations in stochastic chemical kinetics”. In: *Journal of Chemical Physics* 141, 084103 (2014).

[3] D. T. Gillespie. “Stochastic Simulation of Chemical Kinetics”. In: *Annual Review of Physical Chemistry* 58.1 (2007), pp. 35–55.

[4] M. Feinberg. “Chemical reaction network structure and the stability of complex isothermal reactors—I. The deficiency zero and deficiency one theorems”. In: *Chemical Engineering Science* 42.10 (1987), pp. 2229–2268.

[5] D. F. Anderson, G. Craciun, and T. G. Kurtz. “Product-Form Stationary Distributions for Deficiency Zero Chemical Reaction Networks”. In: *Bulletin of Mathematical Biology* 72.8 (2010), pp. 1947–1970.

Dissipation in noisy chemical networks: The role of deficiency

M. Polettini,[1, a)] A. Wachtel,[1, b)] and M. Esposito[1, c)]
Complex Systems and Statistical Mechanics, Physics and Materials Science Research Unit, University of Luxembourg, 162a avenue de la Faïencerie, L-1511 Luxembourg (G. D. Luxembourg)

We study the effect of intrinsic noise on the thermodynamic balance of complex chemical networks subtending cellular metabolism and gene regulation. A topological network property called *deficiency*, known to determine the possibility of complex behavior such as multistability and oscillations, is shown to also characterize the entropic balance. In particular, when deficiency is zero the average stochastic dissipation rate equals that of the corresponding deterministic model, where correlations are disregarded. In fact, dissipation can be reduced by the effect of noise, as occurs in a toy model of metabolism that we employ to illustrate our findings. This phenomenon highlights that there is a close interplay between deficiency and the activation of new dissipative pathways at low molecule numbers.

I. INTRODUCTION

Today, advanced methods in genomics and metabolomics allow to reconstruct the chemical networks (CN) describing the metabolism of complex organisms[1,2]. These reconstructions are graphical repositories of thousands of pathways, metabolites, and their stoichiometry. Much like heat engines, metabolism operates thermodynamic cycles far from equilibrium that transform low chemical potential environmental resources into valuable products, at the expense of high chemical potential waste. Unlike the working substance of heat engines (e.g. steam), some metabolites, enzymes and cofactors might reach very low concentrations. At this level intrinsic noise, due to discreteness and randomness of molecular collisions, enters into play[3]. Suppression of noise and control of correlations in the abundance of regulatory molecules is crucial for the correct functioning of metabolic networks[4–6]. A stochastic description of dynamics and thermodynamics based on jump processes in molecules' populations is then required.

In this direction, the growing field of Stochastic Thermodynamics created the basis for a complete and consistent characterization of irreversibility in small nonequilibrium systems subject to fluctuations. Dissipation is quantified by the rate at which entropy is produced (EPR) and eventually delivered to the environment[7]. The theory has been applied to general CNs[8–10] such as those involved in gene regulation[12], cellular computation[13], copolymerization[14], kinetic proofreading[15], chemical switches[16], and signal transduction[17]. On the other hand, there is a growing body of mathematical literature linking a CN's topology to its dynamics, and still bearing no thermodynamic interpretation. In particular, it has been understood that a topological number called *deficiency* subtends the onset of complex behavior, such as bistability and oscillations[18–20], which are the mechanisms of chemical switches and clocks[21]. When intrinsic noise is important, a crucial result by Anderson, Craciun and Kurtz (ACK)[22] relates the deficiency of the CN to steady statistical properties of the chemical mixture.

In this paper we merge stochastic thermodynamics and deficiency theory, via the ACK theorem. We compare the behavior of an arbitrary CN subject to intrinsic noise and that of the corresponding deterministic model without noise, which follows deterministic rate equations where correlations between species are neglected. In the limit of large particle numbers the deterministic dynamics describes the mode, i.e. the most typical behavior of the system. The difference between the stochastic and the deterministic EPR in the two cases, here named *correlation EPR* (previously known as fluctuating EPR, today ambiguous), is known to vanish at steady states for linear CNs where only input/output and conformational changes of a molecule are allowed, and reaction velocities are linear-affine in the molecules' populations[23].

The main result in this paper is to extend this observation to nonlinear CNs with null deficiency at steady states, and to linear networks at all times. We rely on the following formula for the steady correlation EPR as the weighted difference between the mean and the mode of the reaction velocity v,

$$\text{correlation EPR} = (\text{mean}\, v - \text{most probable}\, v)\, G, \quad (1)$$

where G is the free-enthalpy increase. Hence the correlation EPR might be interpreted as a measure of a system's "propensity to complexity".

The plan of the paper is as follows. In Sec. II B we provide a simple definition of deficiency with the aid of a toy model of metabolism. More generally, under the assumption that the law of mass-action holds and that the mixture is well-stirred, we illustrate the dynamics and thermodynamics of CNs, in the stochastic (II C) and in the deterministic (II D) settings. We then derive the above formula, and by virtue of the ACK theorem (whose proof we briefly sketch in Appendix B) we draw our main conclusion that the correlation EPR vanishes for networks with zero deficiency. Our toy model will finally serve as a testing ground. We employ it to illustrate through Figs. 2, 3 the predictions of the ACK theorem. Incidentally,

a)Electronic mail: matteo.polettini@uni.lu
b)Electronic mail: artur.wachtel@uni.lu
c)Electronic mail: massimilano.esposito@uni.lu

the model displays a non-positive correlation EPR, somewhat contrary to the intuition that "large variability is likely to [...] increase metabolic burden"[6]. We give an explanation of this phenomenon in terms of the topology of the state space where stochastic population dynamics occurs, showing that when deficiency is nonzero, for low molecule numbers certain irreversible closed reaction pathways are switched off.

II. SETUP

A. Notation

As customary in CN studies, we employ a rather compressed notation. Letting $\mathbf{X}$ be the vector of chemical species, a CN is depicted by a set of stoichiometric equations

$$\boldsymbol{\nu}_{+\rho}\cdot\mathbf{X} \underset{k_{-\rho}}{\overset{k_{+\rho}}{\rightleftharpoons}} \boldsymbol{\nu}_{-\rho}\cdot\mathbf{X} \tag{2}$$

where vectors $\boldsymbol{\nu}_{+\rho}$ and $\boldsymbol{\nu}_{-\rho}$ contain, respectively, the numbers of molecules of each species being consumed and produced by reaction ρ, and $\boldsymbol{a}\cdot\boldsymbol{b}$ is the scalar product. The stoichiometric vector is defined as $\boldsymbol{\nabla}_\rho := \boldsymbol{\nu}_{-\rho} - \boldsymbol{\nu}_{+\rho}$, and it describes the net increase of species' populations. The stoichiometric matrix is the matrix that has the stoichiometric vectors as columns, $\nabla = (\boldsymbol{\nabla}_\rho)_{\rho>0}$. We assume that all reactions are strictly reversible, that is, $k_{\pm\rho} > 0$. In sums $\sum_\rho$, index ρ spans over reactions in both directions, unless otherwise specified. Analytic operations between vectors are performed component-wise and imply the scalar product, e.g. $\boldsymbol{a}^{\boldsymbol{b}} := \prod_i a_i^{b_i}$, $\boldsymbol{a}! := \prod_i a_i!$, $\boldsymbol{a}\cdot\ln\boldsymbol{b} := \sum_i a_i \ln b_i$. Boltzmann's constant k_B is set to unity.

B. From metabolism to deficiency

Roughly speaking, the deficiency of a CN is the number of "hidden" closed pathways, or thermdynamic cycles. Let us make this more precise with a simple model inspired by metabolism. Emphasis is on the cycle structure (see[24] for a formal introduction). The model reads

$$\begin{aligned} \emptyset &\xrightarrow{1} \mathrm{N} \\ \mathrm{N} + m\mathrm{E} &\xrightarrow{2} (m+n)\mathrm{E} + \mathrm{W} \\ n\mathrm{E} + \mathrm{W} &\xrightarrow{3} \emptyset, \end{aligned} \tag{3}$$

where $\emptyset$ signifies the "environment" as a whole. The first reaction introduces nutrients N. The second processes the nutrients with the aid of m tokens of energy E to produce more tokens of energy and waste W, and the third delivers waste and excess energy to the environment.

When all three reactions in the above network are performed in a pathway, a thermodynamic cycle is completed, restoring all concentrations in the system to their initial value at the expense of irreversibly dissipated free enthalpy (entropy production). Correspondingly, the stoichiometric matrix

$$\nabla = \begin{pmatrix} +1 & -1 & 0 \\ 0 & +1 & -1 \\ 0 & +n & -n \end{pmatrix} \tag{4}$$

admits $\boldsymbol{c} = (1,1,1)^T$ as a right-null vector, $\nabla\boldsymbol{c} = 0$[10].

The crucial step to understand deficiency is to introduce a symbolic representation of the network in terms of *complexes*, which are aggregates of species appearing as either reactants or products in a reaction. In our case, the complexes are $\mathrm{Y}_1 = \emptyset, \mathrm{Y}_2 = \mathrm{N}, \mathrm{Y}_3 = \mathrm{N} + m\mathrm{E}, \mathrm{Y}_4 = (m+n)\mathrm{E} + \mathrm{W}, \mathrm{Y}_5 = \mathrm{W} + n\mathrm{E}$. We then obtain a representation of the CN as a graph by drawing each reaction as an edge connecting vertices given by the complexes.

For $m = 0$, we notice that $\mathrm{Y}_2 = \mathrm{Y}_3$ and $\mathrm{Y}_4 = \mathrm{Y}_5$ and that a representation of the above network in terms of complexes is a graph consisting of one cycle:

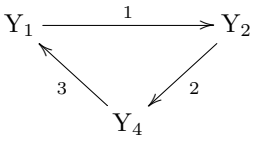

. (5)

Its topology is fully described by its *incidence matrix*

$$\partial = \begin{pmatrix} -1 & 0 & +1 \\ +1 & -1 & 0 \\ 0 & +1 & -1 \end{pmatrix} \tag{6}$$

which admits one right null vector.

For $m > 0$ we obtain the representation

$$\mathrm{Y}_5 \xrightarrow{3} \mathrm{Y}_1 \xrightarrow{1} \mathrm{Y}_2 \ , \qquad \mathrm{Y}_3 \xrightarrow{2} \mathrm{Y}_4 \ , \tag{7}$$

with incidence matrix

$$\partial = \begin{pmatrix} -1 & 0 & +1 \\ +1 & 0 & 0 \\ 0 & -1 & 0 \\ 0 & +1 & 0 \\ 0 & 0 & -1 \end{pmatrix} \tag{8}$$

This graph has no cycles; in fact its incidence matrix admits no right-null vectors.

The *deficiency* δ of a CN is the number of independent closed reaction pathways that cannot be visualized as independent cycles in the graphical representation in terms of complexes, and thus in some sense are "hidden". In our example when $m = 0$ then $\delta = 0$, otherwise the system is deficient, $\delta = 1$. Notice that null deficiency occurs when the autocatalytic mechanism of reaction 2 is not present.

The general recipe to calculate the deficiency is: (i) write down the stoichiometric matrix ∇ of the network; (ii) write down the incidence matrix ∂ of the graph where the reactions are arrows and complexes of reactants distinct vertices of the graph; (iii) then the deficiency is

$$\delta = \dim\ker\nabla - \dim\ker\partial \geq 0 \tag{9}$$

where dim ker calculates the dimension of the null space. The deficiency is non-negative. In fact one can write

$$\nabla = \frac{\partial Y}{\partial X}\partial \tag{10}$$

where the entry $(\partial Y/\partial X)_{ij}$ quantifies the amount of species X_i in complex Y_j. Since by Eq. (10) a right-null vector of ∂ is necessarily a right-null vector of ∇, then $\delta \geq 0$.

C. Average stochastic EPR

The setup of Markovian population dynamics of chemical species is as follows. The number of molecules in the reactor performs a jump process on the discrete lattice orthant $\mathcal{Z}_{\boldsymbol{X}_0}$ of populations that, starting from the initial state $\boldsymbol{X}_0$, are reachable by a finite number of reactions[1]. According to the law of mass-action, transition $\boldsymbol{X} \xrightarrow{\rho} \boldsymbol{X} + \boldsymbol{\nabla}_\rho$ is performed at rate

$$v_\rho(\boldsymbol{X}) = k_\rho \frac{\boldsymbol{X}!}{(\boldsymbol{X} - \boldsymbol{\nu}_\rho)!}. \tag{11}$$

The probability (or *ensemble*) $p_t(\boldsymbol{X})$ that $\boldsymbol{X}$ molecules are present in the reactor at time t obeys the Chemical Master Equation $\dot{p}_t = Lp_t$ with generator

$$Lp_t(\boldsymbol{X}) = -\sum_\rho \Big[v_{+\rho}(\boldsymbol{X}) p_t(\boldsymbol{X}) - v_{-\rho}(\boldsymbol{X} + \boldsymbol{\nabla}_\rho) p_t(\boldsymbol{X} + \boldsymbol{\nabla}_\rho) \Big]. \tag{12}$$

Multiplying by, and summing over $\boldsymbol{X}$, one obtains for the mean populations

$$\frac{d}{dt}\langle \boldsymbol{X} \rangle_t = \sum_\rho \boldsymbol{\nabla}_\rho \langle v_\rho(\boldsymbol{X}) \rangle_t \tag{13}$$

where the average $\langle \cdot \rangle_t$ is taken with respect to $p_t(\boldsymbol{X})$. The equation is not closed, as it involves higher moments on the right-hand side.

For finite $\mathcal{Z}_{\boldsymbol{X}_0}$, it can be proven that any ensemble supported on $\mathcal{Z}_{\boldsymbol{X}_0}$ evolves towards a unique steady ensemble p_∞ such that $Lp_\infty = 0$. We assume that for unbounded $\mathcal{Z}_{\boldsymbol{X}_0}$ conditions are met by which at all times $p_t(\boldsymbol{X} \to \infty)$ decays fast enough (e.g. exponentially) so that no probability leak to infinity occurs, and that a steady ensemble exists.

In this framework, the average EPR characterizing the CN's dissipation is defined as[25]

$$\sigma_t := \sum_\rho \left\langle v_\rho(\boldsymbol{X}) \ln \frac{v_{+\rho}(\boldsymbol{X}) p_t(\boldsymbol{X})}{v_{-\rho}(\boldsymbol{X} + \nabla_\rho) p_t(\boldsymbol{X} + \nabla_\rho)} \right\rangle_t \geq 0 \tag{14}$$

[1] That is, $\mathcal{Z}_{\boldsymbol{X}_0} := \{\boldsymbol{X} = \boldsymbol{X}_0 + \nabla \boldsymbol{n}, \boldsymbol{n} \in \mathbb{Z}^R, \boldsymbol{X} \geq \boldsymbol{0}\}$, sometimes called the *stoichiometric compatibility class*, compatible with $\boldsymbol{X}_0$.

It can easily be proven that the EPR is non-negative, embodying the second law of thermodynamics. The logarithmic term measures the thermodynamic cost of reaction ρ for a given $\boldsymbol{X}$, and it quantifies the degree by which detailed balance is broken.

D. Deterministic EPR

The corresponding deterministic model is obtained by neglecting correlations and higher cumulants, i.e. by replacing $\langle \boldsymbol{X}^{\boldsymbol{\nu}_\rho} \rangle_t \to (\Omega \boldsymbol{x})_t^{\boldsymbol{\nu}_\rho}$, where Ω is a large volume parameter that makes $\boldsymbol{x}$ a continuous variable with the interpretaton of a concentration; in the following we will set $\Omega = 1$ for notational clarity and only resume proper scalings when studying the model systems in Sec. III B. Also, in the large volume limit the approximation $v_\rho(\boldsymbol{x}) \approx k_\rho \boldsymbol{x}^{\boldsymbol{\nu}_\rho}$ is made. Then Eq. (13) yields the rate equation[8]

$$\frac{d\boldsymbol{x}_t}{dt} = \sum_\rho \boldsymbol{\nabla}_\rho v_\rho(\boldsymbol{x}_t) \tag{15}$$

Again, we are interested in steady behavior, when the right-hand side vanishes. Importantly, while the Chemical Master Equation admits one unique steady ensemble, the corresponding deterministic dynamics might admit none or several locally stable fixed points $\boldsymbol{x}_\infty$ and more complicated phenomenology such as limit cycles and fractal attractors[8]. Deterministic multistability corresponds to the steady ensemble being multimodal. Notice that $\boldsymbol{x}$ cannot be interpreted as a mean, as for bistable systems the mean might be far from both stable fixed points. Rather, in a scaling limit with the system size, random jump processes can be shown to typically behave deterministically, as rigorously detailed in Ref. [26].

In this setting, the deterministic EPR is defined as[27]

$$\bar{\sigma}_t := \sum_\rho v_\rho(\boldsymbol{x}_t) \ln \frac{v_{+\rho}(\boldsymbol{x}_t)}{v_{-\rho}(\boldsymbol{x}_t)} \geq 0. \tag{16}$$

The connection to free-energy differences and other thermodynamic potentials in a nonequilibrium setting is detailed in Ref. [10].

III. RESULTS

A. Theoretical

First, we re-work the above expressions for the deterministic and stochastic EPRs to make them closer one to another. Introducing the *thermodynamic forces*

$$G_\rho := \ln \frac{k_{+\rho}}{k_{-\rho}}, \tag{17}$$

that measure the kinetic imbalance of reactions, with a few manipulations we can bring the deterministic EPR

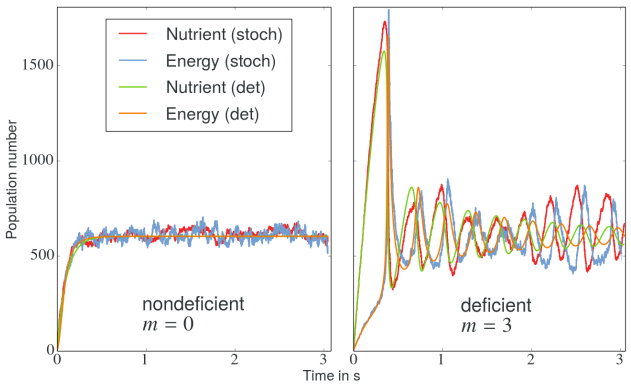

FIG. 1. We consider a class of toy models for metabolism $\emptyset \leftrightharpoons \mathrm{N}, \mathrm{N} + m\mathrm{E} \leftrightharpoons (m+2)\mathrm{E}, 2\mathrm{E} \leftrightharpoons \emptyset$, for varying m. In this figure we compare stochastic and deterministic time evolution of nutrient and energy molecules in the model corresponding to $m = 0$, that has deficiency $\delta = 0$ (on the left), and in model corresponding to $m = 3$, with deficiency $\delta = 1$ (on the right). The reactor is initially empty; rates are scaled according to the volume-parameter $\Omega = 10^{-21} N_A \approx 602$ (see main text), which is the number of molecules at the fixed point, for both models and for both species. In the zero-deficiency case, stochastic dynamics only adds structure-less noise to the deterministic behavior. Instead, in the deficient case, while the deterministic system has damped oscillations towards the fixed point, oscillations are sustained in the corresponding stochastic dynamics, yielding a structural deviation between the two.

to

$$\bar{\sigma}_t = \sum_\rho v_\rho(\boldsymbol{x}_t) G_\rho - \ln \boldsymbol{x}_t \cdot \frac{d\boldsymbol{x}_t}{dt} \tag{18}$$

As regards its stochastic counterpart, plugging the mass-action rates, Eq. (11), into Eq. (14) we obtain

$$\sigma_t = \sum_\rho \langle v_\rho \rangle_t G_\rho - \sum_{\boldsymbol{X}} \ln[p_t(\boldsymbol{X})\boldsymbol{X}!]\, L p_t(\boldsymbol{X}). \tag{19}$$

This is the first main result in our paper. Its most remarkable feature is that in the first term, related to the entropy flow to the environment[9], only the "macroscopic" average reaction velocity appears, and that "microscopic" dependencies on $\boldsymbol{X}$ are within the second term, which is related to the system's entropy change. At the trajectory level, this grants the validity of so-called Fluctuation Theorems[28], hence σ_t is a proper notion of EPR. It is important, and *a priori* not obvious that the thermodynamic force G_ρ is the same in the stochastic and in the deterministic settings.

Second, we define the correlation EPR as $\delta\sigma_t := \sigma_t - \bar{\sigma}_t$ and notice that, in the steady regime, it can be expressed as a weighted difference between the average and the deterministic reaction velocity, as was anticipated in Eq. (1). Explicitly, we obtain a formula for the steady correlation EPR as a weighted sum of population moments:

$$\delta\sigma_\infty = \sum_\rho \Big[\langle v_\rho \rangle_\infty - v_\rho(\boldsymbol{x}_\infty) \Big] G_\rho \tag{20}$$

$$= \sum_\rho G_\rho k_\rho \Big(\langle \boldsymbol{X} \dots (\boldsymbol{X} - \boldsymbol{\nu}_\rho + 1) \rangle_\infty - \boldsymbol{x}_\infty^{\boldsymbol{\nu}_\rho} \Big). \tag{21}$$

The latter expression might pave the way for approximate estimations of the correlation EPR based on Van Kampen's system size expansion, moment-closure techniques or other diffusion approximations, provided due care is paid to the fact that such approximations often fail to reproduce the stochastic thermodynamics out of equilibrium[11] or even the distibution moments[29].

Third, we evaluate the stochastic EPR when the system is in a product-form Poisson-like ensemble[2] with a generic time-dependent parameter $\boldsymbol{y}_t$,

$$\mathrm{Pois}_{\boldsymbol{y}_t}(\boldsymbol{X}) = \frac{1}{Z_{\boldsymbol{X}_0}} \frac{\boldsymbol{y}_t^{\boldsymbol{X}}}{\boldsymbol{X}!}, \tag{22}$$

with $Z_{\boldsymbol{X}_0}$ the normalization factor over $\mathcal{Z}_{\boldsymbol{X}_0}$. In this case it can be shown with few manipulations (see Appendix A for a step-by-step derivation) that $\langle v_\rho \rangle_{\mathrm{Pois}_{\boldsymbol{y}_t}} = v_\rho(\boldsymbol{y}_t)$, and consequently

$$\sigma_{\mathrm{Pois}_{\boldsymbol{y}_t}} = \sum_\rho v_\rho(\boldsymbol{y}_t) G_\rho - \ln \boldsymbol{y}_t \cdot \sum_\rho \nabla_\rho v_\rho(\boldsymbol{y}_t). \tag{23}$$

Notice that this expression coincides with the deterministic EPR at $t \to \infty$ if the Chemical Master Equation admits a steady product-form Poissonian with parameter $\boldsymbol{y}_\infty$ being a deterministic fixed point, and at all times if the system admits a product-form Poissonian with time-dependent parameter solving the deterministic rate equations.

Fourth, we investigate under which conditions such hypothesis are met. The ACK theorem[22] entails that, under our reversibility assumption, if the network has null deficiency, then the Chemical Master Equation admits a product-form Poissonian with parameter $\boldsymbol{x}_\infty$ being the fixed point of the corresponding deterministic dynamics, which by Feinberg's results[18] for $\delta = 0$ is unique and locally stable. Hence the steady correlation EPR vanishes for zero-deficiency networks. For sake of reference we sketch a proof of the theorem in Appendix B. Furthermore, it is known that in linear networks where no more than one molecule is consumed or produced at a time (i.e. $\sum_i \nu_{\rho,i} = 0, 1$), provided the system is prepared in a product-form Poissonian, it maintains such form at all times, with its parameter subjected to the corresponding rate equations[30]. Hence for linear CNs prepared in a product-form Poissonian ensemble, the correlation EPR vanishes at all times. These results thus generalize those by Mou et al.[23], who observed that the correlation EPR vanishes at steady states in linear networks.

[2] Notice that, because the range of summation is the lattice orthant $\mathcal{Z}_{\boldsymbol{X}_0}$ and not $\mathbb{Z}^{|X|}$, $|X|$ being the number of species, a "product-form Poisson-like" distribution is Poissonian in form but not in fact.

B. Numerical

We will now illustrate the consequences of the ACK theorem and our findings with the aid of the above class of toy models. In fact we will further simplify the scenario by eliminating the waste W, which does not play any substantial kinetic role. Details on the simulation methods can be found in Appendix C.

Let Ω be a scaling parameter regulating the system's size and let $x = N/\Omega$ be the concentration of N and $y = E/\Omega$ that of E. A convenient choice of parameters is $k_\rho = K_\pm \Omega^{1-\sum_i \nu_{i\rho}}$, where $K_\pm$ are independent of the reaction, in their respective units (which depend on ρ). Then for given Ω all models turn out to have the same fixed point concentrations and steady EPR, making them easily comparable. Concentrations obey the system of rate equations

$$\begin{aligned} \dot{x} &= K_+ - K_- x - K_+ x y^m + K_- y^{n+m} \\ \dot{y} &= n\left(K_+ x y^m - K_- y^{n+m} + K_- - K_+ y^n\right). \end{aligned} \tag{24}$$

A fixed point is found at $x_\infty = y_\infty = 1$, for all values of m, n. Its stability depends on m, n, K_+, K_-. The deterministic EPR at the fixed point is given by

$$\bar{\sigma}_\infty = 3\Omega(K_+ - K_-)\ln\frac{K_+}{K_-} \tag{25}$$

(notice that parameter Ω cancels within the logarithms, so that the EPR is extensive) and again it is independent of m, n.

We will consider the cases $n = 2$, for values $m = 0, 1, 2, 3$, $m = 0$ being the zero-deficiency case, all others having $\delta = 1$. We take $K_+ = 10$, $K_- = 1$, which signifies that the system is very far from a detailed balanced thermodynamic equilibrium. We start from an empty reactor, $x_0 = y_0 = 0$. For these values the above fixed point is stable for all $m < 4$. For $m = 0$ the dynamics converges uniformly to the fixed point, as shown in the left-hand side of Fig. 1. A more interesting behavior appears for higher m: for $m = 3$ the deterministic system displays damped oscillations towards the fixed point (as shown by the innermost smoother lines in the left-hand side of Fig. 1). Indeed, for $m = 4$ the fixed point becomes unstable and the system displays steady oscillations.

As regards the stochastic setting, so far our framework was that of ensemble thermodynamics, describing a large sample of processes at a given time. From now on we consider one given process in a large time. Indeed, Stochastic Thermodynamics has two complementary formulations: one along ensembles, and one along individual processes[7]. The two frameworks are compatible, since the ergodic principle ensures that long-time averages almost surely (a.s.) equal ensemble averages at the steady state. In particular it can be proven that for the reaction velocity

$$\langle v_\rho \rangle_\infty = \lim_{t\to\infty} \frac{1}{t} \#_t(\rho), \quad a.s. \tag{26}$$

where $\#_t(\rho)$ is the number of times reaction ρ has been performed along the stochastic trajectory up to time t.

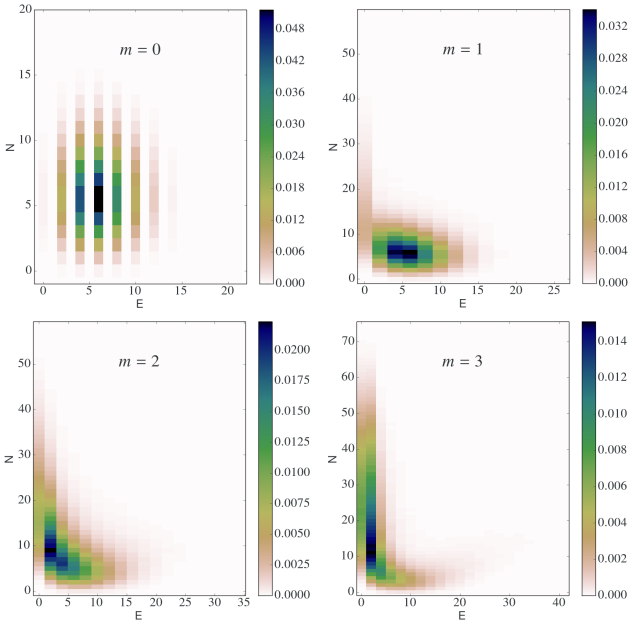

FIG. 2. The ACK theorem states that, if a CN has zero deficiency, then given an initial state (in our case, $N = E = 0$), the steady ensemble of the Chemical Master Equation has product form. Here we display color-plots of the histograms of the steady distribution of nutrient and energy molecules, for our toy models with $m = 0, 1, 2, 3$, and rates scaled down by the volume-parameter $\Omega = 10^{-23} N_A = 6.02$, giving a low number of molecules at the steady state. Zebra lines (present, but not displayed for $m > 0$ for sake of better visualization) indicate that the stochastic dynamics preserves the parity of the energy molecules, which are produced in pairs. Owing to the outer smudge, the deficient models $m = 1, 2, 3$ have a non-product form distribution. The product-form distribution of the zero-deficiency case $m = 0$ is shown in more detail in Fig. 3.

Similarly, a histogram for the steady ensemble $p_\infty(N, E)$ can be obtained by calculating the average time spent by the trajectory at state N, E. Let us then illustrate the ACK theorem. In Fig. 2 we provide color-plots for $p_\infty(N, E)$. For $m = 0$, the color plot renders the distribution's product-form. Zebra-lines are due to the fact that energy tokens are produced in pairs, hence starting from $x_0 = y_0 = 0$ only even numbers of energy molecules can be populated. The same zebra-structure occurs for higher $m > 0$, but for sake of better visualization we drew pixels twice the width, covering the whole area. The smudge in the color plots in Fig. 2 for $m > 0$ reveals that the steady ensemble does not have product form. Instead, in the zero-deficiency case, Fig. 3 compares the histograms of the marginals for the energy and the nutrient, showing that they perfectly agree with the prediction from the product-form Poissonian.

In Fig. 4 we plot the average stochastic EPR as a function of volume Ω. The perfect overlap between the deterministic EPR (upper line) and the dots corresponding

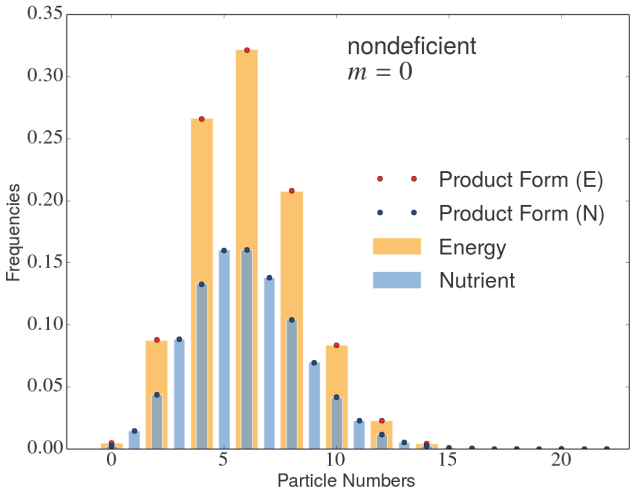

FIG. 3. The nonlinear CN $\emptyset \leftrightharpoons \mathrm{N} \leftrightharpoons 2\mathrm{E} \leftrightharpoons \emptyset$ (corresponding to $m = 0$) has zero deficiency. Hence, by the ACK theorem its corresponding Chemical Master Equation affords a product-form steady ensemble, and the marginals for the number of nutrients and of energy molecules also have Poisson-like distributions. We plot histograms for the populations of nutrient and energy molecules generated by stochastic simulations via Gillespie's algorithm, with rates scaled by a volume parameter $\Omega = 6.02$, showing perfect agreement with the predictions of the ACK theorem.

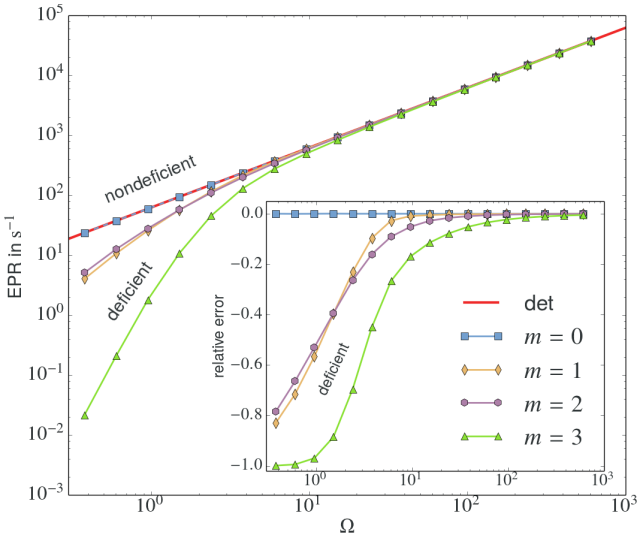

FIG. 4. The main result of our paper is that dissipation (EPR) in stochasic chemical dynamics only coincides with the deterministic EPR when the CN has zero deficiency, and that already in simple systems intrinsic noise affects dissipation. In the main frame we plot in log-log scale the stochastic EPR for our toy models, for all values $m = 0, 1, 2, 3$, as a function of the volume-parameter Ω that sets the average number of molecules present in the reactor at the steady ensemble. The upper straight line represents the deterministic value, Eq. (25). The dots on top of it are the values of the corresponding stochastic zero-deficiency system, $m = 0$. Models $m \geq 1$ with deficiency $\delta = 1$ have lower EPR than the deterministic model. An explanation for this is in Fig. 6. In the inset, we show that the relative error between stochastic and deterministic values decreases with volume.

to the $m = 0$ case confirms our result that for deficiency-zero systems the correlation EPR vanishes. For $m > 0$ this particular class of models has negative correlation EPR. The plots of the relative error in the inset show that the effect vanishes at large system sizes where fluctuations become negligible.

Finally, another interesting aspect to inquire is the dependency of the correlation EPR on the affinity $A = 3 \log K_+/K_-$, which determines the distance from detailed balance, i.e. from thermodynamic equilibrium. In particular, we are interested in the so-called *linear regime* where the affinity is small and stationary currents are approximately linear in the affinity. Then

$$\delta\sigma_\infty = (\ell - \bar{\ell})A^2 \tag{27}$$

with the deterministic *linear response coefficient* $\bar{\ell} = \Omega/3$. The inset in Fig. 5 shows that in a model with nonvanishing deficiency, in the linear regime the correlation EPR, relative to the deterministic linear regime approximation, does not vanish in the limit $A \to 0$, which implies that the stochastic linear response coefficient ℓ differs from the deterministic one.

Our result proves that having $\delta = 0$ is a sufficient condition for a vanishing correlation EPR. A preliminary question is then whether it is also necessary. The answer is trivially negative. In fact, if rates are such that detailed balance holds, then both the stochastic, the deterministic, and hence the correlation EPRs vanish. More generally, for the ACK theorem to hold it is sufficient that the more general condition of *complex balance* holds: even if deficiency is greater than zero, rates can conjure in such a way that currents look "as if" the system had null deficiency. Furthermore, by the theory of Schnakenberg[25] it can be shown that the correlation EPR can be decomposed in fundamental cycles $\delta\sigma(\infty) = \sum_\alpha \left[\langle J_\alpha \rangle_\infty - J_\alpha(\boldsymbol{x}_\infty)\right] A_\alpha$, with index α spanning a basis of the null space of the stoichiometric matrix, A_α a *cycle affinity* and J_α a *cycle current*. Cycle affinities are invariant under a wide range of transformations of the rate constants which affect the cycle currents; hence even for non-complex balanced rates it might be feasible to tune the rates in such a way that several cycle contributions all cancel each other.

The above argument rests on the fact that rate constants might be fine-tuned. The question becomes more interesting if properly reformulated. For systems with nonvanishing deficiency, complex-balanced rates are a set of measure zero in the space of possible rates. So, is the condition $\delta = 0$ necessary for a vanishing correlation EPR, for all possible values of rates? Very special systems with nonvashing deficiency which still have Poissonian steady states have been found[35]. An example is the chemical network $\mathrm{X}+\mathrm{Y} \rightleftharpoons 2\mathrm{X}+\mathrm{Y}$, $\mathrm{X} \rightleftharpoons 2\mathrm{X}$. In this case, the number of molecules of Y is constant and determines

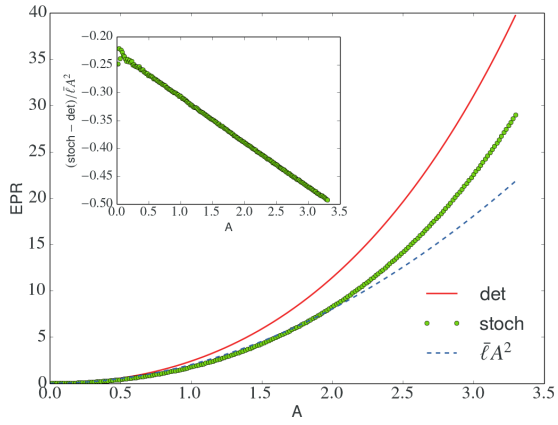

FIG. 5. The affinity $A = 3 \log K_+/K_-$ determines the distance from thermodynamic equilibrium (detailed balance). In this figure we show the dependency of the deterministic and the stochastic EPRs with respect to the affinity, for $m = 3$ and $\Omega = 6.02$, at fixed $K_- = 1$ and variable K_+. The dashed curve is the linear-regime approximation of the deterministic EPR, where the current is approximately linear in the affinity and the EPR is approximated by a quadratic. Clearly the EPRs approach zero for vanishing affinity (no dissipation). The inset shows the error between stochastic and deterministic EPR, relative to the linear approximation. The relative error increases with the affinity and, remarkably, it does not tend to vanish for $A \to 0$. This implies that for nonvanishing deficiency, the Onsager coefficients of the deterministic and stochastic systems differ.

the stoichiometric compatibility class where the dynamics is restricted. The deficiency is $\delta = 1$, still the steady ensemble is a product-form Poissonian with parameter given by the solution of the deterministic equations of motion, and the correlation EPR can be easily shown to vanish. To take this class of cases into the description, Cappelletti and Wiuf have introduced the concept of "stochastically complex-balanced" chemical reaction networks. The analysis of whether correlation EPR vanishes for all values of the rates if and only if the network is stochastically complex-balanced goes beyond the scope of the present paper.

IV. DISCUSSION AND CONCLUSIONS

While it could have been expected that fluctuations would increase dissipation, our simple model displays the opposite behavior. This can be explained as follows. Notice that for $m = 3$ in Fig. 1 the stochastic dynamics has amplified oscillations, such as those characterized in Ref. [36], where a purely stochastic mechanism for biochemical oscillations was proposed. Such oscillations are forcedly stabilized in the deterministic setting. Hence the stochastic model is more flexible and capable of exploring modes that the deterministic system abandons. Lower EPR then occurs when such modes are entropically convenient. A way to characterize these modes is by a switching mechanism of chemical pathways. Fig. 6 details that in deficient networks, at low molecule numbers certain reactions can be effectively shut off because of the temporary absence of a sufficient number of reactants. This phenomenon eventually reshapes the structure of the irreversible closed reaction pathways that the system can locally perform. In our particular model, for low molecule numbers reaction 2 is inhibited, and the other two reactions alone do not contribute to dissipation. Instead, in the CN with $\delta = 0$ the dissipative cycle can be performed at any particle number.

The above example might then lead to hypothesize that the correlation EPR could be non-positive in general. This is not the case though. A counterexample can be found in the literature. The Schlögl model $\emptyset \rightleftharpoons X$, $2X \rightleftharpoons 3X$ has deficiency $\delta = 1$, and its most important feature is that for certain critical values of the parameters it displays a bifurcation. Gaspard compared stochastic and deterministic EPRs for this model[16], and as can be observed from Fig. 2 in Ref.[16], close to the critical point the stochastic EPR is larger than the deterministic one, while in the bistable region it interpolates between the two possible values that the deterministic EPR takes at each of the two stable fixed points.

Despite the fact that our toy model is oversimplified, the mechanisms we observed might carry out to more realistic networks. At the level of gene expression, it is known that intrinsic noise is a crucial factor in phenotypic variation within isogenic populations[3]. One step below, while in cells metabolites might be large in number, gene-expressed regulatory molecules might be very few[3], allowing the switching mechanisms that we described above. In metabolism, the action of enzymes typically adds a level of complexity. In fact, most (if not all) of the reactions in biochemical CNs are not elementary, hence their connectivity and kinetic rules have to be determined *a posteriori* by advanced experimental methods (see[32] for a systematic review). Nevertheless, in our models the inbuilt deficient cycle could be seen as the core structure of any metabolic model. The network should be enriched by resolving individual metabolites within nutrients and waste, adding intermediate reactants such as cofactors and enzymes, resolving the environment and outer thermodynamic cycles, separating time-scales and resorting to effective rate laws when applicable. As a proof of concept, all these operations will in general maintain the core cycle and hence the deficient character of the network, hence it can be argued that, because of its autocatalytic character, metabolism is deficient.

[3] In *E. coli*, the lowest-concentration metabolite, nucleoside adenosine, is present in $\sim 10^2$ copies, but over 80% of the variety proteins is much lower in copy numbers[31]

To conclude, we emphasize that understanding thermodynamic constraints on the regulation of metabolic networks is a crucial problem in CN reconstruction[33,34]. In this work we displayed a close connection between the topological notion of deficiency of a CN and nonequilibrium thermodynamics, proving that at steady states only in zero-deficiency CNs the EPR evaluated by the mean-field deterministic theory coincides with that of the corresponding stochastic model, accounting for stochastic variability in molecules' number at low concentrations. For deficient CNs a nonvanishing correlation EPR quantifies the disagreement between deterministic and stochastic modeling, and at low molecule numbers this disagreement can be understood in terms of a switching mechanisms of reaction pathways. A more detailed study of the conditions for positive vs. negative correlation EPR is demanded to future inquiry. Immediate perspectives also include the study of non-well-stirred mixtures, where reaction-diffusion processes allow for pattern formation, and of systems with separation of time scales and effective enzymatic reactions. On the computational side, the more demanding stochastic techniques can be blended with deterministic algorithms to provide efficient tools for the systematic computation of the entropic balance of a CN, e.g. in software like COPASI[37]. More work has to be done to delineate future application of deficiency theory and stochastic thermodynamics to realistic metabolic networks.

Aknowledgments. The research was supported by the National Research Fund Luxembourg in the frame of project FNR/A11/02, of the AFR Postdoc Grant 5856127 and of the AFR Ph.D. Grant 7865466.

Appendix A: Explicit derivation of Eq. (23)

From Eq. (14), plugging into the rates Eq. (11) and the Poisson-form distribution Eq. (22) we obtain

$$\begin{aligned}\sigma_{\mathrm{Pois}_{\boldsymbol{y}_t}} &= \sum_\rho \sum_{\boldsymbol{X}} \mathrm{Pois}_{\boldsymbol{y}_t}(\boldsymbol{X}) v_\rho(\boldsymbol{X}) \\ &\qquad \ln \frac{v_{+\rho}(\boldsymbol{X})\mathrm{Pois}_{\boldsymbol{y}_t}(\boldsymbol{X})}{v_{-\rho}(\boldsymbol{X}+\nabla_\rho)\mathrm{Pois}_{\boldsymbol{y}_t}(\boldsymbol{X}+\nabla_\rho)} \\ &= \frac{1}{Z_{\boldsymbol{X}_0}} \sum_\rho \sum_{\boldsymbol{X}} k_\rho \frac{{\boldsymbol{y}_t}^{\boldsymbol{X}}}{(\boldsymbol{X}-\boldsymbol{\nu}_\rho)!} \ln \frac{k_\rho \frac{{\boldsymbol{y}_t}^{\boldsymbol{X}}}{(\boldsymbol{X}-\boldsymbol{\nu}_\rho)!}}{k_{-\rho}\frac{{\boldsymbol{y}_t}^{\boldsymbol{X}+\nabla_\rho}}{(\boldsymbol{X}+\nabla_\rho-\boldsymbol{\nu}_{-\rho})!}} \\ &= \frac{1}{Z_{\boldsymbol{X}_0}} \sum_\rho \sum_{\boldsymbol{X}} k_\rho \frac{{\boldsymbol{y}_t}^{\boldsymbol{X}}}{(\boldsymbol{X}-\boldsymbol{\nu}_\rho)!} \left(\ln \frac{k_\rho}{k_{-\rho}} - \nabla_\rho \cdot \ln \boldsymbol{y}_t\right)\end{aligned}$$

We now shift the summation over $\boldsymbol{X}$ to obtain

$$\begin{aligned}\sigma_{\mathrm{Pois}_{\boldsymbol{y}_t}} &= \frac{1}{Z_{\boldsymbol{X}_0}} \sum_{\boldsymbol{X}} \frac{{\boldsymbol{y}_t}^{\boldsymbol{X}}}{\boldsymbol{X}!} \sum_\rho k_\rho {\boldsymbol{y}_t}^{\boldsymbol{\nu}_\rho} \left(\ln \frac{k_\rho}{k_{-\rho}} - \nabla_\rho \cdot \ln \boldsymbol{y}_t\right) \\ &= \sum_\rho k_\rho {\boldsymbol{y}_t}^{\boldsymbol{\nu}_\rho} \left(\ln \frac{k_\rho}{k_{-\rho}} - \nabla_\rho \cdot \ln \boldsymbol{y}_t\right)\end{aligned}$$

which is the desired result, Eq. (23).

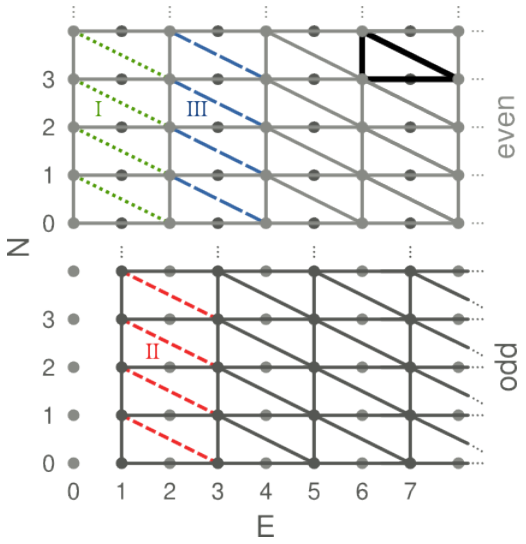

FIG. 6. Chemical stochastic kinetics occurs on lattice orthants, called stoichiometric compatibility classes (SCC). For our class of models, given an initial state, random jumps preserve the parity of the energy molecules (even or odd), hence there are two distinct SCCs. In the zero-deficiency case, $m = 0$, all of the drawn transitions are possible, and both SCCs can be obtained by repeatedly copy-pasting a motif corresponding to the full CN, marked bold in the figure, through the whole lattice orthant. That is, locally each SCC looks like the full CN. Only cycling trajectories that carry a thermodynamic affinity contribute to the steady stochastic EPR[25,28]. Hence, for $m = 0$, even for very low molecule numbers it is always possible to perform the entropy-producing cycle. On the other hand, the structure of the SCCs for deficient networks is: for $m = 1$ dotted transitions type I are not feasible (since at least one energy token is needed to perform reaction $\rho = +2$ and three energy tokens are needed to perform $\rho = -2$), for $m = 2$ dotted transitions type I and II are switched off, and for $m = 3$ transitions type I, II and III are shut. Hence for low-enough molecule numbers, the stochastic trajectory explores a portion of the SCC where there is no possibility of producing entropy along an irreversible cycle (cycles consisting only of reactions $\rho = \pm 1, \pm 2$ don't dissipate). This explains the lower stochastic EPR observed for $m = 1, 2, 3$ in Fig. 4.

Appendix B: Sketch of derivation of the deficiency-zero theorem

One of the corollaries that incarnate the Anderson-Craciun-Kurtz theorem[22] states that if a (weakly) reversible CN has deficiency zero, then on each stoichiometric compatibility classes the Chemical Master Equation admits a product-form Poisson-like steady distribution with parameter given by the unique fixed point of the corresponding rate equations. For sake of completeness, we provide the sketch of a derivation based on the graph-theoretical perspective that was briefly introduced in the main text. For another derivation based on quantum techniques, see[39].

Plugging the product-form Eq. (22) with parameter given by the fixed point $\boldsymbol{x}_\infty$ into the generator Eq. (12), and using rates Eq. (11) one obtains

$$\begin{aligned} &L\mathrm{Pois}_{\boldsymbol{x}_\infty}(\boldsymbol{X}) = \\ &= \frac{1}{Z_{\boldsymbol{X}_0}} \sum_\rho \Big[k_{-\rho} \frac{{\boldsymbol{x}_\infty}^{\boldsymbol{X}+\boldsymbol{\nabla}_\rho}}{(\boldsymbol{X}+\boldsymbol{\nabla}_\rho-\boldsymbol{\nu}_{-\rho})!} - k_{+\rho} \frac{{\boldsymbol{x}_\infty}^{\boldsymbol{X}}}{(\boldsymbol{X}-\boldsymbol{\nu}_\rho)!} \Big] \\ &= \frac{2}{Z_{\boldsymbol{X}_0}} \sum_{\rho>0} \frac{{\boldsymbol{x}_\infty}^{\boldsymbol{X}-\boldsymbol{\nu}_\rho}}{(\boldsymbol{X}-\boldsymbol{\nu}_\rho)!} \Big[v_{-\rho}(\boldsymbol{x}_\infty) - v_{+\rho}(\boldsymbol{x}_\infty) \Big] \end{aligned} \tag{B1}$$

where we used $\boldsymbol{\nabla}_\rho = \boldsymbol{\nu}_{-\rho} - \boldsymbol{\nu}_\rho$, and antisymmetrized. We now observe that the sum over reaction vectors $\rho > 0$ can be commuted with a sum over complexes Y_i, followed by a sum over all reactions ρ that have Y_i as a source complex. The latter information is stored into the incidence matrix ∂ of the graph of complexes. Noticing that ν_ρ only depends on the complex of reactants ahead of ρ, we can write

$$\begin{aligned} L\mathrm{Pois}_{\boldsymbol{x}_\infty}(\boldsymbol{X}) = \frac{2}{Z_{\boldsymbol{X}_0}} \sum_i \frac{{\boldsymbol{x}_\infty}^{\boldsymbol{X}-\boldsymbol{\nu}_i}}{(\boldsymbol{X}-\boldsymbol{\nu}_i)!} \\ \sum_\rho \partial_{i,\rho} \Big[v_{-\rho}(\boldsymbol{x}_\infty) - v_{+\rho}(\boldsymbol{x}_\infty) \Big]. \end{aligned} \tag{B2}$$

After Eq. (15), the fixed point satisfies

$$\sum_{\rho>0} \boldsymbol{\nabla}_\rho \left[v_{+\rho}(\boldsymbol{x}_\infty) - v_{-\rho}(\boldsymbol{x}_\infty) \right] = 0 \tag{B3}$$

which implies that $v_{+\rho}(\boldsymbol{x}_\infty) - v_{-\rho}(\boldsymbol{x}_\infty)$ is a right-null vector of the stoichiometric matrix. But if $\delta = 0$, then $v_{+\rho}(\boldsymbol{x}_\infty) - v_{-\rho}(\boldsymbol{x}_\infty)$ is also a right-null vector of the incidence matrix (see last paragraph in Sec. II B), hence Eq. (B2) vanishes.

Appendix C: Materials and methods

We employed the CN simulation software COPASI[37] to simulate the Chemical Master Equation via Gillespie's algorithm, and the LSODA algorithm implemented in the scientific python stack (SciPy)[38] to solve deterministic rate equations. Histograms in Fig. 3 and Fig. 2 were sampled from stochastic trajectories for random-time change Markov jump processes spanning over 10^5 s with a time resolution of 10^{-1} s, for a total of 10^6 binned particle number pairs, while the stochastic time-courses in Fig.1 employ trajectories of 5 s with a resolution of 10^{-5} s. Each value for the average stochastic EPR in Fig. 4 was calculated along single simulations of 10^5 s. Notice that Gillespie's algorithm keeps track of all reaction events, hence the final result for the stochastic average EPR is independent of time resolution. For the deterministic transients we used the same time-span and resolution as for the stochastic ones. The deterministic EPR was calculated via Eq. (25) and not from the simulation data. Thus it is only valid at the fixed point.

[1] G.J.E. Baart and D.E. Martens, *Genome-scale metabolic models: reconstruction and analysis*, in *Neisseria meningitidis* (Humana Press, 2012), pp. 107–126.

[2] I. Thiele et al., *A community-driven global reconstruction of human metabolism*, Nat. Biotechnol. **31**, 419 (2013).

[3] M.E. Elowitz, A.J. Levine, E.D. Siggia and P.S. Swain, *Sochastic gene expression in a single cell*, Science **297**, 1183 (2002).

[4] E. Levine and T. Hwa, *Stochastic fluctuations in metabolic pathways*, Proc. Natl. Acad. Sci. USA **104**, 9224 (2007).

[5] D.J. Kiviet, P. Nghe, N. Walker, S. Boulineau, V. Sunderlikova, and S.J. Tans, *Stochasticity of metabolism and growth at the single-cell level*, Nature **514**, 376 (2014).

[6] I. Lestas, J. Paulsson, N.E. Ross, and G. Vinnicombe, *Noise in gene regulatory networks*, IEEE **53**, 189 (2008).

[7] C. Van den Broeck and M. Esposito, *Ensemble and trajectory thermodynamics: A brief introduction*, Physica A **418**, 6 (2014).

[8] J. Ross, *Thermodynamics and Fluctuations far from Equilibrium*, (Springer-Verlag Berlin Heidelberg 2008).

[9] T. Schmiedl and U. Seifert, *Stochastic thermodynamics of chemical reaction networks*, J. Chem. Phys. **126**, 044101 (2007).

[10] M. Polettini and M. Esposito, *Irreversible thermodynamics of open chemical networks I: Emergent cycles and broken conservation laws*, J. Chem. Phys. **141**, 024117 (2014).

[11] J.M. Horowitz, *Diffusion approximations to the chemical master equation only have a consistent stochastic thermodynamics at chemical equilibrium*, J. Chem. Phys. **143**, 044111 (2015).

[12] A. Ghosh, *Non-equilibrium dynamics of stochastic gene regulation*, J. Biol. Phys. **41**, 49 (2015).

[13] P. Mehta and D.J. Schwab, *Energetic costs of cellular computation*, Proc. Natl. Acad. Sci. USA, **109**, 17978 (2012).

[14] D. Andrieux and P. Gaspard, *Nonequilibrium generation of information in copolymerization processes*, Proc. Natl. Acad. Sci. USA **105**, 9516 (2008).

[15] R. Rao and L. Peliti, *Thermodynamics of accuracy in kinetic proofreading: Dissipation and efficiency trade-offs*, J. Stat. Mech. P06001 (2015).

[16] P. Gaspard, *Fluctuation theorem for nonequilibrium reactions*, J. Chem. Phys. **120**, 8898 (2004).

[17] H. Qian, *Phosphorylation energy hypothesis: open chemical systems and their biological functions*, Annu. Rev. Phys. Chem. **58**, 113 (2007).

[18] M. Feinberg, *Chemical reaction network structure and the stability of complex isothermal reactors-I. The deficiency zero and deficiency one theorems*, Chem. Eng. Sci. **42**, 2229 (1987).

[19] G. Craciun, Y. Tang, and M. Feinberg, *Understanding bistability in complex enzyme-driven reaction networks*, Proc. Natl. Acad. Sci. USA **103**, 8697 (2006).

[20] D.F. Anderson, G. Craciun, M. Gopalkrishnan, C. Wiuf, *Lyapunov functions, stationary distributions, and non-equilibrium potential for chemical reaction networks*, Bull. Math. Biol., 1 (2015).

[21] J.J. Tyson, R. Albert, A. Goldbeter, P. Ruoff, and J. Sible, *Biological switches and clocks*, J. R. Soc. Interface **5**, S1 (2008).

[22] D.F. Anderson, G. Craciun, and T. Kurtz, *Product-form stationary distributions for deficiency zero chemical reaction networks*, B. Math. Biol. **72**, 1947 (2010).

[23] C.Y. Mou, J.-L. Luo and G. Nicolis, *Stochastic thermodynamics of nonequilibrium steady states in chemical reaction systems*, J. Chem. Phys. **84**, 7011 (1986).

[24] A. van der Schaft, S. Rao, and B. Jayawardhana, *On the mathematical structure of balanced chemical reaction networks governed by mass action kinetics*, SIAM J. Appl. Math. **73**, 953 (2013).

[25] J. Schnakenberg, *Network theory of microscopic and macroscopic behavior of master equation systems*, Rev. Mod. Phys. **48**, 571 (1976).

[26] D.F. Anderson and T.G. Kurtz, *Stochastic Analysis of Biochemical Systems* (Springer, 2015).

[27] H. Qian and D.A. Beard, *Thermodynamics of stoichiometric biochemical networks in living systems far from equilibrium*, Bio-

phys. Chem. **114**, 213 (2005).
[28]M. Polettini and M. Esposito, *Transient fluctuation theorem for the currents and initial equilibrium ensembles*, J. Stat. Mech. P10033 (2014).
[29]D. Schnoerr, G. Sanguinetti and R. Grima, *Validity conditions and stability of moment closure approximations for stochastic chemical kinetics*, J. Chem. Phys. **141**, 084103 (2014).
[30]W.J. Heuett and H. Qian, *Grand canonical Markov model: A stochastic theory for open nonequilibrium biochemical networks*, J. Chem. Phys. **124**, 044110 (2006).
[31]P. Guptasarma, *Does replication-induced transcription regulate synthesis of the myriad low copy number proteins of Escherichia coli?*, Bioessays **17**, 987 (1995).
[32]W. Vance, A. Arkin and J. Ross, *Determination of causal connectivities of species in reaction networks*, Proc. Natl. Acad. Sci. USA, **99** (2002), pp. 5816–5821.
[33]D. A. Beard, S.-D. Liang, and H. Qian, *Energy balance for analysis of complex metabolic networks*, Biophys. J. **83**, 79 (2002).
[34]C.S. Henry, L.J. Broadbelt, and V. Hatzimanikatisy, *Thermodynamics-Based Metabolic Flux Analysis*, Biophys. J. **92**, 1792 (2007).
[35]D. Cappelletti and C. Wiuf, *Product-form Poisson-like distributions and complex balanced reaction systems*, arXiv:1507.02195 (2015).
[36]A.J. McKane, J.D. Nagy, and M.O. Stefanini, *Amplified biochemical oscillations in cellular systems*, J. Stat. Phys. **128**, 165 (2007).
[37]S. Hoops, S. Sahle, R. Gauges, C. Lee, J. Pahle, N. Simus, M. Singhal, L. Xu, P. Mendes and U. Kummer, *COPASI: a COmplex PAthway SImulator*, Bioinformatics **22**, 3067 (2006).
[38]K.J. Millman, M. Aivazis, *Python for Scientists and Engineers*, Computing in Science & Engineering **13**, 9 (2011).
[39]J.C. Baez and B. Fong, *Quantum techniques for studying equilibrium in reaction networks*, Journal of Complex Networks, **3**, 22 (2015).

Part IV.

Macroscopic Thermodynamics of Chemical Reaction Networks

8. Thermodynamics of Enzymatic Reactions

All the results presented in part III started from the chemical master equation with *elementary reactions* as described in section 4.2. In the context of biological applications, however, this is sometimes an unfeasible level of description. Inside a cell there are hundreds and thousands of *enzymes* that enhance the rates of reactions by means of *catalysis*. The action of each enzyme individually needs to be described with several elementary reactions. Describing all of these processes as a big chemical master equation leads to a level of complexity that cannot be handled analytically nor computationally.

A common first simplifying assumption is the deterministic limit for large abundances of particle numbers, as sketched in section 4.3. I addressed especially the *thermodynamic* consistency of this approximation in chapter 7. An additional simplification is the use of *enzyme kinetics* [1] instead of elementary reactions. Enzyme kinetics describe the overall dynamics of the catalytic action of enzymes by means of a *single* reaction per enzyme — thus eliminating the enzymes themselves from the dynamical species, and resulting in a smaller set of dynamical equations that are much easier to handle computationally.

This *coarse graining* of the catalytic mechanism has an impact on the thermodynamic description of the net reaction that needs to be taken care of. An obvious question is whether the single coarse-grained reaction captures all contributions to the dissipation. Another less obvious question is whether a single reaction is even enough to cover all stoichiometric and dynamical properties of the catalytic action. Understanding this is a crucial step on the way to addressing the thermodynamics in real-life chemical reaction networks.

In this chapter, I provide the reprint of an article that I coauthored. We answer the above questions in this article and show that they are related. Our approach starts at the very basis of enzyme kinetics. We exploit the concept of emergent cycles introduced in section 4.1.2 to perform this coarse graining in a thermodynamically consistent way. We especially address the connection between kinetic rates and free-enthalpy differences of reaction, equation (3.19), which is related to the *local detailed balance* from stochastic thermodynamics. As a result, we are able to resolve the confusion that prevailed in the literature with regards to the applicability of this relation for enzymatic reactions: some authors claimed the general validity [2] while others doubted it [3].

References

[1] A. Cornish-Bowden. *Fundamentals of Enzyme Kinetics*. 4th ed. Weinheim: Wiley-Blackwell, 2012.

[2] D. A. Beard and H. Qian. "Relationship between Thermodynamic Driving Force and One-Way Fluxes in Reversible Processes". In: *PLoS ONE* 2.1, e144 (2007).

[3] R. Fleming et al. "Integrated stoichiometric, thermodynamic and kinetic modelling of steady state metabolism". In: *Journal of Theoretical Biology* 264.3 (2010), pp. 683–692.

[1] https://creativecommons.org/licenses/by/3.0/

New Journal of Physics
The open access journal at the forefront of physics

Deutsche Physikalische Gesellschaft DPG
IOP Institute of Physics

Published in partnership with: Deutsche Physikalische Gesellschaft and the Institute of Physics

OPEN ACCESS

RECEIVED
23 November 2017

REVISED
22 February 2018

ACCEPTED FOR PUBLICATION
12 March 2018

PUBLISHED
12 April 2018

FAST TRACK COMMUNICATION

Thermodynamically consistent coarse graining of biocatalysts beyond Michaelis–Menten

Artur Wachtel, Riccardo Rao and Massimiliano Esposito

Complex Systems and Statistical Mechanics, Physics and Materials Science Research Unit, University of Luxembourg, 162a, Avenue de la Faïencerie, 1511 Luxembourg, Luxembourg

E-mail: artur.wachtel@uni.lu

Keywords: coarse graining, biochemical reaction networks, thermodynamics, enzyme kinetics

Abstract

Starting from the detailed catalytic mechanism of a biocatalyst we provide a coarse-graining procedure which, by construction, is thermodynamically consistent. This procedure provides stoichiometries, reaction fluxes (rate laws), and reaction forces (Gibbs energies of reaction) for the coarse-grained level. It can treat active transporters and molecular machines, and thus extends the applicability of ideas that originated in enzyme kinetics. Our results lay the foundations for systematic studies of the thermodynamics of large-scale biochemical reaction networks. Moreover, we identify the conditions under which a relation between one-way fluxes and forces holds at the coarse-grained level as it holds at the detailed level. In doing so, we clarify the speculations and broad claims made in the literature about such a general flux–force relation. As a further consequence we show that, in contrast to common belief, the second law of thermodynamics does not require the currents and the forces of biochemical reaction networks to be always aligned.

1. Introduction

Catalytic processes are ubiquitous in cellular physiology. Biocatalysts are involved in metabolism, cell signaling, transcription and translation of genetic information, as well as replication. All these processes and pathways involve not only a few but rather dozens to hundreds, sometimes thousands of different enzymes. Finding the actual catalytic mechanism of a single enzyme is difficult and time consuming work. To date, for many enzymes the catalytic mechanisms are not known. Even if such detailed information was at hand, including detailed catalytic machanisms into a large scale model is typically unfeasable for numerical simulations. Therefore, larger biochemical reaction networks contain the enzymes as single reactions following enzymatic kinetics. This simplified description captures only the essential dynamical features of the catalytic action, condensed into a single reaction.

The history of enzyme kinetics [1] stretches back more than a hundred years. After the pioneering work of Brown [2] and Henri [3], Michaelis and Menten [4] laid the foundation for the systematic coarse graining of a detailed enzymatic mechanism into a single reaction. Since then, a lot of different types of mechanisms have been found and systematically classified [5]. Arguably, the most important catalysts in biochemical processes are enzymes—which are catalytically active proteins. However, other types of catalytic molecules are also known, some of them occur naturally like catalytic RNA (ribozymes) or catalytic anti-bodies (abzymes), some of them are synthetic (synzymes) [5]. For our purposes it does not matter which kind of biocatalyst is being described by a catalytic mechanism—we treat all of the above in the same way.

From a more general perspective, other scientific fields are concerned with the question of how to properly coarse grain a process as well. While in most applications the focus lies on the dynamics, or kinetics, of a process, it turned out that thermodynamics plays an intricate role in this question [6]. For processes occurring at thermodynamic equilibrium, every choice of coarse graining can be made thermodynamically consistent—after all, the very foundation of equilibrium thermodynamics is concerned with reduced descriptions of physical

phenomena [7]. Instead, biological systems are open systems exchanging particles with reservoirs and as such they are inherently out of equilibrium. Nonequilibrium processes, in general, do not have a natural coarse graining.

When the particle numbers in a reaction network are small, it needs to be described stochastically with the chemical master equation. Indeed, there is increased interest in the correct thermodynamic treatment of stochastic processes [8, 9]. With stochastic processes it is possible to investigate energy-conversion in molecular motors [10–13], error correction via kinetic proofreading [14–16], as well as information processing in small sensing networks [17–19]. In this field, different suggestions arose for coarse grainings motivated by thermodynamic consistency [20–22]. In these cases, the dissipation in a nonequililibrium process is typically underestimated—although also overestimations may occur [23]. For a general overview of coarse-graining in Markov processes, see [24] and references therein.

For large-scale networks however, a stochastic treatment is unfeasable. On the one hand, stochastic simulations quickly become computationally so demanding that they are effectively untractable. On the other hand, when species appear in large abundances (e.g. metabolic networks) the stochastic noise is negligible. This paper is exclusively concerned with this latter case. The dynamics is governed by deterministic differential equations: the nonlinear rate equations of chemical kinetics. Assuming a separation of time scales in these equations, model reduction approaches have been developed [25–27]. However, they do not address the question of thermodynamic consistency. Remarkably, recent development in the thermodynamics of chemical reaction networks [28, 29] highlighted the strong connection between the thermodynamics of deterministic rate equations and of stochastic processes, including the relation between energy, work, and information. Unfortunately, these studies were limited to elementary reactions with mass–action kinetics. The present paper addresses this constraint, thus extending the theory to kinetics of coarse-grained catalysts.

Understanding the nonequilibrium thermodynamics of catalysts is a crucial step towards incorporating thermodynamics into large-scale reaction networks. There is ongoing effort in the latter [30–32] which very often is based on the connection between thermodynamics and kinetics [33–35].

In this paper we show how to coarse grain the deterministic description of any biocatalyst in a thermodynamically consistent way—extending the applicability of such simplifications even to molecular motors [10, 36] and active membrane transport [37]. The starting point is the catalytic mechanism described as a reversible chemical reaction network where each of the M reaction steps ρ is an elementary transition representing a conformational change of a molecule or an elementary chemical reaction with mass–action kinetics. The corresponding rates are given by the fluxes (kinetic rate laws), $\phi_\rho^\pm$, that incorporate the reaction rate constants and the dependence on the concentration of the reactant molecules. The mass–action reaction forces (negative Gibbs free energies of reaction) are $-\Delta_\rho G = RT \ln \phi_\rho^+/\phi_\rho^-$ [38]. At this level, the reaction currents, $J_\rho = \phi_\rho^+ - \phi_\rho^-$, of these elementary steps are aligned with their respective reaction forces [39]: when one is positive, so is the other. From here we construct a reduced set of C reactions with effective reaction fluxes $\psi_\alpha^\pm$ and net forces $-\Delta_\alpha G$. As we will see later, there is a limited freedom to choose the exact set of reduced reactions. Nonetheless, the number of reduced reactions is independent of this choice.

By construction, our coarse graining procedure captures the entropy-production rate (EPR) [39, 40] of the underlying catalytic mechanism,

$$T\sigma := -\sum_\rho^M (\phi_\rho^+ - \phi_\rho^-)\Delta_\rho G = -\sum_\alpha^C (\psi_\alpha^+ - \psi_\alpha^-)\Delta_\alpha G \geqslant 0,$$

even though the number C of effective reactions α is much smaller than the number M of original reaction steps ρ. Therefore, our procedure is applicable in nonequilibrium situations, such as biological systems. In fact, the above equation is exact under steady-state conditions. In transient and other time-dependent situations the coarse graining can be a reasonable approximation. We elaborate this point further in the discussion.

Secondly, we work out the condition for this coarse graining to reduce to a single reaction α. In this case, we prove that the following flux–force relation holds true for this coarse-grained reaction:

$$-\Delta_\alpha G = RT \ln \frac{\psi_\alpha^+}{\psi_\alpha^-}.$$

A trivial consequence is that the coarse-grained reaction current, $J_\alpha = \psi_\alpha^+ - \psi_\alpha^-$, is aligned with the net force, $-\Delta_\alpha G$. In the past, such a flux–force relation has been used in the literature [41, 42] after its general validity was claimed [33] and later questioned [31, 34]. From here the belief arises that in every biochemical reaction network with any type of kinetics the currents and the forces of each reaction individually need to be aligned, a constraint used especially in flux balance analysis [43–45]. However, as we show in this paper, this relation does not hold when the coarse-graining reduces the biocatalyst to two or more coupled reactions.

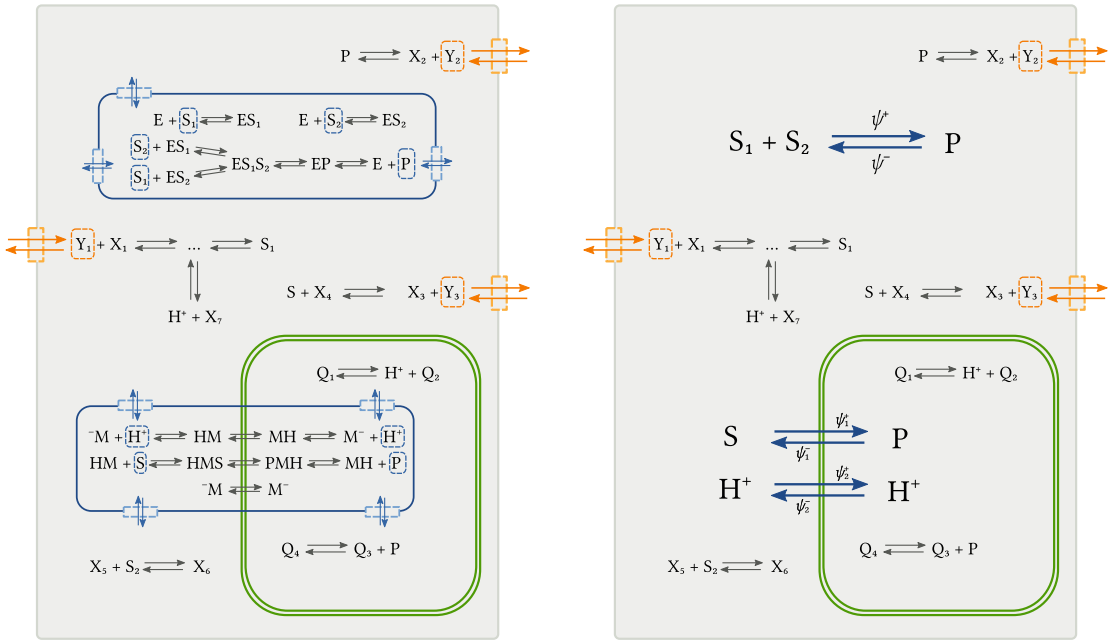

Figure 1. Overview of the coarse-graining procedure: (Left) the starting point is a reaction network with elementary reactions following mass–action kinetics in a steady state. This example contains two catalytic mechanisms [blue boxes] and for illustrative purposes some additional arbitrary reactions. Each of the two catalyst species, E and M, is conserved throughout the network. The reaction partners of the catalysts re-appear in the rest of the network. From the perspective of the remaining network, only the turnover [blue arrows] of these molecules are relevant. The involved concentrations may be global, as for S, or refer to different well stirred sub-compartments [green box], as for P. (Right) The procedure provides few coarse-grained reactions [blue arrows] that replace the originally more complicated mechanisms. The kinetic rate laws, ψ, of the coarse-grained reactions are different from mass–action. We construct them explicitly during the coarse-graining procedure, so that the turnover is correctly reproduced. Combined with the coarse-grained reaction forces [Gibbs free energies] also the entropy-production rate is reproduced exactly. We work out the coarse graining of these two catalysts, E and M, in detail in section 3.

This paper is structured as follows: first we present our results. Then, we illustrate our findings with two examples: the first is enzymatic catalysis of two substrates into one product. This can be reduced to a single reaction, for which we verify the flux–force relation at the coarse-grained level. The second example is a model of active membrane transport of protons, which is a prototype of a biocatalyst that cannot be reduced to a single reaction. Afterwards, we sketch the proofs for our general claims. Finally, we discuss our results and their implications. Rigorous proofs are provided in the appendix.

2. Results

Our main result is a systematic procedure for a thermodynamically consistent coarse graining of catalytic processes. These processes may involve several substrates, products, modifiers (e.g. activators, inhibitors) that bind to or are released from a single molecule—the catalyst. The coarse graining involves only a few steps and is exemplified graphically in figure 1:

(1) Consider the catalytic mechanism in a closed box and identify the internal stoichiometric cycles of the system. An internal stoichiometric cycle is a sequence of reactions leaving the state of the system invariant. Formally, internal stoichiometric cycles constitute the nullspace of the full stoichiometric matrix, $\mathbb{S}$.

(2) Consider the concentrations of all substrates, modifiers, and products (summarized as Y) constant in time—therefore reduce the stoichiometric matrix by exactly those species. The remaining species, X, represent N different states of the catalyst. As a consequence, the reduced stoichiometric matrix, $\mathbb{S}^X$, has a larger nullspace: new stoichiometric cycles emerge in the system. These emergent cycles cause a turnover in the substrates/products while leaving the internal species invariant. Choose a basis, $\boldsymbol{C}_\alpha$, of emergent stoichiometric cycles that are linearly independent from the internal cycles.

(3) Identify the net stoichiometry, $\mathbb{S}^Y\boldsymbol{C}_\alpha$, together with the sum, $-\Delta_\alpha G$, of the forces along each emergent cycle α.

(4) Calculate the apparent fluxes $\psi_\alpha^\pm$ along the emergent cycles at steady state.

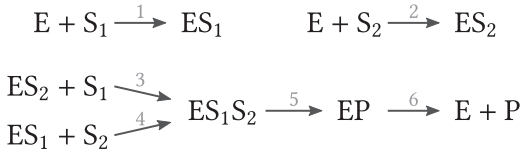

Figure 2. An enzymatic scheme turning two substrates into one product. The substrates can bind in arbitrary order. We adopt a reference direction for the individual reactions: forward is from left to right, as indicated by the arrows. The backward reactions are from right to left, thus every single reaction step is reversible. This scheme has a clear interpretation as a graph: the reactions are edges, reactants/products are vertices, where different combinations of reactants/products are considered different vertices. This graph has three disconnected components and contains no circuit.

For each emergent stoichiometric cycle α this procedure provides a new reversible reaction with net stoichiometry $\mathbb{S}^Y \boldsymbol{C}_\alpha$, net force $-\Delta_\alpha G$, and net fluxes $\psi_\alpha^\pm$. Furthermore, it preserves the EPR and, therefore, is thermodynamically consistent.

Our second result is a consequence of the main result: we prove that the flux–force relation is satisfied at the coarse-grained level by any catalytic mechanism for which only one single cycle emerges in step 2 of the presented procedure, as in example 3.1. When more cycles emerge, the flux–force relation does not hold as we show in the explicit counter-example 3.2.

3. Examples

3.1. Enzymatic catalysis

Let us consider the enzyme E that we introduced in figure 1. It is capable of catalyzing a reaction of two substrates, S_1 and S_2, into a single product molecule, P. The binding order of the two substrates does not matter. Every single one of these reaction steps is assumed to be reversible and to follow mass–action kinetics. For every reaction we adopt a reference forward direction. Overall, the enzymatic catalysis can be represented by the reaction network in figure 2.

We apply our main result to this enzymatic scheme and thus construct a coarse-grained description for the net catalytic action. We furthermore explicitly verify our second result by showing that the derived enzymatic reaction fluxes satisfy the flux–force relation.

3.1.1. Closed system—internal cycles

When this system is contained in a closed box, no molecule can leave or enter the reaction volume. The dynamics is then described by the following rate equations:

$$\frac{\mathrm{d}}{\mathrm{d}t}\boldsymbol{z} = \mathbb{S}\,\boldsymbol{J}(\boldsymbol{z}), \tag{1}$$

where we introduced the concentration vector $\boldsymbol{z}$, the current vector $\boldsymbol{J}(\boldsymbol{z})$, as well as the stoichiometric matrix $\mathbb{S}$:

$$\boldsymbol{z} = \begin{pmatrix} [\mathrm{E}] \\ [\mathrm{ES_1}] \\ [\mathrm{ES_2}] \\ [\mathrm{ES_1S_2}] \\ [\mathrm{EP}] \\ [\mathrm{S_1}] \\ [\mathrm{S_2}] \\ [\mathrm{P}] \end{pmatrix}, \quad \boldsymbol{J}(\boldsymbol{z}) = \begin{pmatrix} k_1[\mathrm{E}][\mathrm{S_1}] - k_{-1}[\mathrm{ES_1}] \\ k_2[\mathrm{E}][\mathrm{S_2}] - k_{-2}[\mathrm{ES_2}] \\ k_3[\mathrm{ES_2}][\mathrm{S_1}] - k_{-3}[\mathrm{ES_1S_2}] \\ k_4[\mathrm{ES_1}][\mathrm{S_2}] - k_{-4}[\mathrm{ES_1S_2}] \\ k_5[\mathrm{ES_1S_2}] - k_{-5}[\mathrm{EP}] \\ k_6[\mathrm{EP}] - k_{-6}[\mathrm{E}][\mathrm{P}] \end{pmatrix}, \quad \mathbb{S} = \begin{pmatrix} -1 & -1 & 0 & 0 & 0 & 1 \\ 1 & 0 & 0 & -1 & 0 & 0 \\ 0 & 1 & -1 & 0 & 0 & 0 \\ 0 & 0 & 1 & 1 & -1 & 0 \\ 0 & 0 & 0 & 0 & 1 & -1 \\ -1 & 0 & -1 & 0 & 0 & 0 \\ 0 & -1 & 0 & -1 & 0 & 0 \\ 0 & 0 & 0 & 0 & 0 & 1 \end{pmatrix}.$$

In the dynamical equations, only the currents $\boldsymbol{J}(\boldsymbol{z})$ depend on the concentrations, whereas the stoichiometric matrix $\mathbb{S}$ does not. The stoichiometric matrix thus imposes constraints on the possible steady-state concentrations that can be analyzed with mere stoichiometry: at steady state the current has to satisfy $0 = \mathbb{S}\,\boldsymbol{J}(\boldsymbol{z}_{\mathrm{ss}})$ or, equivalently, $\boldsymbol{J}(\boldsymbol{z}_{\mathrm{ss}}) \in \ker \mathbb{S}$. In our example, the nullspace $\ker \mathbb{S}$ is one-dimensional and spanned by $\boldsymbol{C}_{\mathrm{int}} = (1 \;\; -1 \;\; -1 \;\; 1 \;\; 0 \;\; 0)^\top$. Hence, the steady-state current is fully described by a single scalar value, $\boldsymbol{J}(\boldsymbol{z}_{\mathrm{ss}}) = J_{\mathrm{int}}\,\boldsymbol{C}_{\mathrm{int}}$. The vector $\boldsymbol{C}_{\mathrm{int}}$ represents a series of reactions that leave the system state unchanged: the two substrates are bound along reactions 1 and 4 and released again along reactions -3 and -2. In the end, the system returns to the exact same state as before these reactions. Therefore, we call this vector *internal stoichiometric cycle*. Having identified this internal cycle renders the first step complete.

Note that this stoichiometric cycle does not correspond to a self-avoiding closed path, or *circuit*, in the reaction graph in figure 2. This is due to the fact that *combinations* of species serve as vertices. If instead each species individually is a vertex, then also each cycle corresponds to a circuit.

In the following we explain why the first step of the procedure is important. The closed system has to satisfy a constraint that comes from physics: a closed system necessarily has to relax to a thermodynamic equilibrium state—which is characterized by the absence of currents of extensive quantities on any scale. Thus thermodynamic equilibrium is satisfied if $J_{\text{int}} = 0$. One can show that this requirement is equivalent to Wegscheider's condition [46]: the product of the forward rate constants along the internal cycle equals that of the backward rate constants,

$$k_1 k_4 k_{-3} k_{-2} = k_{-1} k_{-4} k_3 k_2. \tag{2}$$

Furthermore, irrespective of thermodynamic equilibrium, the steady state has to be stoichiometrically compatible with the initial condition: there are three linearly independent vectors in the cokernel of $\mathbb{S}$:

$$\boldsymbol{\ell}_{\text{E}} = \begin{matrix} \text{E} \\ \text{ES}_1 \\ \text{ES}_2 \\ \text{ES}_1\text{S}_2 \\ \text{EP} \\ \text{S}_1 \\ \text{S}_2 \\ \text{P} \end{matrix} \begin{pmatrix} 1 \\ 1 \\ 1 \\ 1 \\ 1 \\ 0 \\ 0 \\ 0 \end{pmatrix}, \qquad \boldsymbol{\ell}_1 = \begin{matrix} \text{E} \\ \text{ES}_1 \\ \text{ES}_2 \\ \text{ES}_1\text{S}_2 \\ \text{EP} \\ \text{S}_1 \\ \text{S}_2 \\ \text{P} \end{matrix} \begin{pmatrix} 0 \\ 1 \\ 0 \\ 1 \\ 1 \\ 1 \\ 0 \\ 1 \end{pmatrix}, \qquad \boldsymbol{\ell}_2 = \begin{matrix} \text{E} \\ \text{ES}_1 \\ \text{ES}_2 \\ \text{ES}_1\text{S}_2 \\ \text{EP} \\ \text{S}_1 \\ \text{S}_2 \\ \text{P} \end{matrix} \begin{pmatrix} 0 \\ 0 \\ 1 \\ 1 \\ 1 \\ 0 \\ 1 \\ 1 \end{pmatrix}.$$

For each such vector, the scalar $L \equiv \boldsymbol{\ell} \cdot \boldsymbol{z}$ evolves according to $\frac{\partial}{\partial t} \boldsymbol{\ell} \cdot \boldsymbol{z} = \boldsymbol{\ell} \cdot \mathbb{S}\, \boldsymbol{J}(\boldsymbol{z}) = 0$, and thus is a *conserved quantity*. We deliberately chose linearly independent vectors with a clear physical interpretation. These vectors represent conserved moieties, i.e. a part of (or an entire) molecule that remains intact in all reactions. The total concentration of the enzyme moiety in the system is given by L_{E}. The other two conservation laws, L_1 and L_2, are the total concentrations of moieties of the substrates, S_1 and S_2, respectively.

Given a set of values for the conserved quantities from the initial condition, Wegscheider's condition on the rate constants ensures uniqueness of the equilibrium solution [46].

3.1.2. Open system—emergent cycles

So far we only discussed the system in a closed box that will necessarily relax to a thermodynamic equilibrium.

We now open the box and assume that there is a mechanism capable of fixing the concentrations of S_1, S_2 and P to some given levels. These three species therefore no longer take part in the dynamics. Formally, we divide the set of species into two disjoint sets:

$$\underbrace{\{\text{E},\ \text{ES}_1,\ \text{ES}_2,\ \text{ES}_1\text{S}_2,\ \text{EP}\}}_{X} \bigcup \underbrace{\{\text{S}_1,\ \text{S}_2,\ \text{P}\}}_{Y}.$$

The first are the *internal species*, X, which are subject to the dynamics. The second are the *chemostatted species*, Y, which are exchanged with the environment. We apply this splitting to the stoichiometric matrix,

$$\mathbb{S} = \begin{pmatrix} \mathbb{S}^X \\ \mathbb{S}^Y \end{pmatrix},$$

and the vector of concentrations, $\boldsymbol{z} = (\boldsymbol{x}, \boldsymbol{y})$. Analogously, the rate equations for this open reaction system split into

$$\frac{\partial}{\partial t}\boldsymbol{x} = \mathbb{S}^X \boldsymbol{J}(\boldsymbol{x}, \boldsymbol{y}), \tag{3}$$

$$0 \equiv \frac{\partial}{\partial t}\boldsymbol{y} = \mathbb{S}^Y \boldsymbol{J}(\boldsymbol{x}, \boldsymbol{y}) + \boldsymbol{I}(\boldsymbol{x}, \boldsymbol{y}). \tag{4}$$

The equation (4) is merely a definition for the exchange current $\boldsymbol{I}$, keeping the species Y at constant concentrations. Note that the exchange currents $\boldsymbol{I}$ quantify the substrate/product turnover. The actual dynamical rate equations, the equation (3), are a subset of the original equations for the closed system, treating the chemostats as constant parameters. Absorbing these latter concentrations into the rate constants, we arrive at a linear ODE system with new *pseudo-first-order rate constants* $\tilde{k}(\boldsymbol{y})$. For these rate equations, one needs to reconsider the graphical representation of this reaction network: since the chemostatted species now are merely parameters for the reactions, we have to remove the chemostatted species from the former vertices of the network representation and associate them to the edges. The resulting graph representing the open network is drawn in figure 3.

105

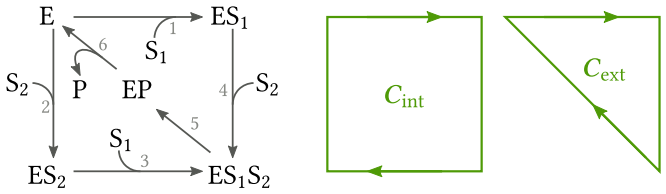

Figure 3. (Left) Enzymatic catalysis as an *open* chemical network. The species S_1, S_2 and P are now associated to the edges of the graph, instead of being part of its vertices as in figure 2. This graph has only one connected component and contains three distinct circuits. (Center, right) Graphical representation of the two circuits spanning the kernel of $\mathbb{S}^X$. The lower left triangle constitutes the third circuit. It can be recovered by a linear combination of the other two circuits.

The steady-state current $\boldsymbol{J}_{ss} = \boldsymbol{J}(\boldsymbol{x}_{ss}, \boldsymbol{y})$ of equation (3) needs to be in the kernel of the internal stoichiometric matrix $\mathbb{S}^X$ only. This opens up new possibilities. It is obvious that $\ker \mathbb{S}$ is a subset of $\ker \mathbb{S}^X$, but $\ker \mathbb{S}^X$ is in fact bigger. In our example we now have two *stoichiometric* cycles,

$$\boldsymbol{C}_{\text{int}} = \begin{pmatrix} 1 \\ -1 \\ -1 \\ 1 \\ 0 \\ 0 \end{pmatrix} \quad \text{and} \quad \boldsymbol{C}_{\text{ext}} = \begin{pmatrix} 1 \\ 0 \\ 0 \\ 1 \\ 1 \\ 1 \end{pmatrix}. \tag{5}$$

The first cycle is the internal cycle we identified in the closed system already: it only involves reactions that leave the closed system invariant, thus upon completion of this cycle not a single molecule is being exchanged. The second cycle is different: upon completion it leaves the internal species unchanged but chemostatted species are exchanged with the environment. Since this type of cycle appears only upon chemostatting, we call them *emergent* stoichiometric cycles. Overall, the steady-state current is a linear combination of these two cycles: $\boldsymbol{J}_{ss} = J_{\text{int}}\, \boldsymbol{C}_{\text{int}} + J_{\text{ext}}\, \boldsymbol{C}_{\text{ext}}$. This completes step 2.

These two stoichiometric cycles correspond to circuits in the open reaction graph. We give a visual representation on the right of figure 3. As a consequence of working with catalysts, the vertices of the reaction graph for the open system coincide with the internal species X. Therefore, for all catalysts the cycles of the open system correspond to circuits in the corresponding graph.

The cycles are not the only structural object affected by the chemostatting procedure: the conservation laws change as well. In the enzyme example we have merely one conservation law left—that of the enzyme moiety, L_E. The substrate moieties are being exchanged with the environment, which renders L_1 and L_2 *broken conservation laws*. Overall, upon adding three chemostats two conservation laws were broken and one cycle emerged. In fact, the number of chemostatted species always equals the number of broken conservation laws plus the number of emergent cycles [47].

3.1.3. Net stoichiometries and net forces

The net stoichiometry of the emergent cycle is $S_1 + S_2 \rightleftharpoons P$. This represents a single reversible reaction describing the net catalytic action of the enzyme. For a complete coarse graining, we still need to identify the fluxes and the net force along this reaction. Its net force is given by the sum of the forces along the emergent cycle. Collecting the Gibbs energies of reaction in a vector, $\Delta_r \boldsymbol{G} := (\Delta_1 G, \ \ldots, \Delta_6 G)^\top$, this sum is concisely written as

$$-\Delta_{\text{ext}} G := -\boldsymbol{C}_{\text{ext}} \cdot \Delta_r \boldsymbol{G} = RT \ln \frac{k_1 k_4 k_5 k_6 [S_1][S_2]}{k_{-1} k_{-4} k_{-5} k_{-6} [P]}. \tag{6}$$

One could also ask about the net stoichiometry and net force along the internal cycle. However, we have $\mathbb{S}\, \boldsymbol{C}_{\text{int}} = 0$ since the internal cycle does not interact with the chemostats. Moreover, the net force along the internal cycle is

$$-\boldsymbol{C}_{\text{int}} \cdot \Delta_r \boldsymbol{G} = RT \ln \frac{k_1 k_4 k_{-3} k_{-2}}{k_{-1} k_{-4} k_3 k_2} = 0 \tag{7}$$

by virtue of Wegscheider's condition.

106

3.1.4. Apparent fluxes

We now determine the apparent fluxes along the two cycles of the system. To that end, we first solve the linear rate equations to calculate the steady-state concentrations and the steady-state currents. For the steady-state

concentrations we use a diagrammatic method popularized by King and Altman [48] that we summarize in appendix A.

As derived in step 2 of the procedure, the steady-state current vector is

$$\boldsymbol{J}_{\rm ss} = \begin{matrix}1\\2\\3\\4\\5\\6\end{matrix}\begin{pmatrix} J_{\rm int}+J_{\rm ext}\\ -J_{\rm int}\\ -J_{\rm int}\\ J_{\rm int}+J_{\rm ext}\\ J_{\rm ext}\\ J_{\rm ext}\end{pmatrix}.$$

Hence the two cycle currents are

$$J_{\rm int} = -J_2 = k_{-2}[{\rm ES}_2] - k_2[{\rm E}][{\rm S}_2], \qquad J_{\rm ext} = J_6 = k_6[{\rm EP}] - k_{-6}[{\rm E}][{\rm P}].$$

With the explicit steady-state concentrations given in appendix A.1, we find (see appendix B.1 for details):

$$J_{\rm int} = k_{-2}[{\rm ES}_2] - k_2[{\rm E}][{\rm S}_2] = \frac{L_{\rm E}k_2k_3}{N_{\rm E}(\boldsymbol{y})k_1}\left(\frac{k_{-1}}{k_4} + [{\rm S}_2]\right)(k_{-1}k_{-4}k_{-5}k_{-6}[{\rm P}] - k_1k_4k_5k_6[{\rm S}_1][{\rm S}_2]).$$

and

$$J_{\rm ext} = k_6[{\rm EP}] - k_{-6}[{\rm E}][{\rm P}] = \frac{L_{\rm E}\xi(\boldsymbol{y})}{N_{\rm E}(\boldsymbol{y})}(k_1k_4k_5k_6[{\rm S}_1][{\rm S}_2] - k_{-1}k_{-4}k_{-5}k_{-6}[{\rm P}]). \tag{8}$$

Here, $L_{\rm E}$ is the total amount of available enzyme, $N_{\rm E}(\boldsymbol{y})$ is a positive quantity that depends on the chemostat concentrations as well as all rate constants, and

$$\xi(\boldsymbol{y}) = k_3[{\rm S}_1] + \frac{k_2k_3[{\rm S}_2]}{k_1} + k_{-2} + \frac{k_{-2}k_{-3}}{k_{-4}}.$$

As expected, the current along the emergent cycle $J_{\rm ext}$ is not zero, provided that its net force is not zero. However, note that the current along the internal cycle does *not* vanish either, even though its own net force is zero. Both currents vanish only when the net force, $-\Delta_{\rm ext}G$, vanishes—which is at thermodynamic equilibrium.

Finally, we decompose the current $J_{\rm ext} = \psi^+ - \psi^-$ into the apparent fluxes

$$\psi^+ = \frac{L_{\rm E}\xi(\boldsymbol{y})}{N_{\rm E}(\boldsymbol{y})}k_1k_4k_5k_6[{\rm S}_1][{\rm S}_2] > 0, \qquad \psi^- = \frac{L_{\rm E}\xi(\boldsymbol{y})}{N_{\rm E}(\boldsymbol{y})}k_{-1}k_{-4}k_{-5}k_{-6}[{\rm P}] > 0. \tag{9}$$

Here, it is important to note that while

$$\psi^+ - \psi^- = k_6[{\rm EP}] - k_{-6}[{\rm E}][{\rm P}],$$

there are several cancellations happening in the derivation of equation (8) implying that

$$\psi^+ \neq k_6[{\rm EP}], \quad \psi^- \neq k_{-6}[{\rm E}][{\rm P}].$$

We elaborate on these cancellations in this special case in appendix B.1 as well as for the general case in appendix B.3.

3.1.5. Flux–force relation

With the explicit expressions for the net force, equation (6), and the apparent fluxes, equation (9), of the emergent cycle we explicitly verify the flux–force relation at the coarse-grained level:

$$RT\ln\frac{\psi^+}{\psi^-} = RT\ln\frac{k_1k_4k_5k_6[{\rm S}_1][{\rm S}_2]}{k_{-1}k_{-4}k_{-5}k_{-6}[{\rm P}]} = -\Delta_{\rm ext}G.$$

This flux–force relation implies that the reaction current is always aligned with the net force along this reaction: $J_{\rm ext} > 0 \Leftrightarrow -\Delta_{\rm ext}G > 0$. In other words, the reaction current directly follows the force acting on this reaction.

In fact, in this case we can connect the flux–force relation to the second law of thermodynamics. The EPR reads

$$\begin{aligned} T\sigma(\boldsymbol{x}_{\rm ss}, \boldsymbol{y}) &= -\boldsymbol{J}_{\rm ss}\cdot\Delta_{\rm r}\boldsymbol{G} = -J_{\rm int}\,\boldsymbol{C}_{\rm int}\cdot\Delta_{\rm r}\boldsymbol{G} - J_{\rm ext}\,\boldsymbol{C}_{\rm ext}\cdot\Delta_{\rm r}\boldsymbol{G}\\ &= -J_{\rm ext}\,\Delta_{\rm ext}G = RT(\psi^+ - \psi^-)\ln\frac{\psi^+}{\psi^-} \geqslant 0. \end{aligned}$$

With this representation, it is evident that the flux–force relation ensures the second law: $\sigma \geqslant 0$. Moreover, we see explicitly that the EPR is faithfully reproduced at the coarse-grained level. This shows the thermodynamic consistency of our coarse-graining procedure.

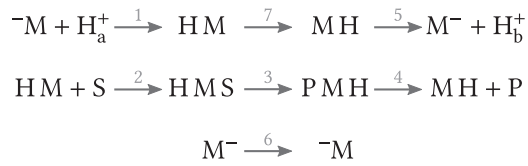

Figure 4. Reaction graph for the mechanism modeling the active transport of protons from one side of a membrane, H_a^+, to the other side, H_b^+. The transport is coupled to the catalysis of a substrate, S, to a product, P. The free transporter itself exists in two different conformations denoted ^{-}M and M^-, respectively. Again, all reactions are considered reversible and to follow mass–action kinetics. A reference forward direction is indicated as arrows from left to right.

3.2. Active membrane transport

We now turn to the second example introduced in figure 1: a membrane protein, M, that models a proton pump similar to the one presented in [37]. It transports protons from one side of the membrane (side a) to the other (side b). The membrane protein itself is assumed to be charged to facilitate binding of the protons and to have different conformations M^- and ^{-}M where it exposes the binding site to the two different sides of the membrane. Furthermore, when a proton is bound, it can either bind another substrate S when exposing the proton to side a—or the respective product P when the proton is exposed to side b. The latter could be some other ion concentrations on either side of the membrane—or an energy rich compound (ATP) and its energy poor counterpart (ADP). The reactions modeling this mechanism are summarized in the reaction graph in figure 4.

In order to find a coarse-grained description for this transporter we apply our result. Since the procedure is already detailed in example 3.1, we omit some repetitive explanations in this example.

3.2.1. Closed system—internal cycles

This closed system has no cycle, therefore Wegscheider's conditions do not impose any relation between the reaction rate constants. There are three conservation laws in the closed system,

$$\ell_M = \begin{matrix} {}^{-}M \\ HM \\ HMS \\ PMH \\ MH \\ M^- \\ H_a^+ \\ H_b^+ \\ S \\ P \end{matrix} \begin{pmatrix} 1 \\ 1 \\ 1 \\ 1 \\ 1 \\ 1 \\ 0 \\ 0 \\ 0 \\ 0 \end{pmatrix}, \qquad \ell_H = \begin{matrix} {}^{-}M \\ HM \\ HMS \\ PMH \\ MH \\ M^- \\ H_a^+ \\ H_b^+ \\ S \\ P \end{matrix} \begin{pmatrix} 0 \\ 1 \\ 1 \\ 1 \\ 1 \\ 0 \\ 1 \\ 1 \\ 0 \\ 0 \end{pmatrix}, \qquad \ell_S = \begin{matrix} {}^{-}M \\ HM \\ HMS \\ PMH \\ MH \\ M^- \\ H_a^+ \\ H_b^+ \\ S \\ P \end{matrix} \begin{pmatrix} 0 \\ 0 \\ 1 \\ 1 \\ 0 \\ 0 \\ 0 \\ 0 \\ 1 \\ 1 \end{pmatrix}.$$

They represent the conservation of membrane protein (L_M), proton (L_H), and substrate moieties (L_S), respectively, showing that these three are conserved independently. For any initial condition, the corresponding rate equations will relax to a unique steady-state solution satisfying thermodynamic equilibrium, $\boldsymbol{J}(\boldsymbol{z}) = 0$.

3.2.2. Open system—emergent cycles

We now fix the concentrations of the protons H_a^+ and H_b^+ in the two reservoirs, as well as the substrate and the product concentrations. The reaction network for this open system is depicted in figure 5. The open system still has a conserved membrane protein moiety while the conservation laws of protons and substrate are broken upon chemostatting. Furthermore, there are two emergent cycles now,

$$C_{cat} = \begin{matrix} 1 \\ 2 \\ 3 \\ 4 \\ 5 \\ 6 \\ 7 \end{matrix} \begin{pmatrix} 0 \\ 1 \\ 1 \\ 1 \\ 0 \\ 0 \\ -1 \end{pmatrix} \quad \text{and} \quad C_{sl} = \begin{matrix} 1 \\ 2 \\ 3 \\ 4 \\ 5 \\ 6 \\ 7 \end{matrix} \begin{pmatrix} -1 \\ 0 \\ 0 \\ 0 \\ -1 \\ -1 \\ -1 \end{pmatrix}. \tag{10}$$

Their visual representation as circuits is given on the right of figure 5.

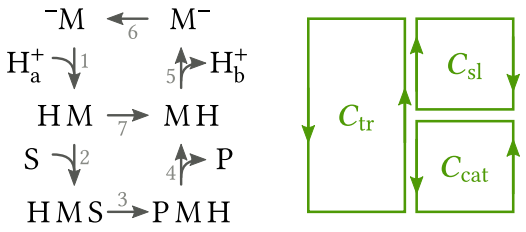

Figure 5. (Left) Active membrane transport as a graph representing the *open* chemical network. The proton concentrations H_a^+ and H_b^+, as well as the substrate and the product are chemostatted, thus are associated to the edges of the graph. (Right) Graphical representations for the three distinct cycles in this graph. Only two of them are independent and we choose $\boldsymbol{C}_{\mathrm{cat}}$ and $\boldsymbol{C}_{\mathrm{sl}}$ as a basis in the main text. The third is their difference $\boldsymbol{C}_{\mathrm{tr}} = \boldsymbol{C}_{\mathrm{cat}} - \boldsymbol{C}_{\mathrm{sl}}$.

3.2.3. Net stoichiometry and net forces

The first emergent cycle has the net stoichiometry $\mathrm{S} \rightleftharpoons \mathrm{P}$, which represents pure catalysis with net force

$$-\Delta_{\mathrm{cat}} G = RT \ln \frac{k_2 k_3 k_4 k_{-7} [\mathrm{S}]}{k_{-2} k_{-3} k_{-4} k_7 [\mathrm{P}]}. \tag{11}$$

The second cycle has net stoichiometry $H_b^+ \rightleftharpoons H_a^+$. This represents the slip of one proton from side b back to side a with net force

$$-\Delta_{\mathrm{sl}} G = RT \ln \frac{k_{-1} k_{-5} k_{-6} k_{-7} [H_b^+]}{k_1 k_5 k_6 k_7 [H_a^+]}. \tag{12}$$

For later reference, we note that the difference $\boldsymbol{C}_{\mathrm{tr}} = \boldsymbol{C}_{\mathrm{cat}} - \boldsymbol{C}_{\mathrm{sl}}$ has net stoichiometry $H_a^+ + \mathrm{S} \rightleftharpoons H_b^+ + \mathrm{P}$. This is the active transport of a proton from side a to side b, under catalysis of one substrate into one product. The net force of this reaction is

$$-\Delta_{\mathrm{tr}} G = -\Delta_{\mathrm{cat}} G + \Delta_{\mathrm{sl}} G = RT \ln \frac{k_1 k_2 k_3 k_4 k_5 k_6 [H_a^+][\mathrm{S}]}{k_{-1} k_{-2} k_{-3} k_{-4} k_{-5} k_{-6} [H_b^+][\mathrm{P}]}. \tag{13}$$

3.2.4. Apparent fluxes

Solving the linear rate equations (see appendix A), we have a solution for the steady-state concentrations. The exact expressions are given in appendix A.2. With the steady-state concentrations, we calculate the contributions of both cycles to the steady-state current: $\boldsymbol{J}(\boldsymbol{x}_{\mathrm{ss}}, \boldsymbol{y}) = J_{\mathrm{cat}}\, \boldsymbol{C}_{\mathrm{cat}} + J_{\mathrm{sl}}\, \boldsymbol{C}_{\mathrm{sl}}$. Each current contribution is given by a single reaction:

$$J_{\mathrm{cat}} = J_2 =: \psi_{\mathrm{cat}}^+ - \psi_{\mathrm{cat}}^-, \qquad J_{\mathrm{sl}} = -J_1 =: \psi_{\mathrm{sl}}^+ - \psi_{\mathrm{sl}}^-.$$

With the abbreviations

$$\xi_{\mathrm{cat}} := k_{-6} k_{-5} [H_b^+] + k_1 k_{-5} [H_a^+][H_b^+] + k_6 k_1 [H_a^+], \qquad \xi_{\mathrm{sl}} := k_3 k_4 + k_{-2} k_4 + k_{-3} k_{-2},$$

we can express the apparent fluxes as

$$\begin{aligned}
\frac{N_{\mathrm{M}}}{L_{\mathrm{M}}} \psi_{\mathrm{cat}}^+ &= k_1 k_2 k_3 k_4 k_5 k_6 [H_a^+][\mathrm{S}] + \xi_{\mathrm{cat}} k_{-7} k_2 k_3 k_4 [\mathrm{S}], \\
\frac{N_{\mathrm{M}}}{L_{\mathrm{M}}} \psi_{\mathrm{cat}}^- &= k_{-1} k_{-2} k_{-3} k_{-4} k_{-5} k_{-6} [H_b^+][\mathrm{P}] + \xi_{\mathrm{cat}} k_7 k_{-2} k_{-3} k_{-4} [\mathrm{P}], \\
\frac{N_{\mathrm{M}}}{L_{\mathrm{M}}} \psi_{\mathrm{sl}}^+ &= k_{-1} k_{-2} k_{-3} k_{-4} k_{-5} k_{-6} [H_b^+][\mathrm{P}] + \xi_{\mathrm{sl}} k_{-1} k_{-5} k_{-6} k_{-7} [H_b^+], \\
\frac{N_{\mathrm{M}}}{L_{\mathrm{M}}} \psi_{\mathrm{sl}}^- &= k_1 k_2 k_3 k_4 k_5 k_6 [H_a^+][\mathrm{S}] + \xi_{\mathrm{sl}} k_1 k_5 k_6 k_7 [H_a^+].
\end{aligned}$$

The derivation for these equations is detailed in appendix B.2. Note that N_{M} depends on all rate constants and all chemostat concentrations.

3.2.5. Breakdown of the flux–force relation

We see that the abbreviated terms ξ appear symmetrically in the forward and backward fluxes. Therefore, when the net forces are zero, necessarily the currents vanish and the system is at thermodynamic equilibrium. However, in general, the currents do not vanish. Moreover, the concentrations of the chemostats appear in the four different fluxes in different combinations—indicating that both net forces couple to both coarse-grained reactions. Due to this coupling, it is impossible to find nice flux–force relations for the two reactions

independently:

$$-\Delta_{\mathrm{cat}} G \neq RT \ln \frac{\psi^{+}_{\mathrm{cat}}}{\psi^{-}_{\mathrm{cat}}}, \qquad -\Delta_{\mathrm{sl}} G \neq RT \ln \frac{\psi^{+}_{\mathrm{sl}}}{\psi^{-}_{\mathrm{sl}}}. \tag{14}$$

To the contrary, it is easy to find concentrations for the four chemostats where the catalytic force is so strong that it drives the slip current against its natural direction—giving rise to a negative contribution in the EPR. Nonetheless, the overall EPR is correctly reproduced at the coarse-grained level:

$$T\sigma = -\boldsymbol{J}_{\mathrm{ss}} \cdot \Delta_{\mathrm{r}} \boldsymbol{G} = -J_{\mathrm{cat}}\, \Delta_{\mathrm{cat}} G - J_{\mathrm{sl}}\, \Delta_{\mathrm{sl}} G \geqslant 0.$$

Since this is, by construction, the correct EPR of the full system at steady state, we know that it is always non-negative—and that the coarse-graining procedure is thermodynamically consistent. This example shows explicitly that biochemical reaction networks need not satisfy the flux–force relation, nor need their currents and forces be aligned to comply with the second law. After all, the function of this membrane protein is to transport protons from side a to side b against the natural concentration gradient.

4. Cycle-based coarse graining

From the perspective of a single biocatalyst, the rest of the cell (or cellular compartment) serves as its environment, providing a reservoir for different chemical species. Our coarse graining exploits this perspective to disentangle the interaction of the catalyst with its environment—in the form of emergent cycles—from the behavior of the catalyst in a (hypothetical) closed box at thermodynamic equilibrium—in the form of the internal cycles. From the perspective of the environment, only the interactions with the catalyst matter, i.e. the particle exchange currents: they prescribe the substrate/product turnover and when combined with the reservoir's concentrations (chemical potentials) also the dissipation. Our coarse graining respects the reservoir's concentrations and incorporates all the emergent cycles that exchange particles with the reservoir. It thus correctly reproduces the exchange currents: this is the fundamental reason why we can replace the actual detailed mechanism of the catalyst with a set of coarse-grained reactions in a thermodynamically exact way. A formal version of this reasoning, including all necessary rigor and a constructive prescription to find the apparent fluxes, is provided in appendix B.

In our examples we illustrated the fundamental difference between the case where a catalyst can be replaced with a single coarse-grained reaction and the case where this is not possible. In the first case, such a catalyst interacts with substrate and product molecules that are coupled via exchange of mass in a specific stoichiometric ratio. This is known as tight coupling. Whether or not the catalysis is additionally modified by activators or inhibitors, does not interfere with this condition. After all, the modifiers are neither consumed nor produced. Thus they appear only in the normalizing denominators of the steady-state concentrations and affect the kinetics while leaving the thermodynamics untouched. Furthermore, if there is only one single emergent cycle in a catalytic mechanism, any product of pseudo-first-order rate constants along any circuit in the network will either (i) satisfy Wegscheider's conditions or (ii) reproduce (up to sign) the net force, $-\Delta_{\alpha} G$, of the emergent cycle. Ultimately, this is why the flux–force relation holds in this tightly coupled case. A formal version of this proof, including all necessary rigor, is provided in appendix C.

In the case where we have to provide two or more coarse-grained reactions, the catalytic mechanism couples several processes that are not tightly coupled via exchange of mass. To the contrary: the turnover of different substrates/products need not have fixed stoichiometric ratios. In fact, their ratios will depend on the environment's concentrations. In this case the flux–force relation does not hold in general, as we proved with our counter-example. After all, when several processes are coupled, the force of one process can overcome the force of the second process to drive the second current against its natural direction. This transduction of energy [12, 49] would not be possible at a coarse-grained level, if the flux–force relation was always true.

We now asses the reduction provided by our procedure: the number C of coarse-grained reactions α is always lower than the number M of reaction steps ρ in the original mechanism. This can be understood from the graph representation of the open system: the number B of circuits in a connected graph is related to its number N of vertices (catalyst states) and the number M of edges (reaction steps) by $B = M - N + 1$ [50]. Some of the circuits represent internal cycles, rendering B an upper bound to the number of emergent cycles C. Since the number N of catalyst states is at least two, these numbers are ordered: $M > B \geqslant C$. This proves that our coarse graining always reduces the number of reactions.

5. Discussion

The original work of Michaelis and Menten [4] was based on a specific enzyme that converts a single substrate into a single product assuming a totally irreversible step. Their goal was to determine the rate of production of product molecule. Later progress in enzyme kinetics extended their method to deal with fully reversible mechanisms, as well as many substrates, many products and modifiers [1]. The focus on the turnover led many people to identify the net effect of the enzyme with a *single* effective reaction, describing its kinetics with the Michaelis–Menten equation (or one of its generalizations). Our coarse-graining indeed incorporates all these special cases: the Michaelis–Menten equation arises from coarse graining a mechanism of the form

$$\mathrm{S} + \mathrm{E} \rightleftharpoons \mathrm{ES} \rightleftharpoons \mathrm{EP} \rightleftharpoons \mathrm{E} + \mathrm{P} \tag{15}$$

and assuming that the last reaction step, the release of the product, is much faster than the other steps. Then the coarse-grained reaction current is identical to the substrate/product turnover. Importantly, our procedure highlights that there is no direct correspondence between the number of required net reactions and the number of circuits in the reaction graph—even of the open system. Some circuits correspond to *internal cycles* that play a kinetic role, not leaving a trace in the thermodynamic forces. Only the *emergent cycles* need to be taken into account for the coarse graining. Thus the net effect of a multi-cyclic catalyst might be consistently expressed as a single effective reaction, as seen in the example 3.1.

Likewise, in theoretical studies of biochemical systems, effective unimolecular reactions of the form

are frequently used, where the reaction rate constants satisfy

$$\frac{k^+}{k^-} = \exp\left[\frac{\mu_A^\circ - \mu_B^\circ + \mu_X - \mu_Y}{RT}\right].$$

Here, the chemical potentials, μ, account for the thermodynamic force exerted by X and Y. Even when the actual effective reaction does not follow mass–action kinetics, this equation is assumed, implying that the effective reaction fluxes are $k^+[A] = \psi^+$ and $k^-[B] = \psi^-$, and the 'constants' k indeed depend on some concentrations. This is only consistent if the implicit conversion mechanism is tightly coupled by exchange of mass: when tightly coupled, the differences of the chemical potentials represent the Gibbs free energy change along the reaction $A + X \rightleftharpoons B + Y$. In this case, the above equation is the flux–force relation. Otherwise, our coarse-graining procedure reveals that this is thermodynamically inconsistent: if the implicitly modeled catalysis is not tightly coupled via the exchange of mass, there is a hidden thermodynamic driving force that is independent of the concentrations of A and B, while the turnover of X/Y is not in a stoichiometric ratio to the turnover of A/B. We have seen in example 3.2 that the flux–force relation indeed does not hold in this case.

The failure of the flux–force relation in the nontightly coupled case does not imply inconsistent thermodynamics. Our coarse-graining procedure indeed deals with this case very easily. The resulting fluxes and forces reproduce the EPR while sacrificing the flux–force relation. The key difference to the original ideas in enzyme kinetics is that the substrate/product turnover is split into *several* effective reactions with their own reaction fluxes and forces, reproducing the EPR. This is especially important for complex catalysts: many models for molecular motors and active transporters are not tightly coupled. These free-energy transducers often display slippage via futile cycles. While some enzymes also show signs of slippage, many simple enzymes are modeled as tightly coupled—which implies they satisfy the flux–force relation. Our coarse graining deals with all these cases and in that sense goes far beyond Michaelis–Menten.

Our procedure greatly reduces the number of species and reactions involved in a network while reproducing the EPR. This comes at the cost of complicated effective fluxes (rate laws). They are rational functions of the involved concentrations and thus more complicated than simple mass–action kinetics. Nonetheless, our procedure is constructive by giving these complicated expressions explicitly. With the explicit solutions at hand, further assumptions can be made to simplify the effective fluxes—as in the case of the original Michaelis–Menten equation. Note that these additional simplifications may have an impact on the EPR, in the worst case breaking the thermodynamic consistency. This trade-off between simplicity and thermodynamic correctness needs to be evaluated case by case.

We now discuss the limitations of our approach. The presented coarse-graining procedure is exact in *steady-state* situations, arbitrarily far from equilibrium. When the surrounding reaction network is not in a steady state, the coarse graining can still be used: then the coarse-grained reaction fluxes and forces have to be considered *instantaneous*—they change in time due to the changing substrate/product (or modifier) concentrations. Underlying this point of view is a separation of time scales: when the abundance of substrates and products is very large, as compared to the abundance of catalyst, then the concentrations of the latter change much more quickly. This results in a quasi-steady state for the catalyst-containing species. Consequently, our coarse graining

111

cannot capture the contribution to dissipation that arises in this fast relaxation dynamics. It only captures the dissipation due to the conversion of substrate into product. This reasoning can be made more rigorous: there are time-scale separation techniques for deterministic rate equations [25, 51] frequently used in biochemical contexts [26], furthermore stochastic corrections due to small copy-numbers [52] and even effective memory effects [27, 53] can be incorporated. However, these techniques do not explicitly address the question of thermodynamic consistency and we think that combining our coarse-graining with these techniques is a promising endeavor for the future.

We restricted the entire reasoning in this paper to catalysts. They follow linear rate equations when their reaction partners have constant concentrations. This linearity allowed us to give explicit solutions for general catalysts. Focusing on the emergent cycles to reproduce the correct thermodynamics paves the way to apply a similar procedure beyond catalysts: reaction networks that remain nonlinear after chemostatting still have emergent cycles [28]. They can be calculated algebraically from bases for the nullspaces of the full and the reduced stoichiometric matrices, $\mathbb{S}$ and $\mathbb{S}^X$. The cycles in nonlinear networks may not have a representation as circuits in the reaction graph, as we have seen with the internal cycle of the enzyme in a closed box. Nonetheless, each of the emergent cycles $\boldsymbol{C}_\alpha$ can serve as an effective reaction: it has a well defined stoichiometry, $\mathbb{S}^Y\boldsymbol{C}_\alpha$, and a well defined net force, $-\Delta_r\boldsymbol{G}\cdot\boldsymbol{C}_\alpha$. The steady state concentrations as well as the fluxes, however, need to be determined case by case. Nonlinear differential equations can be multi-stable, where our coarse graining applies to each stable steady state. Some nonlinear ODEs exhibit limit cycles, thus never reaching a steady state. In this case our procedure is no longer applicable.

6. Summary

We have presented a coarse-graining procedure for biocatalysts and have shown that it is thermodynamically consistent. During this coarse graining procedure, a detailed catalytic mechanism is replaced by a few net reactions. The stoichiometry, deterministic kinetic rate laws and net forces for the coarse-grained reactions are calculated explicitly from the detailed mechanism—ensuring that at steady state the detailed mechanism and the net reactions have both the same substrate/product turnover and the same EPR.

Furthermore, we have shown that in the tightly coupled case where a detailed mechanism is replaced by a single reaction, this net reaction satisfies a flux–force relation. In the case where a detailed mechanism has to be replaced with several net reactions, the flux–force relation does not hold for the net reactions due to cross-coupling of independent thermodynamic forces. Ultimately, this cross-coupling allows the currents and forces not to be aligned—while complying with the second law of thermodynamics.

Overall, we have shown that coarse-graining schemes which preserve the correct thermodynamics far from equilibrium are not out of reach.

Acknowledgments

This work is financially supported by the National Research Fund of Luxembourg in the frame of AFR PhD Grants No. 7865466 and No. 9114110. Furthermore, this research is funded by the European Research Council project NanoThermo (ERC-2015-CoG Agreement No. 681456).

Conflict of interest

The authors declare that they have no conflict of interest.

Appendix A. Diagrammatic method for explicit steady states of linear reaction networks

We consider a catalytic mechanism with a catalyst and several substrates, products, inhibitors or activators. The mechanism is resolved down to elementary reactions following mass–action kinetics.

Upon chemostatting all the substrates, products, inhibitors and activators—summarized as $\boldsymbol{y}$—we are left with rate equations that are linear in the catalyst-containing species—summarized as $\boldsymbol{x}$. While the steady-state equations alone, $0 = \mathbb{S}^X\boldsymbol{J}(\boldsymbol{x}, \boldsymbol{y})$, are under-determined and linearly dependent, the open system still has a conservation law for the total catalyst-moiety concentration $L = \sum_i x_i$, which again is a linear equation. We can replace the first line of the steady-state equations with this constraint to arrive at linear equations $L\boldsymbol{e}_1 = \mathbb{M}(\boldsymbol{y})\boldsymbol{x}$, where $\boldsymbol{e}_1 = (1, 0,...)$ is the first Cartesian unit vector and $\mathbb{M}(\boldsymbol{y})$ is an invertible square matrix that depends on the chemostat concentrations. According to Cramer's rule the unique solution to this problem is given by

$$\frac{x_i^*}{L} = \frac{\det \mathbb{M}_i(\boldsymbol{y})}{\det \mathbb{M}(\boldsymbol{y})}, \tag{A1}$$

where $\mathbb{M}_i(\boldsymbol{y})$ is identical to $\mathbb{M}(\boldsymbol{y})$ just with the ith column replaced by $\boldsymbol{e}_1$. We now provide a diagrammatic method to represent this solution. This diagrammatic method is frequently attributed to King and Altman [48] or Hill [54], while an equivalent approach was already employed by Kirchhoff [55] to solve problems in electric networks. We give the diagrammatic method in the language of graph theory [50, 56], for which we need some definitions.

The open pseudo-first-order reaction network has a simple representation as a connected graph $\mathcal{G}$ where all the catalyst-containing species i form the vertices $\mathcal{V}$ and the reactions $\rho \cup -\rho$ form bidirectional edges $\mathcal{R}$. The reduced stoichiometric matrix $\mathbb{S}^X$ is the *incidence matrix* for this graph.

A closed self-avoiding path in a graph is a *circuit* and can be identified with a vector $c \in \mathbb{R}^{\mathcal{R}}$ over the edges, whose entries are in fact restricted to $\{-1, 0, 1\}$. Since a circuit is a closed path, it satisfies $\mathbb{S}^X c = 0$ and reaches as many vertices as it contains edges. A graph not containing any circuit is called *forest*, a connected forest is called *tree*.

A connected subgraph $\tau \subset \mathcal{G}$ is called *spanning tree* if it spans all the vertices but contains no circuit. The set $\mathcal{T}$ of spanning trees of a finite graph is always finite. A *rooted spanning tree* is a tree where all the edges are oriented along the tree towards one and the same vertex, called the *root*.

With these notions set, the determinants in equation (A1) can be written as

$$\det \mathbb{M}_i(\boldsymbol{y}) = \sum_{\tau \in \mathcal{T}_i} \prod_{\rho \in \tau} \tilde{k}_\rho(\boldsymbol{y}), \qquad \det \mathbb{M}(\boldsymbol{y}) = \sum_i \sum_{\tau \in \mathcal{T}_i} \prod_{\rho \in \tau} \tilde{k}_\rho(\boldsymbol{y}) =: N(\boldsymbol{y}).$$

Here, $\mathcal{T}_i$ is the set of spanning trees rooted in vertex i, and $\tilde{k}_\rho(\boldsymbol{y})$ is the pseudo-first-order rate constant of reaction ρ. Overall, Kirchhoff's formula for the solution to the linear problem is

$$\frac{x_i^*}{L} = \frac{1}{N(\boldsymbol{y})} \sum_{\tau \in \mathcal{T}_i} \prod_{\rho \in \tau} \tilde{k}_\rho(\boldsymbol{y}). \tag{A2}$$

From this result it is easy to confirm that the solution exists and is always unique as long as the chemostat concentrations are finite and positive. Furthermore, the steady-state concentrations are expressed as sums of products of positive quantities, thus themselves are always positive.

While this formula is very compact and abstract, it is not obviously convenient for practical calculations. However, the rooted spanning trees appearing in this formula can be visually represented as diagrams, as we will see in the following examples. These diagrams are intuitive enough to make practical calculations with this formula feasible.

A.1. Steady-state concentrations for the enzymatic catalysis

The enzymatic catalysis example in the main text, when open, is represented by the graph in figure 3. This graph has five vertices and six edges. It contains three distinct circuits and twelve different spanning trees.

A visual representation of Kirchhoff's formula (A2) for its steady-state concentrations is given by the following diagrams:

$$\frac{[\mathrm{E}]}{L_\mathrm{E}} = \frac{1}{N_\mathrm{E}}$$ 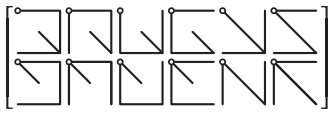

$$\frac{[\mathrm{ES}_1]}{L_\mathrm{E}} = \frac{1}{N_\mathrm{E}}$$ 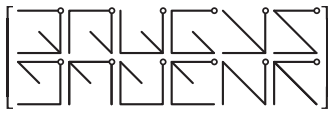

$$\frac{[\mathrm{ES}_2]}{L_\mathrm{E}} = \frac{1}{N_\mathrm{E}}$$ 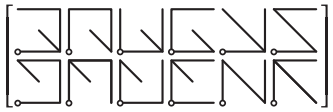

$$\frac{[\mathrm{ES}_1\mathrm{S}_2]}{L_\mathrm{E}} = \frac{1}{N_\mathrm{E}}$$ 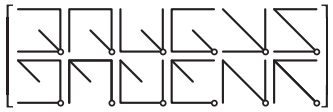

$$\frac{[\mathrm{EP}]}{L_\mathrm{E}} = \frac{1}{N_\mathrm{E}}$$ 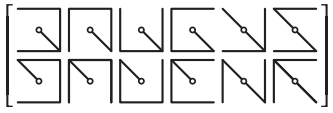

Here, each diagram represents a product of pseudo-first-order rate constants over a spanning tree that is rooted in the (circled) vertex associated with the species we want to solve for (left-hand side). Thus, the concentrations are sums of twelve diagrams each, normalized by a denominator N_E that equals the sum of all the 60 diagrams given above.

A.2. Steady-state concentrations for the active transporter

The active membrane transporter example in the main text, when open, is represented by the graph in figure 5. This graph has six vertices and seven edges. It contains three distinct circuits and 15 different spanning trees.

A visual representation of Kirchhoff's formula (A2) for its steady-state concentrations is given by the following diagrams:

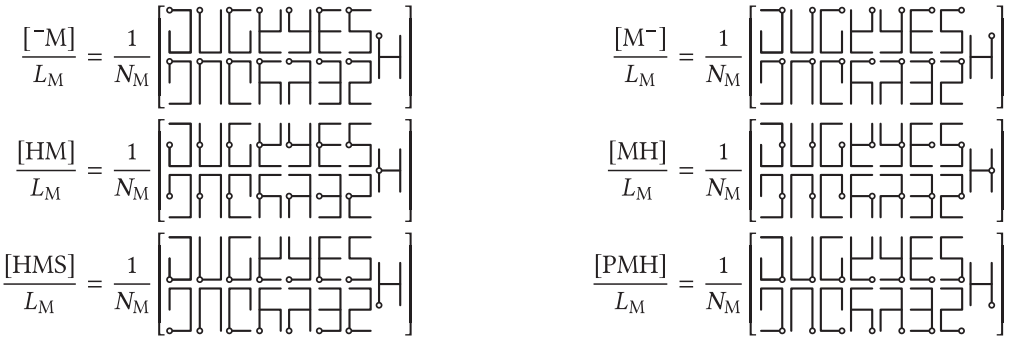

Here, each diagram represents a product of pseudo-first-order rate constants over a spanning tree that is rooted in the (circled) vertex associated with the species we want to solve for (left-hand side). Thus, the concentrations are sums of 15 diagrams each, normalized by a denominator N_M that equals the sum of all the 90 diagrams given above.

Appendix B. Kinetic rate laws for the coarse-grained reactions

We now explicitly construct the kinetic rate laws as apparent cycle fluxes. First, we make use of the diagrammatic method to derive the coarse-grained kinetic rate laws for the two example systems of the main text. Then we generalize these examples to generic catalysts.

B.1. Kinetic rate laws for the enzymatic catalysis

As shown in the main text, the cycle currents are

$$J_{\mathrm{int}} = -J_2 = k_{-2}[\mathrm{ES_2}] - k_2[\mathrm{E}][\mathrm{S_2}], \qquad J_{\mathrm{ext}} = J_6 = k_6[\mathrm{EP}] - k_{-6}[\mathrm{E}][\mathrm{P}].$$

Plugging in the diagrams (appendix A.1) for the steady-state concentrations of the enzyme-containing species we arrive at

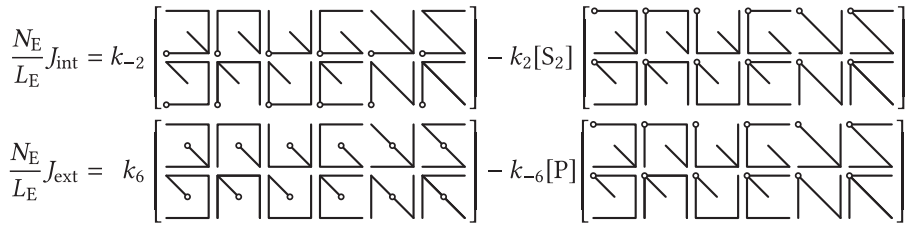

Next, we multiply the remaining pseudo-first-order rate constants into the diagrams and highlight them in blue. This leads us to

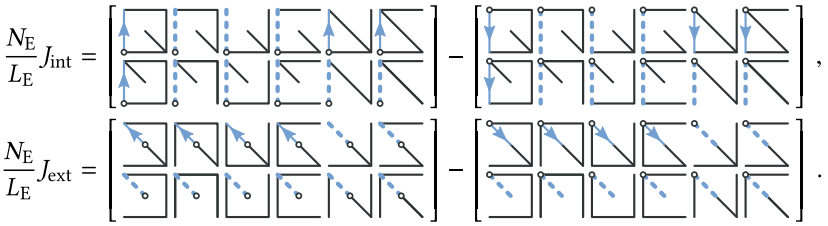

Note how some of the diagrams did not contain that edge before, leading to a circuit in the new diagrams. The new pseudo-first-order rate constant carries an arrowhead to highlight the orientation of that edge. The black edges remain oriented along the other black edges towards the circled vertex. The remaining diagrams already contained the reverse pseudo-first-order rate constant for the newly incorporated edge. The product of these forward and backward pseudo-first-order rate constants is highlighted as a dashed blue edge without arrowhead. The latter tree diagrams appear on both sides of the minus signs and can be canceled. Thus the currents are

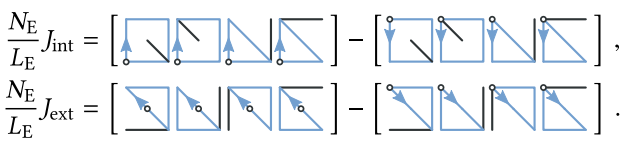

Here, we highlight the entire circuits in blue to emphasize the common factors in the remaining terms. Note that the square representing the internal cycle remained in the internal cycle current on both sides of the minus sign. However, Wegscheider's conditions, equation (2), ensure that these terms cancel as well. Furthermore, Wegscheider's conditions allow us to express the diagrams containing the lower triangle with the upper triangle:

Overall, the currents expressed with rate constants and concentrations are

$$J_{\text{int}} = \frac{L_E k_2 k_3}{N_E k_1}\left(\frac{k_{-1}}{k_4} + [S_2]\right)(k_{-1}k_{-4}k_{-5}k_{-6}[P] - k_1 k_4 k_5 k_6 [S_1][S_2]),$$

$$J_{\text{ext}} = \frac{L_E}{N_E}\left(k_3[S_1] + \frac{k_2 k_3 [S_2]}{k_1} + k_{-2} + \frac{k_{-2}k_{-3}}{k_{-4}}\right)(k_1 k_4 k_5 k_6 [S_1][S_2] - k_{-1}k_{-4}k_{-5}k_{-6}[P]).$$

B.2. Kinetic rate laws for the active transporter

We proceed analogously to the previous calculation for the enzymatic catalysis: plug the tree diagrams from appendix A.2 into

$$J_{\text{cat}} = J_2 = k_2[S][HM] - k_{-2}[HMS],$$
$$J_{\text{sl}} = -J_1 = k_{-1}[HM] - k_1[H_a^+][^-M],$$

and cancel all diagrams that do not contain a circuit. This leads us to

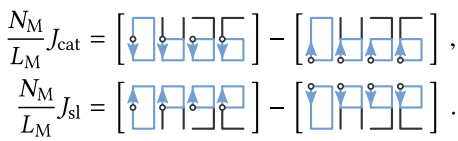

Since this membrane transporter mechanism does not have an internal cycle, we cannot exploit Wegscheider's conditions to cancel more terms. Nonetheless, we see that we can factor the circuits out of some of the terms. Overall, we arrive at the cycle currents

$$J_{\text{cat}} =: \psi^+_{\text{cat}} - \psi^-_{\text{cat}}, \qquad J_{\text{sl}} =: \psi^+_{\text{sl}} - \psi^-_{\text{sl}}.$$

with the fluxes

$$\frac{N_M}{L_M}\psi^+_{\text{cat}} = k_1 k_2 k_3 k_4 k_5 k_6 [H_a^+][S] + \xi_{\text{cat}} k_{-7} k_2 k_3 k_4 [S],$$
$$\frac{N_M}{L_M}\psi^-_{\text{cat}} = k_{-1}k_{-2}k_{-3}k_{-4}k_{-5}k_{-6}[H_b^+][P] + \xi_{\text{cat}} k_7 k_{-2}k_{-3}k_{-4}[P],$$
$$\frac{N_M}{L_M}\psi^+_{\text{sl}} = k_{-1}k_{-2}k_{-3}k_{-4}k_{-5}k_{-6}[H_b^+][P] + \xi_{\text{sl}} k_{-1}k_{-5}k_{-6}k_{-7}[H_b^+],$$
$$\frac{N_M}{L_M}\psi^-_{\text{sl}} = k_1 k_2 k_3 k_4 k_5 k_6 [H_a^+][S] + \xi_{\text{sl}} k_1 k_5 k_6 k_7 [H_a^+],$$

where we used the abbreviations

$$\xi_{\text{cat}} := k_{-6}k_{-5}[H_b^+] + k_1 k_{-5}[H_a^+][H_b^+] + k_6 k_1 [H_a^+], \qquad \xi_{\text{sl}} := k_3 k_4 + k_{-2}k_4 + k_{-3}k_{-2}.$$

B.3. Kinetic rate laws for generic catalysts

By making use of the graph theory notation introduced in appendix A, we can generalize the above calculations to generic catalysts.

Before proceeding with calculations, we need a general method to determine the cycle currents from individual reaction currents. To that end, we construct a special spanning tree τ^* for the graph $\mathcal{G}$ of the open system: (1) we start with the *closed* system and determine its internal cycles $\ker \mathbb{S}$. We take the set $\mathcal{I} \subset \mathcal{R}$ of edges that the internal cycles are supported on. (2) Consider this set of edges $\mathcal{I} \subset \mathcal{G}$ as a subgraph of the *open* network. Choose a spanning tree $\tau_{\mathcal{I}}$ for this subgraph. (3) Complete $\tau_{\mathcal{I}}$ to a spanning tree τ^* of $\mathcal{G}$. All the edges not contained in the spanning tree are the *chords*.

There is a special connection between chords and circuits first highlighted by Schnakenberg [57]: the spanning tree alone, by definition, does not contain any circuit. Adding a chord to the spanning tree gives rise to a circuit composed of the chord together with edges from the spanning tree. Furthermore, by construction every chord gives rise to a *different* circuit and the set of these circuits form a basis of the cycle space $\ker \mathbb{S}^X$. In this

context the circuits associated to chords are also called *fundamental cycles*. The currents on the chords then are identical to the steady-state currents along the fundamental cycles of the chords [57].

The special spanning tree τ^* that we constructed is separating the chords into two sets: each chord in $\mathcal{I}$ gives rise to an *internal cycle*, while the chords not in $\mathcal{I}$ give rise to the emergent cycles. This construction provides a basis for the entire cycle space, yet keeps the internal cycles and the emergent cycles separated. Therefore we call it a *separating spanning tree*.

It is worth noting that not every basis of circuits can be expressed as fundamental cycles of a spanning tree. This technical detail, however, has no impact on our results. Different bases are just different representations of the same space. In the following we assume a spanning tree mainly for convenience.

Let $j \to i$ be the chord of an emergent cycle. Then the current through that chord is

$$J_{ij} = \tilde{k}_{ij}(\boldsymbol{y})x_j - \tilde{k}_{ji}(\boldsymbol{y})x_i = \frac{L}{N(\boldsymbol{y})}\left[\tilde{k}_{ij}(\boldsymbol{y})\sum_{\tau\in\mathcal{T}_j}\prod_{\rho\in\tau}\tilde{k}_\rho(\boldsymbol{y}) - \tilde{k}_{ji}(\boldsymbol{y})\sum_{\tau\in\mathcal{T}_i}\prod_{\rho\in\tau}\tilde{k}_\rho(\boldsymbol{y})\right].$$

Next, we note that a lot of terms cancel by taking this difference. All the spanning trees that contain the edge $i \to j$ or $j \to i$, respectively, appear with both plus and minus sign:

$$J_{ij} = \underbrace{\frac{L}{N(\boldsymbol{y})}\left[\tilde{k}_{ij}(\boldsymbol{y})\sum_{\substack{\tau\in\mathcal{T}_j\\ i\to j\in\tau}}\prod_{\rho\in\tau}\tilde{k}_\rho(\boldsymbol{y}) - \tilde{k}_{ji}(\boldsymbol{y})\sum_{\substack{\tau\in\mathcal{T}_i\\ j\to i\in\tau}}\prod_{\rho\in\tau}\tilde{k}_\rho(\boldsymbol{y})\right]}_{=0}$$
$$+\frac{L}{N(\boldsymbol{y})}\left[\tilde{k}_{ij}(\boldsymbol{y})\sum_{\substack{\tau\in\mathcal{T}_j\\ i\to j\notin\tau}}\prod_{\rho\in\tau}\tilde{k}_\rho(\boldsymbol{y}) - \tilde{k}_{ji}(\boldsymbol{y})\sum_{\substack{\tau\in\mathcal{T}_i\\ j\to i\notin\tau}}\prod_{\rho\in\tau}\tilde{k}_\rho(\boldsymbol{y})\right].$$

After canceling these spanning tree contributions, we define the *apparent cycle fluxes* as

$$\psi_{ij} := \frac{L}{N(\boldsymbol{y})}\tilde{k}_{ij}(\boldsymbol{y})\sum_{\substack{\tau\in\mathcal{T}_j\\ i\to j\notin\tau}}\prod_{\rho\in\tau}\tilde{k}_\rho(\boldsymbol{y}). \tag{B1}$$

We obviously have $J_{ij} = \psi_{ij} - \psi_{ji}$. Thus the apparent cycle fluxes serve as kinetic rate laws for the coarse-grained reactions.

There is, technically speaking, no strict necessity to cancel the spanning tree contributions in order to arrive at expressions that can serve as coarse-grained kinetic rate laws. Keeping the spanning tree contributions results in the apparent fluxes of the substrates/products that are being produced/consumed along the chord. This is a natural choice for dealing with data from isotope labeling experiments. With this definition for kinetic rate laws, however, the flux–force relation is not satisfied—even in the case of a single emergent cycle [34]. In contrast, our definition of apparent fluxes resembles the apparent *cycle* fluxes, rather than apparent exchange fluxes. Comparing the apparent cycle fluxes with the net force along the emergent cycle, we do have a flux–force relation, as shown in the next section.

Appendix C. Proof of the flux–force relation

Before we prove the flux–force relation, we rewrite the apparent fluxes for the emergent cycles derived in equation (B1). This simplifies the final proof considerably. To that end, we observe that adding a chord to a spanning tree not containing this chord always creates a circuit. Since in equation (B1) we sum over all possible spanning trees, the same circuits re-appear in several summands. We now re-sort the sums to first run over distinct circuits, and then sum over the remainders of the spanning trees. For that we need some notation.

For any circuit c we abbreviate the product of pseudo-first-order rate constants along it as $w(c) = \prod_{\rho\in c}\tilde{k}_\rho(\boldsymbol{y})$. The net force along a circuit thus is concisely written as

$$-\Delta_c G = RT\sum_{\rho\in c}\ln\frac{\tilde{k}_\rho(\boldsymbol{y})}{\tilde{k}_{-\rho}(\boldsymbol{y})} = RT\ln\frac{w(c)}{w(-c)}. \tag{C1}$$

Here, $-c$ refers to traversing the circuit c with reversed orientation. For any circuit, c, we furthermore define $\mathcal{F}(c)$ to be the set of subforests of $\mathcal{G}$ that (i) do not contain any edge of c, (ii) span the rest of the graph, and (iii) are directed towards the circuit c. Analogously to the product of rate constants along a circuit, for this set of subforests we denote the sum of products of rate constants as

$$\xi(c) := \sum_{f\in\mathcal{F}(c)} \prod_{\rho\in f} \tilde{k}_\rho(\boldsymbol{y}).$$

By construction, $\xi(c) = \xi(-c)$ since the set $\mathcal{F}(c)$ does not depend on the orientation of c. Let $\mathcal{C}_{ij}$ be the set of circuits traversing the edge $j \to i$. Note that these circuits are exactly the ones appearing in equation (B1) .

With this notation we rewrite the apparent cycle fluxes in the following way:

$$\psi_{ij} = \frac{L}{N(\boldsymbol{y})} \sum_{c\in\mathcal{C}_{ij}} w(c)\xi(c).$$

This rewriting is not limited to the case of a single emergent cycle. In fact, we used this form to express the apparent cycle fluxes of the active membrane transporter in appendix B.2.

We now prove the flux–force relation—under the assumption that there is exactly one emergent cycle c_η with chord $\eta = j \to i$. Let $-\Delta_\eta G$ be the net force along this cycle and let J_η be its current at steady state. Let furthermore τ^* be a separating spanning tree, as we defined in appendix B.3.

Having only one emergent cycle means that for every circuit $c \in \mathcal{C}_{ij}$ we have one of the following cases:

- The circuit is formed by following the separating spanning tree from vertex i back to j, in which case it is exactly the emergent cycle: $c = c_\eta$.
- The circuit is formed by traversing more chords, in which case it can be written as $c = c_\eta + \gamma$ where $\gamma \in \ker \mathbb{S}$ is an internal cycle. In this case we have $\frac{w(c)}{w(-c)} = \frac{w(\gamma)}{w(-\gamma)}\frac{w(c_\eta)}{w(-c_\eta)} = \frac{w(c_\eta)}{w(-c_\eta)}$ due to Wegscheider's conditions.

In any case we can write $w(\pm c) = \zeta(c)w(\pm c_\eta)$ where $\zeta(c) = \zeta(-c)$ is a symmetric factor. Overall, the apparent fluxes for the emergent cycle are

$$\psi_{ij} = \frac{L}{N(\boldsymbol{y})} \sum_{c\in\mathcal{C}_{ij}} w(c)\xi(c) = \frac{L}{N(\boldsymbol{y})}\left[\sum_{c\in\mathcal{C}_{ij}} \xi(c)\zeta(c)\right] w(c_\eta).$$

By construction, ξ and ζ are symmetric and also any sum over these terms is symmetric. Consequently, the apparent forward and backward fluxes of the emergent cycle satisfy

$$\frac{\psi_{ij}}{\psi_{ji}} = \frac{\frac{L}{N(\boldsymbol{y})}\left[\sum_{c\in\mathcal{C}_{ij}} \xi(c)\zeta(c)\right] w(c_\eta)}{\frac{L}{N(\boldsymbol{y})}\left[\sum_{c\in\mathcal{C}_{ij}} \xi(-c)\zeta(-c)\right] w(-c_\eta)} = \frac{w(c_\eta)}{w(-c_\eta)}$$

which, together with equation (C1), concludes the proof.

From this proof it is evident, why the flux–force relation breaks down once there are several emergent cycles with nonzero forces: in the case where a circuit $c \in \mathcal{C}_{ij}$ is not identical to the emergent cycle c_η, we can still write it as $c = c_\eta + \gamma$. However, now γ need not be an internal but might be another emergent cycle. Therefore, Wegscheider's condition does not apply to it, thus $w(\gamma)$ and hence $\zeta(c)$ need not be symmetric. As a consequence, the ratio of apparent forward and backward cycle fluxes cannot be expressed by the force of the emergent cycle $-\Delta_\eta G$ alone.

The proof also shows why the choice of a separating spanning tree is mainly for convenience. In the case of a single emergent cycle, the exact basis for the internal cycles does not matter and you can always find an appropriate separating spanning tree. In the case of several emergent cycles, there is no simple and direct relation between the force and the fluxes of a cycle. The only consistency requirement is the EPR. However, the EPR is a scalar and thus invariant under change of basis. Furthermore, it involves only the forces and the currents of the cycles. This imposes no restrictions on the individual forward and backward fluxes.

ORCID iDs

Artur Wachtel https://orcid.org/0000-0002-6194-6938
Riccardo Rao https://orcid.org/0000-0003-0040-6783
Massimiliano Esposito https://orcid.org/0000-0002-2249-4035

References

[1] Cornish-Bowden A 2013 *FEBS Lett.* **587** 2725
[2] Brown A J 1902 *J. Chem. Soc. Trans.* **81** 373
[3] Henri V 1902 *C. R. Hebd. Acad. Sci.* **135** 916
[4] Michaelis L and Menten M L 1913 *Biochem. Z.* **49** 333

[5] Cornish-Bowden A 2012 *Fundamentals of Enzyme Kinetics* 4th edn (Weinheim: Wiley-VCH)
[6] Puglisi A, Pigolotti S, Rondoni L and Vulpiani A 2010 *J. Stat. Mech.* P05015
[7] Callen H B 1985 *Thermodynamics and an Introduction to Thermostatistics* 2nd edn (New York: Wiley)
[8] Seifert U 2012 *Rep. Prog. Phys.* **75** 126001
[9] Van den Broeck C and Esposito M 2015 *Proc. 13th Int. Summer School on Fundamental Problems in Statistical Physics; Physica* A **418** 6
[10] Jülicher F, Ajdari A and Prost J 1997 *Rev. Mod. Phys.* **69** 1269
[11] Seifert U 2011 *Eur. Phys. J.* E **34** 26
[12] Altaner B, Wachtel A and Vollmer J 2015 *Phys. Rev.* E **92** 042133
[13] Astumian R D, Mukherjee S and Warshel A 2016 *ChemPhysChem* **17** 1719
[14] Murugan A, Huse D H and Leibler S 2012 *Proc. Natl Acad. Sci. USA* **109** 12034
[15] Rao R and Peliti L 2015 *J. Stat. Mech.* P06001
[16] Sartori P and Pigolotti S 2015 *Phys. Rev.* X **5** 041039
[17] Barato A C, Hartich D and Seifert U 2014 *New J. Phys.* **16** 103024
[18] Bo S and Celani A 2016 *J. Stat. Phys.* **162** 1365
[19] Ouldridge T E, Govern C C and ten Wolde P R 2017 *Phys. Rev.* X **7** 021004
[20] Esposito M 2012 *Phys. Rev.* E **85** 041125
[21] Altaner B and Vollmer J 2012 *Phys. Rev. Lett.* **108** 228101
[22] Knoch F and Speck T 2015 *New J. Phys.* **17** 115004
[23] Esposito M and Parrondo J M R 2015 *Phys. Rev.* E **91** 052114
[24] Bo S and Celani A 2017 *Phys. Rep.* **670** 1
[25] Segel L A and Slemrod M 1989 *SIAM Rev.* **31** 446
[26] Gunawardena J 2014 *FEBS J.* **281** 473
[27] Rubin K J, Lawler K, Sollich P and Ng T 2014 *J. Theor. Biol.* **357** 245
[28] Polettini M and Esposito M 2014 *J. Chem. Phys.* **141** 024117
[29] Rao R and Esposito M 2016 *Phys. Rev.* X **6** 041064
[30] Beard D A, dan Liang S and Qian H 2002 *Biophys. J.* **83** 79
[31] Fleming R, Thiele I, Provan G and Nasheuer H 2010 *J. Theor. Biol.* **264** 683
[32] Soh K C and Hatzimanikatis V 2010 *Curr. Opin. Microbiol.* **13** 350
[33] Beard D A and Qian H 2007 *PLoS One* **2** 1
[34] Wiechert W 2007 *Biophys. J.* **93** 2255
[35] Noor E, Flamholz A, Liebermeister W, Bar-Even A and Milo R 2013 *FEBS Lett.* **587** 2772
[36] Liepelt S and Lipowsky R 2007 *Phys. Rev. Lett.* **98** 258102
[37] Pietrobon D and Caplan S R 1985 *Biochemistry* **24** 5764
[38] Alberty R A 2003 *Thermodynamics of Biochemical Reactions* (New York: Wiley)
[39] Kondepudi D and Prigogine I 2015 *Modern Thermodynamics: From Heat Engines to Dissipative Structures* 2nd edn (New York: Wiley)
[40] de Groot S and Mazur P 1984 *Non-equilibrium Thermodynamics, Dover Books on Physics Series* (New York: Dover)
[41] Flamholz A, Noor E, Bar-Even A, Liebermeister W and Milo R 2013 *Proc. Natl Acad. Sci. USA* **110** 10039
[42] Noor E, Bar-Even A, Flamholz A, Reznik E, Liebermeister W and Milo R 2014 *PLoS Comput. Biol.* **10** 1
[43] Henry C S, Broadbelt L J and Hatzimanikatis V 2007 *Biophys. J.* **92** 1792
[44] Orth J D, Thiele I and Palsson B Ø 2010 *Nat. Biotechnol.* **28** 245
[45] Chakrabarti A, Miskovic L, Soh K C and Hatzimanikatis V 2013 *Biotechnol. J.* **8** 1043
[46] Schuster S and Schuster R 1989 *J. Math. Chem.* **3** 25
[47] Polettini M, Wachtel A and Esposito M 2015 *J. Chem. Phys.* **143** 184103
[48] King E L and Altman C 1956 *J. Phys. Chem.* **60** 1375
[49] Hill T L 1977 *Free Energy Transduction in Biology: The Steady-State Kinetic and Thermodynamic Formalism* (New York: Academic)
[50] Tutte W 2001 *Graph Theory* (*Cambridge Mathematical Library*) (Cambridge: Cambridge University Press)
[51] Lee C H and Othmer H G 2009 *J. Math. Biol.* **60** 387
[52] Thomas P, Grima R and Straube A V 2012 *Phys. Rev.* E **86** 041110
[53] Rubin K J and Sollich P 2016 *J. Chem. Phys.* **144** 174114
[54] Hill T L 1966 *J. Theor. Biol.* **10** 442
[55] Kirchhoff G 1847 *Ann. Phys., NY* **148** 497
[56] Knauer U 2011 *Algebraic Graph Theory: Morphisms, Monoids and Matrices De Gruyter Studies in Mathematics* (Berlin: de Gruyter & Co)
[57] Schnakenberg J 1976 *Rev. Mod. Phys.* **48** 571

9. Nonequilibrium Thermodynamics of Linear Reaction Pathways

In the previous chapter, I addressed the thermodynamics of catalytic reactions. These are especially ubiquitous within living cells. Practically all biochemical reactions are enhanced by enzymes — be it the anabolic synthesis of biomass, the processing of chemical signals, the reading and writing of genetic information, or the catabolic breakdown of biomass in order to release the energy stored therein. These processes involve several enzymatic steps after another: the product of one enzyme is the substrate for the next.

This observation leads to a thinking of biochemical logic in terms of *pathways*. Assuming a pathway performs some function in the cell, it will reach some nonequilibrium steady state with concentrations that result from the dynamic coupling of the different intermediate species. Since enzymes mediate the coupling, the enzymes themselves are an ideal point to *regulate* the pathway so that the cell can adjust to some external condition or another. The activity of enzymatic reactions is primarily influenced in the short term by binding of some molecule to the enzyme (allostery) and in the long run by a modified expression level (transcription) of the enzyme itself. It is speculated that the point of regulation within the pathway should be related to thermodynamics [1]: a strongly irreversible reaction needs to be regulated more strongly than a reaction close to equilibrium.

A reasonable first approach to pathway thermodynamics is to consider a linear (or unbranched) chain of reactions, possibly following enzymatic kinetics. While such a system is in principle solvable analytically [2], I was surprised not to find literature addressing specifically the interplay between kinetics and thermodynamics in this setup.

Here, I provide the preprint for a manuscript *in preparation*, which is still very much work in progress. In this manuscript we address the interplay between the chemical potentials, their differences, the current, and the standard-state chemical potentials, which govern the thermodynamic equilibrium. The approach is partially analytical and partially visual. The latter is especially due to the fact that the exact solutions are iterative equations, and as such they are difficult to handle.

Our findings so far recover the common understanding that rate-limiting reaction steps have the strongest effect in reducing the current through the pathway. Additionally, these rate-limiting steps *dissipate* the most — very much irrespective of the equilibrium potential landscape. In addition to the effect of reducing the current, the *location* of the downregulated step has a strong impact on the internal steady-state concentrations. Considering that some intermediary metabolites (at high concentrations) may be dangerous to the cell, this is an important additional factor that needs to be taken into account. Without rate-limiting steps, the equilibrium potential landscape does influence the relative dissipation of the reactions along the pathway. To our surprise, however, individual large jumps in the equilibrium landscape do not indicate the most dissipative reaction. Instead, these are located either *before* the large jump or at the end of the pathway, depending on the strength of the force that drives the pathway out of equilibrium and whether the jump is energetically favorable.

References

[1] D. L. Nelson and M. M. Cox. *Lehninger Principles of Biochemistry*. 5th ed. New York: W. H. Freeman and Co., 2008.

[2] R. Heinrich and E. Klipp. "Control Analysis of Unbranched Enzymatic Chains in States of Maximal Activity". In: *Journal of Theoretical Biology* 182.3 (1996), pp. 243–252.

The following manuscript is a preprint for
[A. Wachtel, M. Esposito. *In preparation.* 2018].
I added pagemarks in the outer margins to provide a continuous pagination throughout the thesis.

Kinetic Effects on Nonequilibrium Thermodynamics of Linear Enzymatic Pathways

Artur Wachtel* and Massimiliano Esposito
Complex Systems and Statistical Mechanics, Physics and Materials Science Research Unit, University of Luxembourg, 162a, Avenue de la Faïencerie, 1511 Luxembourg, G. D. Luxembourg
(Dated: November 16, 2018)

We study the non-equilibrium thermodynamics of linear chemical pathways. For simplicity we assume kinetics of mass–action form that describe enzymatic kinetics in the limit of low concentrations – making the effective rate constants proportional to the available enzyme. We show that a lack of enzymes and thus small fluxes leads to a reorganization of the local dissipation – making the rate-limiting reaction the most dissipative. An abundance of enzymes causes the dissipation of the respective step to go down.

I. INTRODUCTION

Living cells are far from thermodynamic equilibirum. They operate between many reservoirs of chemical species, converting energy-rich species into energy-poor species and extracting some of the energy as usable (chemical) work. This conversion is dissipative, releasing heat into the environment, and it is necessary to keep the cell operative or "alive".

The interior organization of this conversion of chemical compounds is known as *metabolism* and it is frequently understood as being composed of *pathways*: Central energy metabolism, for example, is typically depicted by following the carbon atoms from sugar molecules on their way to carbon dioxide – undergoing glycolysis and the tricarboxylic acid (TCA) cycle. Other metabolic pathways are associated with the storage or release of energetically rich molecules on larger time-scales (starch/glycogen, fatty acids) or with the production of biomass – such as amino-acids or nucleic acids. [1]

Most of the reactions in these pathways do not happen spontaneously, but are mediated by enzymes that enhance the rate of chemical reactions. The kinetics of enzymes is complicated and frequently influenced by inhibitors, activators and other co-factors [2]. Experimental studies to determine the exact kinetic properties of enzymes are hard and time consuming work – rendering the exact kinetic properties of many enzymes still unknown to date.

Enzymes do not modify the thermodynamic equilibrium concentrations of their substrate or product molecules – which is frequently stated as "enzymes do not influence the thermodynamics". The modern understanding of thermodynamics far from thermal equilibrium, however, has revealed that the energetic properties that govern the equilibrium state are not sufficient to characterize the non-equilibrium state – kinetic properties of the system are a crucial ingredient. This implies that the presence of enzymes has an impact on the non-equilibrium properties of a system subject to chemical reactions.

Thermodynamic analysis of actual biochemical pathways is often focused on the calculation or estimation of Gibbs energies of reaction, $\Delta_r G$. The Gibbs energy of a reaction is often used as a measure for the distance from equilibrium. We argue that the *dissipation* of a reaction, being the product of $\Delta_r G$ and reaction current J, is a better measure for the distance from equilibrium – especially when analyzing and comparing reactions from different pathways. After all, two reactions may have the same Gibbs energy difference while carrying different reaction currents and thus contributing differently to the total dissipation of the respective system.

In this paper we consider a linear chain of reactions as an open chemical network [3, 4]. We assume that we know the exact kinetics and that we can control the concentrations of the first and final species in the chain. As a result, we provide the concentrations for the non-equilibrium steady state as functions of the parameters of the system. Knowing the exact state and kinetics of the system, it is possible to study the dissipation in the system, both along each individual reaction, as well as the total dissipation of the entire pathway.

The reversible Michaelis–Menten equation provides the reaction current (reaction velocity) J of an enzymatically catalyzed reaction as

$$J = \frac{L_E}{1 + \frac{[S]}{K_{mS}} + \frac{[P]}{K_{mP}}} (k_S[S] - k_P[P]) = \psi^+ - \psi^- \qquad (1)$$

Here, L_E is the total concentration of the available enzyme E that catalyzes the reaction $S \rightleftharpoons P$. The two *Michaelis constants* K_{mS} and K_{mP} quantify the enzyme saturation and product inhibition, respectively. The *specificity constants* k_S and k_P relate to the equilibrium constant via

$$K^{eq} = \frac{k_S}{k_P} = \frac{[P]^{eq}}{[S]^{eq}} = \exp[-\Delta_r G^\circ] \qquad (2)$$

Thus the forward and backward reaction fluxes relate to the Gibbs energy of reaction via the *flux–force relation*:

$$-\Delta_r G = RT \ln \frac{\psi^+}{\psi^-} \qquad (3)$$

We recently proved that this relation is true for all tightly coupled enzymes [5].

In the limit of low concentrations ($[S] \ll K_{mS}$, $[P] \ll K_{mP}$) the reaction velocity of the reversible Michaelis–Menten equation takes the form of regular mass–action kinetics:

$$J \approx L_E k_S[S] - L_E k_P[P] =: k^+_{eff}[S] - k^-_{eff}[P] \qquad (4)$$

where both effective rate constants $k^\pm_{eff}$ are proportional to the total enzyme abundance.

Thus to first order, one can say that the presence of an enzyme changes the kinetic rate constants *symmetrically*.

* artur.wachtel@uni.lu

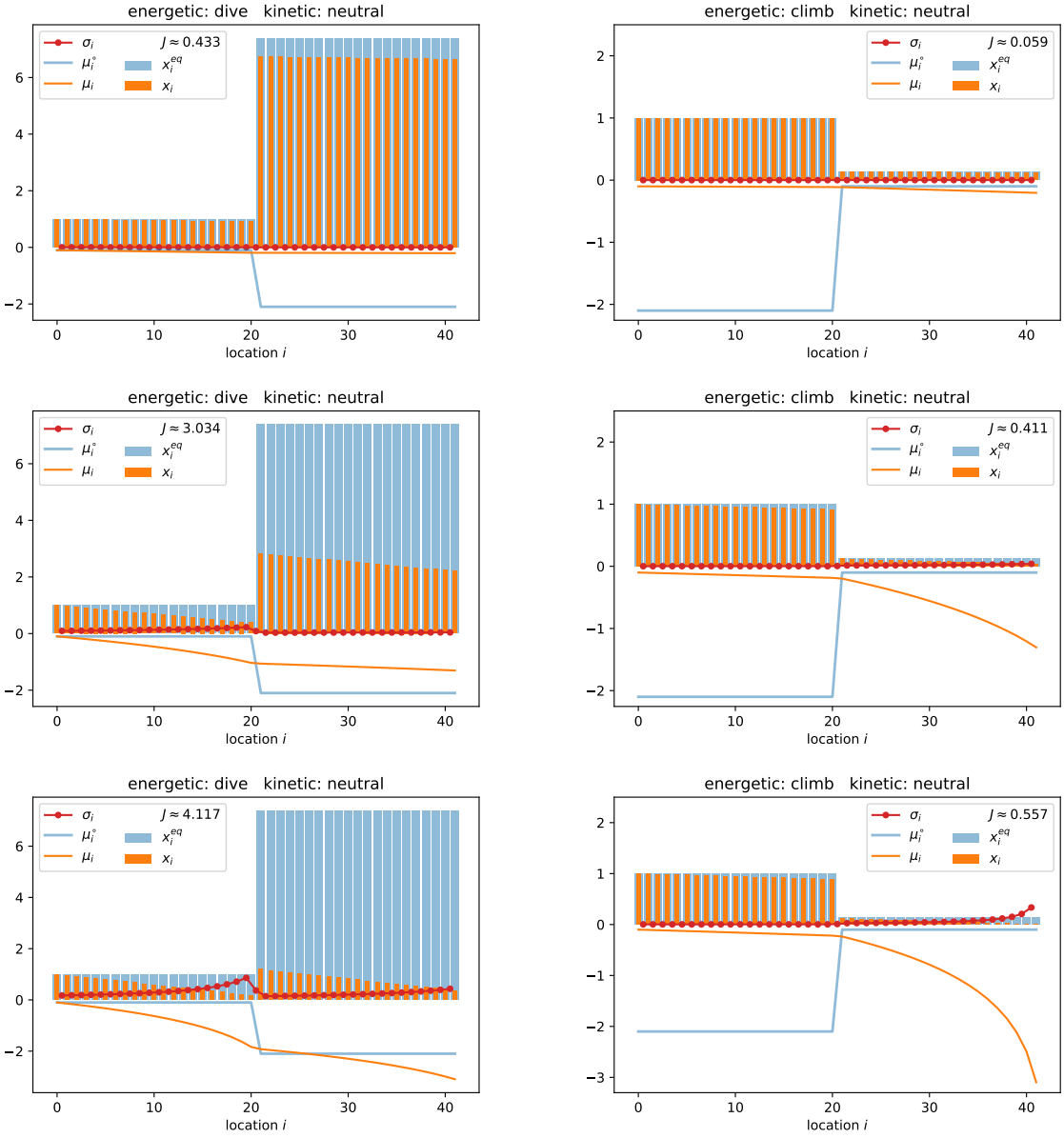

FIG. 1. The path out of thermal equilibrium by sequentially lowering the right-side chemostat concentration. (top: −10%) Here, the chemical potential has almost constant slope – which means the force ΔG is proportional to the globally constant current. (center: −70%) Intermediate regime. (bottom: −95%) This is far from equilibrium. The chemical potential forms a complicated landscape with piecewise exponential behaviour. We discuss these plots in detail in section II B.

II. RESULTS

We consider a linear reaction pathway that transforms a species X_0 to a species X_n in n elementary steps:

$$X_0 \overset{1}{\rightleftharpoons} X_1 \overset{2}{\rightleftharpoons} X_2 \cdots \overset{n-1}{\rightleftharpoons} X_{n-1} \overset{n}{\rightleftharpoons} X_n \tag{5}$$

In section III we derive the full steady-state solution for this linear chain:

- Equilibrium concentations and fluxes with respect to the reference chemostat X_0:

$$x_i^{\mathrm{eq}} = x_0 \exp\left[-\frac{\mu_i^\circ - \mu_0^\circ}{RT}\right] \tag{6}$$

$$\phi_i^{\mathrm{eq}} := \phi_i^+(\boldsymbol{x}^{\mathrm{eq}}) = \phi_i^-(\boldsymbol{x}^{\mathrm{eq}}) = k_{-i} x_i^{\mathrm{eq}} = x_0 k_{-i} \exp\left[-\frac{\mu_i^\circ - \mu_0^\circ}{RT}\right] \tag{7}$$

- Non-Equilibrium concentrations and current:

$$x_i = x_i^{\mathrm{eq}} \cdot (1 + \xi_i) \qquad J = \frac{\xi_0 - \xi_n}{\sum_{j=1}^n \left(\phi_j^{\mathrm{eq}}\right)^{-1}} \tag{8}$$

  Note that X_0 is the reference chemostat, so $\xi_0 = 0$ and $x_0 = x_0^{\mathrm{eq}}$ by definition. Nonetheless, we will keep ξ_0 in all expressions because it highlights the structure of the results.

- The global driving force and dissipation:

$$-\Delta_{\mathrm{tot}} G = -RT \ln \frac{1 + \xi_n}{1 + \xi_0} \tag{9}$$

$$\sigma = -\Delta_{\mathrm{tot}} G\, J = RT \frac{(\xi_0 - \xi_n) \ln \frac{1+\xi_n}{1+\xi_0}}{\sum_{j=1}^n \left(\phi_j^{\mathrm{eq}}\right)^{-1}} \tag{10}$$

- Stepwise ΔG and dissipation:

$$\sigma_i = -\Delta_i G\, J = RTJ \ln\left[1 + \frac{J}{\phi_i^{\mathrm{eq}}(1 + \xi_i)}\right] \tag{11}$$

$$= \frac{RT(\xi_0 - \xi_n)}{\sum_{j=1}^n \left(\phi_j^{\mathrm{eq}}\right)^{-1}} \ln\left[1 + \frac{\xi_0 - \xi_n}{\phi_i^{\mathrm{eq}}(1 + \xi_i) \sum_{j=1}^n \left(\phi_j^{\mathrm{eq}}\right)^{-1}}\right] \tag{12}$$

These equations are not particularly difficult to derive and by themselves may not be too surprising. However, these results are not very intuitive: It is impossible to easily identify

- which reaction in a pathway is the most irreversible
- what is the effect of the energetic landscape μ°.
- what is the actual effect of the kinetics on the non-equilibrium dissipation – in total via the current vs. per reaction on the individual ΔG.

We answer these questions by providing plots of the concentrations at equilibrium x^{eq} and out of equilibrium x, the chemical potentials μ, as well as the reaction-wise dissipation σ_i for different choices of kinetic rate constants and different μ°.

A. Homogeneous pathway

A particularly simple case is when the kinetic rate constants $k_i^\pm = k$ are all identical. Then, the standard-state chemical potentials $\mu_i^\circ = \mu^\circ$, as well as the equilibrium fluxes $\phi_i^{\mathrm{eq}} = \phi^{\mathrm{eq}}$ are all identical. In this case the current is

$$J = \frac{\phi_{\mathrm{eq}}}{n}(\xi_0 - \xi_n) = \frac{\phi^{\mathrm{eq}}}{n}(1 - \exp[\Delta_{\mathrm{tot}} G]) \tag{13}$$

For large forces ($-\Delta_{\mathrm{tot}} G \to \infty \Leftrightarrow \xi_n \to -1$), the current reaches an upper bound of ϕ^{eq}/n.

This simple consideration shows that a chemical pathway displays nonlinear thermodynamic behavior even in the simplest nonequilibrium situation : The global current is not a linear function of the force, but instead reaches an upper bound which is determined by the equilibrium flux and the length of the pathway.

B. Energetic effects on the path out of equilibrium

We now look at the effect of different energetic landscapes μ° that are not entirely homogeneous. To that end, we set the kinetic rate constants to

$$k_{\pm i} = 100 \exp\left[\mp \frac{\Delta_i G^\circ}{2RT}\right] = 100 \exp\left[\mp \frac{\mu_i^\circ - \mu_{i-1}^\circ}{2RT}\right]. \tag{14}$$

In Fig. 1 we have six panels, each representing a linear pathway of 41 reaction steps connecting 42 species. In the two columns we have two different landscapes for the standard state chemical potentials μ° along the pathway: The local differences of μ° are zero except in the central reaction where on the left (right) we have a step down (up) by $\Delta_{21} G^\circ = 2\,RT$. As a direct consequence, the equilibrium concentration distributions x^{eq} directly follow this equilibrium landscape.

Across the different rows we change the last chemostat's concentration. In the first row we fix it to be $\xi_{41} = -10\%$ relative to its equilibrium value. This leads to a global force of

$$-\Delta_{\mathrm{tot}} G = -RT \ln \frac{1 + \xi_{41}}{1 + \xi_0} \approx 0.105\, RT\,. \tag{15}$$

and a steady current from left to right. The value of the current depends on the μ° landscape: On the left, the landscape is favoring the direction of the current, leading to $J_{\mathrm{fav}} \approx 0.433$, while on the right, the current is considerably lower: $J_{\mathrm{unf}} \approx 0.059$. This is caused by the increased (decreased) equilibrium concentrations, and thus fluxes, in the right half of the (un)favorable pathway. As a consequence, the favorable landscape leads to a higher dissipation.

We observe that in both cases the chemical potential μ is approximately a straingt line with constant slope. This is a regime where a linear non-equilibrium thermodynamics may be applicable. The current is in any case linear in ξ_{41}. The local force is $-\Delta_i G \approx RT \frac{J}{\phi_i^{\mathrm{eq}}}$ and thus the stepwise dissipation $\sigma_i \approx RT(J)^2/\phi_i^{\mathrm{eq}}$.

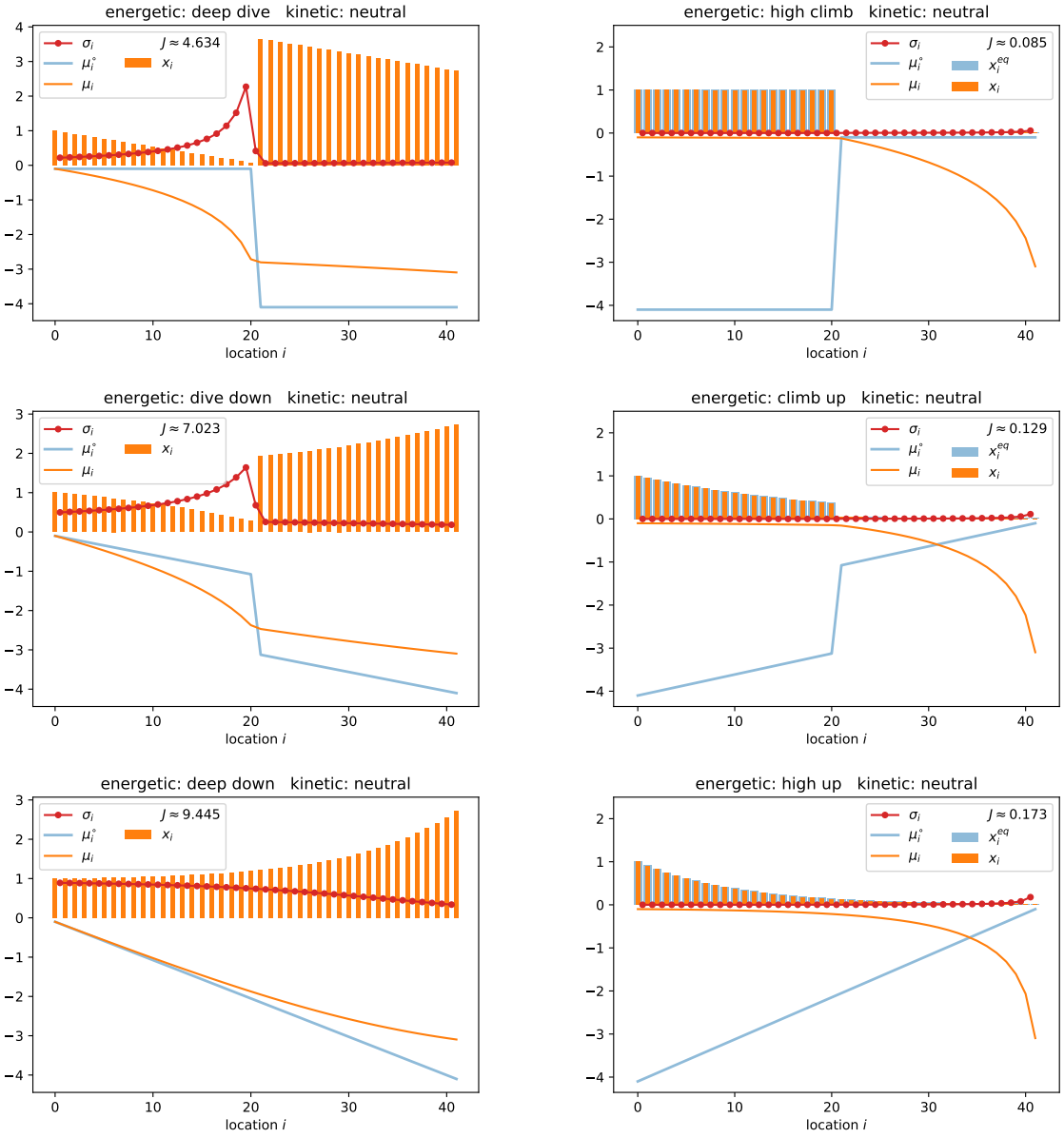

FIG. 2. Impact of different energetic landscapes no the nonequilibrium thermodynamics.

In the second row we have $\xi_{41} = -70\%$ and it becomes more apparent that approximating μ with a constant slope is becoming less reasonable. Bear in mind that in both cases, the global thermodynamic driving force is the same:

$$-\Delta_{\text{tot}}G = -RT \ln \frac{1+\xi_{41}}{1+\xi_0} \approx 1.204\, RT \tag{16}$$

while now the currents are diverging even more:

$$J_{\text{fav}} \approx 3.034 \qquad J_{\text{unf}} \approx 0.411 \tag{17}$$

In the last row, finally, we arrive at $\xi_{41} = -95\%$ and the chemical potential landscape is (approximately) piecewise exponential. The total force is

$$-\Delta_{\text{tot}}G = -RT \ln \frac{1+\xi_{41}}{1+\xi_0} \approx 2.996\, RT\,. \tag{18}$$

and the currents are

$$J_{\text{fav}} \approx 4.117 \qquad J_{\text{unf}} \approx 0.557 \tag{19}$$

Here, the contributions of the individual reactions to the dissipation become clear: On the left (with favorable μ°) the most dissipative step is one before the center – on the right (with unfavorable μ°) the most dissipative step is the last reaction. Irrespective of the landscape, the energetically favored step 21 in the center is not the step that dissipates the most.

The interior shape of the landscape has an imapct on the value of the current. One can as well consider a landscape that favors the current with a linear gradient in μ° while keeping the same overall difference $\mu_0^\circ - \mu_{41}^\circ$ as in the single step. With this energetic landscape we arrive at about 30% stronger currents for $\xi_{41} = -95\%$:

$$J_{\text{fav}} \approx 5.360 \qquad J_{\text{unf}} \approx 0.725\,. \tag{20}$$

For both gradient landscapces, the most dissipative step is the last – even though the favorable gradient landscape has a far more homogeneously distributed dissipation.

Note furthermore that in all these cases, the steps in μ° do not coincide with steps in μ – and out of equilibrium, the local shapes are not immediately linked. This is another indication that the contributions of the individual reaction to the dissipation are not correlated with the energetic bias $-\Delta_i G^\circ = \mu_i^\circ - \mu_{i-1}^\circ$.

An obvious question is whether there is some form of optimal interior landscape for μ° (at fixed global difference $\Delta_{\text{tot}}G^\circ$) to maximize the current. The current as a function of the landscape, however, is unbounded: Setting the interior to very high equilibrium concentrations ($\mu^\circ \to -\infty$) causes the equilibrium fluxes of all reactions to be very high $\phi^{\text{eq}} \to \infty$. As seen for the homogeneous pathway, the current increases with increasing equilibrium flux. When the equilibrium flux of all reactions collectively approaches infinity, the current follows and thus is unbounded. If a single reaction has a considerably smaller equilibrium flux, this flux will limit the current.

The inverse limit $\mu^\circ \to +\infty$ causes the equilibrium fluxes to approach zero $\phi^{\text{eq}} \to 0$ and the current goes to zero as well.

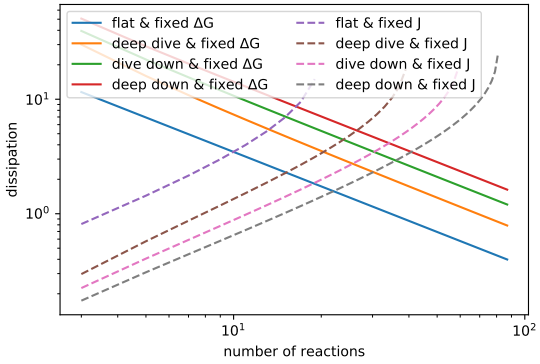

FIG. 3. Scaling of the dissipation with the length of the pathway

C. Scaling with the length

We now address, how the dissipation scales with the length of the pathway. To that end, we note that there is a difference between prescribing the total force $-\Delta_{\text{tot}}G$ (as we did until here) and prescribing the current J through the pathway. In Fig. 3 we see how the dissipation changes as function of length of the pathway (in number of species) – for fixed force given by $\xi_n = -50\%$ (solid lines) and for fixed current $J = 5$ (dashed lines). We provide plots for different energetic landscapes: *neutral*, a favorable *step* of $\Delta G^\circ = 4\,RT$ in the central reaction, a favorable step of $\Delta G^\circ = 2\,RT$ with an additional gradient adding up to $4\,RT$, and a pure favorable *grand*ient of overall $\Delta G^0 = 4\,RT$.

We see that for fixed force, the dissipation reduces with the length of the pathway. This is due to the fact that a longer pathway has a smaller current: For the energetically *neutral* pathway we saw that the current is bounded by ϕ^{eq}/n. A favourable bias increases the current: Among the considered landscapes, the largest current (and therefore the largest dissipation) is found for the strong favorable energetic gradient, while a single energetically favorable step of the same size carries a smaller current.

Conversely, for fixed current the dissipation increases with increasing length of the pathway. This is caused by a larger force that is required to sustain the same current. Moreover, the dissipation diverges when we try to impose a current that exceeds the upper bound for the respective energetic bias.

D. Kinetic effects in energetically biased pathways

We now investigate the kinetic effects for pathways with 41 reaction and 42 species. We begin with the same energetically biased pathways as in the previous subsection: The standard-state chemical potentials are locally flat, except in the central reaction, where we have either a favorable step down or an unfavorable step up by $\Delta G^0 = 2\,RT$. In Fig. 4 we have six panel, again with the favorable landscape on the left while the unvaforable landscape is on the right. In all six panels

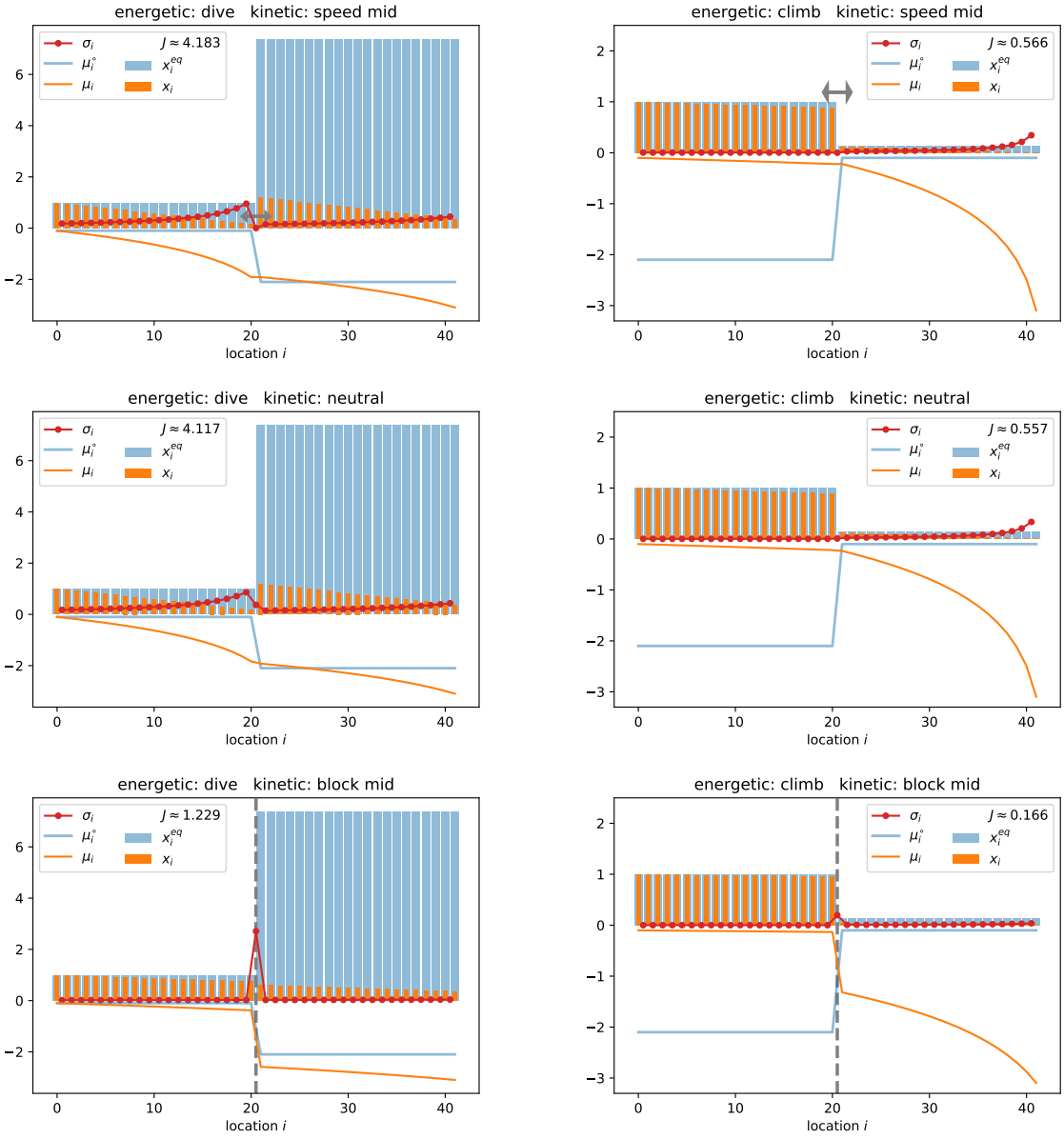

FIG. 4. Several different kinetics for energetically biased pathways.

we keep the left chemostat X_0 at a reference concentration of unity, while the right chemostat is at $\xi_{41} = -95\%$ relative to its equilibrium value, thus the global force is $-\Delta_{\mathrm{tot}}G \approx 2.996\,RT$.

The different rows admit different kinetics for the central reaction: In the central row, all reactions have the same kinetics and thus reproduce the last two panels from Fig. 1. In the top row, the rate constant of the central reaction is increased by a factor of e^5 symmetrically in both directions (indicated by the double headed arrow in gray). In the bottom row, the rate constant of the central reaction is decreased by a factor of e^{-5} symmetrically in both directions (indicated by the gray dashed line).

The increased rate in the center has only a mild influence on the currents:

$$J_{\mathrm{fav}} \approx 4.183 \qquad J_{\mathrm{unf}} \approx 0.566 \tag{21}$$

compared to the

$$J_{\mathrm{fav}} \approx 4.117 \qquad J_{\mathrm{unf}} \approx 0.557 \tag{22}$$

in the central row. The most notable difference is the dissipation of the central step: the increase of the kinetic flux at equilibrium causes the central reaction to have a considerably lower dissipation.

The third row represents systems that are kinetically (almost) split: The flux in the central reaction is so low that the left part of the pathway is almost equilibrated with the reference chemostat, while the right part of the pathway is almost equilibrated with the right chemostat. Consequently, the currents are considerably weaker:

$$J_{\mathrm{fav}} \approx 1.229 \qquad J_{\mathrm{unf}} \approx 0.166 \tag{23}$$

This setting where a single reaction is limiting the overall current considerably is known as "rate-limiting step". We see that this rate-limiting step has a severe influence on the distribution of the dissipation along the pathway: almost all the dissipation is localized on the rate-limiting step, causing the chemical potential μ to develop a considerable jump at that point. We see that the jump always points down und thus is entirely independent from the step in μ°.

E. Kinetic effects in energetically neutral pathways

In Fig. 5 we provide plots for energetically neutral pathways composed of 41 reactions and 42 species: In all these cases, $\mu_0^\circ = \mu_{41}^\circ$. Again, we assume the species X_0 to be a reference chemostat concentration of unity providing a reference equilibrium concentration profile. The right-most species is also chemostatted – and fixed to be at 5 % of its equilibrium value, i. e. $\xi_{41} = -0.95$ which again gives rise to the total force $-\Delta_{\mathrm{tot}}G \approx 2.996\,RT$.

In the left column, the energy landscape goes up along the first 20 reactions, drops along reaction 21, and goes back up along the last 20 reactions. In the right column, the landscape is mirrored.

The different rows indicate different kinetics on the central reaction, again having an enhanced rate by e^5 in the first row, homogeneous kinetics in the central row, and reduced rates by e^{-5} in the last row.

The general dependence on the kinetics is similar to the energetically biased cases:

$$J^{\mathrm{enh}} \approx 2.036\,, \qquad J^{\mathrm{hom}} \approx 1.994\,, \qquad J^{\mathrm{red}} \approx 0.487\,.$$

However, there is no dependence on the orientation of the landscape: From Eq. (8) it is clear that the value of the current is inversely proportional to the total sum over the inverse equilibrium fluxes. Our choice of energetically neutral landscapes, however has a mirror symmetry. This mirror symmetry causes the equilibrium concentrations x^{eq} and consequently the equilibrium fluxes to have the same symmetry. Therefore, neither the currents nor the total dissipation actually depend on the orientation of the landscape.

The only difference we see is in the *localization* of the dissipation: On the left side, where the gradient is unfavorable for the current, but the energetic step in the center is favorable, we see a considerable part of the dissipation located in the first half of the pathway, while the second still dissipates more. On the right, the first half of the pathway contributes basically negligible dissipation. With a rate-limiting step, again, the majority of the dissipation is located on exactly this step.

F. Location of Downregulation

The location of the downregulated reaction step has a strong influence on the dissipation as well as the internal organization of the nonequilibrium concentrations. See figure 6

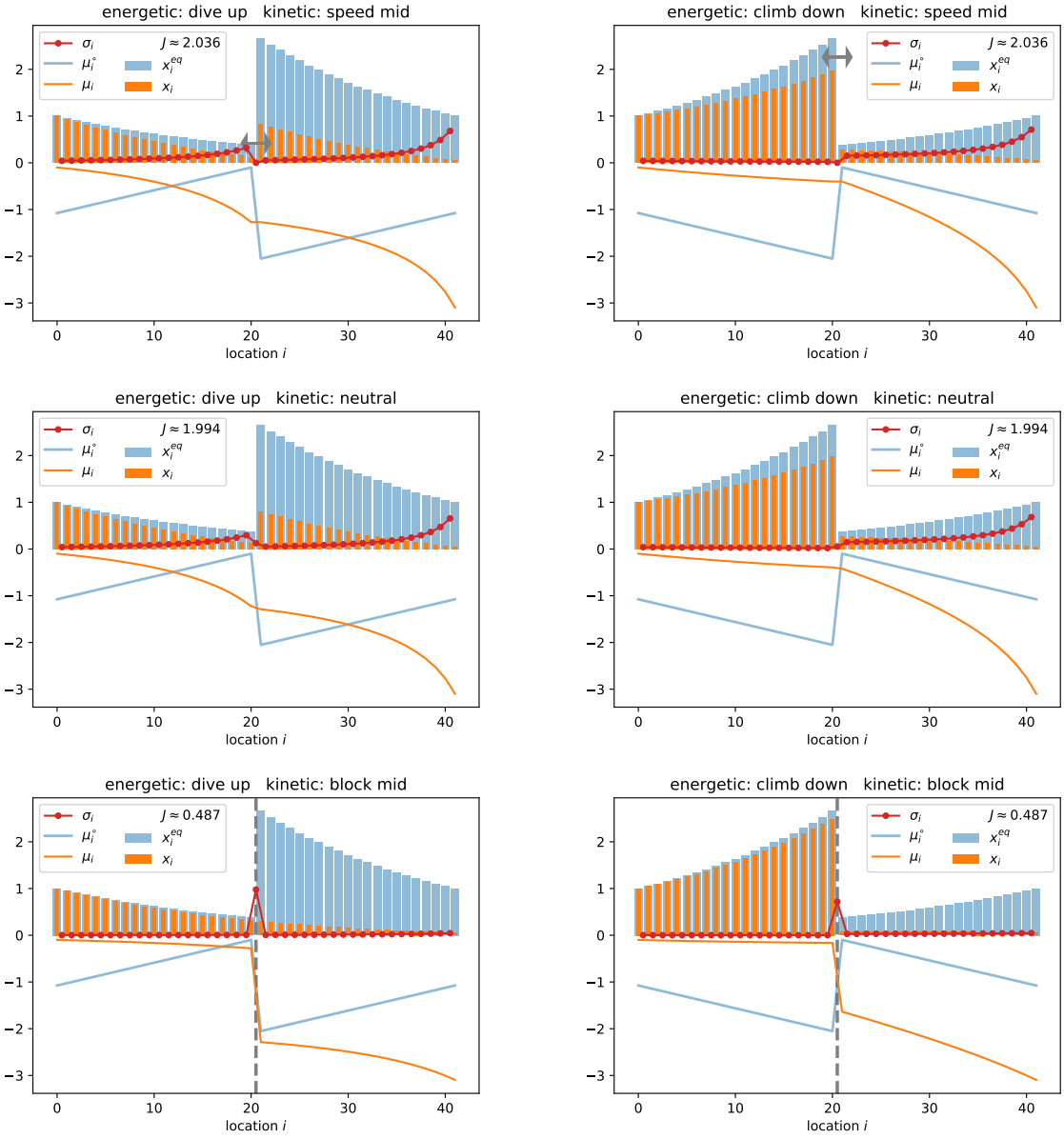

FIG. 5. Several different kinetics for globally energetically neutral pathways.

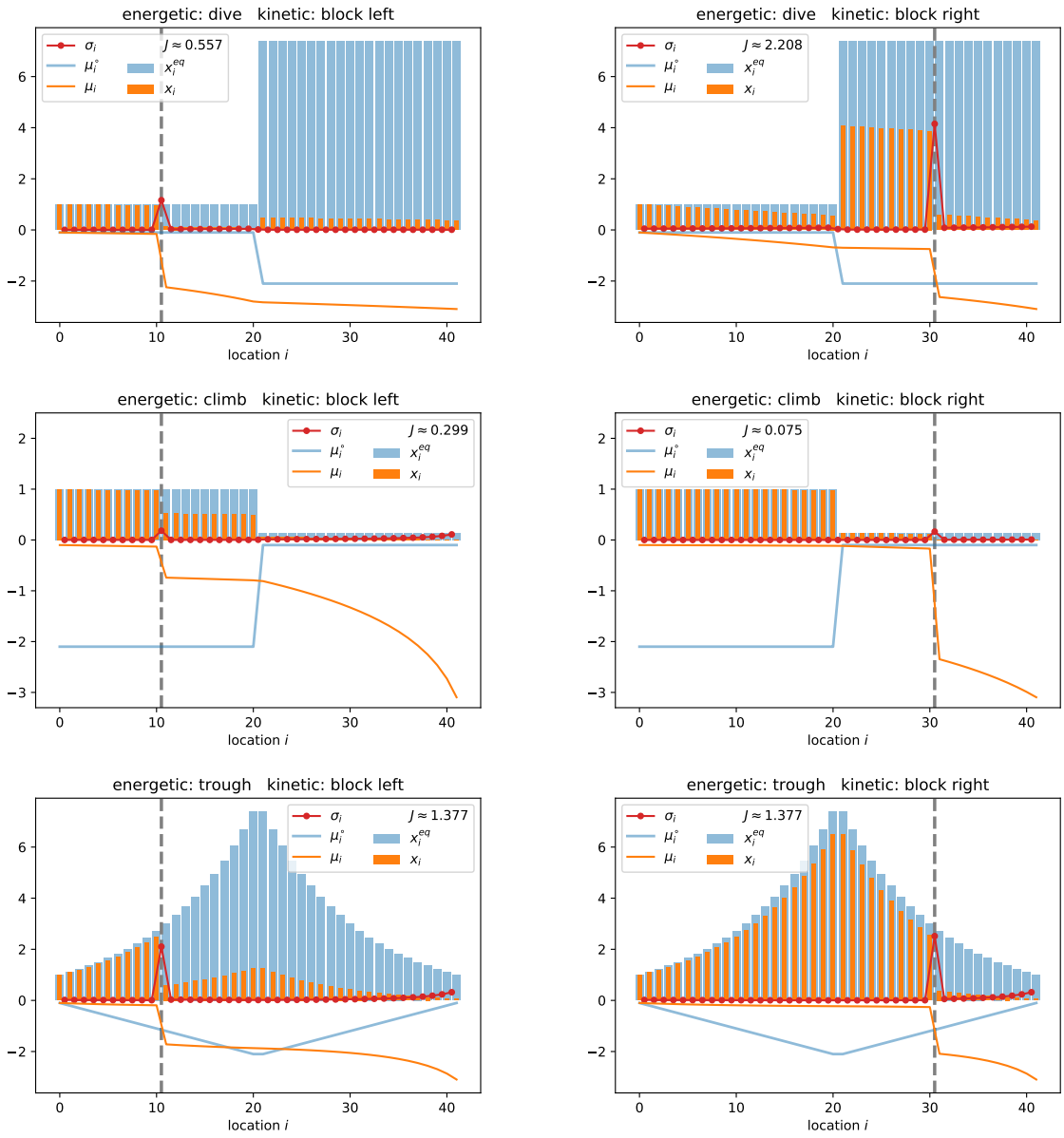

FIG. 6. The location of the downregulated reaction step has a strong influence on the dissipation as well as the internal organization of the nonequilibrium concentrations.

III. METHODS

We now derive the Equations (6–12).

Let us consider a linear pathway transforming a speciess X_0 to a species X_n in n elementary steps:

$$X_0 \overset{1}{\rightleftharpoons} X_1 \overset{2}{\rightleftharpoons} X_2 \cdots \overset{n-1}{\rightleftharpoons} X_{n-1} \overset{n}{\rightleftharpoons} X_n \tag{24}$$

Each step $i = 1, \ldots, n$ follows mass–action kinetic rates

$$\phi_i^+(\boldsymbol{x}) = k_i x_{i-1} \qquad \phi_i^-(\boldsymbol{x}) = k_{-i} x_i \tag{25}$$

and experiences the thermodynamic force

$$-\Delta_i G = RT \ln \frac{k_i x_{i-1}}{k_{-i} x_i} \,. \tag{26}$$

The equilibrium free-energy landscape is characterized by

$$-\Delta_i G^\circ = RT \ln \frac{k_i}{k_{-i}} \tag{27}$$

while the reaction currents are

$$J_i = \phi_i^+ - \phi_i^- = k_i x_{i-1} - k_{-i} x_i \tag{28}$$

A. equilibrium

This reaction network, when considered closed, has a conservation law representing the total concentration of species: $L = \sum_{i=0}^n x_i$. Moreover, in the closed system, the steady state is at thermodynamic equilibrium, i.e. $-\Delta_i G = J_i = 0$. The equilibrium solution is very easy to compute. From $J_i = 0$ we derive a recursive relation

$$x_i^{\mathrm{eq}} = x_{i-1}^{\mathrm{eq}} \frac{k_i}{k_{-i}} = x_{i-1}^{\mathrm{eq}} \exp\left[\frac{-\Delta_i G^\circ}{RT}\right] \tag{29}$$

which relates all concentrations to a single one. We choose x_0 as a reference:

$$x_i^{\mathrm{eq}} = x_0 \prod_{j=1}^{i} \frac{k_i}{k_{-i}} = x_0 \exp\left[-\frac{1}{RT} \sum_{j=1}^{i} \Delta_j G^\circ\right] \tag{30}$$

Since we have a linear pathway we identify $\Delta_i G^\circ = \mu_i^\circ - \mu_{i-1}^\circ$ and thus $\mu_i^\circ - \mu_0^\circ = \sum_{j=1}^i \Delta_j G^\circ$. Therefore,

$$x_i^{\mathrm{eq}} = x_0 \exp\left[-\frac{\mu_i^\circ - \mu_0^\circ}{RT}\right] \tag{31}$$

The unique equilibrium for the system is determined by the initial value of the conservation law, from which we can recover the corresponding value for x_0:

$$L = \sum_{i=0}^n x_i^{\mathrm{eq}} = x_0 \sum_{i=0}^n \exp\left[-\frac{\mu_i^\circ - \mu_0^\circ}{RT}\right] \tag{32}$$

At equilibrium, the currents vanish, but the fluxes have finite values that we denote by

$$\phi_i^{\mathrm{eq}} \coloneqq \phi_i^+(\boldsymbol{x}^{\mathrm{eq}}) = \phi_i^-(\boldsymbol{x}^{\mathrm{eq}}) = k_{-i} x_i^{\mathrm{eq}} = x_0 k_{-i} \exp\left[-\frac{\mu_i^\circ - \mu_0^\circ}{RT}\right] \tag{33}$$

Introducing X_0 as a chemostat changes nothing about these equations – except that the conservation law is broken. We see that at equilibrium, the steady state of the system is fully characterized by the equilibrium landscape μ°, and a value for either the conserved quantity, or the chemostat concentration. The only quantities that actually depend on the individual kinetic rates are the equilibrium fluxes at equilibrium.

B. non-equilibrium

We now consider both X_0 and X_n chemostatted. This breaks the conservation law and creates a cycle with force

$$-\Delta_{\mathrm{cyc}} G = -\sum_{i=1}^n \Delta_i G = -(\mu_n^\circ - \mu_0^\circ) - RT \ln \frac{x_n}{x_0} = \mu_n - \mu_0 \tag{34}$$

The non-equilibrium steady-state solution is characterized by a globally constant current $J_i = J$. In order to actually calculate this solution, let us parameterize it relative to the equilibrium solution we determined from only chemostatting X_0:

$$x_i = x_i^{\mathrm{eq}} \cdot (1 + \xi_i) \,. \tag{35}$$

With this parametrization, the overall force is

$$-\Delta_{\mathrm{cyc}} G = -RT \ln \frac{1 + \xi_n}{1 + \xi_0} \tag{36}$$

while the current is

$$J = k_i x_{i-1}^{\mathrm{eq}}(1 + \xi_{i-1}) - k_{-i} x_i^{\mathrm{eq}}(1 + \xi_i) = \phi_i^{\mathrm{eq}}(\xi_{i-1} - \xi_i) \tag{37}$$

The non-equilibrium solution follows from the recursive relation for the parameters ξ_i:

$$\xi_i = \xi_{i-1} - \frac{J}{\phi_i^{\mathrm{eq}}} \tag{38}$$

$$\Rightarrow \xi_i = \xi_0 - J \sum_{j=1}^{i} \frac{1}{\phi_j^{\mathrm{eq}}} \tag{39}$$

Now we can also express the current via the two chemostats:

$$J = \frac{\xi_0 - \xi_n}{\sum_{j=1}^n \left(\phi_j^{\mathrm{eq}}\right)^{-1}} \tag{40}$$

The overall dissipation for the linear pathway is

$$\sigma = -\Delta_{\mathrm{cyc}} G\, J = \frac{RT}{\sum_{j=1}^n \left(\phi_j^{\mathrm{eq}}\right)^{-1}} (\xi_0 - \xi_n) \ln \frac{1 + \xi_0}{1 + \xi_n} \geq 0 \tag{41}$$

Using the non-equilibrium force of reaction i,

$$-\Delta_i G = RT \ln \frac{1+\xi_{i-1}}{1+\xi_i} = RT \ln \frac{1+\xi_i + \frac{J}{\phi_i^{\mathrm{eq}}}}{1+\xi_i} \tag{42}$$

$$= RT \ln \left[1 + \frac{J}{\phi_i^{\mathrm{eq}} (1+\xi_i)} \right], \tag{43}$$

we can resolve the contributions of the individual steps for the overall dissipation:

$$\sigma_i = -\Delta_i G\, J = RTJ \ln \left[1 + \frac{J}{\phi_i^{\mathrm{eq}} (1+\xi_i)} \right] \tag{44}$$

$$= \frac{RT(\xi_0 - \xi_n)}{\sum_{j=1}^{n} \left(\phi_j^{\mathrm{eq}}\right)^{-1}} \ln \left[1 + \frac{\xi_0 - \xi_n}{\phi_i^{\mathrm{eq}} (1+\xi_i) \sum_{j=1}^{n} \left(\phi_j^{\mathrm{eq}}\right)^{-1}} \right] \tag{45}$$

Please note that from the recursive relation for the parameters ξ we can conclude that each and every individual contribution is positive.

It is worth noting that, while the equilibrium solution is basically characterized by the equilibrium free-energy landscape μ°, the non-equilibrium solution is most conventiently expressed in terms of the equilibrium fluxes. With eq. (33) we can express the equilibrium fluxes with the equilibrium free energy landscape, but the flux still depends on the kinetic rate constants. In other words: while the equilibrium is characterized by the thermodynamic properties, the non-equilibrium depends on both thermodynamic and kinetic properties

IV. CONCLUSION

We have investigated the non-equilibrium thermodynamics of linear reaction pathways following mass–action kinetics. This is a first-order approximation to actual enzymatic kinetics (for low substrate and product concentrations). The total amount of available enzyme causes a change in the kinetic rates symmetrically in both forward and backward direction. We have calculated the full non-equilibrium solution for arbitray energetic biases and arbitrary chemostatting conditions.

Our detailed investigation has highlighted that

- the total force of the pathway is given by the chemostat concentrations. In fact, one concentration relative to the equilibrium provided by the other concentration is enough.
- the direction of the current is directly imposed by the direction of the force $-\Delta_{\mathrm{tot}} G$ along the entire pathway.
- the energetic bias $\Delta_{\mathrm{r}} G^\circ$ of an individual reaction has no direct and simple connection to the actual dissipation $-J\Delta_{\mathrm{r}} G$ along this step.
- the impact of the kinetic equilibrium flux on the dissipation is severe: A rate limiting step is always the single reaction that dissipates the most. A step with enhanced equilibrium flux has negligible dissipation, irrespective of the energetic bias.

Appendix A: Reparametrization of Mass–Action Kinetics

Based on these observations, we now apply a similar parametrization of the kinetic rate constants of the mass–action kinetics:

$$k_i = r \exp\left[\alpha_i + \beta_i\right], \qquad k_{-i} = r \exp\left[-\alpha_i + \beta_i\right]. \tag{A1}$$

Where $r > 0$ while $\alpha_i, \beta_i \in \mathbb{R}$.

With these parameters, we immediately see that the equilibrium free-energy landscape is given by

$$-\Delta G_i^\circ = 2RT\alpha_i, \qquad \mu_i^\circ - \mu_0^\circ = -2RT \sum_{j=1}^{i} \alpha_j \tag{A2}$$

The equilibrum fluxes, consequently, are

$$\phi_i^{\mathrm{eq}} = x_0^{\mathrm{eq}} r \exp\left[\beta_i + 2\sum_{j=1}^{i-1} \alpha_j + \alpha_i\right] \tag{A3}$$

We see that the α determine the equilibrium exclusively – we call them the *thermodynamic parameters*. The remaining parameters, r and β_i, together with the thermodynamic parameters determine the equilibrium kinetic fluxes. Therefore, we call them *kinetic parameters*. Here, r is a global kinetic parameter determining the intrinsic time-scale of the entire system. The β_i act locally on the different reactions.

The non-equilibrium current is

$$J = x_0^{\mathrm{eq}} r \frac{\xi_0 - \xi_n}{\sum_{i=1}^{n} \exp\left[-\beta_i - 2\sum_{j=1}^{i-1} \alpha_i - \alpha_i\right]}. \tag{A4}$$

This current is monotonous in all the parameters: It increases with α, β, x_0 and r and decreases with n.

The non-equilibrium corrections to the equilibrium steady state are

$$\xi_i = \xi_0 - (\xi_0 - \xi_n) \frac{\sum_{j=1}^{i} \exp\left[-\beta_j - 2\sum_{\ell=1}^{j-1} \alpha_\ell - \alpha_j\right]}{\sum_{j=1}^{n} \exp\left[-\beta_j - 2\sum_{\ell=1}^{j-1} \alpha_\ell - \alpha_j\right]} \tag{A5}$$

and hence ordered: $0 = \xi_0 > \xi_1 > \cdots > \xi_{n-1} > \xi_n$. Note that we assume $\xi_0 = 0$ and $-1 < \xi_n < 0$.

1. Homogeneous pathway with localized regulation

Let us now assume the free enthalpy difference is constant along the pathway:

$$-\Delta G_i^\circ = 2RT\alpha_i \equiv 2RT\alpha > 0 \tag{A6}$$

and the kinetic parameters only affect the reaction with index ℓ:

$$\beta_i = \beta\, [\![i = \ell]\!] \quad \text{with } \beta \in \mathbb{R}. \tag{A7}$$

The double stroked bracket $[\![\cdot]\!]$ denotes the Macaulay brackets which evaluate to 0 when the condition inside is violated,

while it evaluates to 1 when the condition inside is satisfied. So in this case $[\![i = k]\!] = \delta_{i,k}$ is the Kroneker symbol.

This parametrization can be interpreted as an upregulation $\beta > 0$ or downregulation $\beta < 0$ for the reaction ℓ while the energetic landscape of the pathway has a constant linear slope.

Using this parametrization, we identify the standard-state chemical potential and the equilibrium fluxes:

$$\mu_i^\circ - \mu_0^\circ = -2RT\alpha i \tag{A8}$$

$$\phi_i^{\mathrm{eq}} = x_0 r \exp\left[\beta\,[\![i = \ell]\!] + \alpha(2i-1)\right] \tag{A9}$$

The sum over the inverse fluxes is a geometric sum and can thus be performed explicitly:

$$\begin{aligned}\sum_{j=1}^{i} \frac{1}{\phi_j^{\mathrm{eq}}} &= \frac{1}{x_0 r} \sum_{j=1}^{i} \exp\left[-\beta\,[\![j = \ell]\!] - \alpha(2j-1)\right] \\ &= \frac{1}{x_0 r}\left\{\sum_{j=1}^{i} \mathrm{e}^{-\alpha(2j-1)} + \mathrm{e}^{-\alpha(2\ell-1)}\left(\mathrm{e}^{-\beta}-1\right)[\![i \geq \ell]\!]\right\} \\ &= \frac{\mathrm{e}^{\alpha}}{x_0 r}\left\{\mathrm{e}^{-2\alpha}\frac{1-\mathrm{e}^{-2\alpha i}}{1-\mathrm{e}^{-2\alpha}} + \mathrm{e}^{-2\alpha\ell}\left(\mathrm{e}^{-\beta}-1\right)[\![i \geq \ell]\!]\right\}\end{aligned}$$

Imposing the first and last species chemostatted with concentrations $\xi_0 = 0$ and $\xi_n < 0$ relative to equilibrium, we find the current

$$J = \frac{x_0 r\,\mathrm{e}^{-\alpha}\,(\xi_0 - \xi_n)}{\mathrm{e}^{-2\alpha}\frac{1-\mathrm{e}^{-2\alpha n}}{1-\mathrm{e}^{-2\alpha}} + \mathrm{e}^{-2\alpha\ell}\left(\mathrm{e}^{-\beta}-1\right)} > 0\,.$$

For upregulation, $\beta > 0$, the current decreases with ℓ. For downregulation, $\beta < 0$, the the current increases with ℓ.

The non-equilibrium steady state follows as

$$\xi_i = \xi_0 - (\xi_0 - \xi_n)\,\frac{\mathrm{e}^{-2\alpha}\frac{1-\mathrm{e}^{-2\alpha i}}{1-\mathrm{e}^{-2\alpha}} + \mathrm{e}^{-2\alpha\ell}\left(\mathrm{e}^{-\beta}-1\right)[\![i \geq \ell]\!]}{\mathrm{e}^{-2\alpha}\frac{1-\mathrm{e}^{-2\alpha n}}{1-\mathrm{e}^{-2\alpha}} + \mathrm{e}^{-2\ell\alpha}\left(\mathrm{e}^{-\beta}-1\right)}\,.$$

We can discuss a couple of interesting limits:

a. Long pathway. We see that the steady-state current is monotonously decreasing with the length n of the pathway. In the limit of an infinitely long pathway, we reach the minimum

$$\lim_{n\to\infty} J = \frac{x_0 r\,\mathrm{e}^{-\alpha}\,(\xi_0 - \xi_n)}{\frac{\mathrm{e}^{-2\alpha}}{1-\mathrm{e}^{-2\alpha}} + \mathrm{e}^{-2\alpha\ell}\left(\mathrm{e}^{-\beta}-1\right)} \tag{A10}$$

This minimum still depends on the strength β as well as the location ℓ of the regulation.

b. One reaction shut down. In the limit of $\beta \to -\infty$, we completely shut down the enzyme that catalyzes reaction ℓ. This causes the current to vanish and the steady-state to become

$$\xi_i = \begin{cases}\xi_0 & \text{if } i < \ell\,,\\ \xi_n & \text{if } i \geq \ell\,.\end{cases} \tag{A11}$$

This means the two parts of the pathway before and after reaction ℓ are completely separated and equilibrated with their respective chemostat. If β is large but finite with a negative value, the concentrations will be very similar to this, with a very small current. Interestingly, for $\beta < 0$ large and finite the dissipation of reaction i,

$$\sigma_i = RTJ \ln\frac{1+\xi_{i-1}}{1+\xi_i}\,, \tag{A12}$$

peaks for $i = \ell$. So while the total dissipation decreases and eventually reaches zero in the limit $\beta \to -\infty$, the dissipation redistributing and localizing on the reaction that is being downregulated.

c. One reaction upregulated. When $\beta > 0$, the relative concentrations of the species $\xi_{\ell-1}$ and ξ_ℓ will become more equal, reaching

$$\lim_{\beta\to\infty} -\Delta_\ell G = -RT \lim_{\beta\to\infty} \ln\frac{1+\xi_\ell}{1+\xi_{\ell-1}} = 0 \tag{A13}$$

making this step basically equilibrated. Note however, that the absolute concentrations $x_{\ell-1}$ and x_ℓ are *not* at the values that the equilibrium with only the chemostat x_0 would impose. See also [6]

2. Energetic Step with localized regulation

Let us now assume the free enthalpy difference is localized as well:

$$-\Delta G_i^\circ = 2RT\alpha\,[\![i = k]\!] \tag{A14}$$

$$\beta = \beta\,[\![i = \ell]\!] \tag{A15}$$

We will assume that $k, \ell > 1$.

Using the Macaulay brackets again, we can express the standard-state chemical potential and the equilibrium flux:

$$\begin{aligned}\mu_i^\circ - \mu_0^\circ &= -2RT\alpha[\![i \geq k]\!] \\ \phi_i^{\mathrm{eq}} &= x_0 r \exp\left(\beta\,[\![i = \ell]\!] + \alpha\,[\![i = k]\!] + 2\alpha\,[\![i > k]\!]\right)\end{aligned}$$

The sums over the inverse fluxes are

$$\sum_{j=1}^{i} \frac{1}{\phi_j^{\mathrm{eq}}} = \frac{1}{x_0 r} \left\{ \sum_{\substack{j=1 \\ j \le i}}^{k-1} \mathrm{e}^{-\beta [\![j=\ell]\!]} + \mathrm{e}^{-\alpha-\beta [\![j=\ell]\!]} [\![i \ge k]\!] + \mathrm{e}^{-2\alpha} \sum_{j=k+1}^{i} \mathrm{e}^{-\beta [\![j=\ell]\!]} \right\} \tag{A16}$$

$$\sum_{j=1}^{n} \frac{1}{\phi_j^{\mathrm{eq}}} = \frac{1}{x_0 r} \left\{ k - 1 + \left(\mathrm{e}^{-\beta} - 1 \right) [\![\ell < k]\!] + \mathrm{e}^{-\alpha-\beta [\![\ell=k]\!]} + \mathrm{e}^{-2\alpha} \left[n - k + 1 + \left(\mathrm{e}^{-\beta} - 1 \right) [\![\ell > k]\!] \right] \right\} \tag{A17}$$

$$= \frac{1}{x_0 r} \begin{cases} k - 2 + \mathrm{e}^{-\beta} + \mathrm{e}^{-\alpha} + \mathrm{e}^{-2\alpha} (n - k + 1) , & l < k \\ k - 1 + \mathrm{e}^{-\alpha-\beta} + \mathrm{e}^{-2\alpha} (n - k + 1) , & l = k \\ k - 1 + \mathrm{e}^{-\alpha} + \mathrm{e}^{-2\alpha} (n - k + \mathrm{e}^{-\beta}) , & l > k \end{cases} \tag{A18}$$

Thus, when applying chemostats $\xi_0 = 0$ and $\xi_n < 0$, the steady-state current amounts to

$$J = \begin{cases} \frac{x_0 r (\xi_0 - \xi_n)}{k - 2 + \mathrm{e}^{-\beta} + \mathrm{e}^{-\alpha} + \mathrm{e}^{-2\alpha} (n-k+1)} , & l < k \\ \frac{x_0 r (\xi_0 - \xi_n)}{k - 1 + \mathrm{e}^{-\alpha-\beta} + \mathrm{e}^{-2\alpha} (n-k+1)} , & l = k \\ \frac{x_0 r (\xi_0 - \xi_n)}{k - 1 + \mathrm{e}^{-\alpha} + \mathrm{e}^{-2\alpha} (n-k+\mathrm{e}^{-\beta})} , & l > k \end{cases} \tag{A19}$$

In contrast to the homogeneously tilted landscape, this current decays to zero when the length n of the pathway approaches infinity.

Following Eqs. (39) and (40), the expressions for the relative concentrations ξ_i at steady state are essentially given by the ratio of Eqs. (A16) and (A18). They appear too complicated to discuss analytically. Therefore, we provide and discuss the plots in the main text.

Appendix B: Reversible Michaelis Menten

It is possible to assume the full reversible Michaelis–Menten kinetics in a linear chain and still give an exact analytical solution:

$$J = \frac{L_{\mathrm{E}}}{1 + \frac{[\mathrm{S}]}{K_{\mathrm{mS}}} + \frac{[\mathrm{P}]}{K_{\mathrm{mP}}}} \left(k_{\mathrm{S}} [\mathrm{S}] - k_{\mathrm{P}} [\mathrm{P}] \right) \tag{B1}$$

Assuming we know the current J and the concentration of S, we can determine the concentration of P:

$$[\mathrm{P}] = \frac{L_{\mathrm{E}} k_{\mathrm{S}} - \frac{J}{K_{\mathrm{mS}}}}{L_{\mathrm{E}} k_{\mathrm{P}} + \frac{J}{K_{\mathrm{mP}}}} [\mathrm{S}] - \frac{J}{\frac{J}{K_{\mathrm{mP}}} + L_{\mathrm{E}} k_{\mathrm{P}}} . \tag{B2}$$

Similarly, we can express the reaction force:

$$-\Delta_{\mathrm{r}} G = RT \ln \frac{k_{\mathrm{S}} [\mathrm{S}]}{k_{\mathrm{P}} [\mathrm{P}]} = -RT \ln \frac{L_{\mathrm{E}} - \frac{J}{k_{\mathrm{S}}} \left(\frac{1}{K_{\mathrm{mS}}} + \frac{1}{[\mathrm{S}]} \right)}{L_{\mathrm{E}} + \frac{J}{k_{\mathrm{P}} K_{\mathrm{mP}}}} \tag{B3}$$

We see that the current is bounded from above by

$$J < \frac{L_{\mathrm{E}} k_{\mathrm{S}}}{\frac{1}{K_{\mathrm{mS}}} + \frac{1}{[\mathrm{S}]}} < L_{\mathrm{E}} k_{\mathrm{S}} [\mathrm{S}] \tag{B4}$$

When combining several Michaelis–Menten enzymes in a linear chain, we can use the above relations in an iterative fashion to determine each concentration and reaction force in the non-equilibrium steady state – expressed via the concentration of the first species and the overall current. We see that a singularity will appear in the force when imposing the current J will cause the concentration of an intermediate species to violate

$$[\mathrm{S}] > \left(\frac{L_{\mathrm{E}} k_{\mathrm{S}}}{J} - \frac{1}{K_{\mathrm{mS}}} \right)^{-1} . \tag{B5}$$

[1] D. L. Nelson and M. M. Cox, *Lehninger Principles of Biochemistry*, 5th ed. (W. H. Freeman and Co., New York, 2008).

[2] A. Cornish-Bowden, *Fundamentals of Enzyme Kinetics*, 4th ed. (Wiley-Blackwell, Weinheim, 2012).

[3] M. Polettini and M. Esposito, Journal of Chemical Physics **141**, 024117 (2014).

[4] R. Rao and M. Esposito, Physical Review X **6**, 041064 (2016).

[5] A. Wachtel, R. Rao, and M. Esposito, New Journal of Physics (2018), 10.1088/1367-2630/aab5c9.

[6] N. Tepper, E. Noor, D. Amador-Noguez, H. S. Haraldsdóttir, R. Milo, J. Rabinowitz, W. Liebermeister, and T. Shlomi, PLOS ONE **8**, e75370 (2013).

Part V.

Conclusion and Perspectives

10. Conclusion

Thermodynamics is a universal theory for exchange processes. It is centered around the exchange of energy in the form of work and heat, and the exchange of matter. In the real world, these exchange processes always come at the cost of irreversible *dissipation*, which we quantify by the *entropy production*. In its modern incarnation, known as *stochastic thermodynamics*, the theory can deal with very small systems that are subject to considerable noise. In these situations also the thermodynamic exchanges are stochastic and possibly discrete. I introduced the general theory in a modern formulation in part I of this thesis. In particular, chapter 1 dealt with the macroscopic formulation, while chapter 2 also incorporated stochasticity.

I accounted for the possibility of chemical reactions in part II. Assuming a dilute reactive solution, I expanded on the properties of *elementary* reactions within a closed container in chapter 3. The following chapter 4 addressed the interactions of many reactions in a *network* and allowed for selective exchange of some of the reactive species with an environment. A central insight for open chemical networks is the crucial role that *stoichiometric cycles* and *conservation laws* play: the conservation of some parts of molecules restricts the dynamics of the network in specific ways, but can be *broken* when species containing these parts are *chemostatted*. The chemostatting can alternatively create new or *emergent* cycles. Along these cycles *thermodynamic forces* act on the reactive system and typically prevent it from from reaching thermodynamic equilibrium, thus driving the exchange *currents*.

Biological cells or cellular substructures fall into the class of systems with exactly these properties: various chemical reactions can proceed inside, thus causing the interconversion of different biochemical species — while their boundaries are semipermeable to the exchange of some chemicals. This continuous exchange of energy and matter is necessary for the cell to stay alive. It is therefore absolutely natural to use tools from nonequilibrium thermodynamics when investigating the structural and dynamical properties of cellular life. This insight, however, faces practical problems. The common modeling of biological systems tries to integrate as much *data* as possible, aiming at a systemic scale — while introducing various approximations along the way. The assumptions typically employed for the further development of nonequilibrium thermodynamics are often selected based on their *theoretical* elegance or simplicity. This situation causes a divide between these two worlds, which this thesis aims to narrow.

In this thesis, I presented my contributions to the nonequilibrium thermodynamics of chemical reaction networks in parts III and IV. I started with a detailed analysis of the thermodynamic and transport properties of stochastic models for the molecular motor kinesin. I addressed the quasi-tight coupling of the chemical turnover and the displacement of the motor, as well as the efficiency of the motor's operation modes. On the one hand, this analysis reveals that an equilibrium-like fluctuation–dissipation relation holds when the displacement velocity is zero, while the chemical turnover does not vanish. On the other hand, the displacement velocity shows negative differential mobility for a large range of driving forces. [1]

I showed how to generalize this analysis technique to provide explicit analytic expressions for the cumulants of arbitrary thermodynamic current observables for finite Markov processes. The general structure in the cumulants delineates the effects of thermodynamic cycle forces from kinetic contributions — thus providing response arbitrarily far from equilibrium, including the corrections to

equilibrium response theory. [2]

For open chemical networks, I addressed the connection between the thermodynamic description of the chemical master equation and the deterministic rate equations of chemical kinetics: when a reaction network satisfies a purely topological condition, the dissipation for both dynamics is exactly identical — even for average particle numbers lower than one, where the deterministic model is not even assumed to reproduce the dynamics correctly. [3]

I furthermore developed a consistent thermodynamic description for coarse-grained catalytic (e.g. enzymatic) reaction kinetics that resolves a long-standing debate in the literature of biochemical reaction networks. This method also deals with catalysts of more complicated nature than simple enzymes: molecular motors and active transporters, thus extending ideas that originated in enzyme kinetics. [4]

With this consistent thermodynamic description of catalytic reactions, I investigated the kinetic effects of enzymes on the nonequilibrium thermodynamics in linear chemical pathways. These investigations reveal that the differences of standard-state chemical potentials (which determine the thermodynamic equilibrium state) have very little influence on the dissipation of the individual reactions. It is rather the kinetic properties that dominate the local dissipation, implying that rate-limiting steps have the highest dissipation in a pathway. [5]

References

[1] B. Altaner, A. Wachtel, and J. Vollmer. "Fluctuating currents in stochastic thermodynamics. II. Energy conversion and nonequilibrium response in kinesin models". In: *Physical Review E* 92, 042133 (2015).

[2] J. Vollmer, B. Altaner, and A. Wachtel. "Fluctuating currents in stochastic thermodynamics. III. Cycle expansion of cumulants". *In preparation.* 2018.

[3] M. Polettini, A. Wachtel, and M. Esposito. "Dissipation in noisy chemical networks: The role of deficiency". In: *Journal of Chemical Physics* 143, 184103 (2015).

[4] A. Wachtel, R. Rao, and M. Esposito. "Thermodynamically consistent coarse graining of biocatalysts beyond Michaelis–Menten". In: *New Journal of Physics* 20, 042002 (2018).

[5] A. Wachtel and M. Esposito. "Kinetic Effects on Nonequilibrium Thermodynamics of Linear Enzymatic Pathways". *In preparation.* 2018.

11. Perspectives

The research on nonequilibrium thermodynamics in biology is far from completed. There are still many open questions, especially regarding the thermodynamics of open chemical reaction networks.

First, I want to briefly discuss two ongoing projects that are a direct continuation of the research already presented in this thesis. Finally, I give an outlook on some more speculative extensions of the theory.

Large Deviations in Open Chemical Networks

The chapters 5 and 6 provided an application as well as a general analytical procedure to calculate the large deviation statistics for currents in finite Markov processes. One of the outcomes of these studies is a fluctuation–dissipation relation for an individual current and its conjugated force, under additional assumptions on how that force couples to the kinetics. In between these studies, Altaner, Polettini, and Esposito [1] identified *locality* as a sufficient condition for this marginal fluctuation–dissipation to occur. This observation was subsequently generalized by Polettini and Esposito [2] to a marginal fluctuation relation. In the light of chemical networks, this begs an obvious question: can we expect a marginal fluctuation–dissipation or even marginal fluctuation relation for a *chemical current* at stalling? The primary problem is that the chemical lattice of an open chemical network is infinitely large and that the chemical current has to account for all the transitions in the lattice which are due to the same *reaction*. Likewise, the emergent cycle forces act anything but locally.

Nonetheless, the study in chapter 7 hints towards a special case: deficiency zero. For deficiency-zero systems, the steady state is uncorrelated and we were able to sum up all the individual transitions into macroscopic chemical currents, proving the equivalence of the dissipation between stochastic and deterministic dynamics. Hence, there is hope that deficiency zero systems do satisfy at least a marginal fluctuation–dissipation relation for macroscopic currents.

I currently investigate this hypothesis in collaboration with Matteo Polettini, where we combine our analytical knowledge with a numerical technique [3] to calculate the scaled cumulant-generating function for the large deviations of currents.

Efficiency in Metabolic Pathways

The central energy metabolism is composed of glycolysis, the tricarboxylic acid cycle, and the electron transport chain. These pathways together degrade glucose sugar into carbon dioxide and store a considerable amount of its energy in ATP. I addressed this kind of energy conversion already in chapter 5, but for a linear system on a finite network of states. The energy transduction in this type of linear systems was pioneered by Hill [4]. Central energy metabolism, however is neither linear, like the unbranched pathway in chapter 9, nor restricted by conservation laws, like molecular motors.

I currently investigate the efficiency of free-energy transduction in open chemical networks and use the central energy metabolism as a guiding example. Following this question turned out to connect our definition of *emergent cycle* to formal definitions of *pathways* [5] and to what in biochemistry is known as *futile cycles* [6].

Extensions

Three central assumptions used in this thesis may be relaxed and further investigated. Firstly, the *existence* of a steady state, be it at thermodynamic equilibrium or not. While this is a mild assumption for the chemical master equation, it is less clear for the deterministic rate equations: the Brusselator reaction system is known to exhibit a stable limit cycle [7]. I may be worthwhile to study the fluctuations of its stochastic trajectories and make sense of their thermodynamics in the light of the fluctuation relation.

Secondly, the treatment of fully time-dependent concentrations [8], including the chemostats, may allow for a broader understanding of the work that chemical networks perform in *finite time*. Moreover, this may be connected to a more rigorous understanding of what it means for a biochemical system to process information [9, 10].

Finally, a complete theory for the nonequilibrium thermodynamics of chemical systems has to account for spatial inhomogeneity. Reaction–diffusion systems are known to produce a variety of dynamical phenomena when driven out of equilibrium. A thermodynamics of pattern formation thus appears to be within reach. Recent progress in this direction looks very promising [11].

Ultimately, the pursuit of nonequilibrium thermodynamics in biology may pave the way for a system-wide treatment of energy, work, heat and information — a theory of *thermodyn**o**mics*.

References

[1] B. Altaner, M. Polettini, and M. Esposito. “Fluctuation-Dissipation Relations Far from Equilibrium”. In: *Physical Review Letters* 117, 180601 (2016).

[2] M. Polettini and M. Esposito. “Effective Thermodynamics for a Marginal Observer”. In: *Physical Review Letters* 119, 240601 (2017).

[3] T. Nemoto et al. “Population-dynamics method with a multicanonical feedback control”. In: *Physical Review E* 93, 062123 (2016).

[4] T. L. Hill. *Free energy transduction in biology: the steady-state kinetic and thermodynamic formalism*. New York: Academic Press, 1977.

[5] C. H. Schilling, D. Letscher, and B. Ø. Palsson. “Theory for the Systemic Definition of Metabolic Pathways and their use in Interpreting Metabolic Function from a Pathway-Oriented Perspective”. In: *Journal of Theoretical Biology* 203.3 (2000), pp. 229–248.

[6] H. Qian and D. Beard. “Metabolic futile cycles and their functions: a systems analysis of energy and control”. In: *IEE Proceedings - Systems Biology* 153.4 (2006), p. 192.

[7] D. Kondepudi and I. Prigogine. *Modern Thermodynamics: From Heat Engines to Dissipative Structures*. 2nd ed. Chichester: John Wiley & Sons, 2015.

[8] R. Rao and M. Esposito. “Nonequilibrium Thermodynamics of Chemical Reaction Networks: Wisdom from Stochastic Thermodynamics”. In: *Physical Review X* 6, 041064 (2016).

[9] A. C. Barato, D. Hartich, and U. Seifert. “Efficiency of cellular information processing”. In: *New Journal of Physics* 16, 103024 (2014).

[10] T. E. Ouldridge, C. C. Govern, and P. R. ten Wolde. “Thermodynamics of Computational Copying in Biochemical Systems”. In: *Physical Review X* 7, 021004 (2017).

[11] G. Falasco, R. Rao, and M. Esposito. “Information Thermodynamics of Turing Patterns”. arXiv: 1803.05378. 2018.

A. Author Contributions

As indicated in the research articles, the authorship of the five included manuscripts is not entirely due to myself.

The first article on kinesin [1] in chapter 5 was a very close collaboration with Bernhard Altaner. He saw that my results on finite Markov processes (part I of the series) were applicable to Kinesin. I contributed to large parts of the theory, the analysis in computer algebra, and the plots. While I also wrote some of the text, he was the leading author. We discussed a lot and at all stages of research with Jürgen Vollmer. The latter especially contributed to the final editing of the text.

The manuscript on the cycle decomposition [2] in chapter 6 was an idea of Jürgen Vollmer, who was not satisfied with the prior state of the theory. He investigated the algebraic properties of the involved determinants. In parallel, and initially independently, Bernhard Altaner did similar calculations based on graph theory. When I realized that both were doing very similar things, I brought them and their ideas together. Subsequently, I contributed significantly to the development of the theory, the notation, and thus simplified a lot of intermediate steps.

The article on deficiency [3] in chapter 7 was initiated by Matteo Polettini, who introduced me to the literature on deficiency. We developed the theory for the article together. I then focussed on numerical simulations and provided all the figures in the article, while he wrote the initial manuscript. Our supervisor Massimiliano Esposito guided us and helped polishing the final version of the article.

The motivation for the article on catalysts [4] in chapter 8 was given by Massimiliano Esposito, who saw a huge gap between the thermodynamics literature and the biochemistry literature. A very illuminating discussion with Riccardo Rao finally sparked the idea for the article, and we then developed the full theory together. I took the lead in writing the text and drawing the figures.

The last manuscript on linear pathways [5] in chapter 9 emerged from several discussions with my supervisor Massimiliano Esposito. The calculations, the figures, and the current state of the text are my work.

References

[1] B. Altaner, A. Wachtel, and J. Vollmer. "Fluctuating currents in stochastic thermodynamics. II. Energy conversion and nonequilibrium response in kinesin models". In: *Physical Review E* 92, 042133 (2015).

[2] J. Vollmer, B. Altaner, and A. Wachtel. "Fluctuating currents in stochastic thermodynamics. III. Cycle expansion of cumulants". *In preparation.* 2018.

[3] M. Polettini, A. Wachtel, and M. Esposito. "Dissipation in noisy chemical networks: The role of deficiency". In: *Journal of Chemical Physics* 143, 184103 (2015).

[4] A. Wachtel, R. Rao, and M. Esposito. "Thermodynamically consistent coarse graining of biocatalysts beyond Michaelis–Menten". In: *New Journal of Physics* 20, 042002 (2018).

[5] A. Wachtel and M. Esposito. "Kinetic Effects on Nonequilibrium Thermodynamics of Linear Enzymatic Pathways". *In preparation.* 2018.